CONSEJO SUPERIOR
DE INVESTIGACIONES
CIENTÍFICAS

Physics at high energies and the dynamics of the universe. A study of inflation and dark energy

Memoria de Tesis Doctoral presentada en la
Facultad de Ciencias de la Universidad Autónoma de Madrid por

Guillermo Ballesteros Martínez

Trabajo dirigido por los doctores

Alberto Casas
(Profesor de Investigación del CSIC)

José Ramón Espinosa
(Investigador Científico del CSIC)

Madrid, 8 de octubre de 2008.

Sólo las páginas de los libros tienen vuelta, las de la vida, no.
18 de Septiembre de 2008. José Saramago.

Don't try to measure feelings by the energy with which they are announced.
Let's imagine this thesis was a journey. I am grateful to the people who helped me to do this work, the people with whom I traveled.

My thesis advisors: Alberto Casas and José Ramón Espinosa. I thank them for the chances they have given me, their support and guidance.
You gave me the map and opened key doors.

Antonio Riotto. Advisor de facto during the last stages. I thank him for that, for support and also for his time.
Thanks for the compass.

Roberto Ruiz de Austri y Roberto Trotta.
Thanks for helping me to go through a dense forest.

Malcolm Fairbairn, Julien Lesgourgues, Subir Sarkar, Luis Álvarez–Gaumé, Andrew Liddle.
Useful gear and boost came from you.

Even the hardest traveler needs shelter in cold nights. Wolfgang Bartmann, Pantelis Tziveloglou, Korinna Zapp and Davide Forcella.
Seriously... Bravo. We once had a castle.

When did men learn to steer by the sun and the stars? Lotta Mether, Nicholas Harries, Cédric Delaunay, Jan de Rydt, Alessandra Gnecchi and Francesco Riva.
Keep shining.

Thanks to Carlos Hoyos, Sergio Montañez, Isabel Pérez, Sergio Montero, África Periáñez, Jesús Moreno, Irene Hidalgo.
Co–walkers, in a sense. We have the same dust on the boots. And the same corns.

There was a spot in the map that I would always find.
Alicia Martínez, Jesús Ballesteros, Miguel Ballesteros Martínez.
You are the place were I come from.

Carlos Tamarit, Juan Cabrera, Caroline Zunckel, Daniel Gerber, Diana Wimmerova, Joaquin López Herráiz, Rosa Castizo, Mikail Acar, Wessel Valkenburg, Mohammed Koujili, Sebastián Pérez, Aurélia Grenier, Laura López–Honórez, Alessio Notari, Alberto Enciso, ...
If I were Perrault's Petit Poucet you would be my pebble stones. Sounds little..? Think twice.

This trip was also yours.

Contents

Chapter 1

Introducción y resumen

El trabajo de investigación resumido en esta tesis consta de dos partes distintas. La primera de ellas trata sobre inflación y la segunda sobre energía oscura. Dicho de otra forma: el tema principal de la primera parte es la aceleración del universo en edades muy tempranas, mientras que el de la segunda es la aceleración en épocas más tardías.

Vamos a comenzar esta introducción revisando brevemente las evidencias observacionales que han llevado a proponer dos fases diferentes de expansión acelerada en la historia del universo. En el caso de la inflación, es decir la aceleración en épocas tempranas, las señales son puramente indirectas. La inflación cosmológica se ideó como una solución a ciertos problemas que la imagen estándar del universo que se tenía a principios de los años ochenta no podía explicar [1]. A lo largo de los años la importancia relativa de estos problemas se ha modificado debido al conocimiento adquirido en este tiempo y también a causa de los cambios en las tendencias investigadoras. Hoy en día, el llamado problema del horizonte es, junto con las propiedades del espectro de perturbaciones primordiales, la mayor motivación en favor de la idea de inflación. El problema del horizonte proviene de la observación de la temperatura del fondo cósmico de microondas (CMB)[1] que es, con un elevado grado de precisión, esencialmente la misma en todo el cielo. Esta notable isotropía parece imposible de explicar usando ningún tipo de proceso físico conocido en el contexto de la cosmología estándar. La razón es que el tamaño del universo observable es demasiado grande para haber permitido en el pasado suficiente contacto causal. El CMB es, por supuesto, también la fuente principal de información sobre la forma y propiedades estadísticas del espectro de perturbaciones primordiales. Su similitud con una distribución gausiana y su invariancia de escala son predichas por la inflación y por tanto sustentan esta teoría. El último aspecto importante en lo que se refiere a la motivación de la idea de inflación es el problema de la planitud del universo (que también proviene de medidas del CMB), y que podríamos dejar de lado si aceptamos un ajuste muy fino de las condiciones iniciales del universo.

Por otra parte, la mayor evidencia en favor de la idea un universo acelerado en el presente es bastante distinta. En este caso proviene de las supernovas de Tipo Ia [2, 3], aunque es cierto que la combinación del CMB con datos sobre las

[1] Las siglas provienen del término inglés: Cosmic Microwave Background

oscilaciones acústicas bariónicas apunta en la misma dirección, al menos en el caso de un universo plano. Un punto clave en la interpretación de los datos es la suposición de que el universo puede ser descrito de acuerdo con el principio cosmológico. Esta información está implícita también en los problemas que motivan la inflación pero allí no surge como un punto tan crucial. Nosotros asumiremos en el trabajo descrito en esta tesis la validez del principio cosmológico.

Dos fases de expansión acelerada que se encuentran absolutamente separadas en escalas de tiempo cosmológicas son actualmente nuestra mejor solución a problemas fundamentales de la cosmología. Obsérvese sin embrago, que hay una diferencia sutil entre los orígenes de las dos fases. Mientras que puede decirse que, teniendo el principio cosmológico para interpretar los datos, la aceleración del universo actual es simplemente una observación; la fase inflacionaria se postula para resolver ciertos problemas provenientes del CMB y que no están tan directamente relacionados con la dinámica del universo. Por lo tanto, parece que cuanto mayor es en el problema la relevancia del trasfondo cosmológico que se asume, más fuerte es la evidencia en favor de la conclusión sobre la dinámica. La pregunta de si estas fases de expansión acelerada son las soluciones reales a los problemas mencionados no la vamos a tratar en esta tesis. En lugar de eso nos centraremos en ciertos aspectos de estas exitosas y ampliamente aceptadas soluciones. En ambos casos, tanto para la inflación como para la energía oscura, la cuestión subyacente fundamental es qué es lo que produce la aceleración.

Durante muchos años una gran cantidad del trabajo realizado en el área de cosmología inflacionaria ha estado dedicado a encontrar, a partir de las observaciones, las propiedades del potencial inflacionario. En el paradigma estándar se asume que la inflación la causa un campo escalar que rueda lentamente y cuyo valor clásico actúa como una constante cosmológica instantánea. Dependiendo de la forma de este potencial, es posible obtener diferentes predicciones para el espectro de perturbaciones primordiales. Por lo tanto, las medidas del espectro pueden en principio ayudar a distinguir enre diferentes clases de potenciales [4]. Desde el punto de vista de la física de partículas los posibles potenciales deberían estar motivados por teorías de física de altas energías. La conexión entre las observaciones y la teoría es muy sutil por varias razones. Ir de las unas a las otras requiere varios pasos que deben darse con cuidado para poder obtener conclusiones con sentido. No entraremos a analizar los efectos astrofísicos y los primeros pasos en el tratamiento de los datos; nos centraremos en las conexiones entre teoría y observaciones asumiendo que disponemos de las segundas en forma adecuada. El primer punto importante que debe tenerse en cuenta son las suposiciones que se hacen a lo largo del proceso.

Una manera común de enfrentarse al problema comienza con la elección de una parametrización lo suficientemente general del espectro de potencias, que entonces se aplica para realizar una ajuste de los datos. Los parámetros que se infieren de este modo se comparan después con las predicciones teóricas de diferentes modelos [5]. Esta es posiblemente la estrategia que más se ha utilizado hasta el momento. Claramente, este método solamente puede resultar útil si las predicciones de los modelos inflacionarios que se quiere analizar pueden ser descritas con suficiente precisión por la parametrización escogida. Además, si las predicciones de los modelos son muy diferentes entre si no será posible usar una única parametrización, y si son

muy semejantes no se podrá distinguir entre ellas. Es costumbre caracterizar las desviaciones de la invariancia de escala del espectro primordial con una cantidad llamada "índice espectral". Un refinamiento sería la adición de un parámetro de segundo orden, el "running", que cuantifica la dependencia del propio índice con la escala. Podríamos incluso ir más allá, añadiendo parámetros en una serie, pero los datos no son lo suficientemente buenos como para que ese procedimiento sea de alguna utilidad a día de hoy. El problema que motiva la primera parte de esta tesis surge si uno incluye el running en la parametrización del espectro de perturbaciones primordiales y mide su valor. Volveremos a esto en un momento.

Otra forma posible de caracterizar el potencial inflacionario es intentar reconstruirlo de forma numérica usando directamente una parametrización adecuada del mismo o de una cantidad relacionada como el parámetro de Hubble [6, 7]. En aplicaciones prácticas este segundo método también se basa en una expansión en serie y esencialmente puede ponerse en correspondencia con con la expansión del espectro primordial que hemos mencionado antes. La tercera estrategia que uno podría imaginar consiste en utilizar las predicciones reales para el espectro de una clase particular de modelos para diseñar una parametrización que se adecue especialmente a esos modelos. Aunque es correcto decir que esta manera de afrontar el problema no es tan general como las dos anteriores, tiene claras ventajas sobre ellas, especialmente si las desviaciones de invariancia de escala son importantes. Es este tercer método el que vamos a utilizar principalmente en esta tesis.

Volvamos ahora al problema que motiva la primera parte del trabajo aquí resumido. Cuando se ajustan los datos permitiendo la posibilidad de que haya un running constante del índice espectral, resulta que su valor no se puede acomodar a las predicciones de la mayor parte de los modelos inflacionarios. Esto sucede porque la magnitud del running es demasiado grande para que dichos modelos puedan mantener un periodo inflacionario durante un tiempo suficiente como para resolver el problema del horizonte. Existe una tensión entre obtener expansión acelerada suficientemente prolongada y un espectro dependiente de la escala como sugieren las medidas del running [8]. Está claro que podríamos olvidarnos de este problema si pudiéramos argumentar que realmente no existe necesidad de ajustar los datos usando una parametrización que incluya el running. Esto nos lleva a una segunda sutileza presente en la conexión entre teoría y observaciones: las técnicas estadísticas que se usan para interpretar los datos y la robustez de las conclusiones que de ellas se extraen. El punto de vista actualmente aceptado sobre el running del índice espectral es que no hay suficiente evidencia en favor de la necesidad de incluirlo o para concluir que debe ser desechado. En cualquier caso es interesante mantener abierta la posibilidad de que el running este realmente presente en los datos debido a las implicaciones físicas que tendría y su potencial discriminador entre modelos.

La primera parte de la investigación recogida en esta tesis tiene como punto de partida las indicaciones del satélite WMAP sobre el running del índice espectral y describe una amplia clase de modelos inflacionarios basados en física de partículas que son compatibles con ellas y con los demás requisitos de un período inflacionario que resuelva los problemas del horizonte y de la planitud. Es razonable esperar que el potoencial que resuelva este problema no sea demasiado plano de manera que pueda proporcionar un running considerable, pero al mismo tiempo su pen-

diente no puede ser excesivamente grande porque eso echaría a perder la llamada "aproximación de slow–roll". Podría pensarse que las correcciones radiativas combinan ambas características; así que primero consideraremos el efecto que tienen en potenciales que son planos a nivel árbol y haremos un análisis general de sus predicciones en relación con el espectro primordial. Como veremos, el caso más sencillo que uno puede imaginar no es suficiente para resolver el problema y por lo tanto extenderemos nuestro análisis para tener en cuenta el umbrales de masa extra. Después incluiremos los efectos de posible física que pudiera haber a energías más altas que aquellas a las cuales la inflación tiene lugar. En general, el potencial en la teoría efectiva a bajas energías se verá modificado por términos extra que son no renormalizables y relevantes para superar la tensión entre el running del índice espectral y la cantidad de inflación que es necesaria. Una vez hecho un análisis global de estos efectos, que aplicaremos a algunos ejemplos concretos, pasaremos a utilizar datos cosmológicos para estudiar estas clases de modelos. Para ello diseñamos una parametrización específica del espectro de perturbaciones primordiales en la aproximación de slow–roll que nos permite estudiar su eficiencia al ser confrontados con los datos. Aplicaremos técnicas estadísticas bayesianas y frecuentístas para evaluar el ajuste a los mismos. Finalmente, compararemos los resultados con aquellos que provienen de la parametrización estándar y explicaremos las conexiones existentes entre ellos. Los resultados de esta investigación pueden ser encontrados en [9, 10].

Vamos a ocuparnos ahora del segundo tema principal de esta tesis: la aceleración del universo hoy en día. Como antes hemos dicho, las observaciones de supernovas de Tipo Ia plantean un gran problema para nuestra comprensión del universo porque no tenemos una explicación satisfactoria de la fuente de esta aceleración. La explicación más simple posible es la adición de una constante cosmológica en las ecuaciones de Einstein. Esto es suficiente para satisfacer los requisitos observacionales pero conlleva dificultades de tipo conceptual porque la constante cosmológica puede interpretarse como la energía del vacío y al calcular su valor obtenemos un resultado que se encuentra a muchos órdenes de magnitud del minúsculo número que medimos. La constante cosmológica también puede verse como un fluido perfecto tal que su presión y densidad de energía son de igual magnitud pero signo opuesto. Una pequeña modificación de esta idea consiste en cambiar la relación de proporcionalidad entre estas dos cantidades pero manteniéndola lo suficientemente negativa como para que permita producir aceleración. El reto no es solamente que no hay ninguna forma de materia conocida con una ecuación de estado así, sino también que esta energía oscura debe constituir casi tres cuartas partes de la energía del universo. Como un campo escalar acoplado de forma mínima en relatividad general es un fluido perfecto, es posible establecer una analogía inmediata con el caso de la inflación y suponer que la aceleración actual es producida por un campo de "quintessence" como ese. Por último, podría ser también que la teoría gravitatoria adecuada a escalas cosmológicas no fuera la relatividad general sino alguna modificación de ella. Si ese fuera el caso, las ecuaciones en las que se basa la interpretación de la energía oscura podrían ser sustituidas por otras que incorporaran la expansión acelerada sin asumir la existencia de energía oscura o de una constante cosmológica. Ninguna de las tres formas de tratar con el problema de la aceleración actual del universo está libre de dificultades pero posiblemente son nuestras mejores ideas teóricas dentro del marco del principio cosmológico.

Incluir la constante cosmológica como una forma particular de energía oscura es perfectamente válido desde un punto de vista práctico y si así lo hacemos nos quedamos con dos alternativas para describir la aceleración del universo. Se está llevando a cabo un gran esfuerzo para descubrir de que manera podría distinguirse entre la energía oscura y las teorías de gravedad modificada. Si fuéramos capaces de descartar claramente una de las dos daríamos un gran paso en nuestra comprensión del problema de la aceleración. Los datos sobre la expansión del universo no son suficientes para distinguir entre estas dos explicaciones. La razón es que cualquier evolución que podamos imaginar para la expansión puede ser reproducida con una ecuación de estado para la energía oscura que sea lo suficientemente complicada [11]. Por lo tanto, cualquier expansión predicha por una teoría gravitatoria puede ser imitada en el contexto de la relatividad general por una componente de materia extraña.

Se propuso que la forma en que la materia se agrupa en el universo para formar grandes estructuras como galaxias podría ayudar a resolver el problema [12]. La teoría de formación de estructuras describe la forma en que pequeñas inhomogeneidades, perturbaciones, evolucionan en el tiempo creciendo hasta convertirse en sistemas de materia gravitacionalmente ligados. La propuesta que se hizo es que tal vez las predicciones para la evolución de estas perturbaciones en diferentes teorías de gravedad pueda ser usada para poner a prueba las teorías y discriminar entre ellas. Tenemos que aclarar que cuando hablamos de materia nos referimos tanto a bariones como a materia oscura, que es otra componente notable del universo cuyo lugar en el mundo de la física de partículas no conocemos con precisión. Se supone que la materia oscura se comporta gravitatoriamente como la materia ordinaria pero no interacciona (o lo hace muy poco) con la radiación electromagnética. Por lo tanto la materia oscura resulta ser invisible y la evidencia de su existencia proviene precisamente de la física de la gravitación. Las medidas indican que la materia oscura es aproximadamente seis veces más abundante en el universo que que la materia corriente de la que estamos hechos (y que da cuenta de solamente un pequeño 5% de la energía total del universo). Claramente, la naturaleza de la materia oscura es otro gran problema de la cosmología y de la física de partículas; un problema que no vamos a analizar en esta tesis. Simplemente asumiremos (sobre una base bien firme) que la materia oscura existe y usaremos sus propiedades gravitacionales para tratar de aprender sobre la naturaleza de la energía oscura.

La pregunta de si el crecimiento de las perturbaciones de materia oscura puede ser usado de manera fiable para discriminar entre energía oscura y teorías de gravedad modificadas no tiene una respuesta clara todavía. Se ha argumentado que, al igual que sucede con la expansión del universo, la evolución del crecimiento de las perturbaciones predicha por las teorías de gravedad modificada puede ser reproducida en relatividad general si se permiten ciertas características en la energía oscura [13]. La evolución de perturbaciones de materia es en cualquier caso una herramienta que podemos usar para aprender sobre la energía oscura en un sentido amplio del término. Posiblemente, el crecimiento de las perturbaciones nos ayudará en el futuro cercano a desvelar las propiedades de la energía oscura gracias a varios experimentos que están previstos.

En esta tesis se estudia el efecto que fluctuaciones en la energía oscura pueden

tener en la formación de estructuras. Así como las perturbaciones de materia oscura son un requisito para el crecimiento de estructuras, pequeñas perturbaciones en la energía oscura son también posibles. De hecho, el acoplo gravitacional entre la materia oscura y la energía oscura hace que las perturbaciones en uno de estos fluidos se propaguen al otro. Por lo tanto, es natural esperar fluctuaciones en la energía oscura; incluso si inicialemente fueran cero serían inducidas por las perturbaciones de la materia oscura. Hemos obtenido las ecuaciones diferenciales de segundo orden que gobiernan la evolución de las perturbaciones en relatividad general en el caso simplificado en el que ningún otro tipo de fluido aparte de materia y energía oscuras es tenido en cuenta. Asumimos que la energía oscura no presenta tensión de cizalla[2] y que su ecuación de estado es constante. Hemos resuelto las ecuaciones de manera numérica y calculado el índice de crecimiento, que parametriza la forma en que las perturbaciones de materia oscura evolucionan. Tras comparar los resultados con los del caso límite en el que la energía oscura no tiene perturbaciones, nos centramos en los diferentes parámetros cosmológicos que afectan al crecimiento de las perturbaciones. Hemos diseñado una parametrización del índice de crecimiento que tiene en cuenta la dependencia con el corrimiento al rojo, la ecuación de estado de la energía oscura y su velocidad del sonido, la escala de las perturbaciones y la abundancia relativa de materia oscura. Los resultados de este trabajo se encuentran en [14].

Después de estas primeras páginas introductorias la tesis se estructura en tres partes principales. Primero hay una revisión general de cosmología que hace énfasis en los problemas y herramientas que nos interesan. Le sigue un capítulo dedicado al running del índice espectral del espectro de perturbaciones primordiales. Ese capítulo contiene los resultados que han sido publicados en el Journal of Cosmology and Astroparticle Physics [9, 10]. El siguiente capítulo trata sobre los efectos de las perturbaciones de energía oscura en el crecimiento de estructuras que acabamos de introducir en los párrafos anteriores. Esta parte está basada en un trabajo más reciente [14], que ha sido publicado en Physics Letters B. Finalmente, hay un breve capítulo de conclusiones.

[2] El término inglés es 'shear', que hemos traducido aqui como usualmente se hace en otros campos donde aparece la dinámica de fluidos

Chapter 2

Introduction and overview

The research work that this thesis summarizes consists of two distinct parts. The first one deals with inflation and the second with dark energy. In other words: the main theme of the former is the acceleration of the universe at very early times while the object of the latter is the late time acceleration of the cosmos. These pages are therefore about the dynamics of the universe and the possible physical descriptions of it that have been proposed.

Let us commence this introduction by briefly reviewing the observational evidence that has lead to postulate two different phases of accelerated expansion in the history of the universe. In the case of inflation, i.e. early time acceleration, the signs are purely indirect. Inflation was devised as a solution to certain problems which the standard picture of the universe that we had in the beginning of the eighties could not account for [1]. Over the years the relative importance of these problems has changed due to the knowledge acquired and also because of the natural shift in research trends. Today, the so called horizon problem, together with the properties of the spectrum of primordial fluctuations form arguably the greatest motivation in favour of inflation. The horizon problem comes from the observation of the temperature of the cosmic microwave background (CMB) which is essentially the same in all the sky with very high accuracy. This remarkable isotropy seems to be impossible to explain using any known physical process in the framework of standard cosmology. The reason is that the size of the observable universe is far too large for having allowed sufficient causal contact in the past. The CMB is, of course, also the key source of information on the shape and statistical properties of the spectrum of primordial perturbations. Its gaussianity and approximate flatness are predicted by inflation and therefore support this paradigm. The last important issue as regards to the motivations for inflation is the flatness problem (also resulting from CMB measurements), which we could leave aside by accepting a tremendous fine tuning.

On the other hand, the main support for the idea of a present accelerated expansion of the universe is rather different. Here the evidence mainly comes from supernovae Type Ia data [2,3]; although it is true that the combination of CMB and baryon acoustic oscillation (BAO) data clearly points toward the same conclusion, at least for a flat universe. A key in the interpretation of the data is the assumption that the universe can be described according with the cosmological principle.

This piece of information is also implicit in the problems that motivate inflation, but there it does not appear as such an obvious crucial point. We will assume the cosmological principle through all the work that is described in this thesis.

Two phases of accelerating expansion which are absolutely apart from each other in cosmological timescales are currently our better solutions to cornerstone cosmological problems. Let us notice that there is however a subtle difference in their origins. While it is fair to say that, having the cosmological principle to interpret the data, the present accelerated expansion is just observed; the inflationary phase is postulated to solve a few problems that come from (CMB) observations and are less directly related to the dynamics of the universe. So, it seems that the greater it is the relevance of the assumed background cosmology in the problem, the stronger the evidence for the dynamical conclusion becomes. The question of whether these phases of accelerated expansion are the actual solutions to those problems is one that we will not address in this thesis. We will instead focus on certain aspects of these successful and widely ackwnoledged descriptions. In both cases, for inflation and for dark energy as well, a basic underlying question which motivates the research presented here is: what drives the acceleration?

For several years a great amount of work in the area of inflationary cosmology has been devoted to finding out the properties of the scalar inflationary potential from cosmological observations. In the standard paradigm, it is assumed that inflation is produced by a slowly rolling scalar field whose classical background value acts as an instantaneous cosmological constant. Depending on the shape of this potential different predictions for the spectrum of primordial perturbations can be obtained. Therefore, observations of the spectrum can in principle help to distinguish among different classes of potentials [4]. From the perspective of theoretical particle physics the possible potentials should be motivated by high energy theories, which are mostly beyond reach of collider experiments. Therefore, in the framework of inflation, cosmological observations (mainly of the CMB) can be used as an indirect window into the physics of very high energies. The connection between the observations and the theoretical predictions is a subtle one for several reasons. Going from one to the other requires various steps that must be done with great care in order to get meaningful conclusions. We will not enter here into astrophysical effects and the first steps in data handling but will focus on the links between theory and observations assuming that these are already given in an appropriate form. The first important point to keep in mind is are the assumptions that made along the process of linking both.

A common approach to the problem starts with the choice of a sufficiently general parameterization of the power spectrum which is then applied to fit the data. The inferred parameters are compared with the theoretical predictions of different models in a second stage [5]. This is perhaps the strategy that has been most extensively used so far. It is clear that this method can only be useful as far as the predictions of the inflationary potentials we are interested in can be described with sufficiently high accuracy by the chosen parameterization of the spectra. Moreover, if the predictions of the models are too dissimilar it will not be possible to use a single parameterization and if they are too close we will not be able to tell them apart. It is customary to measure the deviation from scale invariance of the primordial spectrum with

a number called the tilt or spectral index. A further refinement is the addition of a second order parameter, the running, which is meant to quantify the scale dependence of the index itself. We could even go on adding parameters in a series but the data is not really good enough for that procedure to be of much use today. The problem that motivates the first part of this thesis arises if one includes the running of the spectral index in the parameterization of the primordial perturbations and measures its value. We will come back to this in a moment.

Another possible way to characterize the inflationary potential is trying to reconstruct it numerically by directly using a suitable parameterization of it or an intimately related quantity such us the Hubble parameter [6, 7]. In practical applications this second method also relies in a series expansion around a fiducial point and can be essentially matched with the aforementioned expansion of the primordial spectrum. Finally, the third strategy that one could devise consists in using the actual predictions for the spectrum of a particular class of models to design a parameterization which is specially well suited for those models. Although it is possibly fair to say that this approach is not as generic as the previous two, it has clear advantages over them, particularly when the deviations from scale invariance are important. It is this third method the one we mainly exploit in this thesis.

Let us now come back to the problem that motivates the first core of the work summarized here. When one fits the data allowing the possibility of a constant running of the spectral index it turns out that the measured value of this parameter is very difficult to reconcile with the greatest majority of single field inflationary models. The reason is that its magnitude turns out to be too large for most models to be capable of sustaining inflation long enough to solve the horizon problem. There is a tension between producing enough accelerated expansion and a spectrum that deviates from scale invariance as the measurements of the running suggest [8]. It is clear that we could simply forget about this issue if we could argue that there is really no need to fit the data using a parameterization that includes the running. This leads us to a second subtlety in the connection between theory and observations: the statistical tools used to interpret the data and the robustness of the conclusions that we draw from them. The presently accepted point of view about the running of the spectral index is that there is not sufficient evidence in favour of the need to include it or to conclude that it must be disregarded altogether. It is nevertheless worth to keep open the possibility that such a running may actually be present in the data because of the physical implications that it brings and its potential as a model discriminator.

The first part of the research that this thesis reports takes as starting point the Wilkinson Microwave Anisotropy Probe (WMAP) indications in favour of a running spectral index, and finds out a broad class of particle physics models that are compatible with them and the other requirements of a successful inflationary period that solves the horizon and flatness problems. It is reasonable to expect that the potential should not be too flat in order to give a sizable running but at the same time it cannot be to steep because that would spoil the slow–roll approximation. Therefore, one would think that loop corrections can combine both features and so we first consider the effect of radiative corrections on potentials that are flat at tree level and make a general analysis of their predictions for the primordial spectrum.

As we will see the simplest case that one can devise is not sufficient for our aim and therefore we extend our analysis to take into account extra mass thresholds. Then, we include the effect of possible physics present at energies higher than those at which inflation takes place. In general, the potential in the low energy effective theory gets modified by extra terms, which are non–renormalizable, and relevant to overcome the tension between the running spectral index and the amount of inflation that is needed. After performing a general theoretical analysis of these effects and applying them to some concrete examples we move on to use cosmological data to test these classes of models. For this aim we designed a specific parameterization of the spectrum of primordial perturbations in the slow–roll approximation to study the performance of the models when confronted with real data. We apply Bayesian and frequentist statistical techniques to asses the goodness of the fits. Finally, we compare the results with those that come from the standard parameterization and explain the connections between them. The results of this research can be found in [9] and [10].

Let us now turn our attention to the second main topic of this thesis: the present accelerated expansion of the Universe. As we have said before, the observations of Type Ia supernova data pose a big problem for our understanding of the Universe because we do not have a satisfactory explanation for the source of this acceleration. The simplest possible description of it is the addition of a cosmological constant term in the Einstein equations. This is sufficient to satisfy the observational constraints but leads us to conceptual difficulties since the cosmological constant can be interpreted as vacuum energy and when we compute its value it turns to be many orders of magnitude away from the minuscule number that we measure. The cosmological constant can be thought of as a perfect fluid such that its pressure and energy density are of equal magnitude but opposite sign. A small modification of this picture consists in changing the proportionality relation between these two quantities but keeping it negative enough to still provide acceleration. The challenge then is not only the fact that there is no known form of matter with such an equation of state but also that this dark energy should amount to nearly three quarters of the total content of the universe. Since a minimally coupled homogeneous scalar field in general relativity is a perfect fluid, it is possible to make an immediate analogy with the case of inflation and suppose that the present acceleration is driven by this quintessence field. Last but not least, it could be that the theory of gravitation that is valid at cosmological scales were not Einstein's general relativity but some modification of it. If that were the case, the equations on which the dark energy interpretation relies could be replaced by others that would incorporate the accelerated expansion without assuming the existence of dark energy or a cosmological constant. None of the three ways of dealing with the present acceleration is free of problems but they are probably our current best theoretical ideas in the playground of the cosmological principle.

Including the cosmological constant as a particular form of dark energy is perfectly valid for practical purposes and doing so we remain with two alternatives to describe the present accelerated expansion of the Universe. A great amount of effort is currently being put into inventing ways that can help to distinguish between modified gravity and dark energy. If we were able to clearly discard one of

the two it would signify an important step for our understanding of the problem of the acceleration. It turns out that the mere data on the expansion history of the universe, is not enough to tell them apart [11]. The reason is that any expansion history we can think of can be reproduced if the equation of state of dark energy is a sufficiently complicated function of time. Therefore, any expansion predicted by a gravity theory can be mimicked in the context of general relativity with a strange matter component.

It was suggested that the way in which the matter clusters in the Universe to form large structures like galaxies could help to circumvent this problem [12]. The theory of structure formation describes the way in which small inhomogeneities, perturbations, evolve in time growing to become gravitationally bounded systems of matter. The proposal was that perhaps the predictions for the evolution of these perturbations in different theories of gravity can be used to test the theories and discriminate between them. Let us clarify that when we talk about matter here we mean baryons as well as dark matter; which is yet another remarkable component of the Universe whose actual place in the particle physics world we do not know. This dark matter is supposed to behave gravitationally in the same way as ordinary matter but to interact very lightly or nothing at all with electromagnetic radiation. Therefore the dark matter happens to be invisible and the evidence for its existence comes precisely from gravitational physics. The measurements indicate that dark matter is approximately six times more abundant in the Universe than the normal matter we are made of (and which comprises just a tiny 5% of the total energy budget of the Universe). Clearly, the nature of dark matter is another big problem in cosmology and particle physics; a problem we do not deal with in this thesis. We will simply assume (on a rather firm basis) that dark matter is there and use its gravitational properties for the purpose of trying to learn about the nature of dark energy.

The question of whether the growth of dark matter perturbations can be reliably used to discriminate between dark energy and modified gravity has no clear answer so far. It has been argued that, as it happens with the expansion history, the growth history predicted by modified gravity theories can be reproduced by general relativity if certain conditions on the dark energy component are allowed [13]. The evolution of matter perturbations is nonetheless a tool that we can use for learning about dark energy in an ample sense. The growth of matter perturbations will possibly help us in the near future to unveil the properties of dark energy thanks to future envisaged probes.

In this thesis it is studied the effect that dark energy fluctuations can have on the growth of structure. As well as dark matter perturbations are a requirement for the growth of structure, small perturbations in the dark energy fluid are also possible. In fact, it turns out that the gravitational coupling between dark matter and dark energy propagates perturbations in any of these fluids into the other one. Therefore, it is natural to expect dark energy fluctuations, even if they are set to zero at an early time, because they will be induced from the dark matter perturbations. We have obtained the second order differential equations that govern the evolution of perturbations in general relativity in the simplified case in which no other fluid apart from dark matter and dark energy is taken into account. We assumed that

the dark energy has no shear and that its equation of state is constant. We solved the equations numerically and compute from them the growth index, which parameterizes the way in which dark matter perturbations grow. After comparing the results with the ones for the limiting case of smooth dark energy, we focused on the effect of the different cosmological parameters that affect the growth. We built a parameterization of the growth index that takes into account its redshift dependence as well as the dependence on the equation of state of dark energy and its speed of sound, the comoving scale of the perturbations and the present relative dark matter abundance. The results of this work can be found in [14].

After these introductory first pages the dissertation is structured in three main parts. First, there is a general review of cosmology which makes emphasis on the problems and tools that we are interested in. Then it comes a chapter devoted to the issue of the running spectral index of the spectrum of primordial perturbations. As we mentioned above, that chapter comprises the research results that were made available in two research articles [9] and [10] (which are both published in the Journal of Cosmology and Astroparticle Physics). The next chapter deals with the effect of dark energy perturbations on the growth of structure that we just introduced in the previous paragraphs. That part is based on a more recent work [14], which has been published in Physics Letters B. Finally, there is a brief chapter with some concluding remarks.

Chapter 3

Review of cosmology

Here we intend to provide an overview of cosmology in the FLRW framework, including basic and more advanced topics that we will need in the subsequent chapters. We will focus on those aspects that are most relevant for this thesis and many of the concepts and ideas that we will present will be of direct use in the two chapters that come afterwards. Most of the points concerning the cosmology that we consider are well developed in [15] and [16]. Also [17, 18] are very good sources. For reviewing certain ideas in general relativity that we will simply assume it can be useful to check [19, 20]. We set $\hbar = c = 1$ and define the reduced Planck Mass as $M_p = (8\pi G)^{-1} = 2.44 \times 10^{18}\text{GeV}$, where G is Newton's constant.

3.1 The homogeneous and isotropic universe

In this first section we are going to review essential aspects of FLRW cosmologies. We will start introducing the cosmological principle and deriving the form of the metric that it implies. Then, we will explain the idea of the cosmological redshift and finally we will define the two basic horizons that we can have in this framework.

3.1.1 The cosmological principle

The current standard description of the Universe is based on the assumption that the universe is spatially homogeneous and isotropic on very large scales. This is called the *cosmological principle* and it means that for any free falling observer, regardless of its location, the Universe should appear the same in any direction. This assumption, that greatly reduces the class of allowed General Relativity metrics, is backed by Large Scale Structure (LSS) and Cosmic Microwave Background Observations. Although the cosmological principle is being theoretically and observationally challenged nowadays, there is no compelling evidence to abandon it. We will assume its validity through this work. For some comments about the cosmological principle and its observational basis see Section 3.2.7.

Robertson and Walker showed that the metric that is termed 'FLRW' is the most general one permitted by the cosmological principle [21, 22]. Previously, Friedmann

and Lemaître had derived its solution from Einstein equations independently from each other [23–25]. The cosmological principle tells us that the spacetime metric in a system of coordinates comoving with free falling observers must be of the form

$$\mathrm{d}s^2 = -\mathrm{d}t^2 + [R(t)]^2\,\mathrm{d}\Sigma^2\,, \tag{3.1}$$

where $\mathrm{d}\Sigma^2$ is the space metric constrained to describe homogeneity and isotropy and $R(t)$ is some time dependent function. There are only three independent possible constructions that lead to homogeneous and isotropic three–dimensional spaces [15]. A proof based on the maximum number of isometries of a space of a given dimension can be found in [16]. The first possibility is simply a flat space, with line element

$$\mathrm{d}\Sigma^2 = \delta_{ij}\mathrm{d}x^i\mathrm{d}x^j\,. \tag{3.2}$$

The second is a spherical hypersurface of radius a:

$$\delta_{ij}x^i x^j + z^2 = a^2 \tag{3.3}$$

in four-dimensional Euclidean space:

$$\mathrm{d}\Sigma^2 = \delta_{ij}\mathrm{d}x^i\mathrm{d}x^j + \mathrm{d}z^2\,. \tag{3.4}$$

The third and last one is obtained reversing a sign in the previous two equations:

$$\delta_{ij}x^i x^j - z^2 = a^2\,, \tag{3.5}$$

$$\mathrm{d}\Sigma^2 = \delta_{ij}\mathrm{d}x^i\mathrm{d}x^j - \mathrm{d}z^2\,, \tag{3.6}$$

which corresponds to a hyperspherical surface in pseudo Euclidean four–dimensional space. Rescaling the variables by a and expressing $\mathrm{d}z$ in terms of the other three coordinates, we can rewrite the line element that defines the last two cases:

$$\mathrm{d}\Sigma^2 = a^2\left[\delta_{ij}\mathrm{d}x^i\mathrm{d}x^j \pm \frac{\left(\delta_{ij}x^i\mathrm{d}x^j\right)^2}{1 \mp \delta_{ij}x^i x^j}\right]\,. \tag{3.7}$$

This formula can be easily generalized to include the flat three–dimensional case and finally the FLRW metric is

$$\mathrm{d}s^2 = -\mathrm{d}t^2 + a^2\left[\delta_{ij}\mathrm{d}x^i\mathrm{d}x^j + \kappa\,\frac{\left(\delta_{ij}x^i\mathrm{d}x^j\right)^2}{1 - \kappa\,\delta_{ij}x^i x^j}\right]\,, \quad \kappa = \{-1, 0, 1\}\,. \tag{3.8}$$

This is the most general metric (up to coordinate transformations) for a universe that looks spherically symmetric and isotropic to a set of typical free falling observers, as we are supposed to be ourselves. The scale factor $a(t)$ is proportional to the distance between any two comoving observers, so the rate change of such distance is proportional to the rate change of a itself. It can be easily checked applying the general relativity equations of motion for free falling particles (the geodesics equations) that a particle which is initially at rest in the comoving coordinates (3.8) will remain at rest.

It is often convenient to work with the conformal comoving time, defined as

$$a\,\mathrm{d}\tau \equiv \mathrm{d}t\,, \tag{3.9}$$

so the FLRW metric reads

$$\mathrm{d}s^2 = a^2\left[-\mathrm{d}\tau^2 + \delta_{ij}\mathrm{d}x^i\mathrm{d}x^j + \kappa\,\frac{\left(\delta_{ij}x^i\mathrm{d}x^j\right)^2}{1-\kappa\,\delta_{ij}x^ix^j}\right], \quad \kappa = \{-1,0,1\}\,. \tag{3.10}$$

A perfect fluid is a medium which has the property that in every point of the space that it fills it is possible to define a comoving inertial Cartesian frame where the fluid appears isotropic [15, 18]. According to this definition the components of the energy momentum tensor of a perfect fluid in such a frame must be

$$T^{ij} = P\delta^{ij}\,, \qquad T^{i0} = T^{0i} = 0\,, \qquad T^{00} = \rho\,. \tag{3.11}$$

This means that locally the energy momentum tensor of a perfect fluid appears

$$T^{\mu}{}_{\nu} = P\eta^{\mu}{}_{\nu} + (\rho + P)U^{\mu}U_{\nu}\,, \tag{3.12}$$

where U^μ is a vector under the Lorentz group with components $U^0 = 1$ and $U^i = 0$ in the local inertial comoving frame. By definition, the functions ρ and P in these equations are the energy density and the pressure of the perfect fluid. In general, one can define a perfect fluid as medium whose energy momentum tensor is

$$T^{\mu}{}_{\nu} = Pg^{\mu}{}_{\nu} + (\rho + P)U^{\mu}U_{\nu}\,, \qquad g_{\mu\nu}U^{\mu}U^{\nu} = -1\,, \tag{3.13}$$

where ρ and P are subject to the condition of being equal to the coefficients in a locally comoving inertial frame and U^μ must be a vector under general coordinate transformations and have components $U^0 = 1$ and $U^i = 0$ in that frame.

The Einsten equations

$$G_{\mu\nu} = 8\pi G\,T_{\mu\nu}\,, \tag{3.14}$$

for a homogeneous perfect fluid of energy density $\rho = -T^0{}_0$ and pressure $T^i{}_0 = P\delta^i_j$ in a FLRW background are called 'Friedmann equations' and take the form:

$$\mathcal{H}^2 = \frac{8\pi G}{3}a^2\rho - \kappa\,, \tag{3.15}$$

$$-\mathcal{H}' = \frac{4\pi G}{3}a^2\,(\rho + 3P)\,, \tag{3.16}$$

where we have introduced the 'conformal Hubble parameter'

$$\mathcal{H} \equiv \frac{a'}{a} = \frac{1}{a}\frac{\mathrm{d}a}{\mathrm{d}\tau}\,. \tag{3.17}$$

Differentiating (3.15) with respect to τ and using (3.16) one finds the conservation law

$$\rho' + 3\mathcal{H}\,(\rho + P) = 0\,. \tag{3.18}$$

To solve these equations it is necessary to specify some extra information regarding the energy momentum tensor T^μ_ν. This is typically done relating the energy density and the pressure through a condition of proportionality:

$$P = w\rho\,, \tag{3.19}$$

where the 'equation of state' w specifies the properties of the fluid and is typically assumed to be a constant. For instance, w is equal to 0 if it represents cold dark matter; and it is 1/3 for radiation. Let us suppose that the universe is filled with radiation, matter and a certain unspecified fluid with equation of state w_x. Moreover let us assume that these three components do not interact with each other and therefore satisfy (3.18) separately. The equation (3.15) is

$$\mathcal{H}^2 = \frac{8\pi G}{3} a^2 \left(\rho_r + \rho_m + \rho_x\right) - \kappa \,. \tag{3.20}$$

This equation can be rewritten in a convenient way by defining the critical density:

$$\rho_c \equiv \frac{3\mathcal{H}^2}{8\pi G a^2} \,, \tag{3.21}$$

the relative energy densities for the fluids:

$$\Omega_i \equiv \frac{\rho_i}{\rho_c} \,, \quad {}_{i=\{r,m,x\}} \,, \tag{3.22}$$

and an analogous quantity for the curvature term:

$$\Omega_\kappa = -\frac{\kappa}{\mathcal{H}^2} \,. \tag{3.23}$$

Then, the equation (3.20) becomes

$$\Omega_r + \Omega_m + \Omega_x + \Omega_\kappa = 1 \,. \tag{3.24}$$

From (3.18) it is immediate to obtain the dependence of the energy density of the fluids on a

$$\rho_i = \rho_{i0}\, a^{-3(1+w_i)} \,, \quad {}_{i=\{r,m,x\}} \,, \tag{3.25}$$

where we have chosen to normalize to 1 the scale factor today: $a_0 = 1$. We will take this normalization from now on, although we will sometimes keep the notation a_0 for clarity. Also, in what follows, the subscript '$_0$' will refer to quantities evaluated at the present time. Hence,

$$\frac{\mathcal{H}^2}{\mathcal{H}_0^2} = \Omega_{r0}\, a^{-2} + \Omega_{m0}\, a^{-1} + \Omega_{x0}\, a^{-(1+3w_x)} + \Omega_{\kappa 0} \,. \tag{3.26}$$

Given the present relative amounts of the different fluids and the current Hubble parameter, we can use (3.26) to compute the scale factor at any time. This is useful, among other things, to obtain the age of the universe, which in conformal time reads:

$$\tau_0 = \frac{1}{\mathcal{H}_0} \int_0^1 \frac{\mathrm{d}a}{\sqrt{\Omega_{r0} + \Omega_{m0}\, a + \Omega_{x0}\, a^{1-3w_x} + \Omega_{\kappa 0}\, a^2}} \,. \tag{3.27}$$

The critical density ρ_c tells valuable information about the spatial curvature of the universe. By definition, it is clear than ρ_c is the value that the energy density would have at any time in a universe in which $\kappa = 0$.

3.1.2 The cosmological redshift

The probably most important source of information about the scale factor and the kinematics of the universe is the observation of the displacement in the frequency of light that arrives to us from sources, like other galaxies, that are far away. From (3.8) we see that the light emitted at time t_1 from a galaxy located at a comoving distance r_1 apart from our location will reach us at t_0, given by

$$\int_{t_1}^{t_0} \frac{\mathrm{d}t}{a} = \int_0^{r_1} \frac{\mathrm{d}r}{\sqrt{1-\kappa r^2}}\,. \tag{3.28}$$

The right hand side of this equation is time independent and therefore one can easily relate the time lapses of emission Δt_1 and arrival Δt_0 between subsequent wave crests:

$$\int_{\Delta t_1}^{\Delta t_0} \frac{\mathrm{d}t}{a} = 0\,. \tag{3.29}$$

Since the typical wavelengths are much smaller than the distances between galaxies, we obtain the following expression that connects the measured frequency ν_0 with the frequency of emission ν_1

$$\frac{\nu_0}{\nu_1} = \frac{\Delta t_1}{\Delta t_0} = \frac{a\,(t_1)}{a\,(t_0)}\,. \tag{3.30}$$

This effect is quantified with the 'redshift' z defined as:

$$z \equiv \frac{\lambda_0 - \lambda_1}{\lambda_1} = \frac{a_0}{a_1} - 1\,. \tag{3.31}$$

For not too large variations of the scale factor we can use a Taylor series expansion:

$$a(t) = a(t_0)\left[1 + (t - t_0)\,H_0 + \ldots\right]\,, \tag{3.32}$$

where the current Hubble factor H_0, usually called 'Hubble constant', is related to its conformal counterpart $\mathcal{H}_0$ by

$$H \equiv \frac{1}{a}\frac{\mathrm{d}a}{\mathrm{d}t} = \frac{1}{a}\mathcal{H}\,. \tag{3.33}$$

The metric (3.8) can be expressed in spherical polar coordinates, becoming diagonal

$$(3.4.1)\mathrm{d}s^2 = \mathrm{d}t^2 - a^2\left[\frac{\mathrm{d}r^2}{1-\kappa r^2} + r^2\mathrm{d}\Omega\right]\,, \tag{3.34}$$

where

$$\delta_{ij}\mathrm{d}x^i\mathrm{d}x^j = \mathrm{d}r^2 + r^2\mathrm{d}\Omega\,, \tag{3.35}$$

$$\mathrm{d}\Omega = \mathrm{d}\theta^2 + \sin^2\theta\,\mathrm{d}\phi^2\,. \tag{3.36}$$

The proper distance, at a certain time t, from the origin to a comoving object at radial coordinate r is

$$d(r,t) = a(t)\int_0^r \frac{\mathrm{d}r}{\sqrt{1-\kappa r^2}}\,. \tag{3.37}$$

Since in a system of comoving coordinates r does not depend on time, the proper distance time variation is exclusively given by the scale factor of the universe. Moreover, the difference $t - t_0$ is precisely equal to the proper distance and therefore

$$z \simeq H_0\, d\,. \tag{3.38}$$

Several kinds of observations that rely on different distance indicators allow to measure the Hubble constant. Some of these methods are the Tully-Fisher relation (based on the 21 cm absorption line in spiral galaxies), surface brightness fluctuations in galaxies and; most importantly for us, Type Ia supernovae luminosity distance measurements. For an overview of some of the techniques see [15] and references therein. The currently accepted value of the Hubble constant is around $70\,\mathrm{km\,s^{-1}Mpc^{-1}}$ with a 7% error. It is customary to use a dimensionless parameter $h \simeq 0.7$ to express the Hubble constant:

$$H_0 = 100\, h\,\mathrm{km\,s^{-1}Mpc^{-1}}\,. \tag{3.39}$$

The fact that h is a positive number means that the wavelengths of radiation that is emitted from distant sources are stretched as they travel towards us and therefore the universe is expanding.

The expression (3.38) works well for measurements of distances at redshift $z < 1$ approximately. However, for larger redshifts that approximation is not good enough and another formula is used:

$$d_L = H_0^{-1}\left(z + \frac{1}{2}\,(1 - q_0)\, z^2 + \dots\right)\,. \tag{3.40}$$

where the 'deceleration parameter' is defined as

$$q_0 \equiv -\frac{\ddot{a}\,(t_0)}{H_0^2 a\,(t_0)}\,, \tag{3.41}$$

and d_L is the 'luminosity distance' that we are going to introduce next. In a static universe, if we consider a source of radiation, the relation between the energy that it emits per unit of time (the absolute luminosity, L) and the energy received at a distance D per unit of time and area (the relative luminosity, l) is

$$L = 4\pi\, D^2\, l \tag{3.42}$$

if the emission is isotropic and there is no energy loss. Since measurements at low redshifts tell us that the Hubble constant is positive, we must rewrite (3.42) to account for the expansion of the universe. Due to the cosmological redshift, we have to include a factor $(1 + z)^{-2}$ because the energy and the frequency of arrival of photons is diminished by $(1 + z)^{-1}$ in a expanding universe. Moreover, the surface of the radiation sphere at the time t_0 in which the radiation reaches us is $4\pi\, r_1^2 a(t_0)$, where r_1 is the comoving coordinate of the emitter. Therefore,

$$d_L = a(t_0) r_1 (1 + z) \tag{3.43}$$

is the luminosity distance that should be used in place of D in equation (3.42) to relate apparent and absolute luminosities in a FLRW background. For not too large

redshifts we can use (3.28) to expand r_1 in a series of z, obtaining the expression (3.40). This expression can be used at moderate redshifts to determine the second time derivative of the scale factor from the deceleration parameter, obtaining information about the acceleration of the universe. For redshifts of order unity the expansion in z is not convenient and the full Friedmann equations are the tool that is actually employed to interpret the observations.

3.1.3 Horizons

A 'particle horizon' in FLRW cosmology is determined by the maximum distance at which past events can be observed. Assuming that the big bang started at time $t = 0$, we see from equation (3.37) that this distance, $r_M(t)$, is given by the following integral equation:

$$\int_0^t \frac{\mathrm{d}\tilde{t}}{a\left(\tilde{t}\right)} = \int_0^{r_M(t)} \frac{\mathrm{d}r}{\sqrt{1-\kappa r^2}}\,. \tag{3.44}$$

According to this, the only way in which there could be no such horizon would be a divergence in the left integral. However, since the radiation density decays much faster than any component (matter or dark energy), the scale factor goes as the square root of the proper time at early stages and the integral is convergent. The proper distance to the horizon can be read from (3.37):

$$d_M(t) = a(t) \int_0^{r_M(t)} \frac{\mathrm{d}r}{\sqrt{1-\kappa r^2}} \tag{3.45}$$

In Section 3.1.1 we obtained the age of the universe in conformal time, equation (3.27). This can be rewritten in proper time to get the particle horizon today:

$$d_{M0} = \frac{1}{H_0} \int_0^1 \frac{\mathrm{d}a}{\sqrt{\Omega_{r0} + \Omega_{m0}\, a + \Omega_{x0}\, a^{1-3w_x} + \Omega_{\kappa 0}\, a^2}}\,. \tag{3.46}$$

By definition, according to the standard big bang cosmology, this is the limiting distance beyond which we do not recieve any photons in our instruments. We will later see that the particle horizon plays a central role in the motivation of inflationary theory.

Let us suppose now that the universe will end up recollapsing at a time t_F. By simply relabeling the limits of integration in equation (3.44), the maximum value of the radial coordinate from which an observer can possibly get signals emitted at any instant later than a given time t comes from

$$\int_t^{t_F} \frac{\mathrm{d}t}{a\left(t\right)} = \int_0^{r_F(t)} \frac{\mathrm{d}r}{\sqrt{1-\kappa r^2}}\,. \tag{3.47}$$

This equation defines the 'event horizon', r_F at proper time t. In the case that there is no future collapse ($t_F \to \infty$) the integral on the left can still be convergent and there will also be a horizon. In analogy to (3.45), the proper distance to the event horizon is

$$d_F(t) = a(t) \int_0^{r_F(t)} \frac{\mathrm{d}r}{\sqrt{1-\kappa r^2}}\,. \tag{3.48}$$

This integral can be written in the following way in the case when $t_F \to \infty$:

$$d_F^{(\infty)}(t) = \frac{a(t)}{H_0} \int_{a(t)}^{a(t_F \to \infty)} \frac{\mathrm{d}a}{\sqrt{\Omega_{r0} + \Omega_{m0}\, a + \Omega_{x0}\, a^{1-3w_x} + \Omega_{\kappa 0}\, a^2}}\,. \tag{3.49}$$

This quantity represents the maximum proper distance of future events that we can ever observe.

3.2 The present accelerated expansion of the universe

This section is devoted to one of the biggest misteries in cosmology. We will explain under which conditions the universe can undergo a phase of accelerated expansion and we will comment on the current evidence in favour of this idea. Then, we will introduce the cosmological constant problem and the coincidence "problem". These will serve us to present the best known theoretical approaches to the question of the acceleration that have been proposed. We will conclude commenting on some other possibilities that have also been put forward and are gaining importance lately.

3.2.1 Accelerated expansion

In order to be able to use luminosity observations at redshifts around unity and beyond to learn about the expansion of the universe we need to express $a(t_0)r$ in Equation (3.43) as a function of the redshift. Let us consider a FLRW universe that contains radiation, matter and some other fluid with equation of state w_x, as in Section 3.1.1. We can rewrite Equation (3.26) using proper time as follows:

$$\frac{H^2}{H_0^2} = \Omega_{r0}\, a^{-4} + \Omega_{m0}\, a^{-3} + \Omega_{x0}\, a^{-3(1+w_x)} + \Omega_{\kappa 0}\, a^{-2}\,. \tag{3.50}$$

Therefore, from (3.28) we get

$$\int_0^r \frac{\mathrm{d}\tilde{r}}{\sqrt{1-\kappa\tilde{r}^2}} = \frac{1}{H_0} \int_{1/(1+z)}^1 \frac{\mathrm{d}a}{\sqrt{\Omega_{r0} + \Omega_{m0}\, a + \Omega_{x0}\, a^{1-3w_x} + \Omega_{\kappa 0}\, a^2}}\,. \tag{3.51}$$

Using (3.23) we can express the solution of (3.51) for r in a compact way for any of the three possible values of κ. The luminosity distance (3.43) then becomes

$$d_L(z) = \frac{(1+z)}{H_0\, \Omega_{\kappa 0}^{1/2}} \sinh\left[\int_{1/(1+z)}^1 \frac{\Omega_{\kappa 0}^{1/2}\, \mathrm{d}a}{\sqrt{\Omega_{r0} + \Omega_{m0}\, a + \Omega_{x0}\, a^{1-3w_x} + \Omega_{\kappa 0}\, a^2}} \right]. \tag{3.52}$$

This formula is valid regardless of the sign of κ. In the case of zero spatial curvature it must be understood that the limit $k \to 0$ has to be taken to solve the indeterminacy that appears. Combining (3.52) and (3.42) it is possible to study the redshift dependence of the relative luminosity for sources whose absolute luminosity is known. In this way one can extract conclusions about the composition of the universe by finding out which combination of the present relative energy densities

makes the best fit to the observations. The deceleration parameter can be computed as a linear combination of the relative energy densities:

$$q = \frac{1}{2}\left(\Omega_m + 2\Omega_r + (1+3w_x)\,\Omega_x\right) . \tag{3.53}$$

This equation is valid at any time and can be easily obtained computing the second derivative of the scale factor from the Friedmann equations and using the definition of the critical density. It is remarkable that the curvature term does not appear in (3.53) . This is because the acceleration of the scale factor with respect to proper time,

$$\frac{\ddot{a}}{a} = -\frac{4\pi G}{3} a^2(\rho + 3P) , \tag{3.54}$$

does not depend on the curvature. If we had defined the deceleration parameter using conformal time we would have found a term proportional to Ω_κ . The Equation (3.53) tells us that the acceleration of a FLRW universe measured by a comoving observer in his proper frame does not depend on the geometry of the spatial sections of the universe but only on its energy density content. Moreover, we see from (3.26) that the expansion of the universe will stop only if the equation

$$\Omega_r + \Omega_m\, a + \Omega_x\, a^{1-3w_x} + a^2\Omega_k = 0 \tag{3.55}$$

has a solution for positive a . Naively, it seems reasonable to think that the energy densities of any fluid one could imagine would be positive and therefore the existence of a solution for (3.55) depends on the value of κ . For $\kappa = 1$ the curvature term Ω_κ is negative and, depending on w_x , there may be a value of the scale factor $1 \geq a > 0$ that satisfies the equation. For $\kappa = \{0, -1\}$ this cannot occur. Under the assumption of positive energy densities, since

$$\Omega_i\, H^2 = \Omega_{i0}\, H_0^2\, a^{-3(1+w_i)} , \tag{3.56}$$

we see that (3.53) implies that a necessary condition for $\ddot{a}$ to be positive is that

$$1 + 3w_x < 0 . \tag{3.57}$$

Moreover (3.56) and (3.50) show that at late times, provided that (3.57) is satisfied, Ω_x tends to unity and Ω_m and Ω_r go to zero. This means that if q is negative at certain proper time it will remain so forever. We have seen that the Equations (3.53) and (3.55) can be used to read the overall evolution of the scale factor in time if w_x is known. We will later explain that Type Ia supernova data indicate that the deceleration parameter is indeed negative and therefore some fluid that satisfies (3.57) is required to explain the observations in the framework of FLRW cosmology. This component of the universe would not be needed if the observations would only tell us that there is expansion but gave us no information about the acceleration. The Equation (3.50) is perfectly compatible with $\Omega_{x0} = 0$ and an expanding universe for any value of κ .

In Section 3.1.3 we defined the event horizon and wrote the Equation (3.49) for the proper distance to it at a given time t . If the condition (3.57) is satisfied, the integral (3.49) converges for $t_F \to \infty$:

$$d_F^{(\infty)}(t) \simeq -\frac{2}{1+3w_x}\, a^{\frac{3}{2}(1+w_x)}\, \Omega_{x0}^{1/2}\, H_0^{-1} \simeq -2(1+3w_x)^{-1} H(t)^{-1} . \tag{3.58}$$

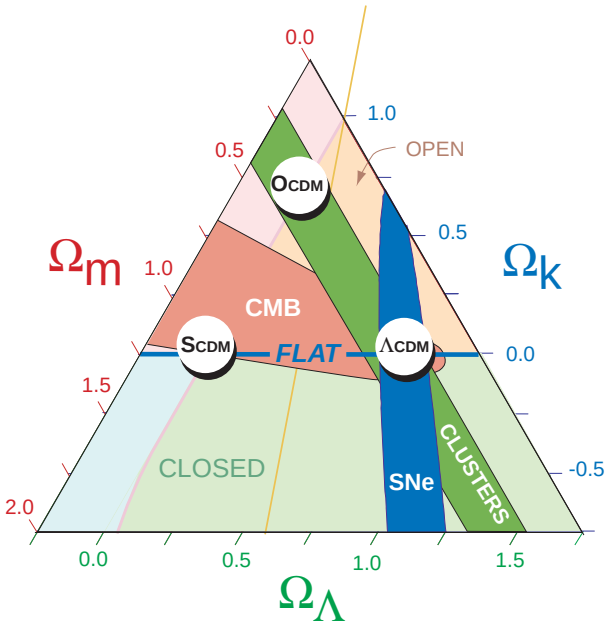

Figure 3.1: The cosmic triangle of [26]. The models at the right of the yellow line that starts near $\Omega_{m0} = 0.5$ and ends at $\Omega_{\kappa 0} = 1.0$ have $\ddot{a} > 0$ while those at the left of it have $\ddot{a} < 0$. The violet line that runs almost parallel to the Ω_m edge from $\Omega_{\kappa 0} = 1.0$ until $\Omega_{m0} \simeq 0.1$ separates the models that expand forever (at the right of it) from those that end up recollapsing. The horizontal line that marks the models with $\Omega_{\kappa 0} = 1.0$ separates open and closed universes. The figure shows the constraints on the parameter space from the data sets that were available in 1999. In particular, for the cosmic microwave background the data came from COBE [27], SP94 [28] , SK95 [29], MSAM [30] and MAX [31] among others. The CMB seems to indicate a high degree of flatness. The clusters measurements give the value of Ω_{m0}. The supernova data selects a set of universes that lays in the region that corresponds to accelerated expansion.

If $w_x = -1$ we get the very neat expression: $d_F^{(\infty)}(t) \simeq H(t)^{-1}$.

Our standard cosmological picture says that the energy density in radiation today is much less than that in matter. Photons, which can be seen in the cosmic microwave background, amount to about $10^{-5}\%$ of the total energy density in the universe. Neutrinos can be considered as relativistic particles in the limit of very small masses and their contribution is also of that order of magnitude. Other sources of photons like gamma rays are negligible. A very convenient way of representing the sum rule (3.24), neglecting the contribution of radiation, is by means of an equilateral triangle [26], as in Figure 3.1 . In this diagram, lines of constant Ω_{m0} , $\Omega_{\kappa 0}$ and Ω_{x0} are parallel to the corresponding edges of the triangle. The sum rule is satisfied at any point inside it. The circles inside the figure exemplify the positions of three different cosmological models, characterized by their composition. The open cold dark matter model (OCDM) has low matter density and no dark energy, while in the standard cold dark matter case (SCDM) all the energy density is in Ω_{m0} and the curvature component is zero. In the ΛCDM model the energy density is distributed between cold dark matter and dark energy with $w = -1$. This last model

is still today in agreement with the data [32, 33].

3.2.2 Type Ia supernovae

The supernovae of Type I are those whose spectra do not display hydrogen lines. Among them there is the subclass of supernovae Type Ia, which are supposed to occur when a white dwarf star explodes because its mass reaches the Chandrasekhar limit by accretion from a partner star. The variation in the absolute luminosity of these phenomenons is rather small since the explosion takes place when the mass of the star is very close to the Chandrasekhar limit of roughly 1.4 solar masses. Therefore Type Ia surpenovae are good distance indicators. In fact, it is possible to calibrate the absolute luminosity using the time that it takes to reach the peak luminosity and the relaxation time after the explosion.

The Type Ia supernovae are an essential piece of information in our current understanding of the cosmological picture. In the late nineteens the observations started to show evidence for the acceleration of the universe in the flat case [34–36] and also allowing a non zero curvature term [37, 38]. They are now widely used for determining cosmological parameters in combination with data sets of different physical origin such as the cosmic microwave background [32]. In Figure 3.2 we show the latest joint constraints from supernovae, CMB and Baryon Acoustic Oscillations on the equation of state of dark energy and the present relative energy density of matter for a flat universe [33]. A detailed description of the supernova data used to obtain this result and the statistical analysis done for combining sets associated to different redshifts can be found in [3]. The CMB data that was consider comes from the latest WMAP release [32]. As shown in Figure 3.2, the conclusion for the FLRW metric is that the universe is accelerating, driven by a dark energy component whose relative energy density constitutes approximately three quarters of the total one. As we already anticipated with Figure 3.1, the supernova data alone indicates the acceleration of the universe, since it selects values of w more negative than $-1/3$. It is interesting that the same conclusion can be reached combining CMB and BAO data but none of these probes is sufficient on its own.

3.2.3 The cosmological constant problem

Undoubtedly, one of the most central and intriguing questions of current research in cosmology is what makes the universe accelerate, as it has been observed. This phenomenon can be simply described by including in Einstein equations a cosmological constant that would account for roughly three quarters of the energy density of the universe. This constant term, which was originally introduced by Einstein [39] as an addend to $G_{\mu\nu}$ for a very different purpose, is enough to get an agreement with the data under the assumption that the universe is homogeneous and isotropic at large scales, but gives us little or no insight into the underlying physics.

What is behind this cosmological constant? The widely accepted interpretation is that it represents the energy of the vacuum in which we happen to live. This leads to a fundamental question for particle physics, since the vacuum energy should in principle be computable from the theory describing interactions at the deepest

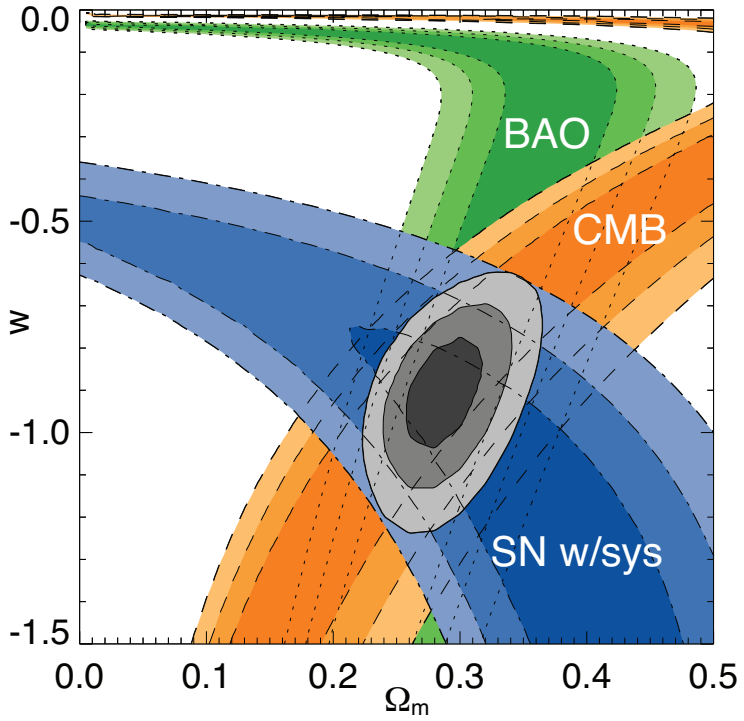

Figure 3.2: The 68.3%, 95.4%, and 99.7% confidence level contours on the equation of state of dark energy w and the present matter density Ω_{m0} are shown in the flat universe case (Rubin et al. [33]). The systematical and statistical errors on the supernovae measurements are included in the contours.

fundamental level. However, we lack such a complete theory; and performing an approximation using the normal tools of effective field theory, assuming the validity of the Standard Model of particle physics (SM) up to the Planck Mass, gives a result which is away from the measured value by many orders of magnitude. This is the cosmological constant problem, which is studied in depth in [40], for example.

In Section 3.1.1 we considered a universe that contains matter, radiation and a dark energy fluid with an equation of state w_x that relates its energy density and pressure. If $w_x = -1$ the dark energy is a cosmological constant term in Einsten equations:

$$G_{\mu\nu} = 8\pi G T_{\mu\nu} - \Lambda g_{\mu\nu} \,. \tag{3.59}$$

From (3.13) we see that a cosmological constant can be interpreted as a perfect fluid with a negative pressure that is equal in magnitude to the fluid's energy density.

Due to Lorentz invariance the energy momentum tensor in vacuum must be proportional to the metric since this is the only tensor that there can be in that situation. Therefore, if we denote the vacuum with brackets we have

$$\langle T_{\mu\nu} \rangle = -8\pi G \rho_V g_{\mu\nu} = -\Lambda g_{\mu\nu} \,, \tag{3.60}$$

and we conclude that any contribution to the vacuum energy acts as a cosmologi-

cal constant Λ in (3.59) . Vacuum energy has been theoretically and experimentally studied in scales much smaller than cosmological ones through the Casimir effect [41]. Two parallel plate conductors effectively determine the boundary conditions for the vacuum between them. The energy stored in between the plates will depend on these boundary conditions which can be changed by modifying the distance between the plates. This in turn produces a force between the metallic plates that can be measured. The Casimir effect is a quantum phenomenon. Classically, the force between uncharged plates would be zero, but virtual photons exchanged between the plates alter this picture. The effect can be described in terms of the zero–point electromagnetic energy of the vacuum. The Casimir force has been measured relatively recently [42] using parallel conducting plates separated approximately 1μm.

In a FLRW universe with a cosmological constant we have:

$$\mathcal{H}^2 = \frac{8\pi G}{3} a^2 \rho_M - \kappa + \frac{\Lambda}{3} a^2 \,, \tag{3.61}$$

where the energy density ρ_M contains the general matter components (radiation, cold dark matter, ...). Equivalently, we can write from (3.26):

$$\frac{\mathcal{H}^2}{\mathcal{H}_0^2} = \Omega_{r0}\, a^{-2} + \Omega_{m0}\, a^{-1} + \Omega_\Lambda\, a^2 + \Omega_{\kappa 0} \,, \tag{3.62}$$

where we have substituted the generic dark energy component by a cosmological constant so

$$\Omega_\Lambda = \frac{\Lambda}{3} \frac{a^2}{\mathcal{H}^2} = \frac{\Lambda}{3} \frac{1}{H^2}. \tag{3.63}$$

Since the current critical density is measured to be approximately

$$\rho_{c\,0} \simeq 2 \times 10^{-29} h^2 \,\mathrm{g\,cm^{-3}} \,, \tag{3.64}$$

it turns out that the value of the cosmological constant is

$$\Lambda \simeq 10^{-35}\,\mathrm{s^{-2}} \,, \tag{3.65}$$

which in reduced Planck units is

$$\Lambda \simeq 3 \times 10^{-122} \,. \tag{3.66}$$

The problem with this tiny value is that the number that one would naively expect is much larger. In [40] there is a very rough estimation that serves to illustrate this issue. If one considers the sum of the zero–point energies of all normal modes of a free field of mass m up to some cut–off $\Lambda \gg m$, the result is $\Lambda/16\pi^2$. Taking the cut–off to be the reduced Planck mass, this sum is approximately $2 \times 10^{71}\mathrm{GeV}^4$. However, the measured value of the cosmological constant gives in in these units a vacuum energy of $\rho_V \simeq 10^{-47}\mathrm{GeV}^4$. The comparison of these two hugely different numbers is typically used to phrase the cosmological constant problem by saying that it is a concern of about 120 orders of magnitude.

Another way of looking into the problem is considering the Higgs potential in the Standard Model of particle physics which tells us that the electroweak scale is

approximately 250 GeV. This corresponds to a vacuum energy which we could say that is different from the one associated to the cosmological constant by some 56 orders of magnitude already, without having to go up to the Planck scale. We can even extend the argument down to the QCD scale, getting in that case $\rho_V \simeq 10^{-3}\mathrm{GeV}^4$, also far away from the measured value. In summary, the problem is that Λ is really is small in comparison with any other fundamental energy scale that we know about. However it is worth to remark that this problem does not come from general relativity itself, which tells us nothing about what the "natural" value of Λ should be, but from particle physics arguments, as we have just seen.

Further understanding into the meaning of Λ can be gained from the Lagrangian formulation of general relativity [19, 43]. The calculus of variations says that extremizing

$$\mathcal{S} = \frac{1}{16\pi G}\int \mathrm{d}^4x\,\sqrt{-g}\,R + \int \mathrm{d}^4x\,\sqrt{-g}\,\mathcal{L}_m\,, \tag{3.67}$$

we obtain

$$G_{\mu\nu} = 8\pi G\,T_{\mu\nu}\,, \tag{3.68}$$

where

$$T_{\mu\nu} = -\frac{2}{\sqrt{-g}}\frac{\delta\mathcal{S}_m}{\delta g^{\mu\nu}}\,, \tag{3.69}$$

being $\mathcal{S}_m$ the part of the action that contains the matter lagrangian $\mathcal{L}_m$. The inclusion of a cosmological constant is done adding to the total action the term

$$\mathcal{S}_\Lambda = -\frac{\Lambda}{8\pi G}\int \mathrm{d}^4x\,\sqrt{-g}\,. \tag{3.70}$$

The action

$$\mathcal{S}_H + \mathcal{S}_\Lambda = \frac{1}{16\pi G}\int \mathrm{d}^4x\,\sqrt{-g}\,(R - 2\Lambda) \tag{3.71}$$

is the most general covariant one that can be built from the metric and its second derivatives. Therefore, the Λ term in (3.59) must be regarded from a field theory point of view as one of the possible terms allowed by the symmetries of general relativity. At this level, there is no evident particular theoretical reason for Λ to take one value or another.

Considering the full action $\mathcal{S}_H + \mathcal{S}_\Lambda + \mathcal{S}_m$ the total cosmological constant would also have a contribution from the potential contained in $\mathcal{L}_m$:

$$\Lambda_T = \Lambda + V\,. \tag{3.72}$$

The potential energy V would in general have a classical (tree–level) part plus quantum corrections. Moreover, using ideas based on the renormalization group, it has recently been argued that Λ should also be scale dependent and therefore get quantum corrections in a well defined theory in which the spacetime is curved [44].

One could think that the solution of the cosmological constant problem may come from a delicate cancellation of the different contributions that we have commented above, in such a way that the final measured value Λ_T would be as small as it is required by the observations. Unfortunately we know of no mechanism that could produce that effect.

Many different ideas inspired in high energy physics theories have been tried to be connected to the cosmological constant problem: supersymmetry [45] and supergravity [46], extra dimensions [47–49], string theory [50,51] and even anthropic arguments based on constructions allowing multiple different vacua have been used [52–55]. Also, many other ideas have been proposed to address the problem; for example mass varying neutrinos [56], novel phase transitions [57, 58] and the backreaction of cosmological perturbations [59]; to name some of them. There are also several works that try to the reinterpret the mathematical structure of the action $\mathcal{S}_H + \mathcal{S}_\Lambda + \mathcal{S}_m$, for instance considering Λ as a Lagrange multiplier, an stochastic variable or even a constant of integration. A short summary of ideas along these last lines can be found in [60]. For reviews on the cosmological constant, including theoretical and observational aspects see [40, 43, 60–65].

3.2.4 The coincidence "problem"

The data indicates that the present relative energy densities of dark matter and dark energy are roughly of the same order of magnitude:

$$\Omega_{x0} \simeq 0.72\,, \tag{3.73}$$

$$\Omega_{m0} \simeq 0.24\,, \tag{3.74}$$

with the concrete values depending on the data sets considered and the corresponding errors for dark matter being somewhat larger than those for dark energy; approximately 6% and 2% respectively. See [32], for instance.

Looking at (3.24) and (3.26) it is clear that if these equations are valid for $a \to 0$ the relative energy densities must have been exceedingly different from each other in the far past and so will be far in the future. This feature is illustrated in Figure 3.3 taken from [43]. The so called 'coincidence problem' can be formulated as the following question: Why should we observe the dark matter and dark energy relative densities to be so close now? This numerical similarity causes certain discomfort among several cosmologists because it seems to indicate that we are in a rather peculiar moment in the history of the universe. It is argued that if there were no particular reason for this fact, we would have to accept a coincidence that seems in disagreement with the *style* of the successful trend of research in modern cosmology that was initiated with the cosmological principle, according to which the universe looks the same in any direction everywhere at large scales.

The importance of this coincidence is by no means as big as that of the cosmological constant problem. A widely extended opinion is that there is actually no problem at all with $\Omega_{\Lambda 0}$ and Ω_{m0} being similar. While the cosmological constant problem directly targets the nature of the vacuum energy, which is a question of fundamental significance, the coincidence problem does not seem to have such deep physics implications. However, its relevance for current research in theoretical cosmology is undeniable since it has been used as a motivation for studying dynamical dark energy models, which in turn also address the cosmological constant problem.

The coincidence problem has even been extended to include the energy density of radiation Ω_r [66]. There is an epoch in the history of the universe where Ω_Λ , Ω_m

and Ω_r become comparable within a few orders of magnitude and, since $\Omega_{r0} \simeq 10^{-4}$, this period is happening now. Its length, for comparison with Figure 3.3, can be estimated knowing the values of the scale factor at which $\Omega_\Lambda = \Omega_m$ and $\Omega_m = \Omega_r$ which are approximately 10^{-4} and 1 respectively, with the normalization convention introduced in Section 3.1.1. In view of Figure 3.3 this is a narrow lapse which starts in between the big bang nucleosynthesis and today. Formulated in this way, the coincidence problem reminds of the gauge coupling unification around 10^{16}GeV that is known to happen to some extent in the Standard Model and much improved in the Minimal Supersymmetric Standard Model. This analogy has lead to the suggestion of trying to explain the cosmological coincidence from arguments of symmetry [66].

To finish this discussion about the coincidence problem, it is important to draw attention to an "aesthetic" feature of Figure 3.3 that can be misleading and should not be unnoticed. Although we have introduced the coincidence problem in terms of epochs in the history of the universe, the figure shows the evolution of Ω_Λ as a function of the scale factor. If we assume that there was an inflationary period in the very early universe and consider the typical 60 efolds requirement, which corresponds to a change in the scale factor of 26 orders of magnitude, we realize that basically all the region of the plot to the left of $a = 1$ happens in next to no time in comparison with the evolution that is taking place today. Therefore, restricting the width of the plot to a symmetric region around $a = 1$ that extends in the past until radiation domination at most, the sharp step–like shape of the plot disappears and one would think that the coincidence between the present values of the relative energy densities is not as severe as Figure 3.3 may suggest.

3.2.5 Quintessence

The quintessence proposal [67] was partly motivated by searching for a solution of the coincidence "problem" [68] and partly by trying to understand the meaning of the cosmological constant. The basic idea is that the value of the cosmological constant in general relativity may actually be time dependent. This dependence should be small over cosmological timescales and an easy way to implement it is using a scalar field. The idea is completely analogous to that of primordial inflation driven by a rolling scalar. Since a great part of this thesis is concerned with inflationary dynamics and its predictions, while we do not really need to enter in so much detail concerning quintessence, we will avoid writing twice the same equations and make reference here to those of Section 3.4.3 when necessary.

The equation of motion of a minimally coupled homogeneous scalar field in general relativity (3.188) can be understood as a damped harmonic oscillator where the damping term is played by the Hubble parameter. If the square of H is bigger than the second derivative of the scalar potential the system will be essentially overdamped and the field will remain approximately constant. In the opposite case, the contribution from H can be neglected and the scalar would be basically free rolling. We see in Equation (3.186) that the equation of state of the fluid represented by the scalar field will be time dependent but very close to -1 (the cosmological constant case) if the speed of the field can be neglected in comparison with the potential. In this situation the potential would effectively act as a (normally slightly varying)

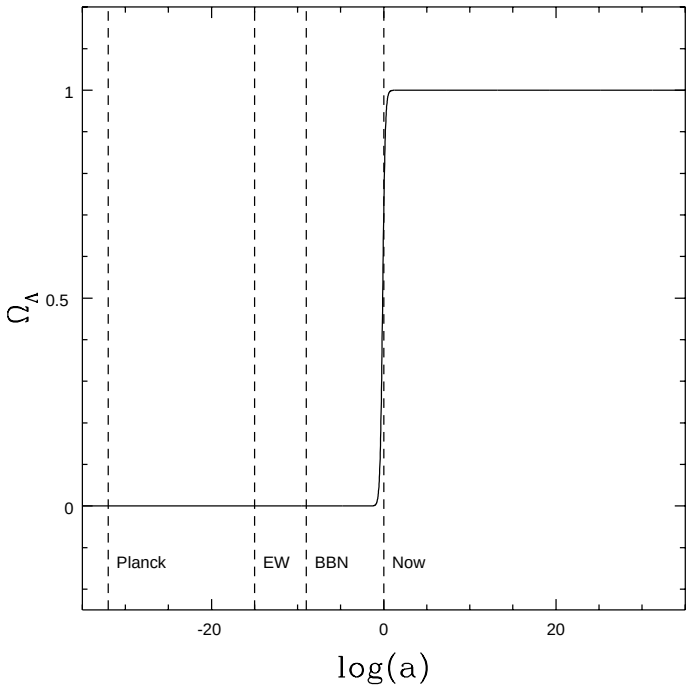

Figure 3.3: Ω_Λ as a function of the natural logarithm of scale factor a, for a universe with $\Omega_{x0} = 0.3$ and $\Omega_{x0} = 0.7$ [43]. Vertical dashed lines indicate the scale factors corresponding to the Planck era, the electroweak phase transition, and big bang nucleosynthesis.

cosmological constant. An interesting property of certain quintessence models is that the evolution of the scalar field can track that of the energy density in matter or radiation [69–72] which in some settings helps to alleviate the fine–tuning that can be viewed in the coincidence "problem". This happens, for instance, with exponential potentials. It is also said quite often that dark energy in the form of a rolling field would agree with the possibility that the energy of the true vacuum is exactly zero. This is a theoretically appealing possibility, but even if the minimum of the hypothetical scalar potential that would be driving inflation today were zero we would still have to account for quantum corrections and background values of other scalars that are not contemplated in this framework. This would be another source of fine–tuning, to say the least. On the other hand, the slow–roll of the quintessence field, which is required in order to have an equation of state close to -1, means that the Hubble parameter must be comparable to the square root of the second derivative of the potential. This is giving us an estimate on the effective mass of the scalar field around $10^{-33}\,\mathrm{eV}$, which is extremely tiny in comparison with any mass that we know about in the Standard Model. A mass of this size would necessarily produce a long range force if coupled to other fields. Since the quintessence field is obviously coupled to gravity this might have observational consequences [73, 74]. There are currently several bounds on the variation of fundamental constants that these kind of couplings could produce and also on a fifth force from the same origin. It seems quite reasonable that solving these issues in quintessence would require

imposing some extra symmetry. Indeed many of the specific models that have been built are based on theories with an underlying possible fundamental symmetry such as supersymmetry [75] or supergravity [76]. Another popular example is the assumption that the quintessence field is a pseudo–Goldstone boson [77]. Actually, many of the motivations that have been used in the context of inflation are also present in the ample spectrum of quintessence models and there are even examples in which a single scalar field has been proposed to deal with both periods of accelerated expansion [78, 79]. Moreover, apart from the generic case of a minimally coupled scalar field, there are more exotic variations of dynamical dark energy. The first one is k–essence [80] (see [81] for the original work in the context of inflation), where the kinetic part of the action is a functional of $\partial^\mu \partial_\mu \phi$ which can be motivated in some examples of low energy string theory. There are even models based on a rolling tachyon (a field with negative mass squared) [82, 83], a phantom field (with equation of state smaller than -1) [84] and a Chaplygin gas [85], which does not contain a scalar field but a fluid in which the energy density and the pressure and inversely proportional to each other.

3.2.6 Modified gravity

It is possible to look at the problem of the accelerated expansion of the universe from a conceptually different perspective that tries to get rid of scalar fields and dark energy [86]. From Equation (3.68) and the definition (3.69) we see that the left hand side of Einstein equations is purely geometric, because it depends only on the metric, while the right hand side encodes the matter content of the universe. However, we can always rewrite (3.68) splitting the energy momentum tensor and moving one of the parts to the left side of the equality, obtaining a new gravity source $G_{\mu\nu}$. This simple reshuffling tells us that general relativity in a FLRW background with a particular energy content can be in principle equivalent to a different gravity theory with another matter content. The idea behind the theories of modified gravity can be understood as reinterpreting the dark content of the universe in terms a geometrical effect in a gravity theory that is qualitatively different from general relativity. Clearly, great care must be taken if we want to avoid breaking general covariance by splitting the tensors in (3.68). Indeed, for this reason, this procedure is not usually followed to build theories of modified gravity and the starting point that is typically taken is a modification of (3.67). However, it is useful to keep in mind this dual picture that connects gravity and matter in different backgrounds.

Modified gravity theories have been used not only to address the problem of the present acceleration of the universe but also attempting to describe the observations that lead to the introduction of dark matter, like those related to the rotation curves of galaxies and gravitational lensing in galaxy clusters. However, with the discovery of the 'bullet cluster' [87] and a recently found similar system [88], this potential use of modified gravity seems to be under serious threaten, although there are works that challenge this conclusion [89, 90]. In any case, we are interested in gravity at the cosmological level, and a change in the theory of gravitation at very large distances can in principle be perfectly compatible with having dark matter as an explanation of the observations at smaller scales.

Modified gravity theories are an attractive possibility for describing the dynamics of the universe as a whole. A wide class of them is the $f(R)$ theories, which are characterized by an action of the form:

$$\mathcal{S}_{mg} = \int \mathrm{d}^4x\sqrt{-g}f(R) + \int \mathrm{d}^4x\,\sqrt{-g}\,\mathcal{L}_m\,, \tag{3.75}$$

where $f(R)$ is a function that normally includes the normal R term of the Einstein-Hilbert action (3.67). For instance, it was shown in [86] and [91] that late time acceleration can be obtained with terms that contain inverse powers of the Ricci scalar added to the Einstein Hilbert action. In particular, the case $1/R$ was studied in detail in these works. It turns out that this case is equivalent to certain class of scalar–tensor theories of gravity which are incompatible with the dynamics at the Solar System scale. Moreover, the addition of non–linear R terms gives rise to higher order equations of motion which can be a source of instabilities [92,93]. In [94] more general actions including terms depending on $R_{\mu\nu}R^{\mu\nu}$ and $R_{\mu\nu\alpha\beta}R^{\mu\nu\alpha\beta}$ are studied. Interestingly a modification of the form R^2 can serve to provide a period of (early time) inflation but is not useful for late time acceleration [65]. For a review about modified gravity theories see [95].

We have mentioned above that extra dimensional models have been used to attack the cosmological constant problem. Indeed, a whole class of modified gravity theories is constituted from many of these constructions, basically 'braneworlds'. A prototypical example is the DGP model [96]. In this model a four–dimensional 3–brane is embedded in (five–dimensional) Minkowski space with an infinite extra dimension. At short distances gravity looks like general relativity but the effect of the extra dimension is relevant at larger scales. This is controlled by a parameter which is sometimes called the cross–over scale:

$$r_c \equiv \frac{G_5}{2G_4}\,. \tag{3.76}$$

The constants G_5 and G_4 are related to the two mass scales that appear in the action:

$$\mathcal{S}_{DGP} \supset \frac{1}{2}M_5^{-3}\int \mathrm{d}^5x\sqrt{-g_5}R_5 + \frac{1}{2}M_4^{-2}\int \mathrm{d}^4x\,\sqrt{-g}R\,, \tag{3.77}$$

by

$$8\pi G_5 = M_5^{-3}\,, \quad 8\pi G_4 = M_4^{-2}\,. \tag{3.78}$$

The Ricci scalar and determinant coming from the five-dimensional metric are denoted R_5 and g_5 respectively. The four–dimensional constant G_4 is related to Newton's constant G (defined as the one appearing in the Newtonian potential) by

$$G = \frac{4}{3}G_4\,, \tag{3.79}$$

because of the presence of an extra scalar degree of freedom as described in [97] and [98]. The mass scales in (3.78) need not be related to each other and r_c can be regarded as a free parameter of the model. For a flat FLRW brane the analogous of the Friedmann equation (3.15), written in proper time is,

$$H^2 - \frac{\varepsilon}{r_c}H = \frac{8\pi G_4}{3}\rho\,, \tag{3.80}$$

where $\varepsilon = \pm 1$. When $1/r_c \ll H$ the usual form of the Friedmann Equation (3.15) is recovered. In the case $\varepsilon = 1$ a universe filled with cold dark matter evolves towards the de Sitter solution $H = 1/r_c$, giving accelerated expansion at late times without dark energy. Therefore, in order to explain the present acceleration of the universe within this model we need $H_0 \simeq 2M_5^3/M_4^2$. The acceleration would be interpreted as the weakening of gravity in the 3–brane. On the other hand, the case with negative ε requires a dark energy component on the brane in order to have acceleration. The equation for $\kappa \neq 0$ is a little bit more complex but the behaviour is qualitatively the same.

In [99] and [100] the DGP model was tested against the gold sample of Type Ia supernovae [101], the first year data from the Supernova Legacy Survey [2] and the BAO peak in the Sloan Digital Sky Survey [102]. The data favours a closed ($\kappa = 1$) universe with a best fit $\Omega_{m0} \simeq 0.27$ and $\Omega_{r0} \equiv 1/(4r_c H_0^2) \simeq 0.22$. The result of the second of these analyses is shown in Figure 3.4(a). When cosmic microwave background Radiation data is included, the goodness of the fit decreases considerably as it can be seen in Figure 3.4(b) from [33]. This figure represents confidence level contours for $\Omega_{\kappa 0}$, defined as in (3.23), versus Ω_{r0}. The best fit is displaced towards a flat model with respect to 3.4(a) and it is clear that the compatibility of the three data sets (the same that were used for Figure 3.2) is only marginal, although it is still too early to discard the dynamics of the DGP model on these grounds.

There are concerns regarding the reliability of using Baryon Acoustic Oscillations and (perhaps even more) cosmic microwave background radiation data to asses the DGP model. The reason is that the study of cosmological perturbations in the DGP model is a quite subtle issue [103, 104] which is probably not fully understood yet. For earlier works on the same topic one may check [105, 106]. Apart from the analyses mentioned above there are several other studies that have tried to test the DGP model with different data sets combinations, for instance [107, 108].

Taking into account that there is no contradiction between the DGP model and the available supernova data one may wonder if it would be possible at all to distinguish its dynamics from those of standard Einstein gravity with a dark energy component. It is known that if the equation of state of dark energy is not constant, the expansion histories predicted by the two models can be matched. The question that was raised was if subhorizon perturbations and the growth of structure could be used to differentiate the two models. It was argued in [11] that this can only be possible under certain restrictions upon the dark energy fluid. In general, the two descriptions of the present acceleration could not be told apart because they would predict equivalent evolutions for the matter perturbations. However, as we have discussed above, there is still room for study concerning perturbations in the DGP model and it is not clear yet if it is really possible to discriminate between the two cases using the growth of structure.

The DGP model has received various criticisms for having a ghost degree of freedom in the accelerating solution that is relevant for describing the observations (see [110] for example). This is actually a generic concern for modified gravity theories. A description of the problem for the generic gravitational actions that were introduced in [91] to generalize $f(R)$ gravity, can be found in [111]. The DGP

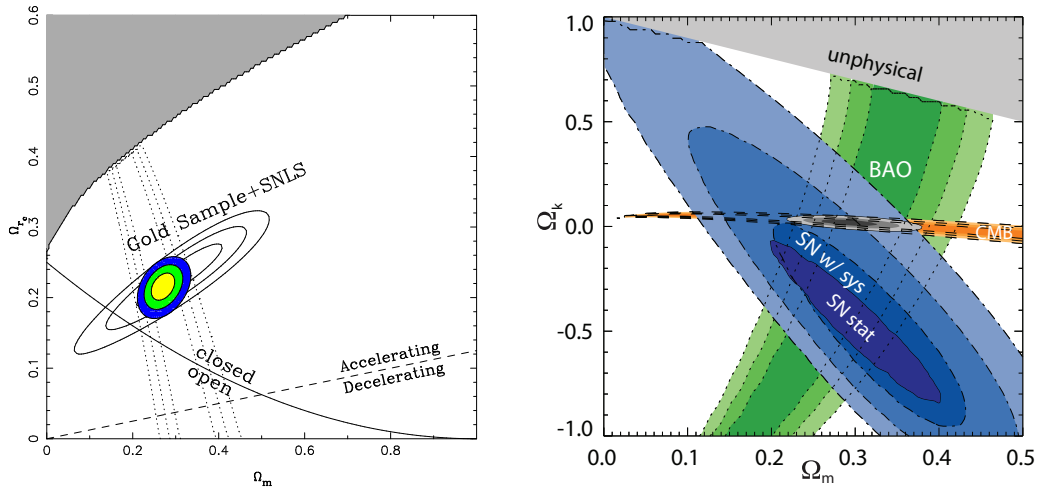

(a) Guo et al. [100] (b) Rubin et al. [33]

Figure 3.4: For the DGP model, 68.3%, 95.4% and 99.7% confidence level contours in Ω_{r0} versus Ω_{m0} (left) and $\Omega_{\kappa 0}$ versus Ω_{m0} (right). The baryon acoustic oscillations data (dotted lines in the left figure) are orthogonal to the supernovae data. The inclusion of the latest WMAP data release [109] introduces a qualitative change in the meaning of the fit from (a) to (b). The flat $\kappa = 0$ case, which is almost selected by the CMB data, corresponds to the oblique line that divides the parameter space into closed and open models in the left figure. The dark shaded upper areas in both plots represent the "no big-bang" region. In the figure on the right, the statistical contours of the Union Supernova Compilation data are displayed alone only for the smallest confidence level.

model is nonetheless an interesting case for exploring alternative possibilities to explain the acceleration of the universe and analysing how the data can be used to constrain other models than those described by (3.50).

3.2.7 Other approaches to the acceleration problem

There are two important ways of approaching the problem of the present accelerated expansion of the universe that are not directly related to the research in this thesis but deserve to be mentioned nonetheless. The first one consists in dropping the working assumption that the universe should be described by a FLRW metric. We will leap over the discussion of whether this condition is backed by observations or not. Let us just say that the strongest evidence in favour of it comes from the CMB temperature, whose relative variation in the sky does not exceed approximately 10^{-5}. It can be argued that the CMB has little to do with the total matter and energy density distribution which is what determines the geometry according to general relativity. However, taking into account the large distances that photons originated in the CMB have traveled before reaching us, it would be rather surprising such a high degree of isotropy if the universe where inhomogeneous. Therefore it does not seem unreasonable to conclude that on very large scales that will be precisely the case. In reality, the fact that the universe looks isotropic from a certain point does not imply that it is homogeneous; that would be the case if

the universe were isotropic around every point, which is something we cannot test. The success of the cosmological principle greatly comes from its simplicity, which makes it an attractive framework. Testing homogeneity in the universe is not easy simply because the observations (basically light of different wavelengths) have to be interpreted according with a particular model to give it meaning. There some works that support the homogeneity hypothesis from LSS data (see [112] for instance) as well as others that challenge it at certain scales [113, 114] reporting the existence of matter voids.

If those voids existed they could be a possible explanation of the (apparent) acceleration of the universe. If we were located inside an underdense region of the universe, the Type Ia luminosity observations might be explained without requiring dark energy [115–121]. There are however some difficulties with this models, mainly that it is unclear how the voids could have formed since they do not seem to fit within the standard theory of structure formation. Another problem is that in order to fit the observations, it has to be required that the position of the observers inside the (supposedly spherical) void is not more than a 10% away from the center, which obviously means that the allowed region inside the void is just a 10^{-3} of the total volume. The metric that is used to modelize this structures is the Lemâitre–Tolman–Bondi (LTB) one. This metric has also been used to describe other proposals like the Swiss–cheese universe [122–124] that try to reinterpret the cosmological data. Other not so well–known metrics have been used for the same purpose, see [125] for an example.

A different way in which it may be possible to explain the observed accelerated expansion without a dark energy fluid or a modification of gravity is through the effect of backreaction perturbations. Very roughly speaking, the idea is that the perturbations induced in the matter content of the universe would backreact on the metric providing an effective cosmological constant [59]. See also [126, 127]. Although there are claims that it is impossible that this kind of process could be the explanation of the accelerated expansion [128], the question is far from being fully settled and many articles have been published on the topic since it was proposed.

3.3 Small inhomogeneities

In this section we are going to deal with the theory of small cosmological perturbations at the linear level. Some of the equations that we will introduce will be relevant in subsequent chapters in relation to inflation and dark energy. We will devote a few pages to explain the idea of a gauge in general relativity. The last part of this section serves to define the speed of sound, which will be essential in our treatment of dark energy perturbations.

3.3.1 Linear perturbations

Let us assume a universe that can be described by a FLRW metric with small perturbations. We will assume that the departure from perfect homogeneity and isotropy is small enough to guarantee that the fluctuations can be studied at the

linear level. This means that the equations that describe their evolution will be linear in the perturbations themselves. Moreover, we impose $\kappa = 0$ because the most recent observations [32] indicate that the spatial curvature is negligible. Background quantities will be denoted with bars over them. The quantities without bars are the perturbed ones. For instance:

$$g_{\mu\nu} = \bar{g}_{\mu\nu} + h_{\mu\nu}\,, \tag{3.81}$$

means that the actual metric $g_{\mu\nu}$ is the sum of a background (FLRW) metric $\bar{g}_{\mu\nu}$ plus a small perturbation $h_{\mu\nu}$. Since we decide to neglect curvature effects we can write:

$$\mathrm{d}s^2 = a^2(\tau)\left[-\mathrm{d}\tau^2 + (\delta_{ij} + h_{ij})\,\mathrm{d}x^i\mathrm{d}x^j\right]\,, \tag{3.82}$$

where h_{ij} encodes the perturbation and can be decomposed into a trace part $h \equiv h^i_i$ and a traceless one. The expression (3.82) is valid in the synchronous gauge, in which the components g_{00} and g_{0i} of the metric tensor are by definition unperturbed. We choose to work in this gauge for convenience. We will later comment on other possible gauges and the relations among them. The traceless part of h_{ij} can be decomposed in three pieces in such a way that

$$h_{ij} = \frac{h}{3}\delta_{ij} + h^{\parallel}_{ij} + h^{\perp}_{ij} + h^{T}_{ij}\,, \tag{3.83}$$

where, by definition,

$$\epsilon_{ijk}\,\partial_j\partial_l h^{\parallel}_{lk} = 0\,, \tag{3.84}$$

$$\partial_i\partial_j h^{\perp}_{ij} = 0\,, \tag{3.85}$$

$$\partial_i h^{T}_{ij} = 0\,. \tag{3.86}$$

The first two of these three equations imply that $h^{\parallel}_{ij}$ can be expressed in terms of a scalar field μ and $h^{\perp}_{ij}$ can be obtained from a vector $\mathbf{A}$ with zero divergence:

$$\begin{aligned} h^{\parallel}_{ij} &= \left(\partial_i\partial_j - \frac{1}{3}\delta_{ij}\nabla^2\right)\mu\,, \\ h^{\perp}_{ij} &= \partial_i A_j + \partial_j A_i\,, \qquad \partial_i A_i = 0\,. \end{aligned} \tag{3.87}$$

The two scalar fields h and μ characterize the scalar modes of the metric perturbations, $\mathbf{A}$ represents the vector ones and h^T_{ij} encodes the tensor modes. This classification of the degrees of freedom of the perturbations is motivated by their spin with respect to a local rotation of the spatial coordinates on spacetime slices of constant time [18]. Tensor, vector and scalar perturbations have spin 2, 1 and 0, respectively. We can easily check that the conditions we have imposed above to define the synchronous gauge are such that they select all the possible degrees of freedom of the metric without leaving any redundancy or eliminating relevant variables. In four dimensions, any metric contains at most 10 independent quantities because it is a symmetric tensor. From this point of view, the FLRW metric is certainly rather simple, since it can be defined from a single function, the scale factor a. With 4 coordinate transformations we can reduce the original 10 degrees of freedom to just 6. To see how these 6 degrees of freedom can be distributed we have to determine

how many functions are needed to define vectors and tensors in three–dimensional spaces (the hypersurfaces of constant time that we mentioned above). Any vector in three dimensions can be decomposed into the sum of the directional derivative of a scalar which is irrotational, and a divergenceless vector. The actual number of degrees of freedom in a vector is equal to the number of functions we use to define it (4 scalar quantities) minus the number of conditions we impose upon them (2 equations), which amounts to 2 . Similarly, a symmetric traceless tensor in three dimensions contains just 2 degrees of freedom. This is because it can be decomposed into a scalar, a divergenceless vector; and a pure tensor part, each of which components is divergenceless as well. So, the real number of degrees of freedom for such a tensor is $1\,[\text{scalar}] + (3-2)\,[\text{vector}] + (3-3)\,[\text{tensor}] = 2$. Therefore, the 6 metric degrees of freedom that remain after gaugeing out 4 components by coordinate transformations, are in fact 2 tensor degrees of freedom, 2 vector ones and 2 scalars. This is precisely what we have used above for the synchronous gauge. It turns out that the equations for the evolution of the perturbations that come from Einstein equations can be distributed in three independent sets which correspond to the splitting that we have described. This happens even if one starts writing the perturbed FLRW metric in the most general way without considering first how many degrees of freedom can be gauged. The choice of a gauge leaves away the possibility of unphysical solutions of the perturbation equations that correspond to coordinate transformations of the FLRW metric. We will later see in more depth what a gauge actually means.

It is useful to apply perturbation theory using Fourier space. The fluctuations are described in spacetime by partial differential equations in which the variables are the spacetime coordinates. Since the background metric does not have any degrees of freedom that depend on space coordinates, the coefficients multiplying the derivative terms in the equations only depend on time. Therefore, for each wavenumber, the equations in Fourier space only contain time derivatives; and different wavenumbers do not mix. We will focus on scalar perturbations since these are the ones that we will later be interested in. It is customary to write the scalar part or the metric perturbation in Fourier space in the synchronous gauge as follows [129]:

$$h_{ij}(\mathbf{x},\tau) = \int \mathrm{d}^3k\, e^{i\mathbf{k}\cdot\mathbf{x}} \left(\hat{k}_i\hat{k}_j\, h(\mathbf{k},\tau) + (\hat{k}_i\hat{k}_j - \frac{1}{3}\delta_{ij})\, 6\,\eta(\mathbf{k},\tau) \right) , \quad \mathbf{k} = k\,\hat{\mathbf{k}} . \quad (3.88)$$

The functions $h(\mathbf{k},\tau)$ and $\eta(\mathbf{k},\tau)$ are the two independent degrees of freedom and the first one of them represents the trace of the perturbation. This is the same notation that we have used above for the trace in real spacetime, but the two traces will never appear in the same equation, so there is no risk of confusion.

We consider an anisotropic fluid which is almost perfect, so the anisotropies are small perturbations. There are two possible ways to convert a perfect fluid into an anisotropic one by introducing small perturbations. The first one is adding a small velocity $v^i = \mathrm{d}x^i/\mathrm{d}\tau$ that will appear in the off–diagonal entries of the energy momentum tensor. The second one is a pure traceless shear perturbation Σ^i_j . We also want to allow the possibility of small inhomogeneous perturbations and therefore the pressure and the energy density are $P = \bar{P} + \delta P$ and $\rho = \bar{\rho} + \delta\rho$, where the quantities with a bar are understood to be homogeneous. Remembering

the Equation (3.13), the components of the energy momentum tensor of the fluid can be written as

$$T^0{}_0 = -(\bar{\rho} + \delta\rho)\,, \tag{3.89}$$
$$T^0{}_i = (\bar{\rho} + \bar{P})v_i = -T^i{}_0\,, \tag{3.90}$$
$$T^i{}_j = (\bar{P} + \delta P)\delta^i{}_j + \Sigma^i{}_j\,, \qquad \Sigma^i{}_i = 0\,, \tag{3.91}$$

The background part of the Einstein equations gives the Friedmann equations (3.15) and (3.16), while the part that contains the perturbations,

$$\delta G_{\mu\nu} = 8\pi G \delta T_{\mu\nu}\,, \tag{3.92}$$

gives in Fourier space

$$k^2\eta - \frac{1}{2}\mathcal{H}h' = 4\pi G\, a^2\, \delta T^0{}_0\,, \tag{3.93}$$
$$k^2\eta' = 4\pi G\, a^2\, \left(\bar{\rho} + \bar{P}\right)\theta\,, \tag{3.94}$$
$$h'' + 2\mathcal{H}h' - 2k^2\eta = -8\pi G\, a^2\, \delta T^i{}_i\,, \tag{3.95}$$
$$h'' + 6\eta'' + 2\mathcal{H}\left(h' + 6\eta'\right) - 2k^2\eta = -24\pi G\, a^2\, \left(\bar{\rho} + \bar{P}\right)\sigma\,, \tag{3.96}$$

where the functions θ and σ are defined as

$$\left(\bar{\rho} + \bar{P}\right)\theta \equiv ik^j \delta T^0{}_j\,, \tag{3.97}$$
$$\left(\bar{\rho} + \bar{P}\right)\sigma \equiv -\left(\hat{k}_i\hat{k}_j - \frac{1}{3}\delta_{ij}\right)\Sigma^i{}_j\,. \tag{3.98}$$

It is clear that

$$\Sigma^i{}_j \equiv T^i{}_j - \frac{1}{3}\delta^i{}_j T^k{}_k \tag{3.99}$$

is the traceless component of $T^i{}_j$, as we just explained, and

$$\theta = i\, k^j v_j \tag{3.100}$$

is simply the divergence of the perturbation in the fluid velocity. If we assume that the background pressure and energy density are linked by an equation of state $\bar{P} = w\bar{\rho}$, the energy momentum tensor conservation

$$T^{\mu\nu}{}_{;\,\mu} = 0\,, \tag{3.101}$$

implies the following differential equations for the perturbations:

$$\delta' = -(1+w)\left(\theta + \frac{h'}{2}\right) - 3\mathcal{H}\left(\frac{\delta P}{\delta\rho} - w\right)\delta\,, \tag{3.102}$$
$$\theta' = -\mathcal{H}(1-3w)\theta - \frac{w'}{1+w}\theta + \frac{1}{1+w}\frac{\delta P}{\delta\rho}\,k^2\delta - k^2\sigma\,, \tag{3.103}$$

where we have defined

$$\delta \equiv \frac{\delta\rho}{\bar{\rho}}\,. \tag{3.104}$$

Since we only consider non interacting fluids, these equations can be applied for a single fluid or for a mass average mixture of several fluids.

The gauge choice

In conformal time, the perturbation $h_{\mu\nu}$ in Equation (3.81) for an arbitrary background metric can always be expressed in the following general way [15]:

$$h_{00} = -E\,, \tag{3.105}$$

$$h_{i0} = \frac{\partial F}{\partial x^i} + G_i\,, \tag{3.106}$$

$$h_{ij} = A\delta_{ij} + \frac{\partial^2 B}{\partial x^i \partial x^j} + \frac{\partial C_i}{\partial x^j} + \frac{\partial C_j}{\partial x^i} + D_{ij}\,, \tag{3.107}$$

where D_{ij} is symmetrical and

$$\frac{\partial C_i}{\partial x^i} = \frac{\partial G_i}{\partial x^i} = 0\,, \quad \frac{\partial D_{ij}}{\partial x^i} = 0\,, \quad D_{ii} = 0\,. \tag{3.108}$$

Clearly, this last set of equations looks very similar to (3.89), (3.90) and (3.91) and indeed they reduce to them in the case of a FLRW metric in the synchronous gauge.

Similarly, the perturbations of the energy momentum tensor can be decomposed in a set of functions that, used into the Einstein equations, should match the degrees of freedom of the metric perturbation.

$$\delta T_{ij} = \bar{P}h_{ij} + \delta P\delta_{ij} + \frac{\partial^2 \pi^S}{\partial x^i \partial x^j} + \frac{\partial \pi_j^V}{\partial x^i} + \frac{\partial \pi_i^V}{\partial x^j} + \pi_{ij}^T\,, \tag{3.109}$$

$$\delta T_{i0} = ph_{i0} - \left(\bar{\rho} + \bar{P}\right)\left(\frac{\partial \delta u}{\partial x^i} + \delta u_i^V\right)\,, \tag{3.110}$$

$$\delta T_{00} = = -\bar{\rho}h_{00} + \delta\rho\,, \tag{3.111}$$

where π_{ij}^T is symmetrical and, in analogy to the metric perturbation,

$$\frac{\pi_i^V}{\partial x^i} = \frac{\delta u_i^V}{\partial x^i} = 0\,, \quad \frac{\pi_{ij}^T}{\partial x^i} = 0\,, \quad D_{ii} = 0\,. \tag{3.112}$$

With this decomposition of the metric and the energy momentum tensor, it is possible to study separately the scalar, vector and tensor degrees of freedom for the perturbations. For non perfect fluids there are several quantities in the resulting equations that have to be specified in order to get a final complete set of equations. These quantities are $\delta\rho$, δP, π^S, π_i^V and π_{ij}^T. Usually this is done through the 'Boltzmann Equations' which describe changes in the positions and momenta of point particles. We will not need these equations and therefore we are not going to describe them here. They can be found in [129] or [15], for instance.

However, even if one provides expressions or equations for those functions, what happens in general is that the Einstein equations turn out to have solutions that correspond to scalar and vector modes related to coordinate transformations and that hence are unphysical. This problem can be avoided eliminating these (gauge) degrees of freedom by working with gauge invariant quantities [130] or by choosing a gauge. For example, the synchronous gauge is defined taking $E = F = 0$. We are going to focus now on this problem of gauge freedom.

Let

$$\hat{x}^\mu = x^\mu + \psi^\mu \tag{3.113}$$

be a coordinate transformation with the peculiarity that

$$\psi^\mu = \psi^\mu(x) \tag{3.114}$$

is a small displacement in the sense that it can be considered on the same footing as other perturbations such as $h_{\mu\nu}$. It is straightforward to see how the general perturbed metric (3.81) changes under this type of transformation:

$$\hat{g}_{\mu\nu}(\hat{x}) = \frac{\partial x^\rho}{\partial \hat{x}^\mu}\frac{\partial x^\sigma}{\partial \hat{x}^\nu} g_{\rho\sigma}(x) \simeq \bar{g}_{\mu\nu}(x) + h_{\mu\nu} - \bar{g}_{\mu\sigma}\frac{\partial \psi^\sigma}{\partial x^\nu} - \bar{g}_{\rho\nu}\frac{\partial \psi^\rho}{\partial x^\mu}\,, \tag{3.115}$$

being the equation exact at first order in perturbation theory. After the change of coordinates, we can still write:

$$\hat{g}_{\mu\nu}(\hat{x}) = \bar{g}_{\mu\nu}(\hat{x}) + \hat{h}_{\mu\nu}\,. \tag{3.116}$$

Comparing (3.115) and (3.116) we conclude that

$$\hat{h}_{\mu\nu} = h_{\mu\nu} - \frac{\bar{g}_{\mu\nu}}{x^\lambda}\psi^\lambda - \bar{g}_{\mu\sigma}\frac{\partial \psi^\sigma}{\partial x^\nu} - \bar{g}_{\rho\nu}\frac{\partial \psi^\rho}{\partial x^\mu}\,, \tag{3.117}$$

where we have used

$$\bar{g}_{\mu\nu}(x) \simeq \bar{g}_{\mu\nu}(\hat{x}) - \frac{\partial g_{\mu\nu}}{\partial x^\rho}\psi^\rho\,. \tag{3.118}$$

The gauge transformation (3.117) relates the metric perturbations in the two coordinate systems. The spatial part of ψ^μ can be decomposed into a gradient and a divergenceless vector:

$$\psi_j = \partial_j\varphi + \xi_j\,, \tag{3.119}$$

which allows us to write

$$\begin{aligned}
\Delta A &= 2\mathcal{H}\psi_0\,, && (3.120)\\
\Delta B &= -2\varphi\,, && (3.121)\\
\Delta C_j &= -\xi_j\,, && (3.122)\\
\Delta D_{ij} &= 0\,, && (3.123)\\
\Delta E &= 2\psi_0'\,, && (3.124)\\
\Delta F &= 2\mathcal{H}\varphi - \psi_0 - \varphi'\,, && (3.125)\\
\Delta G_j &= 2\mathcal{H}\xi_j - \xi_j{}'\,, && (3.126)
\end{aligned}$$

where we have defined

$$\Delta h_{\mu\nu}(x) = \hat{h}_{\mu\nu}(x) - h_{\mu\nu}(x)\,. \tag{3.127}$$

And for the perturbations of the energy momentum tensor we have

$$\begin{aligned}
\Delta\delta P &= \bar{P}'\psi_0\,, && (3.128)\\
\Delta\delta\rho &= \bar{\rho}'\psi_0 && (3.129)\\
\Delta\delta u &= -\psi_0\,, && (3.130)
\end{aligned}$$

while the other components are gauge invariant

$$\Delta\pi^S = \Delta\pi_i^V = \Delta\pi_{ij}^T = \Delta\delta u_i^V = 0\,. \tag{3.131}$$

It is worth to remark that the Equations (3.128), (3.129), (3.130) and (3.131) apply to each individual component in the case of a universe filled with several species. This is so because these equations do not depend on the conservation laws even though the different components may not be conserved separately.

As we have said before one possibility to eliminate the gauge freedom is fixing the gauge; i.e. writing the perturbation equations in a system of coordinates in which some of the functions that define the perturbations vanish. The tensor part of the perturbations is gauge invariant and so we do not need to consider it for the gauge fixing. There are four functions with vector character, two of them are gauge invariant and the remaining two can be combined to create a third gauge invariant quantity:

$$\tilde{G}_i \equiv G_i - C_i{}'\,. \tag{3.132}$$

It is possible to work using the three vector invariants or fixing the gauge by taking either G_i or C_i to zero. In any case $\tilde{G}_i$ decays in time as $1/a^2$ in an expanding universe and we will not need to worry later about vector modes. Similarly, for the scalar perturbations, to get rid of spurious modes we can either fix a gauge or use gauge invariant variables such as

$$\tilde{\Phi} \equiv E + \frac{1}{a}\left[a\left(F - B'\right)\right]'\,, \tag{3.133}$$

$$\tilde{\Psi} \equiv -A - \mathcal{H}\left(F - B'\right)\,, \tag{3.134}$$

which were introduced by Bardeen [130] and by Kodama and Sasaki [131]. The two most common gauge choices are the conformal Newtonian gauge (also known as longitudinal) and the synchronous gauge, which is is the one used in the work of this thesis. We will now define these two gauges and comment on their properties.

Newtonian Gauge

This gauge is defined by choosing a ψ^μ displacement such that

$$B = 0, \quad F = 0\,. \tag{3.135}$$

The remaining scalar degrees of freedom are customarily denoted by

$$E \equiv \Phi, \quad A = -2\Psi\,. \tag{3.136}$$

If we focus in the scalar perturbations, the metric in this gauge reads

$$ds^2 = a^2(\tau)\left\{-(1+2\Phi)d\tau^2 + (1-2\Psi)dx^i dx_i\right\}\,. \tag{3.137}$$

It is remarkable that in the Newtonian gauge the Ψ and Φ only differ if the anisotropic part of the energy momentum tensor is negligible. In Fourier space:

$$k^2(\Phi - \Psi) = 12\pi G a^2(\bar{\rho} + \bar{P})\sigma\,. \tag{3.138}$$

This means that $\Phi = \Psi$ for a perfect fluid. Notice that (in this gauge) these two variables, which are usually termed scalar potentials, are related to the gauge invariant quantities that we defined above: $\Phi = \tilde{\Phi}$, $\Psi = \tilde{\Psi}/2$.

Synchronous gauge

This gauge, that we have been using, it is defined through the conditions

$$E = 0, \quad F = 0\,. \tag{3.139}$$

The scalar part of the metric can be read from (3.82):

$$\mathrm{d}s^2 = a^2(\tau)\left\{-\mathrm{d}\tau^2 + \left[\left(1+\frac{h}{3}\right)\delta_{ij} + \left(\partial_i\partial_j - \frac{1}{3}\delta_{ij}\nabla^2\right)\mu\right]\mathrm{d}x^i\mathrm{d}x^j\right\}\,. \tag{3.140}$$

This form of the metric can be easily related to the scalar quantities of (3.120)–(3.126). The synchronous gauge is not a real gauge because after imposing (3.140) we are not really fixing all the gauge degrees of freedom. A clear explanation of this is given in [15]. In general, under a coordinate transformation of the form (3.113) with

$$\psi_0 = \psi_0\left(x^j\right)\,, \tag{3.141}$$

$$\varphi = -a^2\,\psi_0\left(x^j\right)\int\frac{\mathrm{d}\tau}{a^2}\,, \tag{3.142}$$

where ψ_0 is an arbitrary function of x^j but not of x^0, the quantities E and F are invariant but A and B change. Besides, the Einstein equations are invariant under this coordinate transformation. Since this happens for any solution

$$S = \{\delta P, \delta\rho, \delta u, \ldots\}\,, \tag{3.143}$$

there will be another solution of the form

$$S + \Delta S = \{\delta P + \Delta\delta P, \delta\rho + \Delta\delta\rho, \delta u + \Delta\delta u, \ldots\}\,. \tag{3.144}$$

Therefore, in the synchronous gauge one should check that any solution of the Einstein equations is a physical one and not a mere (gauge) change of coordinates. In spite of this problem the synchronous gauge is still very useful, specially if the residual gauge symmetry can be eliminated. If one of the components of the universe is a non relativistic fluid such as dark matter, the corresponding homogeneous background pressure $\bar{P}_m$, the pressure perturbation δP_m and the scalar stress anisotropy π_m^S will be zero because the components T_j^i are negligible. The Einstein equations in this case imply that δu_m is time independent. Moreover, the velocity perturbation changes as

$$\Delta\delta u = -\psi_0 \tag{3.145}$$

under any coordinate transformation given by (3.141) and (3.142). Since this holds for each species separately, a time independent velocity perturbation in one component can be removed in the synchronous gauge by making a residual gauge transformation with $\psi_0 = \delta u_m$, and this choice fixes the gauge completely. As it is explained in [15], this makes the synchronous gauge convenient to study any late epoch of the history of the universe, when dark matter is a key ingredient. This is exactly what we will apply in Chapter 5 where we will work in the synchronous gauge, making use (in Fourier space) of the fact that the dark matter velocity perturbation vanishes. Taking into account what we have explained here, we will be sure that the solutions obtained there will be physical.

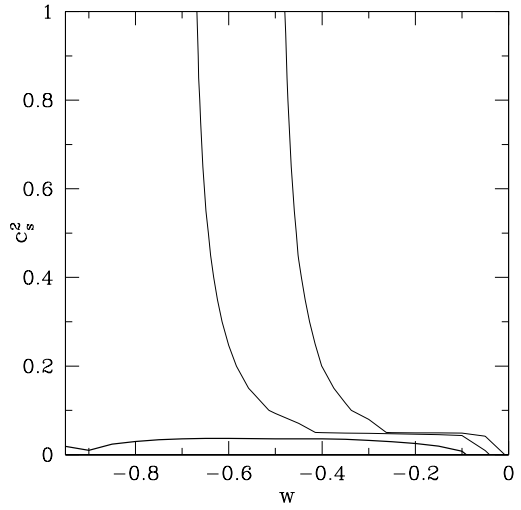

Figure 3.5: Likelihood contour plot for the dark energy component in the $\{w, \hat{c}_s^2\}$ plane showing 1, 2 and 3σ contours. This figure has been taken from [132] and shows the weakness of the constraint in $\hat{c}_s^2$ for reasonable values of w.

3.3.2 The speed of sound

The speed of sound of a fluid can be defined as the ratio [132]

$$c_s^2 \equiv \frac{\delta P}{\delta \rho}\,, \tag{3.146}$$

between the pressure and the energy density perturbations of the fluid. It is important to recall that the speed of sound defined in this way is a gauge dependent quantity. However, the speed of sound is gauge invariant when measured in the rest frame of the fluid. For a perfect homogeneous fluid the speed of sound would be

$$c_a^2 \equiv \frac{\dot{\bar{P}}}{\dot{\bar{\rho}}} = w - \frac{\dot{w}}{3\mathcal{H}(1+w)}\,, \tag{3.147}$$

because it comes from adiabatic (that is the reason for the subscript '$_a$' in the notation) perturbations in the pressure and the energy density. The right hand side of (3.147) comes from differentiating (3.19) with respect to conformal time and applying the conservation (3.18). If the equation of state w is constant, the adiabatic speed of sound turns out to be equal to w itself. In a more general case the fluid may also have entropy perturbations denoted by Γ. If the total speed of sound of the fluid is given by (3.146), the entropy perturbation can be defined as

$$w\Gamma \equiv \left(c_s^2 - c_a^2\right)\frac{\delta\rho}{\rho} = \frac{\dot{P}}{\rho}\left(\frac{\delta P}{\dot{P}} - \frac{\delta\rho}{\dot{\rho}}\right)\,. \tag{3.148}$$

It is convenient to express the gauge invariant (rest frame) density perturbation, that we will denote $\hat{\delta}$, in terms of the density and velocity perturbations in any

other frame [131]

$$\hat{\delta} = \delta + 3\mathcal{H}(1+w)\frac{\theta}{k^2}\,. \tag{3.149}$$

From (3.148) and (3.149), the pressure perturbation of a fluid component with constant equation of state can be written in any reference frame in terms of its rest frame speed of sound $\hat{c}_s$ as follows [132]

$$\delta P = \hat{c}_s^2\,\delta\rho + 3\mathcal{H}\,(1+w)\left(\hat{c}_s^2 - w\right)\rho\frac{\theta}{k^2}\,. \tag{3.150}$$

In our computations we will restrict the squared speed of sound of dark energy to be positive and smaller than unity. The sound speed of dark energy is essentially unconstrained [132–141]. The attempts that have been made to measure its value are based on different kinds of data sets such as cosmic microwave background radiation, large scale structure and supernovae Type Ia data and large neutral hydrogen galaxy surveys. The only bound on this quantity that we have managed to find in the literature is given in [132] and was obtained from the CMB alone. The concrete figure is $\hat{c}_s^2 < 0.04$ at 1σ level. All the other references mentioned above conclude that it is not possible to bound the speed of sound with present data; and detection forecasts made in [142] state that it will be difficult to do it by cross–correlating future data sets. The "tentative" bound of [132] is only valid when a very broad range of values is allowed for the equation of state of dark energy: $w \in (-1, 0)$, and the result disappears due to cosmic variance if this range is reduced by neglecting the values of w bigger than -0.3. It is fair to say that there are basically no observational constraints in the dark energy speed of sound, since the values of w that lead to that weak bound are ruled out. Figure 3.5 has been taken from [132] and is illustrative of how weak the bound on $\hat{c}_s^2$ is. This figure and the corresponding numerical bound were obtained using the first year WMAP likelihood code and a partial marginalization over the remaining cosmological parameters. Values of $\hat{c}_s^2$ close to unity enhance the power of the CMB spectrum at large scales but the effects gets ameliorated when w is decreased, due to the integrated Sachs–Wolfe (ISW) effect, in such a way that it is not easy to constrain $\hat{c}_s^2$ from the low multipoles of the CMB if w is near -1.

There is an interesting result in [141] concerning the prospects for measuring the speed of sound of dark energy. A detection of models with sound speeds close to zero, $\hat{c}_s^2 \lesssim 0.01$, using the clustering of hydrogen galaxies and the ISW, will be possible for dark energy models with $w \gtrsim -0.9$. It turns out that a low value of w enhances the ISW effect at recent times but this can be compensated by reducing the sound speed of dark energy. As we will later see, the fact that small speeds of sound and values of the equation of state greater than -1 favour the detection of dark energy perturbations is consistent with our results. This is because the relevance of the dark energy fluctuations is more important in that case than in other regions of the parameter space.

3.4 Inflation and the spectrum of primordial perturbations

In this last section of our review of cosmology we will introduce the idea of inflation starting from the problems that motivated it around thirty years ago. We will explain how an early stage of accelerated expansion can solve these problems and then we will focus on inflation driven by a scalar field. After reviewing a classical way of grouping inflationary models we will present the basic dynamical equations. Then, we will provide the formulas that connect single field slow–roll inflation with the spectrum of primordial perturbations and sketch how to derive them. The section concludes commenting on how to relate the primordial spectrum with the actual cosmological observations and with some remarks concerning the use of effective field theories.

3.4.1 The need for inflation

Cosmological inflation was first proposed by Alan Guth in the beginning of the eighties [1] in relation to the monopole problem in the early universe. He realized that inflation would also serve as a solution to the flatness and horizon problems. For a historical account of the development of the idea and an introductory explanation to the concepts of the theory see [143]. At that time, the standard hot big bang was an extremely successful idea that could account for several observational facts like the expansion of the universe, the cosmic microwave background radiation, the abundances of light elements and the estimated age of the universe. However, it lacked an explanation for the rather peculiar initial conditions that lead to what we observe today. Basically, the hot big bang assumes a homogeneous and isotropic universe whose dynamics is governed by the relativistic perfect fluid that it contains. This is in accordance with the cosmological principle, which states that the universe must look the same to all observers within it. With this setup it is possible to explain the evolution of the universe since the formation of nucleons up to now. In what follows we will introduce the main problems with this picture.

The flatness problem

We have earlier commented that current observations favour a universe whose density is nearly critical and has $\Omega_{\kappa 0} \simeq 0$. From (3.23) we see that the time dependence of Ω_κ is given by the square of the inverse of the derivative of the scale factor:

$$\Omega_\kappa = -\frac{\kappa}{\dot{a}^2}\,. \tag{3.151}$$

According to the thermal history of the standard big bang cosmology, a period of matter domination was preceded by another one in which radiation was the leading component. For the argument that we are going to present now, the current accelerated expansion is irrelevant. During the matter period the scale factor grows as $t^{2/3}$ which means that Ω_k also increases as $t^{2/3}$. The temperature T of the universe today is about $3K$ and during that period the temperature is proportional to $t^{-2/3}$.

Since, at the time of matter–radiation equality the temperature was about $10^4 K$ we conclude that, at that time the value of Ω_κ must have been roughly 10^{-4} at most. In the earlier radiation period the time dependence of the scale factor was $t^{1/2}$ and the temperature changed with time as $t^{-1/2}$, so Ω_k evolved as T^{-2}. Going back until the time when the neutron–proton conversion started to take place, at a temperature around $10^{10} K$, we see that Ω_κ had to be as as small as 10^{-16}. If we go even further, down to the electroweak scale, the value of the curvature energy density must had been roughly 10^{-27}. Only a narrow range of values for κ at any time in the far past can produce a universe like ours today. Small deviations from the conditions in the early universe could have lead to very different dynamics such as recollapsing universes or very fast expanding ones. The question is: Why the energy density of the universe is so close to the critical one? We see that in the context of big bang cosmology, this issue can be traced back to a big fine tuning of the curvature at early times. The problem, as in the case of the cosmological constant, is not associated to the smallness itself but to the related physics. In the case of the cosmological constant, we do not have a satisfactory explanation for its tiny value and our crude estimations are very far from it. Here, with the early value of the curvature, it may seem reasonable to accept a big fine tuning because we have a good description for the subsequent evolution. However, as we do the *Gedanken* experiment of going back in time, we realize that we do not know any mechanism that would set κ to a certain value at a particular time in the history of the universe and this makes the fine tuning more troublesome. Still, it can be argued that the flatness problem is perhaps the lesser of those that can be used to motivate inflation.

The horizon problem

The spherical polar form of the FLRW metric tells us that an object, with radial coordinate r_1 that we observe to subtend a small angle θ in the sky and whose radiation reaching us today was emitted at a time t_1, occupies a proper distance approximately equal to $s = a(t_1)\, r_1\, \theta$ that is orthogonal to the line of sight. We define the 'angular diameter distance' by the euclidean relation that associates the angle θ to the arc length s:

$$s = \theta\, d_A\,. \tag{3.152}$$

Therefore

$$d_A = a(t_1)\, r_1\,. \tag{3.153}$$

Comparing this with Equation (3.43) and using (3.31) we see that

$$d_L = (1+z)^2 d_A\,. \tag{3.154}$$

The particle horizon at the time of last scattering, when the cosmic microwave background was released, is given by an expression analogous to (3.46):

$$d_{LS} = \frac{1}{H_0}\int_0^{a_{LS}} \frac{\mathrm{d}a}{\sqrt{\Omega_{r0} + \Omega_{m0}\, a + \Omega_{x0}\, a^{1-3w_x} + \Omega_{\kappa 0}\, a^2}}\,. \tag{3.155}$$

In a matter or radiation universe this distance is of order t as it can be immediately seen expressing it as a function of time and recalling that in matter a goes as $t^{2/3}$

while in radiation it goes as $t^{1/2}$. Assuming matter domination, this means that the size of the horizon at the time of last scattering was

$$d_{LS} \simeq H_0^{-1} \left(1 + z_{LS}\right)^{-3/2} , \tag{3.156}$$

where $z_{LS} \simeq 1100$ is the redshift that corresponds to the last scattering surface. The angular diameter distance to this surface can be computed from (3.52) and (3.154) and it turns to be approximately $H_0^{-1} \left(1 + z_{LS}\right)^{-1}$. Therefore, using (3.152), the angle subtended today by a length of the size of the particle horizon at the time of last scattering is approximately $\theta_{LS} \simeq \left(1 + z_{LS}\right)^{-1/2}$. This is roughly equal to just $2^{\rm o}$. However, the temperature of the cosmic microwave background is isotropic to the level of 10^{-5} all over the sky. How is this possible if only regions that today appear to be smaller than $2^{\rm o}$ were in causal contact when that radiation was produced? Clearly some explanation is needed to justify this apparently extraordinary agreement between different parts of the universe. The horizon problem is the most important of the three that we are reviewing here and perhaps the only one that cannot be circumvented in a simple way without relying on inflation or some other alternative mechanism. We will later see that if inflation solves the horizon problem it will automatically solve the other two.

The monopole problem

In grand unified theories, the Standard Model of particle physics is the result of a spontaneous symmetry breaking at scale around $10^{16}\,{\rm GeV}$. A group $\tilde{\mathcal{G}}$ that contains the Standard Model group $SU(3) \times SU(2) \times U(1)$ can in general allow the generation of charged monopoles that we have not observed in nature. This may also happen for topological defects of other dimensionalities: cosmic strings and domain walls, for instance. If we assume that the Standard Model does indeed come from a theory with a greater symmetry, we should wonder if any defects are created in the phase transition that corresponds to the symmetry breaking. Then, if they can survive during the subsequent evolution of the universe, we have to explain why we have not found them.

In general, topological defects are solutions of the classical equations of motion for the scalar fields of a theory. These solutions have the property that they interpolate between different vacua of the theory. For instance, a scalar field with two possible vacua may give rise to a domain wall. Monopoles can appear if there is a symmetry breaking with three scalar fields, in which case the vacuum manifold is topologically equivalent to a two–dimensional sphere. Mathematically, if the group $\tilde{\mathcal{G}}$ is semisimple, its breaking to the Standard Model group will generate magnetic monopoles because the second homotopy group, π_2, of the vacuum manifold is non–trivial. These monopoles are called magnetic because they are charged under the electromagnetic $U(1)$ group of the Standard Model. The topological defects are local or global depending on the symmetry that is broken. In usual grand unified theories, the symmetry is gauge and the defects will be local. The masses of the monopoles depend on their gauge character.

At least one topological defect is created per horizon volume in the symmetry breaking. When the temperature of the universe is $T_{GUT} \simeq 10^{16}\,{\rm GeV}$, the horizon

scale is approximately $t_H \simeq T_{GUT}^{-2}$ and the average number of monopoles per photon would be

$$\frac{n_\odot}{n_\gamma} \simeq T_{GUT}^{-3} t_H^{-3} = T_{GUT}^3 \,. \tag{3.157}$$

This quotient remains of the same order during the subsequent expansion of the universe. To obtain the present energy density of monopoles we just have to compute $\rho_{\odot 0} \simeq m_\odot n_\odot(t_0) \simeq m_\odot T_{GUT}^{-3} T_0^3$, where T_0 is the temperature of the universe today and $m_\odot$ denotes the monopole mass. Dividing by the critical density of the universe we get:

$$\Omega_{\odot 0} = \frac{\rho_{\odot 0}}{\rho_{c0}} \simeq 10^{47} m_\odot[\mathrm{GeV}]\, T_{GUT}^4[\mathrm{GeV}] \tag{3.158}$$

where $m_\odot[\mathrm{GeV}]$ and $T_{GUT}[\mathrm{GeV}]$ are the monopole mass and the grand unified theory temperature at which the breaking occurs, both in GeV . For a mass of 10^{16}GeV and a temperature of 10^{14}GeV we would have a relic abundance of 10^{11} , which is clearly a huge number for a relative energy density and far much bigger than the current experimental bounds.

Under a certain condition: that the reheating temperature does not exceed the grand unified scale, inflation can cure this problem. In any case, it is obvious that there is no concern to deal with if there is no grand unified theory and, in this sense, monopoles are the weakest support for inflation among the three problems that we have reviewed. However, it is interesting that the monopole problem was actually the original motivation of Guth for developing the idea of inflation.

We will later explain that the most common way of implementing inflation is through a slowly rolling scalar field, in a similar fashion as quintessence models of dark energy. In many high energy extensions of the SM there are several extra scalar fields and an enhanced symmetry of the SM group. If scalar fields are really a necessary ingredient for inflation, it is reassuring that no unwanted relics such as monopoles will be present if these fields are associated to a bigger group. Therefore, although the monopole problem is not there without grand unified theories (or other similar high energy variants) it a good feature of inflation that the problem is naturally solved in the cases where it might potentially appear.

A comment about the motivation for inflation

Leaving aside the grand unified theories and the monopole problem, it is noteworthy how the arguments we use to motivate inflation come in one way or another from the cosmic microwave background. The horizon problem, which should be regarded as the greatest concern of the three problems that we have presented is intimately connected with the isotropy of the CMB. The flatness problem is also related to the CMB, although in a not so obvious way. If we come back the cosmic triangle introduced in Section 3.2.1 (see Figure 3.1) we can observe that the CMB data seems to determine an area in the parameter space that is characterized by $\Omega_{\kappa 0} = 0$. This can also be seen in Figure 3.6 from [3] which is to the ΛCDM model the analogous of Figure 3.4(b) to the DGP case. It is clear that if it were not for the CMB, the class of allowed models would include not only the flat case but also a substantial amount of open and closed ones. Moreover, as we will see later, inflation provides a

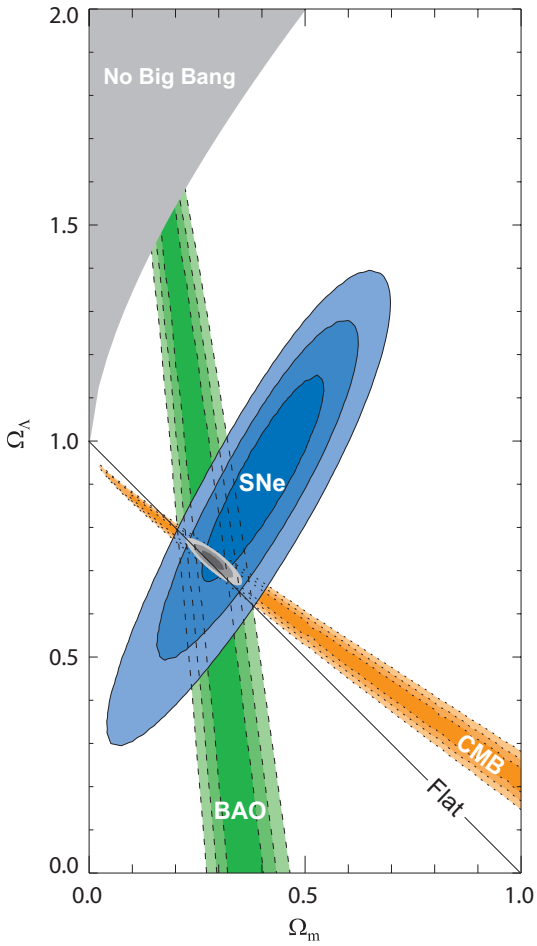

Figure 3.6: 68.3 %, 95.4 % and 99.7% confidence level contours on $\Omega_{\Lambda 0}$ and Ω_{m0} obtained from CMB, BAO and the Union Supernova set, as well as their combination. See [3].

quantum mechanical mechanism for the generation of the cosmological fluctuations observed in the CMB (and also in the LSS distribution of matter). The properties of these fluctuations (scale invariance, gaussianity and adiabaticity) are predicted by inflation and this made it a very popular framework. The modern point of view is that the generation of these fluctuations together with the horizon problem are two main motivations for inflation. Any other theory of the early pre–big bang universe should be able to address these two points satisfactorily.

Solving the problems

In this section we are going to explain how inflation can solve the three problems that we have presented as a motivation. The only assumption we need to make at this point is a period of early accelerated expansion that precedes the radiation and matter dominated phases of the universe. In fact, we can take this assumption as our definition for inflation, regardless of the mechanism that sustains the acceleration. If we also wanted to explain the generation of primordial fluctuations in the CMB

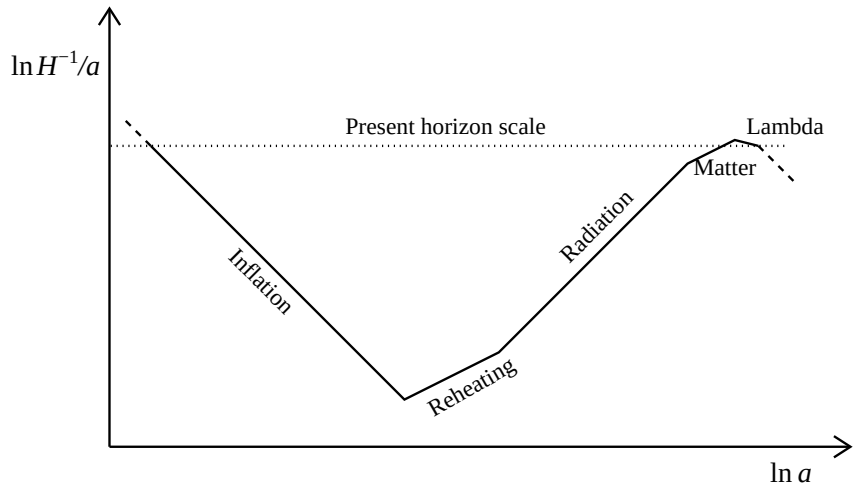

Figure 3.7: Schematic representation of the evolution of the Hubble parameter as a function of the scale factor of the universe. Figure from [144], Liddle et al.

and LSS we would have to work in a more detailed framework and we will leave that for a later section.

To quantify the amount of expansion that is produced during inflation (or any other process where the scale factor of the universe changes) it is customary to use the 'number of efolds', defined as the following integral:

$$N_e\left(t_i\,,t_f\right) \equiv \int_{t_i}^{t_f} H\mathrm{d}t \;= \int_{\tau_i}^{\tau_f} \frac{\mathcal{H}}{a}\mathrm{d}\tau\,, \tag{3.159}$$

where t_i denotes the time at which inflation starts and t_f marks its end. The solution to the problems comes from the fact that H is nearly constant during inflation, which is a qualitatively different behaviour from that of radiation or matter domination. The Equations (3.23) and (3.33) tell us that during inflation Ω_κ decreases roughly like a^{-2}. This means that if the period of inflation is sufficiently long, the value of Ω_κ can be reduced to any small value that may be required to explain the present $\Omega_{\kappa 0} \simeq 0$, in accord with the evolution in the matter and radiation phases. The value of Ω_κ at the end of inflation is

$$\Omega_{\kappa f} = -\frac{\kappa}{a_f^2 H_f^2}\,. \tag{3.160}$$

Then, the value today can be expressed as

$$\Omega_{\kappa 0} = \Omega_{\kappa f}\frac{a_f^2 H_f^2}{a_0^2 H_0^2}\,. \tag{3.161}$$

In Figure 3.7 there is an schematic representation of the evolution of the natural logarithm of $1/\dot{a}$ as a function of a during the different epochs of the universe [144]. We will assume that the period indicated as *reheating* is irrelevant and therefore the values of the scale factor and the Hubble parameter do not change between the end

of inflation and the beginning of the radiation period. Therefore:

$$\Omega_{\kappa 0} = \Omega_{\kappa r} \frac{a_r^2 H_r^2}{a_0^2 H_0^2}\,, \tag{3.162}$$

where the subindex '$_r$' corresponds to the beginning of the radiation period. From (3.56) we see that the value of the scale factor for which $\Omega_m = \Omega_r$ is precisely

$$a_{eq} = \frac{\Omega_{r0}}{\Omega_{m0}}\,. \tag{3.163}$$

Using Equation (3.50) we can express the Hubble factor during the epoch that encompasses matter and radiation as

$$\frac{H^2}{H_0^2} \simeq \Omega_{r0}\, a^{-4} + \Omega_{m0}\, a^{-3}\,, \tag{3.164}$$

where we have neglected the terms related to curvature and dark energy. Evaluating (3.162) at a_{eq} we obtain

$$H_{eq}^2 \simeq 2 H_0^2 \Omega_{0m} \left(\frac{\Omega_{0m}}{\Omega_{r0}}\right)^3\,. \tag{3.165}$$

Doing the same at a_f and taking into account that the cubic term is negligible in comparison to the quartic one we get

$$H_r^2 \simeq \frac{H_{eq}^2}{2} \left(\frac{a_{eq}}{a_r}\right)^4\,. \tag{3.166}$$

Recalling our convention, $a_0 = 1$, and making use of (3.166) and (3.165) to eliminate a_r; and then H_{eq} in (3.162) we arrive to

$$\Omega_{\kappa 0} \approx \Omega_{\kappa r} \frac{H_r}{H_0} \sqrt{\Omega_{r0}}\,. \tag{3.167}$$

Since $\Omega_{\kappa r}$ is the value of (3.23) at the end of inflation, we can write

$$\Omega_{\kappa r} = -\frac{\kappa}{a_r^2 H^2} \simeq \Omega_{\kappa i}\, e^{-2N_e}\,, \tag{3.168}$$

where we have used that the Hubble parameter is almost constant during inflation and $a_r = a_f = a_i e^{N_e}$ to write the result in terms of Ω_κ at the beginning of inflation. Therefore, we finally get

$$\Omega_{\kappa 0} \approx \Omega_{\kappa i}\, e^{-2N_e} \frac{H_r}{H_0} \sqrt{\Omega_{r0}}\,. \tag{3.169}$$

The first Friedmann equation, (3.15), can be written as

$$\frac{H^2}{H_0^2} = \frac{\rho}{\rho_{c0}} \left(1 + \Omega_k\right)^{-1}\,, \tag{3.170}$$

which particularized for the beginning of the radiation period is just

$$\frac{H_r^2}{H_0^2} \simeq \frac{\rho_r}{\rho_{c\,0}}\,. \tag{3.171}$$

Then, taking (3.64) into account, the Equation (3.169) becomes

$$\Omega_{\kappa 0} \approx \Omega_{\kappa i}\, e^{-2N_e} \sqrt{\frac{\rho_r}{\rho_{c0}}\Omega_{r0}}\,, \tag{3.172}$$

where the critical density today is $\rho_{c\,0}^{1/4} = 3 \times 10^3 h^{1/2}\,\mathrm{eV}$ and

$$\Omega_{r0} = \Omega_\gamma(1 + 0.2271 N_{\mathrm{eff}})\,, \tag{3.173}$$

with $\Omega_\gamma = 2.469 \times 10^{-5} h^{-2}$ for $T = 2.725K$ [32]; and $N_{\mathrm{eff}} = 3.04$. If we assume that $\Omega_{\kappa i} \simeq 1$ (it cannot be bigger) and take the energy scale at the end of inflation that defines ρ_r to be about $2 \times 10^{16}\mathrm{GeV}$, since $\Omega_{\kappa 0} \simeq 10^{-2}$ [32], we find that N_e has to be bigger than approximately 62 in order to solve the flatness problem. If we choose the nucleon mass (1MeV) or the Planck Mass as the scales for the end of inflation (these are broad lower an upper limits) we would get that inflation must last roughly for at least 17 or 68 efolds respectively. The result that we have obtained can be summarized with the following formula which works approximately well:

$$N_e \simeq 26.5 + \frac{1}{2}\ln\frac{\Omega_{\kappa i}}{\Omega_{\kappa 0}} + \ln M_f[\mathrm{GeV}]\,, \tag{3.174}$$

where M_f is the energy scale that corresponds at the end of inflation and should be expressed in GeV in the equation.

The horizon problem in the standard big bang cosmology has to do with the fact that the size of the universe is too large for its different regions to have been in causal contact in the past and so allowing thermal equilibrium at the time of decoupling. Inflation tells us that the observable part of the universe might have had a very small size in the far past, in such a way that causal contact was possible in reality. If we assume that the Hubble parameter is constant during inflation (this can usually be done during at least one Hubble time [145]), the scale factor in that period grows exponentially

$$a = a_i e^{H_I(t-t_i)}\,, \tag{3.175}$$

where the initial time of inflation is t_i and the total number of efolds is

$$N_e = H_I(t_f - t_i)\,, \tag{3.176}$$

where t_f marks the end of inflation and we denote by H_I the value of the Hubble factor during inflation. We saw in Section 3.1.3 that the proper horizon size at the time of last scattering can be expressed as

$$d_{LS} = a_{LS}\int_{t_i}^{t_{LS}} \frac{\mathrm{d}t}{a(t)} \simeq a_{LS}\int_{t_i}^{t_f} \frac{\mathrm{d}t}{a(t)} \simeq \frac{a_{LS}}{a_f H_I}\left(e^{N_e} - 1\right) \simeq \frac{a_{LS}}{a_r H_I} e^{N_e}\,, \tag{3.177}$$

where we have assumed that the integral is dominated by the inflationary period and the effect of reheating is negligible so $a_f = a_r$. To solve the horizon problem

this distance must be larger than the angular diameter distance of the surface of last scattering which, as we said when we introduced the horizon problem, is

$$d_A(t_{LS}) \simeq \frac{1}{(1+z_{LS})H_0} = \frac{a_{LS}}{H_0}\,. \tag{3.178}$$

Hence

$$e^{N_e} > \frac{a_r H_I}{H_0}\,, \tag{3.179}$$

which leads us to the same number of efolds of inflation as the solution of the flatness problem, using the same approximations.

Finally, the monopole problem is solved in inflation if the production of monopoles takes place before photons are created in a period of reheating. We assume a grand unification theory and inflation ending at a temperature below T_{GUT} , so monopoles are produced due to a symmetry breaking of the grand unification group during the course of the accelerated expansion. The current searches for monopoles indicate that there are less than 10^{-30} per photon [146], which means that even if they were as heavy as the Planck Mass their contribution to the energy density of the universe would be negligible. Assuming that the initial amounts of photons and monopoles where comparable when these where formed, in order to produce a present ratio as low as the previous bound, inflation must have increased the horizon size of the universe by a factor 10^{10} before photons are produced at reheating. This corresponds to approximately 23 efolds, and therefore if inflation solves the flatness and horizon problems it will also do the same concerning monopoles.

3.4.2 Classifying inflationary models

As we will see in the next section, a simple and widely employed way of describing accelerated expansion in the very early universe is through a scalar field coupled to general relativity in a FLRW background. Within this framework, a model of inflation is essentially characterized by the potential of the field, which determines its classical dynamics. There are however many other possibilities that have been explored, some of which do not require scalar fields. Therefore, in a broader sense, we can think of a model of inflation as any mechanism which solves the horizon and flatness problems by producing an early phase of accelerated expansion. Since there is a huge variety of different models, there are several classifications that have been put forward according to criteria like the predictions of the models and the shape of their potentials or the number of fields involved. An extensive review of inflation models inspired by particle physics can be found in [145].

In the case of single field inflation models (see Section 3.4.3) there is a simple classification [147] that turns out to be useful for certain purposes such us the interpretation of fits to the primordial power spectrum from the standard parameterization described in Section 3.4.4. In [148] this was used for the third year release of WMAP data and the same kind of analysis was recently updated for the latest release [5]. According to this classification the models are divided into three general types: 'large–field', 'small–field', and 'hybrid', with a fourth set, 'linear models', which are those in the boundary between the first two classes. This grouping is

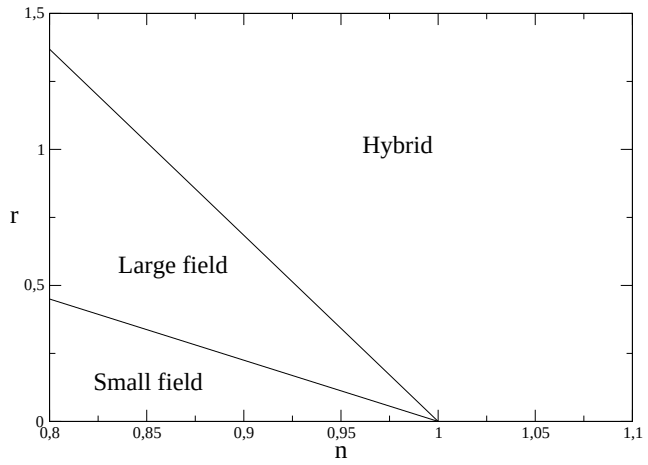

Figure 3.8: Regions in the $\{n, r\}$ plane for the three types of single field models according to [147].

valid when first order slow–roll inflation is sufficient to describe the dynamics and hence the first two slow–roll parameters ϵ and η (introduced in Section 3.4.3) can be used to define the classes.

Large–field models are characterized by 'chaotic' initial conditions [149], in which the inflaton field is displaced far from its minimum, usually to values near the Planck Mass or even above, and rolls toward a minimum at the origin. These large values of the inflaton have raised some concerns in the literature although it is sometimes argued that they pose no real problem since the value of the potential can be well below M_p^4 provided that the self–coupling of the inflation is small enough. This is for instance the case of the widely advertised $\lambda\phi^4$ model, in which the smallness of the coupling comes as a requirement imposed by the measurement of the amplitude of primordial perturbations 3.219, the so called COBE bound. This example, together with the ϕ^2 case are typically called chaotic inflation and there is recently some interest in finding out whether these potentials can be obtained from high energy theories like supergravity [150,151]. See also [152–154] for earlier works on the same question. Generically, any potential of the form $V = \lambda_p M_p^{4-p}\phi^p$ is referred to as chaotic inflation. For these models inflation ends for $\phi \sim pM_p$ due to the breaking of the slow–roll approximation (see Section 3.4.3) and then oscillates about the minimum of the potential at $\phi = 0$.

Another example of large–field models is given by an exponential potential $V = \exp(\alpha\phi/M_p)$ with constant α, which produces an exact power–law spectrum and constant slow–roll parameters [155, 156] as defined in Section 3.4.3. The exponential potentials arise as the effective low energy description of degrees of freedom related to extra spatial dimensions in Kaluza Klein models. They also appear associated to dilatons and moduli fields in superstring theories. Since the slow–roll parameters are constant in this case, as it can be checked for instance by integrating the equations of motion analytically, inflation cannot end due to the breaking of slow–roll conditions. Therefore, another mechanism is required; otherwise the

model would not be fully satisfactory. Having noticed this point gives us the chance of going back to discuss of how ambitious should be the description of what we call a model of inflation. For the purpose of this section and the largest part of this work we are mostly concerned with the dynamics of the inflationary phase itself and therefore we do not worry about other subsequent processes such as reheating. In fact, as we will later see, the classes of inflationary models introduced in Sections 4.2 and 4.6 (that constitute the theoretical part of one of the two cores of this thesis), without being part of the class of large field models as defined here, do not include a description of reheating since their potentials are not bounded from below.

Making a simple sign redefinition, the inflaton can be made to roll from smaller to larger values in many large field models (those that are even) and in this sense the naming may not be the most fortunate one. In fact, one typically assumes that the field is positive, keeping in mind the possibilities cut by this choice (to which we will stick).

Most small field models have a form that typically comes from spontaneous symmetry breaking. The field is initially near the origin or right at it from the classical point of view and rolls towards a minimum of the potential at $\phi \neq 0$. So, inflation occurs when the field value is smaller than its classical vacuum expectation value. Clearly, the behaviour of the field is different from that of large field models. The typical example is a potential of the form $\Lambda^4 \left(1 - (\phi/\mu)^p\right)$ with $\phi \ll \mu \ll M_p$ and $p \geq 2$. These kind of potentials can be seen as the Taylor approximation near the origin of a function whose first non zero derivative at that point is of order p [157]. A particle physics motivation for the $p = 2$ case [158, 159] is a pseudo–Nambu–Goldstone boson such as the axion [160].

The linear models are defined as those that satisfy that the first derivative of the potential is constant. This makes the corresponding potential slow–roll parameters to be constant and therefore inflation does not end because of the breaking of slow–roll, as it also happens in the case of an exponential potential. Large field and small field cases cover adjacent regions in the space of observable parameters (see Figure 3.8), and the signs of the curvature of their potentials are different. For the large field models, the second derivative of the potential is $V'' > 0$, and for the small field models, $V'' < 0$. Clearly, the linear models are at the boundary between those two classes.

Normally, for large and small field models the vacuum energy of the inflaton at the end of the process is zero. On the contrary, in hybrid inflation models the inflaton keeps a significant energy, i.e. $V(\phi_{end}) \neq 0$. The end of inflation in these models takes place by means of the action of a second scalar field. In spite of the fact that there are two relevant fields, this class of models actually belongs to the single field class because inflation is driven just by one of the fields. Hybrid inflation was first introduced in [161] and many variations of it have risen afterwards; see [162–165] for instance. For a complete review of a large part of the literature on hybrid inflation (up to 1999) one can check [145]. The inflationary phase of these models can be typically described by a potential $V = \Lambda^4(1 + (\phi/\mu)^p)$, with $p \geq 2$. Since the minimum of the potential gives $V \neq 0$, once the field reaches this point inflation would go on as in the case of a cosmological constant. However, if there is

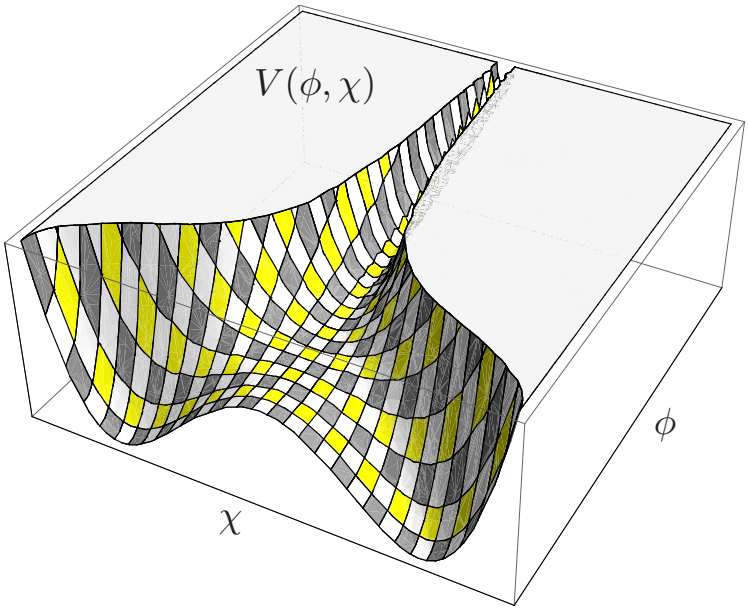

Figure 3.9: The hybrid inflation potential (3.180). The inflaton field ϕ rolls along the valley until it approaches the point $\phi = 0$, and then the waterfall field χ starts moving as well. Classically, the final state of the system corresponds to any of the two equivalent absolute minima that are depicted, with $\phi = 0$ and $\chi = \pm M$

a second field, inflation can finish if the previous minimum is actually just a relative or metastable point. This is illustrated in Figure 3.9 .

The simplest example of hybrid inflation [166] has two fields, ϕ and χ , interacting through the potential

$$V(\phi,\chi) = \frac{\lambda_1}{4}(\chi^2 - M^2)^2 + \frac{1}{2}m^2\phi^2 + \frac{1}{2}\lambda_2\phi^2\chi^2 \ . \tag{3.180}$$

If ϕ^2 is large enough, the minimum of the potential along the χ–direction is at $\chi = 0$, as Figure 3.9 shows. Classically, ϕ changes with time until it acquires the value $\phi_0 = \lambda_1 M^2/\lambda_2$ and then rolls down into one of the two possible true minima at $\phi = 0$ and $\chi = \pm M$. The role of the inflaton in this dynamical model is played by ϕ , which has an effective potential

$$V_{\rm eff}(\phi) = \frac{\lambda_1}{4}M^4 + \frac{1}{2}m^2\phi^2 \ , \tag{3.181}$$

during the period of accelerated expansion, and therefore the model can be viewed as one example of single field inflation. It is customary to call the field χ a 'waterfall' since it is due to its presence that inflation can terminate by allowing ϕ to end its evolution in the true minimum with $V = 0$. Hybrid models are therefore characterized by a small value of the field and $V'' > 0$ during the inflationary phase. This makes them a mixture of the large and small field cases, and hence they recieve that appellative.

This classification of single field models has been widely used since the different groups make distinct predictions for the scalar spectral index and the tensor–scalar ratio, as shown in Figure 3.8, which can help to discriminate among them. However, it is important to notice that this figure is generically valid only if certain potentials that involve different functional forms of the inflaton are discarded. If these potentials where to be taken into account the different classes in Figure 3.8 would mix. We will later see that this is actually what happens for the potential that contains a non–renormalizable operator studied in Chapter 4. In this concrete example there is a strong scale dependence of the scalar spectral index which makes $n-1$ change sign during inflation (while the tensor contribution to the spectrum remains small) in such a way that the model travels from the hybrid to the large field class, crossing the border between the two sets. The primordial power spectra (with constant spectral indexes) is behind this figure; which means that its appearance will vary if other parameterizations are considered. In fact the Figure 3.8 should be in general understood making reference to a particular wavenumber k_0 , the fiducial scale at which the power law approximation of the spectrum with constant spectral index is applied. See Section 3.4.4 for the definition of this parameterization and its connection to single field inflation models.

Other ways of producing inflation

Finally let us just mention some examples of the many other inflationary models that have been invented. First, there are those that cannot be considered single field models because there is more than one degree of freedom involved in the process of accelerated expansion. See [167–173] for an incomplete list of references on this broad topic. Another kind of models contains those coming from theories of modified gravity, in the same fashion as for dark energy; for example, we can have higher order derivative dynamics, Jordan–Brans–Dicke and other scalar–tensor gravity theories among others. But also, open inflation [174, 175], k–inflation [81], fast roll inflation [176,177], spinflation [178], vector inflation [179,180], inflation from extra dimensions [181–183] and branes [184–186]. Interestingly, branes can be used to build scenarios which solve the flatness and horizon problems without requiring a phase of inflation [187]. In fact there are several proposals to address those problems which do not relay on accelerated expansion; many of them can be categorized within the so called bouncing models [188].

3.4.3 Slow–roll inflation

The most popular way to implement inflation is using a scalar field ϕ with a self–coupling given by a potential $V(\phi)$. The field initiates its evolution at some value ϕ_i and the classical equations of motion make it evolve, rolling down its potential, until it stabilizes in a minimum. If there is a period during which the field changes very slowly, the value of the potential will remain approximately constant for that lapse of time, acting effectively as a cosmological constant and therefore producing an accelerated expansion of the universe. Inflation would end if the field gains too much speed or when it stops at a position where the potential becomes zero.

Hence, a condition to obtain successful inflation in this framework is a relatively flat potential that would maintain a moderate speed of the field to solve the horizon and flatness problems by producing enough efolds of expansion. This way of modeling inflation owes its popularity not only to its simplicity but also to the great number of variants that it permits, just by modifying the potential $V(\phi)$. Although no fundamental scalar field has been observed in nature so far, they are very useful for making contact with high energy theories and many works have been done to constrain these using the observable consequences of inflation, mainly in the cosmic microwave background.

Let us focus on a generic cosmological inflationary process driven by a single real scalar field. The dynamics of this system can be encoded in the action (3.67) which reads

$$\mathcal{S} = \frac{1}{16\pi G}\int \mathrm{d}^4x\,\sqrt{-g}\,R + \int \mathrm{d}^4x\,\sqrt{-g}\,\mathcal{L}_m\,, \tag{3.182}$$

where the matter lagrangian minimally couples the 'inflaton' ϕ to the metric

$$\mathcal{L}_m = -\frac{1}{2}\partial_\mu\phi\partial^\mu\phi - V(\phi)\ . \tag{3.183}$$

We will assume that the field ϕ is a function of time but does not depend on the spatial coordinates. In this case, the corresponding energy momentum tensor is that of a perfect fluid (3.13) with energy density and pressure:

$$\rho = \frac{1}{2}\dot{\phi}^2 + V(\phi)\,, \tag{3.184}$$

$$P = \frac{1}{2}\dot{\phi}^2 - V(\phi)\,. \tag{3.185}$$

Therefore, the equation of state is time dependent:

$$w = \frac{\frac{1}{2}\dot{\phi}^2 - V(\phi)}{\frac{1}{2}\dot{\phi}^2 + V(\phi)}\,, \tag{3.186}$$

but, if as we said, the speed of the field is very slow, the kinetic term is much smaller than the potential and then $w \simeq -1$, resembling a cosmological constant. The field equations can be obtained imposing the requirement that the action must be stationary under variations in ϕ. The result in a flat FLRW background is:

$$H^2 = \frac{1}{3M_p^2}\left(\frac{1}{2}\dot{\phi}^2 + V(\phi)\right)\,, \tag{3.187}$$

$$\ddot{\phi} + 3H\dot{\phi} = -V'\,, \tag{3.188}$$

$$2\dot{H} = -\frac{1}{M_p^2}\dot{\phi}^2\,, \tag{3.189}$$

where we denote

$$V' = \frac{\mathrm{d}V}{\mathrm{d}\phi}\,, \tag{3.190}$$

that should not be confused with the derivative with respect to conformal time. Clearly, the Equation (3.187) is nothing but (3.15), while (3.16) can be obtained

expressing $\dot{\phi}$ in (3.189) in terms of ρ and P and using (3.187) together with (3.33). Only two of the equations of motion are independent. It can be easily checked that (3.189) is obtained differentiating (3.187) with respect to t and then using (3.188) to eliminate $\ddot{\phi}$. By definition, an inflationary expansion satisfies

$$\ddot{a} > 0 \, . \tag{3.191}$$

From (3.189) and (3.187) the second derivative of the scale factor can be expressed as

$$3\frac{\ddot{a}}{a} = V(\phi) - \dot{\phi}^2 = -\frac{1}{2M_p^2}(\rho + 3P) \, , \tag{3.192}$$

which is equivalent to (3.54). The condition (3.191) will hold whenever

$$V(\phi) > \dot{\phi}^2 \tag{3.193}$$

is satisfied; or equivalently

$$w < -\frac{1}{3} \, , \tag{3.194}$$

the same as (3.57). Let us suppose that the difference between the kinetic and the potential terms is so big that we can neglect $\dot{\phi}$ in (3.187). In that case, the condition (3.193) is approximately equivalent to

$$\dot{H} \ll -H^2 \, , \tag{3.195}$$

which tells that the expansion is nearly exponential because the relative change in H during a Hubble time H^{-1} is much less than unity. We can also assume that $\ddot{\phi}$ is negligible in (3.188) so the equations of motion become

$$H^2 \simeq \frac{1}{3M_p^2}V(\phi) \, , \tag{3.196}$$

$$3H\dot{\phi} \simeq -V' \, , \tag{3.197}$$

and the relation between $\dot{H}$ and $\dot{\phi}$, Equation (3.189) still holds. When these two approximations are valid (3.189) can be written as follows

$$\frac{\ddot{a}}{a} \simeq \frac{V}{3}\left(1 - \frac{2}{3}\epsilon\right) \, , \tag{3.198}$$

where

$$\epsilon \equiv \frac{1}{2}M_p^2\left(\frac{V'}{V}\right)^2 \, . \tag{3.199}$$

Within these approximations, if ϵ is small compared to 1 the dynamics will be inflationary. There is another useful parameter that is related to both (3.196) and (3.197):

$$\eta \equiv M_p^2\frac{V''}{V} \, . \tag{3.200}$$

These two functions of ϕ, ϵ and η are called 'potential slow–roll parameters' (PSR). We will refer to the Equations (3.196) and (3.197) as the 'slow–roll approximation'. If the dynamics encoded in (3.187) and (3.188) can be satisfactorily described by

(3.196) and (3.197) we will say that the slow–roll approximation holds. It can be easily checked that the slow–roll approximation implies the so called 'slow–roll conditions'

$$\epsilon \ll 1\,, \tag{3.201}$$
$$|\eta| \ll 1\,. \tag{3.202}$$

Simply, starting from (3.196) and (3.197), and then using $\dot{\phi}^2 \ll V$ and (3.189) we see:

$$\frac{V'}{V} \simeq \frac{\dot{\phi}}{HM_p^2} \ll \frac{2V}{HM_p^2\dot{\phi}} = -\frac{6V}{M_p^2V'}\,, \tag{3.203}$$

and hence $\epsilon/3 \ll 1$. On the other hand, differentiating (3.197) with respect to time we have

$$3\dot{H}\dot{\phi} + 3H\ddot{\phi} + V''\dot{\phi} \simeq 0\,, \tag{3.204}$$

which implies

$$1 \gg \left|\frac{1}{3}\eta - 2\frac{\ddot{\phi}}{3H\dot{\phi}}\right|\,; \tag{3.205}$$

and from here, using (3.188) and (3.197) in the second term, we get $|\eta|/3 \ll 1$. Although, as we have just seen, the smallness of these parameters is a necessary consistency condition for the slow–roll approximation, it is not a sufficient one to guarantee its validity [189]. The reason can be understood from the previous argumentation where we have used the 'attractor solution' (3.197) to compute the second derivative of the field. If we start from the full equations of motion, (3.187) and (3.188), and the slow–roll conditions, (3.201) and (3.202), it turns out that (3.197) is an extra condition that we have to impose in order to get the slow–roll approximation.

Provided that the evolution of the field is monotonic, i.e. that $\dot{\phi} = 0$ does not occur during the evolution, it is possible to use ϕ itself as a parameter to describe the dynamics. In this case the Hubble parameter can be seen as field function and $\dot{H} = H'\dot{\phi}$, so (3.189) can be rewritten in the following way:

$$\dot{\phi} = -2M_p^2H'\,, \tag{3.206}$$

and (3.187) becomes

$$\left[H'(\phi)\right]^2 - \frac{3}{2}M_p^2H(\phi)^2 = -\frac{1}{2M_p^2}V(\phi)\,. \tag{3.207}$$

In analogy to the definitions of the potential slow–roll parameters we introduce the parameters ϵ_H and η_H, by

$$\epsilon_H \equiv 2M_p^2\left(\frac{H'}{H}\right)^2\,, \tag{3.208}$$
$$\eta_H \equiv 2M_p^2\frac{H''}{H}\,. \tag{3.209}$$

These are usually called 'Hubble slow–roll parameters' (HSR) to distinguish them from those of equations (3.199) and (3.200), that are simply termed 'slow–roll parameters' very often. The HSR parameters have some advantages over the PSR parameters. From the equations of motion one finds that

$$\frac{1}{3}\epsilon_H = \frac{\dot{\phi}^2}{\dot{\phi}^2 + 2V}, \tag{3.210}$$

$$\eta_H = \frac{\ddot{\phi}}{\dot{\phi}H}\,. \tag{3.211}$$

Obviously, $\epsilon_H \ll 1$ is the condition for neglecting $\dot{\phi}^2$ in favour of V in equation (3.187); and $|\eta_H| \ll 1$ is the condition for neglecting $\ddot{\phi}$ in (3.188). These conditions are sufficient to guarantee the slow–roll approximation. Besides, it can be easily checked that inflation will happen if and only if

$$\epsilon_H < 1\,. \tag{3.212}$$

The formulation of the equations of motion in terms of the Hubble parameter allows to obtain inflationary solutions by choosing $H(\phi)$ and solving (3.207) for $V(\phi)$. This procedure is valid if H' does not pass through zero; otherwise the change of variable from t to ϕ is not an adequate reparameterization. Clearly, for an arbitrary $H(\phi)$ the obtained potential need not have any physical origin at all. The Hubble formulation is useful for general analyses of inflationary dynamics, but if we are interested in studying a particular potential we may better use the most common formulation of the equations of motion (3.187) and (3.188). In this case it is more convenient to work with the PSR parameters, provided that the attractor condition (3.197) is satisfied.

It is possible to define a whole hierarchy of slow–roll parameters, of which those we have already introduced are the lowest order elements. For instance, in the case of the PSR parameters we have

$${}^{(n)}\beta \equiv M_p^{2n}\,\frac{(V')^{n-1}\,V^{(n+1)}}{V^n}\;,\; n>1\,. \tag{3.213}$$

In particular we will later need

$$\xi \equiv {}^{(2)}\beta = M_p^4\frac{V'V'''}{V^2}\,. \tag{3.214}$$

Similar expressions can be defined for the HSR parameters using $H(\phi)$ instead of $V(\phi)$ and there are exact and approximate formulas that serve to relate both sets of parameters [189]. We will later see that the slow–roll parameters are useful because they allow us to compute quantities that are related to the observations.

In Section 3.4.1 we introduced the number of efolds (3.159) as a measure of the efficiency of inflation. Using (3.206) we see that the number of efolds can be computed as an integral over field values.

$$N_e\,(t_i\,,t_f) = \frac{1}{M_p}\int_{\phi_f}^{\phi_i}\frac{1}{\sqrt{2\epsilon_H}}\mathrm{d}\phi\,, \tag{3.215}$$

Let us remark again that the change of variables is only valid if $\dot{\phi} \neq 0$ during the whole process. Under this condition, the number of efolds can be used as another parameter to describe the evolution of the field, we just have to take t to be the upper limit of integration. Besides, if the slow–roll approximation holds, we can trade ϵ_H by ϵ in the previous expression.

$$N_e\left(t_i\,,t_f\right) \simeq \frac{1}{M_p}\int_{\phi_f}^{\phi_i}\frac{1}{\sqrt{2\epsilon}}\mathrm{d}\phi\,. \tag{3.216}$$

It is clear that the smaller ϵ is the bigger the amount of expansion that takes place. This is partly the reason why slow–roll inflation is so useful.

For later use, it is convenient to explain how to relate in the slow–roll approximation physical inverse distance scales k (wavenumbers) with the inflaton field ϕ. This is done using the following derivative:

$$\frac{\mathrm{d}\phi}{\mathrm{d}\ln k} \simeq -M_p\sqrt{2\epsilon_H}\,. \tag{3.217}$$

A very simple argument to understand this formula is given in [145]. We just take logarithms in the equation $k = aH$, that relates the scale factor at a certain t with the scale k that leaves the horizon in that moment, and then differentiate with respect to ϕ. Taking into account that during inflation the Hubble parameter remains approximately constant, and using the slow–roll approximation, we reach (3.217). Clearly, what that equation tells is that during inflation

$$N_e\left(t_i\,,t_f\right) \simeq \ln\left(\frac{k_f}{k_i}\right)\,, \tag{3.218}$$

where the subscripts on k match those on t, denoting the scales that leave the horizon at those times. The definition (3.159) means that the number of efolds represent the logarithmic change of the scale factor. In differential form we can write $\mathrm{d}N_e = \mathrm{d}\ln a$; from here, and using the approximate constancy of H during inflation, we see that a change of a certain number of efolds in the scale factor corresponds to the same range of scales stretched outside the horizon. For instance, if the number of efolds of inflation were 60, we would know that there are approximately 26 order of magnitude between the smallest and largest scales to leave the horizon.

3.4.4 Primordial spectrum from slow–roll

In the slow–roll picture different models can be devised depending on the choice of the potential $V(\phi)$. The prediction for the total number of efolds of inflation depends on the model but we cannot use that information to distinguish between different potentials because the cosmological data only probes the first 10 efolds or so. The usual strategy to test inflationary potentials is the comparison of theoretical predictions for the spectrum of primordial cosmological perturbations with data. In this section we are going to provide the expressions of the primordial spectrum in terms of the slow–roll parameters and we will briefly comment how to obtain them later on. We will also introduce the standard parameterization that is commonly used to fit the data and explain its usefulness and extent of generality.

Let us remark that we are using here the term "model" in a rather broad and unambitious way to refer to a particular choice of the potential $V(\phi)$. It is clear though that this puts at the same level models that have very different degrees of justification from the point of view of particle physics. A completely satisfactory model of inflation cannot be just limited to specifying the inflationary potential [145] and should also address important questions like how it does relate to the fields of the Standard Model, for instance. Besides, as we explain in Section 3.4.2, slow–roll single field inflation is only one possible way (albeit a broad one) of making inflation theoretically possible. In this respect, let us remark that the solutions via inflation of the horizon and flatness problems do not require any scalar field whatsoever. In any case, we shall focus now on inflation driven by a scalar field.

In the slow–roll approximation the scalar and tensor components of the spectrum of primordial perturbations are respectively given by:

$$P_s(k) \simeq \frac{1}{24\pi^2\epsilon}\frac{V}{M_p^4}\,, \tag{3.219}$$

$$P_t(k) \simeq \frac{3}{2\pi^2}\frac{V}{M_p^4}\,. \tag{3.220}$$

Thus the tensor to scalar ratio simply reads

$$r \equiv \frac{P_t}{P_s} \simeq 16\epsilon\,. \tag{3.221}$$

It is worth noticing that the tensor part of the spectrum is proportional to the potential, which is approximately constant during inflation, and therefore the detection of primordial gravitational waves can help to determine the scale of inflation. The tilt of the scalar part of the spectrum is measured by the scalar 'spectral index'. It tells us whether the spectrum gains or looses power when the wave number is increased. The scalar spectral index itself is a function of the wavenumber and its definition is the following:

$$n - 1 \equiv \frac{\mathrm{d}\ln P_s}{\mathrm{d}\ln k}\,. \tag{3.222}$$

Using the Equation (3.217) in the slow–roll approximation, where $\epsilon_H \simeq \epsilon$, we can apply the previous definition (3.222) to express the scalar spectral index in terms of the first order slow–roll parameters:

$$n - 1 \simeq 2\eta - 6\epsilon\,. \tag{3.223}$$

Differentiating once more we obtain the 'running' of the spectral index:

$$\frac{\mathrm{d}n}{\mathrm{d}\ln k} \simeq -2\xi + 16\epsilon\eta - 24\epsilon^2\,, \tag{3.224}$$

in which the second order slow–roll parameter appears from the third derivative of the inflaton potential. Similar expressions, involving the tensor spectral index can be written for the tensor part of the primordial spectrum $P_t(k)$. In particular, the tensor spectral index is defined as

$$n_t \equiv \frac{\mathrm{d}\ln P_t}{\mathrm{d}\ln k}\,, \tag{3.225}$$

and, in the slow–roll approximation,

$$n_t \simeq -2\epsilon\,. \tag{3.226}$$

The corresponding running is

$$\frac{\mathrm{d}n_t}{\mathrm{d}\ln k} = 16\epsilon\eta - 24\epsilon^2\,, \tag{3.227}$$

which at lowest order in slow–roll does not depend on derivatives of the potential of order higher than 2. The simple equation

$$r \simeq -8n_t\,, \tag{3.228}$$

is said to be a consistency equation for slow–roll inflation because a measurement of the two quantities involved in it might disprove this framework if they were found not to satisfy that proportionality relation. The current data is not good enough to probe the tensor part of the spectrum properly, which is much smaller than its scalar counterpart, and the tensor spectral index is completely unconstrained. In fact, this index is not normally considered a free parameter when fits are performed and its value is usually enforced by the consistency condition (3.228).

Standard parameterization of the primordial spectrum

Since the spectrum of primordial perturbations predicted by slow–roll inflation is nearly scale invariant, a common approach to determine it from CMB and LSS data is to perform a Taylor expansion of $\ln P_s(k)$ and $\ln P_t(k)$ in $\ln k/k_0$ around zero, where k_0 is a fiducial scale, that will later choose to be $k_0 \equiv 0.002$ Mpc^{-1}, as it is customary.

$$\ln P_s(k) = \ln P_s(k_0) + [n(k_0) - 1] \ln \frac{k}{k_0} + \frac{1}{2}\frac{\mathrm{d}n}{\mathrm{d}\ln k}\bigg|_{k_0} \left(\ln \frac{k}{k_0}\right)^2 + \cdots \tag{3.229}$$

$$\ln P_t(k) = \ln P_t(k_0) + n_t(k_0) \ln \frac{k}{k_0} + \cdots\,. \tag{3.230}$$

Usually, one does not go beyond the order shown in these equations. In particular, a running of the tensor spectral index has not been considered because presently the tensor contribution to the spectrum is only weakly constrained by the data. Therefore, one typically fits four independent parameters, namely: $\{\ln P_s, n, \mathrm{d}n/\mathrm{d}\ln k, r\}_{k_0}$ and often the running of the spectral index, $\mathrm{d}n/\mathrm{d}\ln k|_{k_0}$, and the tensor to scalar ratio, $r(k_0)$, are set to zero. In general, the issue of whether an extra parameter is needed or not is a difficult one and has to be addressed with care. See for example [190, 191] for a discussion about this question to which we will return in Section 4.11. For the latest results using this parameterization see Section 4.1.2.

The normal procedure for comparing models basically consists in using the previous expansions to fit the data. The numbers obtained are then compared with the theoretical predictions for the different inflationary models. We would like to stress for the purposes of our discussion that these simple functional forms that

are typically assumed for $P_s(k)$ and $P_t(k)$ may not be accurate enough to describe the actual power spectrum of potentials which are slightly more complicated than just a monomial and still physically well motivated. In this sense, although (3.229) and (3.230) can be useful as phenomenological approximations, it is important to be open to other parameterizations. We will later show explicit examples of this. At the end of the day, the best fit together with the best physical motivation will determine the preferred functional form.

3.4.5 The primordial perturbations

In the case of single field slow–roll inflation the spectrum of scalar perturbations comes from the curvature perturbation

$$\mathcal{R}_{\mathbf{k}} = \frac{1}{4}\frac{a^2}{k^2} R_3(\mathbf{k}) \,, \tag{3.231}$$

where R_3 is the spatial curvature in a comoving frame, $\mathbf{k}$ is the wavenumber vector of Fourier space and k is its modulus. On the other hand, the tensor part h_{ij}^T of the metric perturbation, Equation (3.83), has two degrees of freedom, as we explained in Section 3.3.1. These can be split in two polarizations $h^\times$ and h^+ in such a way that the two degrees of freedom are $h_{11} = -h_{22} = h^+$ and $h_{12} = h_{21} = h^\times$. Although there are two different gravitational degrees of freedom they have the same spectrum due two rotational invariance and therefore the spectrum of primordial perturbations is composed of $\mathcal{P}_\mathcal{R}$ and $\mathcal{P}_h$. The tensor perturbations are gaussian because they behave as massless scalar fields. So it is the curvature perturbation if the fluctuation of the inflaton is not coupled to other fields during its evolution. The assumption that the inflaton does not interact with other fields it is equivalent to work with linear perturbation theory. Gaussianity means that the Fourier components of the perturbation evolve independently from each other and their phases are random. This property let us define the spectra that we have introduced before in a precise way. For instance, in the case of the curvature perturbation we have

$$\langle \mathcal{R}^*_{\mathbf{k}} \mathcal{R}_{\mathbf{k}'} \rangle = \frac{2\pi^2}{k^3} \mathcal{P}_\mathcal{R} \, \delta^{(3)} \left(\mathbf{k} - \mathbf{k}' \right) \,. \tag{3.232}$$

An analogous expression holds for the tensor component of the spectrum. The only difference comes from the fact that a factor of 1/2 has to be included in the right hand side when we substitute $\mathcal{R}$ by $h^\times$ or h^+ to account for the equal contributions of the two polarizations.

Now the question is what is the relation between $\mathcal{P}_\mathcal{R}$ and its tensor counterpart and the expressions (3.219)and (3.220). Although we do not measure directly the curvature perturbation at horizon exit during inflation, this quantity has the property of becoming time independent once it leaves the horizon. Therefore, when inflation ends and H can no longer be approximated by a constant, the horizon grows in time and we are gradually able to detect *frozen* primordial perturbations at increasingly larger scales as they enter the horizon. This behaviour is illustrated in Figure 3.10 from [192].

There are several ways in which one can compute the curvature perturbation and prove that it really remains constant after it exits the horizon. We could just use the

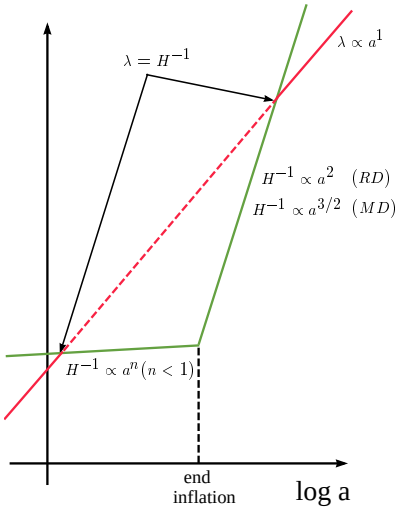

Figure 3.10: The size of the "horizon" H^{-1} remains approximately constant during inflation while a comoving length $\lambda = 2\pi/k$ (in red) grows like the scale factor a therefore crossing the horizon at some point during inflation and entering later during matter or radiation domination. The curvature perturbations generated during inflation associated to a scale k are time independent while $\lambda > H^{-1}$.

equations of Section 3.3.1 particularized for the energy momentum tensor of a scalar field (see Equations (3.184) and (3.185)), working either in the conformal Newtonian gauge or using gauge invariant variables, as it is usually done. These procedures are detailed in [193], for instance. Another possibility is using a calculational framework based on the fact that the evolution along a comoving worldline is approximately the same as in the background (non–perturbed) universe after smoothing on scales much larger than H^{-1}. This is explained in [18] and [145] and was done in [194] for a general case with several scalar fields.

We are going to explain now how to get the curvature perturbation spectrum in a very straightforward way. More detailed and thorough explanations can be found in [18] and [193]. The equation of motion of a scalar field which depends on all four spacetime coordinates is

$$\ddot{\phi} + 3H\dot{\phi} + \frac{1}{a^2}\partial_i\partial_i\phi + \frac{\mathrm{d}V}{\mathrm{d}\phi} = 0\,. \tag{3.233}$$

Writing

$$\phi(\mathbf{x}, t) = \phi(t) + \delta\phi(\mathbf{x}, t)\,, \tag{3.234}$$

the equation for the perturbation is

$$(\delta\phi)^{\cdot\cdot} + 3H(\delta\phi)^{\cdot} - \frac{1}{a^2}\partial_i\partial_i\delta\phi + \frac{\mathrm{d}^2V}{\mathrm{d}\phi^2}\delta\phi = 0\,, \tag{3.235}$$

which becomes

$$(\delta\phi_{\mathbf{k}})^{\cdot\cdot} + 3H(\delta\phi_{\mathbf{k}})^{\cdot} + \frac{k^2}{a^2}\delta\phi_{\mathbf{k}} + \frac{\mathrm{d}^2V}{\mathrm{d}\phi^2}\delta\phi_{\mathbf{k}} = 0\,, \tag{3.236}$$

after going to Fourier space with

$$\phi(\mathbf{x},t)=\frac{1}{(2\pi)^{3/2}}\int\phi_{\mathbf{k}}e^{i\mathbf{k}\cdot\mathbf{x}}\mathrm{d}^3\mathbf{k}\,. \tag{3.237}$$

The last term in Equation (3.236) contains the mass of the inflaton. Let us suppose for a moment that this term is negligible. Then, it is easy to understand the behaviour of the solutions. The horizon crossing condition, $k=aH$, tells us that for wavelengths within the horizon ($k\gg aH$) the perturbations are oscillatory. Well after horizon crossing, when $k\ll aH$, the perturbations become time independent, and it is said that they *freeze*. The mass term in (3.236) is negligible in inflation for wavelengths within the horizon. The smallness of $|\eta|$ and the approximation (3.196) guarantee that this is so because they imply that the second derivative of the potential is much smaller than H^2. However, a few Hubble times after horizon exit the mass term cannot be generally neglected and therefore the solution will have an extra time dependence. In the pure massless case and well outside the horizon, it can be easily checked, going to conformal time, that

$$|\delta\phi_{\mathbf{k}}|^2\simeq\frac{H^2}{2k^3}\,, \tag{3.238}$$

and since H is almost constant during inflation, it is clear that the perturbations do not change considerably after leaving the horizon. In the massive case the solution for the perturbations equation has a small time dependence. It can be expressed in terms of Hankel functions for sufficiently small masses. Concretely,

$$|\delta\phi_{\mathbf{k}}|^2\simeq\frac{H^2}{2k^3}\left(\frac{k}{aH}\right)^{3-2\nu}\,, \tag{3.239}$$

where

$$\nu^2=\frac{9}{4}-\frac{1}{H^2}\left(\frac{\mathrm{d}^2V}{\mathrm{d}\phi^2}\right)^2\,. \tag{3.240}$$

See [193] for details. As we explained before, a slowly rolling inflaton has a mass which is much smaller than the Hubble rate and therefore $\nu\simeq 3/2$, which means that the extra time dependence in (3.239) is indeed very small.

For the quantum perturbation field, from (3.232) we have

$$\int\frac{\mathrm{d}k}{k}\mathcal{P}_{\delta\phi}=\langle\delta\phi(\mathbf{x},t)^2\rangle=\int\frac{\mathrm{d}k}{k}\frac{k^3}{2\pi^2}|\delta\phi_{\mathbf{k}}|^2\,, \tag{3.241}$$

and in consequence

$$\mathcal{P}_{\delta\phi}=\frac{k^3}{2\pi^2}|\delta\phi_{\mathbf{k}}|^2\simeq\frac{1}{4\pi^2}H^2\left(\frac{k}{aH}\right)^{3-2\nu}\,. \tag{3.242}$$

We have just obtained the primordial spectrum for the inflaton perturbation but we still have to connect this result with the curvature perturbation $\mathcal{R}_{\mathbf{k}}$ to write its own spectrum. The link is provided by

$$\mathcal{R}_{\mathbf{k}}=-\frac{H}{\dot\phi}\delta\phi_{\mathbf{k}}\,, \tag{3.243}$$

which implies

$$\mathcal{P}_{\mathcal{R}}(k) = \frac{1}{2M_p^2\epsilon_H}\left(\frac{H}{2\pi}\right)^2\left(\frac{k}{aH}\right)^{3-2\nu}, \tag{3.244}$$

where we have used the definition (3.208) of the first HSR. At horizon crossing during inflation this expression is precisely (3.219). In general, the curvature perturbation is defined as

$$\mathcal{R} = -\Psi + H\delta u\,, \tag{3.245}$$

in terms of the potential Ψ and the velocity perturbation δu that we introduced in Equations (3.136) and (3.110) respectively. Using the equations of Section 3.3.1 it is easy to check that

$$\Delta\mathcal{R} = 0\,, \tag{3.246}$$

which means that the curvature perturbation is gauge invariant. When the energy and matter content of the universe are given by a single scalar field

$$\delta u = -\frac{\delta\phi}{\dot{\phi}}\,, \tag{3.247}$$

and therefore:

$$\mathcal{R} = -\Psi - H\frac{\delta\phi}{\dot{\phi}}\,. \tag{3.248}$$

This expression is very close to (3.243). Before seeing how to get there, we will introduce the concepts of 'slicing' and 'threading' [18, 193]. In general relativity, choosing a gauge is equivalent to selecting a particular coordinate system in which the equations that define the gauge are satisfied. For instance, let us recall for a moment the way in which the Newtonian gauge was defined in Section 3.3.1 by choosing a particular coordinate displacement. A gauge choice defines a threading of the spacetime manifold in lines of fixed spatial coordinates and a slicing in hypersurfaces of fixed time. If we choose a slicing which is comoving, i.e. orthogonal to the worldlines of comoving observers, we can move to it from an arbitrary slicing with perturbation $\delta\phi$ using the time displacement

$$\delta t = \frac{\delta\phi}{\dot{\phi}}\,. \tag{3.249}$$

This is simply because in such a comoving slicing the field perturbation is zero. By definition $\mathcal{R}$ is the gravitational potential on comoving hypersurfaces where the field perturbation is zero. Similarly, in a spatially flat gauge (the slicing makes $\Psi = 0$) we get the expression (3.243). Since the curvature perturbation is gauge invariant, once we know its spectrum in a particular gauge we will also know it in any other coordinate choice and so the result (3.219) holds in general.

Clearly we haven't done a complete computation of the spectrum of the comoving curvature perturbation because we started from the equation for the perturbation of a single massive field disregarding metric perturbation degrees of freedom. A more rigorous approach would have been to take the full set of equations for the coupled perturbations and then work with gauge invariant quantities or choosing a specific gauge. However, our approach is not completely inconsistent because if we had chosen to work in the conformal Newtonian gauge we would have found

that for the case of single field inflation the energy momentum tensor off–diagonal terms are zero and that would have lead us to work with only one metric degree of freedom. This degree of freedom, any of the quantities E or A of Equations (3.136), has a equation of motion that can be written with coefficients that depend on the slow–roll parameters and from there we would have arrived to (3.219) rather straightforwardly [193].

The computation of the tensor primordial spectrum is somewhat simpler. This is due to the fact that the two (gauge invariant) physical degrees of freedom satisfy the equation of motion of a massless scalar field (see Equation (3.236) and take the last term to zero). The canonical normalization of the two polarizations that we mentioned in the beginning of this section are

$$\psi_\times = \frac{M_p}{\sqrt{2}} h^\times \,, \quad \psi_+ = \frac{M_p}{\sqrt{2}} h^+ \,. \tag{3.250}$$

As we saw before, the solution for both will be of the form

$$|\psi_{\mathbf{k}}|^2 = \left(\frac{H}{2\pi}\right)^2 \left(\frac{k}{aH}\right)^{3-2\nu_t} \,, \tag{3.251}$$

with

$$\nu_t \simeq \frac{3}{2} - \epsilon \,. \tag{3.252}$$

The primordial tensor spectrum is

$$\frac{1}{2} P_t = 4 \frac{k^3}{2\pi^2} |\psi_{\mathbf{k}}|^2 = \frac{8}{M_p} \left(\frac{H}{2\pi}\right)^2 \left(\frac{k}{aH}\right)^{n_t} \,, \tag{3.253}$$

where we have taken into account the polarization multiplicity and $n_t = -2\epsilon$, in accord with Equation (3.226). Notice that this is the spectrum for scales much larger than the horizon, where the perturbations are almost constant, as the smallness of the slow–roll parameter ϵ guarantees.

3.4.6 Linking observations and the primordial spectrum

The final question we should analyse is how do we connect the observations with the primordial perturbations that we have studied in the previous sections. Basically, there are two kinds of measurements that are useful: the CMB and the energy density distribution (large scale structure data). The CMB can be decomposed into two kinds of observables which are the temperature anisotropy and its polarization. Reviews on the physics of the CMB can be found in [195] and also [196, 197]. These data, CMB and LSS, are related to the primordial quantities by different time dependent 'transfer functions' through proportionality relations. The spectrum of the energy density distribution is

$$\mathcal{P}_\delta(k,t) = \mathcal{T}^2(k,t) \mathcal{P}_\mathcal{R}(k) \,. \tag{3.254}$$

In the case of the CMB anisotropy we have

$$a_{lm} = \frac{4\pi}{(2\pi)^{3/2}} \int \mathcal{T}_\Theta(k,l) \mathcal{R}_{lm}(k)\, k \,\mathrm{d}k \,, \tag{3.255}$$

where

$$\mathcal{R}_{lm}(k) = k\, i^l \int \mathcal{R}(k\hat{\mathbf{k}}) Y_{lm}(\hat{\mathbf{k}}) \mathrm{d}\Omega_{\mathbf{k}}. \tag{3.256}$$

Using the properties of spherical harmonics (rotational invariance) [198] we define

$$\langle a^*_{lm} a_{l'm'} \rangle = C_l \delta_{ll'} \delta_{mm'}\,, \tag{3.257}$$

where

$$C_l = 4\pi \int_0^\infty \mathcal{T}^2_\Theta(k,l) \mathcal{P}_\mathcal{R}(k) \frac{\mathrm{d}k}{k}, \tag{3.258}$$

which is called the angular power spectrum. Two similarly defined spectra give information on correlation and polarization but we are not providing the corresponding formulas here. Notice that we have neglected the contribution from the tensor part of the spectrum. Interestingly, the higher sensitivity of the Planck probe in comparison with WMAP will allow to measure the polarization spectrum much better. Roughly speaking, the number of standard cosmological parameters that can be determined from the data is proportional to the number of available spectra and the number of acoustic peaks in these spectra. In consequence, Planck will be able to test many cosmological hypotheses beyond the capabilities of WMAP. This is the reason why, as we will later comment in greater depth, Planck data may be able to clarify the WMAP indications concerning the running of the scalar spectral index.

The previous equations indicate that testing the predictions of a particular model of inflation using CMB and LSS data is an indirect process in the sense that they have to be convoluted with the transfer functions to get the observable quantities. This integration explains that different primordial spectra can give equally good fits to the data, even if the spectra are qualitatively different.

3.4.7 Some words on effective field theories in inflation

Since inflation must have happened at very high energies in order to comply with the observational requirement of the amplitude of primordial perturbations and solve the horizon problem, there is the possibility of using the CMB for probing energy scales which otherwise would be unattainable. It has even been argued in several works that effects of physics coming from beyond the Planck scale could have left an imprint in the CMB [199–201]. Since we do not really know what is the theory that describes physical phenomena at these formidable energies the most useful tool to deal with this question is that of effective field theories. A study of the potentialities of this kind of techniques for learning about the implications of high energy physics in inflation and the cosmology of the very early universe has been done in [202], where hybrid inflation in supersymmetry and supergravity models are considered. A general effective field theory for inflation is constructed in [203]. As it is explained in [204], effective field theories are appropriate for analysing the existence of hierarchies of scale in a physical problem. According to our current understanding of particle physics, any field theory is effective in the sense that its validity is restricted to a certain range of energies. Perhaps string theory or some unknown ultraviolet completion of gravity might be the only case of a theory which could be used in

principle at any energy. However, it is a matter of debate if such a theory may actually exist and for practical reasons effective field theories are just very convenient to use. A general feature of quantum field theories is that the coupling and mass values vary with the energy scale at which physics takes place. This can be described using renormalization group techniques which are also a powerful tool in other branches of physics such as statistical mechanics. For a thorough review of the renormalization group method see [205]; or check [206] for a shorter introduction. This *running* of the lagrangian parameters turns out to be of great importance for inflation. We will later see that the intrinsic energy scale dependence of the theory is connected with the distance scale dependence of observables like the scalar spectral index. This is particularly so for the case of flat directions (for instance, those that naturally appear in supersymmetric theories) in which case the dynamics of inflation is almost entirely determined by radiative corrections coming from a proper treatment of quantum energy effects. In consequence, the inflaton value, the energy scale of the process and the wavenumber of the primordial perturbations are all related.

The renormalization group methods and loop corrections are adequate to deal with quantum corrections to a theory within its own domain of validity. However, it may be the case that physics from higher energy scales have a relevant contribution to an inflationary process that happens at a lower scale. It is in this situation when the power of effective field theories is realized. There is a general well defined procedure for taking into account these effects which does not require a detailed knowledge of the physical theory at high scales. Using just the fields relevant in the low energy theory, it is possible to make an expansion of the action which includes those effects and may contribute to give us hints of the possible nature of the physics at high energy from observations or measurements performed at lower scales.

The fact that in quantum field theories there appear to be ultraviolet divergences at small distances (i.e. at high energies) can be interpreted as a signature that the connection between the lagrangian parameters and their true values comes from physics beyond the quantum field theory itself. The approximate energy scale at which new physics effects start to become so relevant that the low energy theory should be substituted is called an (ultraviolet) *cut–off*. This upper limit typically marks the degree of validity of an effective field theory. In an effective field theory framework the effects from high energy physics are manifest at lower scales through an explicit cut–off dependence in the effective lagrangian. The cut–off scale enters as a suppression factor in high dimensional operators of the low energy fields. These operators are *non–renormalizable* from the point of view of power counting and the resulting theory will be non–renormalizable in general in the strict sense that amplitudes are divergent at sufficiently high order in perturbation theory. As it is emphasized in [204], effective field theories can be used to study quantum effects on non–renormalizable theories provided that the application is restricted to low enough energies. See [205] for a discussion about the possible situations that may appear in non–renormalizable theories. For other introductions on renormalizability and the physical meaning of a cut–off see [207, 208].

As we said above, effective field theories are an essential tool for analyzing systems which have two very different energy (or mass) scales. In these situations it is usually convenient to use series expansions in the ratio of the two scales. The key

issue behind this kind of calculations is reliably taking into account the high energy effects in the low energy field theory. This procedure, together with an appropriate choice of the renormalization scale in dealing with radiative corrections, can simplify the mathematical aspects of a problem and lead to an accurate description of it. We will have the chance of seeing how this works in practice in application to specific examples later on (see Sections 4.3 and 4.5). When more than two mass scales that are wide apart appear in the problem the situation becomes more involved and there are several choices of the renormalization scale that can be made in order to minimize the impact of large logarithms [209–211]. It turns out that the most convenient one is usually simply taking the smallest of them [212], which can be seen using the decoupling theorem [213].

The quantity to which effective field theories are applied in the context of inflation is the effective scalar potential that describes the interactions of the system. Its most remarkable property is that it is scale invariant, which means that it satisfies the following relation, usually called Callan-Symanzik equation [205]:

$$\mathcal{D}V \equiv \left(Q\frac{\partial}{\partial Q} + \beta_a \frac{\partial}{\partial \lambda_a} - \gamma\phi\frac{\partial}{\partial \phi} \right) V = 0\,. \tag{3.259}$$

The definitions of the beta functions, β_a, and the anomalous dimension, γ, that enter into this equation are as follows:

$$\beta_a = \frac{\partial \lambda_a}{\partial \ln Q}\,, \tag{3.260}$$

$$\gamma = -\frac{\partial \ln \phi}{\partial \ln Q}\,. \tag{3.261}$$

The quantities λ_a represent the couplings of the model, being the subscript just a label to distinguish between them. Let us notice that the definitions (3.260) and (3.261) can be read off from (3.259) just knowing the symmetry that this last equation describes.

A useful property of the effective potential is that the n–loop improved effective potential with (n+1)–loop renormalization group equations is equivalent to the nth–to–leading–log order effective potential [214–216]. This fact can be used order by order in perturbation theory in (3.259) to obtain a series of recursion relations that allows to find higher order corrections from lower order ones. In particular the case of a tree level potential improved with one–loop renormalization group equations describes the leading–log approximation. Similarly, the one–loop effective potential improved with two–loop renormalization group equations corresponds to the next–to–leading–log approximation. With this method the complication of the computation of high order contributions to the beta functions can be greatly reduced. We will use this technique in Section 4.5 to compute two–loop corrections to the effective potential of a model of inflation in which there are two different mass scales.

Chapter 4

The running spectral index as a probe of physics at high energies

4.1 Cosmological data and the running spectral index

The two works, [9] and [10], on which this part is based, were done after the releases of the first and second WMAP data sets respectively. In this section we review those results including other complementary data sets paying special attention to the analyses of the WMAP team itself, although we also mention other related ones that appeared at the time. After that, we comment on the latest WMAP data release and the current status concerning the running spectral index. Let us recall that the objective of the research that this whole chapter summarizes is to find a general class of particle physics inflationary potentials that can account for these WMAP indications on the running of the spectral index an sustain inflation for long enough to solve the horizon and flatness problems.

4.1.1 Early indications

In what follows we review the results of the analyses of WMAP and other data that lead to an indication of a large running of the spectral index. The contents of this subsection correspond to the first two WMAP data releases. As we have said, we will focus on the analyses done by the WMAP team itself.

The Wilkinson Microwave Anisotropy Probe (WMAP) mission has been taking data since October 2001. The first results [217,218] where released in February 2003 and we will refer to them as WMAP1. In March 2006 appeared the second analysis release [219] that we will call WMAP3 because it came three years after the first release of the data collected by the probe. Very roughly speaking, the main difference between the two data analyses is that the second one focuses not only on the CMB temperature but also on its polarization. Also, according to the WMAP team, more efficient algorithms were used for the data processing to obtain the WMAP3 results. The first work on which this thesis is based [9] was presented a few months ahead of WMAP3 and so it was based on the indications given by WMAP1. The second

Table 4.1: Best fit values at $k = 0.05\,\mathrm{Mpc}^{-1}$ for the ΛCDM model with running in WMAP1.

	WMAP	WMAPe	WMAPe +2dFGRS	WMAPe +2dFGRS+Lymanα
n	$0.93^{+0.07}_{-0.07}$	0.91 ± 0.06	$0.93^{+0.04}_{-0.05}$	0.93 ± 0.03
$\frac{\mathrm{d}n}{\mathrm{d}\ln k}$	-0.047 ± 0.04	-0.055 ± 0.038	$-0.031^{+0.023}_{-0.025}$	$-0.031^{+0.016}_{-0.017}$

work [10], which is a continuation of the first one, used the data of WMAP3, which was the latest available one in that moment.

The Table 4.1 shows the result of the analysis done by the WMAP team for the first data release and other relevant data sets. On this table, the label WMAP corresponds to the analysis considering only WMAP data. WMAPe refers to the data coming from WMAP and two different ground based telescopes, the Cosmic Background Interferometer (CBI) [220,221] and ACBAR, the Arcminute Cosmology Bolometer Array Receiver [222]. CBI is a ground based interferometer placed in Chile and designed to study the cosmic microwave background radiation on angular scales from 5 arc minutes to 1 degree which corresponds to the spherical harmonic scales from l = 3000 down to l = 300, approximately. ACBAR is a telescope in the South Pole working in a range of angular scales $l = \{200, 3000\}$. Apart from these three CMB data sets, there are other relevant spectral observations employed to get the cosmological parameters. In particular, 2dFGRS, The Two Degree Field Galaxy Redshift Survey [223, 224] of the Anglo–Australian Observatory measured the redshift of about twenty thousand galaxies for $z \in \{0, 0.3\}$. There is also the Lyman α data set which is a survey of quasars done with the Keck telescopes in Hawaii for redshifts between 2 and 4. The data that came from these surveys is included in the results of the last column of Table 4.1. These two pieces of information are important because they span the range of cosmological scales in the analysis beyond WMAP data. Concretely, Lyman α data covers a range of scales between roughly $10^{-1}\mathrm{Mpc}^{-1}$ and $1\mathrm{Mpc}^{-1}$, while WMAP goes from $10^{-4}\mathrm{Mpc}^{-1}$ to almost 10^{-1} Mpc^{-1}, as can be seen in Figure 4.1 from [218]. However, the Lyman α data appears to be problematic due to systematics. We will further comment on this later on.

Allowing the presence of non negligible tensor perturbations (ΛCDMr model) the results for the spectral index and its running in WMAP1 change as shown in Table 4.2. We see that in this case higher values of the running were preferred, but also the associated errors increased. The employed parameter estimation technique is explained in [225].

The data in Tables 4.1 and 4.2 come from references [217] and [218] respectively. Notice that the fiducial scale chosen differs from one table to the other. This means that one cannot compare directly the values quoted in both tables, being necessary

Table 4.2: Mean values and 68% probability level at $k = 0.002\,\mathrm{Mpc}^{-1}$ of the 1-d marginalized likelihood for the ΛCDMr model with running in WMAP1.

	WMAP	WMAPe+2dFGRS	WMAPe+2dFGRS+Lymanα
n	$1.20^{+0.12}_{-0.11}$	$1.18^{+0.12}_{-0.11}$	1.13 ± 0.08
$\frac{\mathrm{d}n}{\mathrm{d}\ln k}$	$-0.077^{+0.050}_{-0.052}$	$-0.075^{+0.044}_{-0.045}$	$-0.055^{+0.028}_{-0.029}$

to apply the adequate parameterizations to know the numbers at a different scale. There are about 3.2 efolds of inflation between the two scales quoted. The WMAP1 analysis found a 2σ marginal preference for a non zero running when the analysis is carried allowing tensor perturbations, but also without them. In particular, when tensors are considered, the data pointed towards a running index going from blue ($n > 1$) at large scales to red at small scales. This feature is not easy to reproduce in an inflationary setup. The conclusion of [218] was that more data was required to confirm such a behaviour of the CMB power spectrum. Independent analyses of WMAP first year data reaching similar conclusions about the running spectral index are [223, 224, 226]. In particular it is interesting to mention the analysis done by the SDSS team [227] which included WMAP data and was in agreement with the results of the WMAP group. There are also other statistical studies worth mentioning. For instance in [228] it was concluded (using WMAP and Lyman α data) that there was no necessity of a running spectral index from a statistical point of view. Similar arguments can be found in [229]. We will come back to the effect of Lyman α data when we talk about the three year WMAP release. For the moment, let us just mention that, on the contrary, in [230] it was argued that $\mathrm{d}n/\mathrm{d}\ln k \neq 0$ was not only allowed by WMAP1 data but was actually favoured. Finally, we want to remark that the detailed analysis procedures employed in the works cited differ from each other; and the issue of which is the best way to take into account several data sets with different systematics is rather open to discussion and still an interesting question. As we will see next, with the WMAP year three data, there seemed to be no definite statistical evidence for or against a running spectral index.

The WMAP3 analysis [219] included not only the measurements of the temperature (TT) and the temperature polarization power spectrum (TE), but also measurements of the polarization spectra. The statistical analysis techniques were improved with respect to WMAP1, particularly as regards to the data corresponding to the lowest and highest multipoles of the spectrum. WMAP3 showed that the fit to the ΛCDMr and ΛCDM models with a running spectral index was better than the one to ΛCDM assuming $\mathrm{d}n/\mathrm{d}\ln k = 0$. However, in [219] it was said that the fit improvement was not statistically significant in the sense that it did not justify the addition of new parameters beyond those of the ΛCDM model. To reach this claim a goodness of fit analysis in terms of the χ^2 estimator was performed. The conclu-

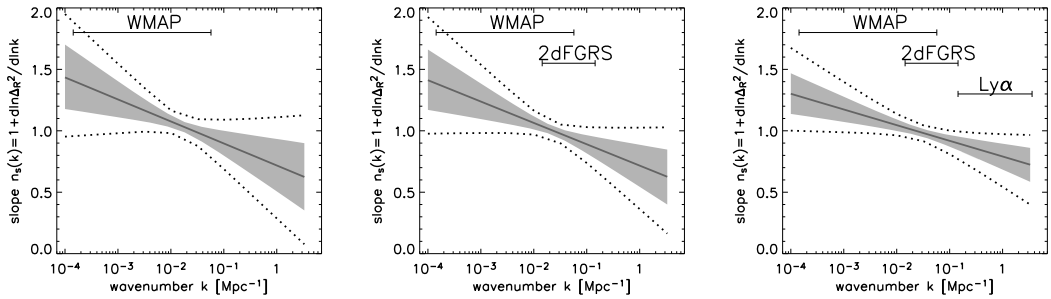

Figure 4.1: These plots from [218] show the scalar spectral index as a function of the scale for the three data sets considered in WMAP1. The mean (solid line), the 68% (shaded area) and 95% (dashed lines) intervals are shown.

sion in that work was that the data favoured numerically a large running spectral index but the evidence was not compelling. It was suggested that additional WMAP data and future small–scale CMB surveys were required to settle an answer to this question.

The numbers in Tables 4.3 and 4.4 were taken from LAMBDA, the Legacy Archive for Microwave Background Data Analysis [231] of the WMAP team. Apart from ACBAR and the latest CBI data, other new information from different surveys was used in the WMAP3 analysis that was not present in WMAP1. The most complete analysis was done for the ΛCDM model and the numbers obtained are shown in Table 4.3. Every pair $(n, \mathrm{d}n/\mathrm{d}\ln k)$ corresponds to the result of the analysis of WMAP information *and* the extra data from the surveys indicated after the '+' sign. The new surveys that were considered are SDSS, the Sloan Digital Sky Survey; BOOMERANG (Balloon Observations of Milimetric Extragalactic Radiation and Geophysics); VSA, The Very Small Array; and WL whose data comprises the results of the Canada–France–Hawaii Telescope Legacy Survey (CFHTLS) observations of weak lensing of distant galaxies [232]. The SDSS [233, 234] is a project intended to get an optical detailed map of one quarter of the entire sky and a three dimensional map of about one million galaxies and quasars. It uses a telescope in New Mexico. The information from SDSS used by the WMAP team is related to galaxy clustering observations. BOOMERANG is a balloon experiment that has flown twice around Antarctica carrying several detectors to study the CMB [235, 236]. Finally, VSA is an interferometer in Tenerife studying the CMB and capable of working on angular scales between 6 and 30 arc min and a range of multipoles between 100 and 2500 [237]. Finally, VSA is an interferometer in Tenerife studying the CMB and capable of working on angular scales between 6 and 30 arcmin and a range of multipoles between 100 and 2500 [237]. Moreover the 2dFGRS data used in the WMAP3 release increased with respect t the previous analysis [238].

The last column of Table 4.3 shows the values obtained for the combination of all data sets except WL. It is interesting to compare Tables 4.1 and 4.3, but being careful of taking into account the different fiducial scales. The first conclusion that could be drawn is that WMAP3 strengthened the evidence for a running spectral index. This is simply because adding a much wider amount of data coming from

Table 4.3: Marginalized 1-d values and 68% probability level at $k = 0.002\,\mathrm{Mpc}^{-1}$ for the ΛCDM model with running in WMAP3

	WMAP	+2dFGRS	+SDSS	+BOOM+ACBAR
n	$1.050^{+0.059}_{-0.058}$	1.034 ± 0.052	$1.056^{+0.052}_{-0.053}$	1.055 ± 0.056
$\frac{\mathrm{d}n}{\mathrm{d}\ln k}$	$-0.055^{+0.030}_{-0.035}$	-0.048 ± 0.027	-0.060 ± 0.028	-0.058 ± 0.029

	+CBI+VSA	+WL	+all (except WL)
n	1.066 ± 0.055	1.061 ± 0.048	$1.054^{+0.047}_{-0.046}$
$\frac{\mathrm{d}n}{\mathrm{d}\ln k}$	$-0.066^{+0.029}_{-0.028}$	-0.059 ± 0.025	-0.061 ± 0.023

unrelated experiments the results do not change much with respect to those of WMAP1. In fact, a detailed study of both analyses shows that the indication of a running spectral index for the ΛCDM model is statistically more significant than before. A graphical comparison between the fits with and without running to the ΛCDM model can be seen in Figure 4.2.

In Table 4.4 the results for the ΛCDMr model that came from WMAP3 can be read. This set of numbers is not as complete as the one for the ΛCDM because some of the analyses had not been done at the time that this compilation was performed. As it happened in WMAP1, we also see in WMAP3 that non negligible tensor perturbations meant higher values of the running spectral index in general. Overall, the conclusions of WMAP3 are similar to those of WMAP1. The fit to the data assuming a non zero running scalar spectral index is better than the one obtained for zero running, but according to [219] there is no significant statistical evidence in favour of a running model. In this respect it is interesting to remark that inflationary models that produce an important amount of tensor perturbations were ruled out by the data unless a scalar running spectral index is assumed, in which case they were compatible and produced a better fit to the power spectrum than a simple ΛCDM model.

The WMAP collaboration decided to exclude Lyman α data in WMAP3. In [239] such a joint analysis assuming no tensors was done with two different sets of Lyman α data that cover a redshift range of z between 2.2 and 4.2 . The result of this analysis was a very modest $\mathrm{d}n/\mathrm{d}\ln k = -0.002 \pm 0.015$ at $k = 0.002\,\mathrm{Mpc}^{-1}$, which is a much smaller running than the one of WMAP3. According to [240] the same happens when WMAP data is combined with Lyman α data from SDSS. The SDSS information used by the WMAP team in the WMAP3 analysis comes from galaxy clustering and not from Lyman α absorption lines. In [240] it was claimed that the WMAP3

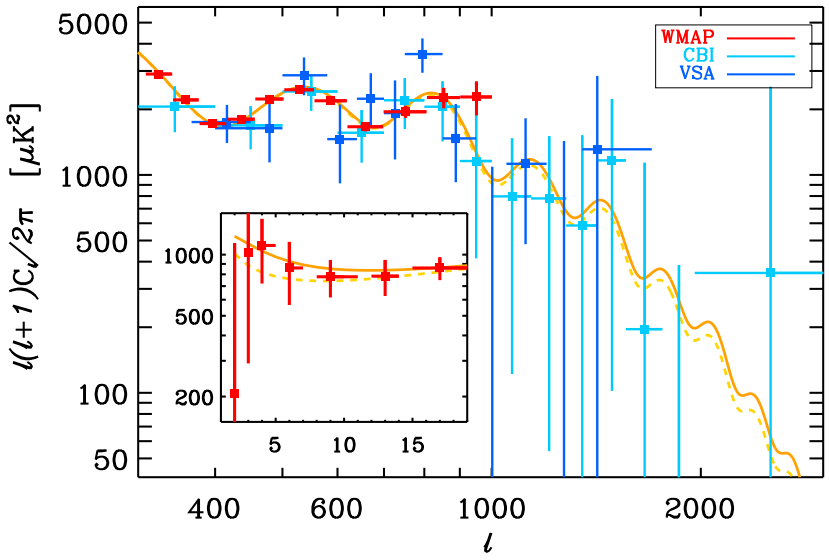

Figure 4.2: This plot from [219] shows the fits to the WMAP3, CBI and VSA power spectrum data with the ΛCDM model including a running of the scalar spectral index (dashed line) and without running (solid line). The insert for l below 20 may be interpreted as the effect of the running helping to suppress the power spectrum and therefore reproducing better the mean values of the lowest multipoles.

Table 4.4: Marginalized 1-d values and 68% probability level at $k = 0.002\,\mathrm{Mpc}^{-1}$ for the ΛCDMr model with running in WMAP3

	WMAP	+2dFGRS	+SDSS
n	1.16 ± 0.10	$1.057^{+0.066}_{-0.064}$	1.009 ± 0.043
$\frac{\mathrm{d}n}{\mathrm{d}\ln k}$	-0.085 ± 0.043	-0.042 ± 0.028	-0.024 ± 0.020

	+BOOM+ACBAR	+CBI +VSA
n	$1.157^{+0.095}_{-0.096}$	$1.167^{+0.096}_{-0.094}$
$\frac{\mathrm{d}n}{\mathrm{d}\ln k}$	-0.082 ± 0.040	$-0.090^{+0.038}_{-0.039}$

Table 4.5: Marginalized 1-d 95% confidence intervals for $1-n$ and the running at $k = 0.002\,\mathrm{Mpc}^{-1}$ for the ΛCDM model with running in WMAP5.

	WMAP	+ACBAR	+BAO+SNALL
$1-n$	$[-0.135,\ 0.075]$	$[-0.125,\ 0.063]$	$[-0.0014,\ 0.0608]$
$\frac{\mathrm{d}n}{\mathrm{d}\ln k}$	-0.037 ± 0.028	$-0.035^{+0.024}_{-0.025}$	$-0.032^{+0.021}_{-0.020}$

	BAO+SNALL+LYAPOST	CMB
$1-n$	$[-0.038,\ 0.0490]$	$[-0.154,\ 0.038]$
$\frac{\mathrm{d}n}{\mathrm{d}\ln k}$	-0.012 ± 0.012	-0.053 ± 0.025

indication of a running spectral index is just a statistical fluctuation that disappears when Lyman α data is added. There were some other relevant works after WMAP3 addressing the issue of a running spectral index through a statistical treatment of the data. In the analyses of references [241, 242] the evidence in favour of a non zero $\mathrm{d}n/\mathrm{d}\ln k$ was stronger than the one found by the WMAP team. In [148] broad groups of inflationary models were studied using WMAP3 and SDSS data; it is shown that the data was compatible with a large running and a large value of r, but it was argued that this was not statistically required, in agreement with [219]. Reference [243] is a brief summary of the situation after WMAP3. It stresses the tension between CMB and Lyman α data as regards to the inferred amplitudes of the power spectrum and how the running spectral index worsened it.

4.1.2 Status after WMAP5 and Planck forecasts

The fifth WMAP data release, together with the corresponding analysis, was in March 2008 [32,244]. In Tables 4.5 and 4.6 the results for the spectral index and its running at $k = 0.002\,\mathrm{Mpc}^{-1}$ obtained by the WMAP team are shown. These results have been extracted from LAMBDA [231]. The first numerical column in each table corresponds to WMAP5 data alone. In the other columns the data indicated after the '+' sign has also been included in the analyses. The Table 4.5 refers to the ΛCDM model and the effect of gravitational waves is accounted for in Table 4.6. The extra data sets that were considered in these analyses are the following:
– SNALL: Supernova Gold Sample [101], Legacy Survey [2] and Essence [245].
– ACBAR: The complete data set as described in [246].
– BAO: Baryonic Acoustic Oscillations [247].
– LYAPOST: Post-processing including the Lymanα forest data [240].
– CMB: Boomerang + CBI + VSA + ACBAR (2006) [248].

Table 4.6: Marginalized 1-d 95% confidence intervals for $1-n$ and the running at $k = 0.002\,\mathrm{Mpc}^{-1}$ for the ΛCDMr model with running in WMAP5.

	WMAP	+ACBAR	+BAO+SNALL
$1-n$	$[-0.250,\ 0.044]$	$[-0.232,\ 0.039]$	$[-0.256,\ 0.025]$
$\frac{\mathrm{d}n}{\mathrm{d}\ln k}$	-0.050 ± 0.034	-0.048 ± 0.027	$-0.055^{+0.027}_{-0.028}$

	BAO+SNALL+LYAPOST	CMB
$1-n$	$[-0.088,\ 0.048]$	$[-0.2890,\ 0.0047]$
$\frac{\mathrm{d}n}{\mathrm{d}\ln k}$	$-0.017^{+0.014}_{-0.013}$	$-0.072^{+0.031}_{-0.030}$

As it happened with previous data releases, the inclusion of tensors in the analysis enhances the running of the spectral index. It is remarkable that when WMAP data alone is employed in the fits, the obtained values for the running are closer to zero than in the case of the three–year release. This is interpreted in [32] as a slight increment of the power of the lower multipoles of the spectrum due to three distinct effects that have to do with having a a higher integration time, the use of an improved beam model and the resolution of the temperature data. This means that previous hints that suggested that the running is related to the lowest multipoles of the spectrum are still valid in WMAP5 data. It is concluded in [32] that no significant evidence for the running is found using CMB, baryonic acoustic oscillations and supernova data; and stressed that the allowed window for the running becomes narrower when Lyman α data is considered. Another interesting feature of the data to look at is the central value of the index at $k = 0.002\,\mathrm{Mpc}^{-1}$. The analyses of WMAP3 including a running indicated that $n-1$ was positive regardless of the inclusion of tensors. This did not occur in the case of WMAP1 and the ΛCDM with running. Looking at the intervals given in Tables 4.5 and 4.6 , we can check that this characteristic remains in WMAP5 for the two models and we can even say that is reinforced. However, including supernova and Lyman α data the effect diminishes, specially when the second of these two sets is taken into account. Indeed, we see that the effect of Lyman α , as it happened in WMAP1, tends to reduce the evidence in favour of a running spectral index. As we have said, this data set was excluded from the analysis of the year–three release. On the other hand, the inclusion of the supernova data is a new characteristic of the analysis as far as the running is concerned. It seems that as in the older WMAP analyses, the indications of a running are stronger when only CMB data is included. One may try to guess that this is because the running is more relevant for the lowest multipoles than for bigger ones, but there may be other reasons, related to the statistical treatment of the

uncertainties.

The last lines of [32] are a comment about the need of improving the determination of parameters such us the tilt of the scalar power spectrum, the running and the tensor–scalar ratio. The conclusion is that not only higher precision data are needed, in particular for constraining the running better, but also improved statistical techniques to deal, for instance, with data sets of different physical origin and different systematics. In summary, after WMAP5 the situation regarding the running of the spectral index has not changed qualitatively with respect to the previous releases. Although there is no compelling evidence in favour of its need, it is an open possibility.

It is worth mentioning the work of [249] where using a splines reconstruction technique it is found that a running of the spectral index is not required by the current data. The same conclusion is obtained in [5] with a Montecarlo Markov Chain analysis in `cosmomc`. In fact, it is pointed out there that the data are in good agreement with a Harrison–Zeldovich primordial spectrum (without running) and zero tensor amplitude.

The Planck probe [250, 251] will have the ability to handle small–scale fluctuations that are very difficult to measure with WMAP. Perhaps data coming from this mission will be able to clarify the issue of the running scalar spectral index. In practice this is so because the higher precision of Planck will effectively reduce the degeneracies between cosmological parameters to a level that will allow much more confidence in the statistical analysis. Thanks to the better determination of the CMB polarization, Planck will produce an improved determination of the tensor modes, helping to disentangle the present correlation in the data between $\mathrm{d}n/\mathrm{d}\ln k$ and r. In [252] simulated data was used to conclude by means of model selection techniques that Planck will find evidence of the running if its absolute value is larger than 0.02. In fact, it was already known that Planck would be able to detect the scale dependence of the spectral index if it is bigger than a few times 10^{-3} [145]. It will also be interesting to see how the effects depend on which fiducial scale is chosen for the analyses. If the running appears to be large it may be sensible to redo them at different scales to see how strong is the result and which variations are there in its central value. According to [253], the scale $k = 0.017\,\mathrm{Mpc}^{-1}$ minimizes the correlation between the spectral index and the running for WMAP3 data. However, this k value is further away from the lowest multipoles of the spectrum than $k = 0.002\,\mathrm{Mpc}^{-1}$, and so perhaps from that point of view it may not be the best choice if the running is really particularly affected by that region of the spectrum.

4.2 A large class of inflation models

In this section we introduce a broad group of inflationary models: those characterized by a flat inflaton scalar potential at tree level. Radiative corrections allow the slow–roll of the inflaton field by altering slightly the flatness of the potential. As we will shortly see, the values of the scalar spectral index and its running can be quite generally characterized for these models. It is important to stress that these models include as a subclass many supersymmetric hybrid inflation models.

Indeed, these potentials appear typically in supersymmetric (SUSY) theories: the tree level effective potential ordinarily has plenty of *accidental* flat directions. A familiar example of this is the Minimal Supersymmetric Standard Model (MSSM). Such accidental flatness is broken by radiative corrections since there is no symmetry protecting it.

Any of the models we are interested in is defined by a tree level potential independent of the inflaton field. This means that the slope of the inflaton potential arises from radiative corrections. Typically, at one loop order we will have:

$$V = \rho + \beta \ \ln \frac{m(\phi)}{Q} \ , \tag{4.1}$$

$$\frac{\partial \rho}{\partial \phi} = 0 \ , \tag{4.2}$$

where Q is the renormalization scale and $m(\phi)$ is a function of the inflation field with mass dimensions. The generic definition of Q that we have chosen implies that it might have absorbed a finite constant contribution which depends on the regularization scheme. Normally, $m(\phi)$ is the most relevant ϕ–dependent mass, but there could be different masses, which is a complication we will ignore for the moment. Note that ρ depends on Q through its renormalization group equation (RGE) and that the Q–invariance of the effective potential implies that

$$\beta = \frac{\mathrm{d}\rho}{\mathrm{d}\ln \mathrm{Q}} \ , \tag{4.3}$$

at one loop order.

Since these "almost flat" directions are so common in SUSY scenarios, they are natural candidates to drive inflation, provided that the potential stores large enough energy density. As a matter of fact, particular examples of these approximate flat directions have been used in the literature to implement inflation, e.g. the first D–hybrid inflation model belongs to this class [254]. See [255–258] for inflation from flat directions in the MSSM. The important point is that, whatever it is the model considered, the slope of $V(\phi)$, and thus the dynamics of inflation, are determined by radiative corrections. Since the latter have a very generic functional form (logarithmic), it is possible to make very model–independent predictions without relying on a particular model [9]. Next we work out these statements in a more detailed way.

The leading–log approximation (which amounts to summing the leading logarithmic contributions to all loops) is implemented in this context simply by taking $Q = m(\phi)$, so that

$$V(\phi) \simeq \rho(Q = m(\phi)) \ . \tag{4.4}$$

This choice eliminates the potentially large (and thus dangerous) logarithms, improving the convergence of the perturbative expansion.

Generally, $m(\phi)$ is of the form $m^2(\phi) = M^2 + c^2\phi^2$, where M does not depend on ϕ and c is some coupling constant. To make the analysis simpler we will take $M = 0$ for the time being because this is what actually happens for many hybrid

inflation models. For very small values of the inflaton field the presence of M^2 avoids an infrared logarithmic singularity. In practice, inflation ends before reaching this regime in most models. Moreover, in the hybrid models, the inflaton eventually gets a value where some waterfall fields come into play and the inflaton potential changes dramatically (stopping inflation in any case). So one can assume a purely logarithmic form of the potential during all the inflationary process before reheating. Choosing $Q = m(\phi)$ we are associating a single value of Q to a particular value of ϕ because c depends on Q according to its own RGE. With this choice of the renormalization scale we set its relationship to the inflaton by the RGEs of the model.

In the leading–log approximation

$$\frac{\mathrm{d}Q}{\mathrm{d}\phi} = \frac{Q}{\phi}\alpha = c\alpha \,, \tag{4.5}$$

where

$$\frac{1}{\alpha} \equiv 1 - \frac{\beta_c}{c}\,, \tag{4.6}$$

$$\beta_c \equiv \frac{\mathrm{d}c}{\mathrm{d}\ln Q}\,. \tag{4.7}$$

In consequence,

$$V' = \alpha\,\frac{\beta}{\phi}\,, \tag{4.8}$$

$$V'' = -\,\alpha\,\frac{\beta}{\phi^2}\left[1 - \alpha\frac{\dot\beta}{\beta} - \alpha^2\left(\frac{\dot\beta_c}{c} - \frac{\beta_c^2}{c^2}\right)\right], \tag{4.9}$$

being

$$V' \equiv \frac{\mathrm{d}V}{\mathrm{d}\phi}\,, \tag{4.10}$$

$$\dot\beta \equiv \frac{d\beta}{d\ln Q}\,. \tag{4.11}$$

We use here overdots to indicate logarithmic derivatives with respect to the renormalization scale and primes for the derivatives with respect to the inflaton field. This notation is in conflict with the one used in the previous chapter for other derivatives, but this will not be a problem since those will not appear here. Also, it will be clear from the context what primes and overdots mean.

4.2.1 Small-coupling regime

Provided that

$$\frac{\beta_c}{c} \ll 1\,, \tag{4.12}$$

α will be approximately equal to 1 and we can neglect all but the first term within the square brackets in (4.9). Then

$$\epsilon \simeq \frac{1}{2}\frac{M_p^2}{\phi^2}\left(\frac{\beta}{\rho}\right)^2\,, \qquad \eta \simeq -\frac{M_p^2}{\phi^2}\frac{\beta}{\rho} \simeq -2\left(\frac{\beta}{\rho}\right)^{-1}\epsilon\,, \qquad \xi \simeq 2\eta^2\,, \tag{4.13}$$

so $\epsilon \ll \eta$, and thus

$$n - 1 \simeq 2\eta\,. \tag{4.14}$$

The running of the spectral index with the scale will be given by:

$$\frac{\mathrm{d}n}{\mathrm{d}\ln k} \simeq -2\xi \simeq -4\eta^2 = -(n-1)^2\,. \tag{4.15}$$

From these equations we see that there are strong and model independent relations in this regime among the parameters. Obviously, $\mathrm{d}n/\mathrm{d}\ln k$ is negative, as suggested by the WMAP analysis, though its value tends to be small. In fact the sign of $n-1$ cannot change along the inflationary process, which would contradict the WMAP indication of n crossing the $n = 1$ value. The sign of $\mathrm{d}n/\mathrm{d}\ln k$ and the correlation of its absolute value with that of $n-1$ are quite model independent: they apply whenever the field dependence of the inflaton potential is well described simply by a $\ln\phi$. If the value of β changes along the inflationary course, e.g. if some threshold of extra particles is crossed, this correlation still holds except in the neighbourhood of the threshold, provided that the small–coupling regime approximation is valid everywhere else.

The previous formulas can be obtained and understood from a slightly different approach. In the regime of very small coupling constants we have

$$\frac{\mathrm{d}\beta}{\mathrm{d}\ln Q} \ll \beta\,, \tag{4.16}$$

since the former is higher order in the couplings and has a loop suppression factor. Then we can consider β as constant in the range of $Q \propto \phi$ of interest (which is never too wide). Now the scalar potential (4.4) can be easily written in terms of its value at a certain ϕ_0 in that range[1], which is the value of the inflaton related to the inverse distance scale k_0, integrating Equation (4.3):

$$V(\phi) = \rho_0 + \beta\ \ln\frac{\phi}{\phi_0}\ , \tag{4.17}$$

where $\rho_0 \equiv \rho(\phi_0)$. Clearly, (4.17) can also be obtained from (4.1) by choosing $Q = c\phi_0$.

Since $\ln\phi = \lim_{\alpha\to 0}\alpha^{-1}(\phi^\alpha - 1)$ the logarithmic potential (4.17) can be considered in many respects as a monomial potential with $\alpha = 0$. In particular all the derivatives, which are crucial for the cosmology of the model, follow that pattern. On the other hand, as argued above, this potential is physically as well motivated as the monomial forms.

The signs of the first derivative of the potential V', the slow–roll parameter η and $n-1$ are also correlated; namely

$$\mathrm{sign}(n-1) = -\mathrm{sign}\left(V'\right) = -\mathrm{sign}(\beta)\ . \tag{4.18}$$

Notice that a change in the sign of $n-1$ can only occur if V' vanishes, indicating the presence of a local extremum. Usually β is positive and therefore we naturally

[1] Notice that the meaning of the subindex '$_0$' has changed once more. Now it is associated to the fiducial scale.

expect $n < 1$. In typical hybrid inflation models [166] the field ϕ rolls towards the origin, where the true minimum of the potential is. Inflation ends either because the flatness condition gets violated below some critical value of the inflaton or because $|\eta|$ becomes of order 1. Notice that ϵ and $|\eta|$ increase as ϕ rolls to smaller values.

On the contrary, if β is negative, then $n > 1$, ϕ grows and the slow–roll parameters ϵ and η get smaller as time goes by. Inflation would not stop unless ϕ reaches some critical value where the tree level flatness ends and all the fields go to the true minimum. This is not the most common situation, but it cannot be excluded. See for instance [159, 202, 259].

In the usual case, with inflation ending because $|\eta|$ becomes of order unity, and in the absence of thresholds of new physics during the inflationary process, the number of efolds, N_e, since the beginning of inflation $t_\star$ until the end at t_e can be easily computed plugging (4.13) in equation (3.159) and is simply

$$N_e \simeq -\frac{1}{2}\left[\frac{1}{\eta(\phi_\star)} - \frac{1}{\eta(\phi_e)}\right] \simeq -\frac{1}{2\eta(\phi_\star)} \ . \tag{4.19}$$

If there are no other steps of inflation, then N_e must be roughly between 50 and 60 in order to solve the flatness and horizon problems; otherwise it could be smaller. Then, the value of the spectral index at the beginning of inflation is given by

$$n_\star \equiv n(k_\star) \simeq 1 + 2\eta(\phi_\star) \simeq 1 - \frac{1}{N_e} \ , \tag{4.20}$$

which means $n_\star \lesssim 0.98$, with the approximate equality valid for $N_e = 60$. For a given value of the quotient β/ρ this also fixes the initial value $\phi_\star$ through (4.13). In addition, we can use (4.20) to write equation (4.15) in an integrated form as

$$n = 1 - \frac{1}{N_e - \ln(k/k_\star)} \ . \tag{4.21}$$

For later use, it is convenient to rewrite the previous expression in terms of the initial value of the spectral index, given by equation (4.20), as

$$n = n_\star + \frac{1}{N_e} - \frac{1}{N_e - \ln(k/k_\star)} \ . \tag{4.22}$$

This is also true for the $\beta < 0$ (and thus $n > 1$) case.

Finally, note that there is no problem in reproducing the observed scalar power spectrum; for a given value of β/ρ, this can be achieved with an appropriate value of ρ, according to equation (3.219).

In summary, in the small-coupling regime the predictions of tree level flat inflation models (including many hybrid inflation models) concerning the size and running of the spectral index are quite neat and model independent.

4.2.2 The regime of not-so-small coupling

If the β functions are positive as usual, the couplings grow in the ultraviolet and there will be a scale where the second and third terms within the square brackets in

(4.9) will compete with the first one. Since they naturally have the opposite sign, one can expect that at sufficiently high energy scales (which means initial stages of inflation) the sign of $n-1$ may get positive, which therefore could account for the indication of WMAP. Notice in particular that, since equation (4.13) for η is not a valid approximation anymore, the previous correlation (4.18) between the signs of V' and η does not hold, which allows η to pass from positive to negative values without the presence of an extremal point of the potential V. This behaviour is completely natural, and even unavoidable in this regime. However, reproducing the WMAP indication on the running spectral index *and* the other physical requirements at the same time (in particular, a sufficient number of efolds) is not simple. This is something we will carefully check in the next section.

The running of the spectral index can still be computed, taking into account that, as long as $\beta/\rho \ll 1$, then $\epsilon \ll |\eta|$ (except within the close neighborhood of the point where η vanishes), so $n \simeq 1 + 2\eta$, and

$$\frac{\mathrm{d}n}{\mathrm{d}\ln k} \simeq 2\frac{\mathrm{d}\phi}{\mathrm{d}\ln k}\frac{\mathrm{d}\eta}{\mathrm{d}\phi} = -2M_p\sqrt{2\epsilon}\frac{\mathrm{d}\eta}{\mathrm{d}\phi} \ , \tag{4.23}$$

where $\mathrm{d}\eta/\mathrm{d}\phi$ can be straightforwardly evaluated using the whole expression for η from (4.9), taking into account the dependence on ϕ through the one on Q with the help of equation (4.5). Similarly, the number of efolds is computed using equations (3.159, 4.8). In the next Section we will show explicit expressions for these quantities in a concrete case.

4.3 A detailed example, D–term inflation

In the previous Section we claimed that, within the hybrid inflation framework, it is natural to expect a running spectral index, even crossing the $n = 1$ value, if the scale of the initial stages of inflation is high enough. Now we will explicitly show that this is the case in a popular example of hybrid inflation, namely the first example of hybrid D–term inflation, proposed by Binétruy and Dvali [254].

We will use a notation similar to that of [202] where the superpotential is written in the following way

$$W = \Phi(\lambda H_+ H_- - \mu^2) \ , \tag{4.24}$$

with a tadpole for the chiral superfield Φ. The quantities λ and μ^2 are real constants and H_+, H_- are chiral superfields, charged under a U(1) gauge group with gauge coupling g. The corresponding charges are ± 1 for $H_\pm$ (and 0 for Φ). The associated tree level scalar potential is given by

$$V_0 = V_F + V_D, \tag{4.25}$$

with

$$\begin{aligned} V_F &= \left|\lambda H_+ H_- - \mu^2\right|^2 + \lambda^2\left(|H_-|^2 + |H_+|^2\right)|\Phi|^2 \ , \\ V_D &= \frac{g^2}{2}\left(|H_+|^2 - |H_-|^2 + \xi_D\right)^2 \ , \end{aligned} \tag{4.26}$$

being ξ_D a Fayet–Iliopoulos term. The fields in these expressions are the scalar components of the chiral superfields.

The global minimum of the potential is supersymmetric ($V_F = 0\,,\ V_D = 0$) and occurs at

$$\Phi = 0\,, \tag{4.27}$$

$$2|H_\pm|^2 = \mp\xi_D + \sqrt{\xi_D^2 + 4\frac{\mu^4}{\lambda^2}}\,. \tag{4.28}$$

However, for large enough $|\Phi|$, i.e.

$$|\Phi|^2 > |\Phi_c|^2 = \frac{1}{\lambda^2}\Delta\ , \quad \Delta \equiv \sqrt{g^4\xi_D^2 + \lambda^2\mu^4}\ , \tag{4.29}$$

the potential has a minimum at $H_\pm = 0$ and is flat in Φ. This flat direction[2] is two dimensional because $\Phi = (\phi_R + i\phi_I)/\sqrt{2}$ is a complex superfield. In the following, we will examine the potential along the real part $\phi \equiv \phi_R$. All our results would be the same along any other radial direction. It is in this flat region where inflation takes place. The tree level potential during this period is simply

$$V_0 \equiv \rho = \mu^4 + \frac{1}{2}g^2\xi_D^2\ . \tag{4.30}$$

And the one loop correction is given by

$$\Delta V_1 = \frac{1}{32\pi^2}\sum_{i=\pm}\left[\tilde{m}_i^4 \ln\frac{\tilde{m}_i^2}{Q^2} \ - \ m_i^4 \ln\frac{m_i^2}{Q^2}\right]\ , \tag{4.31}$$

where m_i^2 and $\tilde{m}_i^2$ are the ϕ–dependent square masses of the fermionic and scalar components of the H_+ and H_-superfields respectively:

$$m_\pm^2 = m^2(\phi) \equiv \frac{1}{2}\lambda^2\phi^2\ , \qquad \tilde{m}_\pm^2 = m^2(\phi) \pm \Delta\ . \tag{4.32}$$

In practice, $\tilde{m}_\pm^2$ is dominated by the $m^2(\phi)$ contribution. To see this, notice that the condition $m^2(\phi) = \Delta$, which is equivalent to $\tilde{m}_-^2 = 0$, precisely corresponds to the point $\phi = \phi_c$, below which the flatness of the potential breaks down and inflation cannot continue. Since the number of efolds goes roughly as ϕ^2, most of the efolds are produced at larger (usually much larger) values of ϕ^2, where $m^2(\phi) \gg \Delta$. This is particularly true in the region of interest for us, i.e. the initial stages of inflation. Furthermore, as we will see below, inflation ordinarily ends before $\phi^2 = \phi_c^2$, namely when $|\eta|$ becomes of order 1, which normally occurs at $\phi^2 \gg \phi_c^2$. In consequence, ΔV_1 can be written as

$$\Delta V_1 = \frac{1}{8\pi^2}\Delta^2 \ln\frac{m(\phi)}{Q} \ + \ \mathcal{O}\left(\frac{\Delta^2}{m^4(\phi)}\right)\ , \tag{4.33}$$

so $V = V_0 + \Delta V_1$ is of the generic form shown in equation (4.1).

[2]It is normal usage to speak about flat directions for spaces of dimensionality higher than 1.

The various β–functions, defined as derivatives with respect to $\ln Q$, are given by

$$\beta = \frac{1}{8\pi^2}\Delta^2 , \tag{4.34}$$

$$\beta_g = \frac{1}{8\pi^2}g^3 , \tag{4.35}$$

$$\beta_\lambda = \frac{1}{16\pi^2}\lambda(3\lambda^2 - 4g^2) , \tag{4.36}$$

$$\beta_{\mu^2} = \frac{1}{16\pi^2}\lambda^2\mu^2 , \tag{4.37}$$

$$\beta_{\xi_D} = 0 . \tag{4.38}$$

For example $\beta \equiv \mathrm{d}V/\mathrm{d}\ln Q$.

In the leading–log approximation the radiatively corrected potential is simply given by ρ evaluated at the scale $Q = m(\phi) = \lambda\phi/\sqrt{2}$; in the notation of Section 4.2, $c \equiv \lambda/\sqrt{2}$. As we have already mentioned, the end of inflation occurs at $\phi_{\rm end} = \mathrm{Max}\{\phi_c, \phi_\eta\}$, where ϕ_c marks the end of tree level flatness and is given in equation (4.29); and ϕ_η approximately corresponds to the point where $|\eta| \simeq 1$. Using equation (4.13) to make an estimate one can check that

$$\phi_\eta^2 \simeq M_p^2\frac{\beta}{\rho} , \tag{4.39}$$

and therefore $\phi_c < \phi_\eta$ is satisfied for a wide range of the parameters so normally inflation would end when $|\eta| \simeq 1$.

A successful inflationary process, consistent with the WMAP constraints for a running spectral index, should satisfy the following requirements:

i) At least produce about 50 or 60 efolds of inflation.

ii) A correct amplitude of primordial perturbations as measured at the fiducial scale, that we choose $k_0 = 0.002\ \mathrm{Mpc}^{-1}$,

iii) A running spectral index with $n - 1$ passing from positive to negative during the very first few efolds of inflation, with $-\mathrm{d}n/\mathrm{d}\ln k \simeq 0.05$.

It is worth to remark that the condition ***i)*** can be relaxed if there are several steps of inflation. In such a situation about 7 or 10 efolds, which is the range covered by WMAP with the optional complement of additional observations, can be acceptable. In any case we will examine the possibilities of fulfiling the conditions as we have stated them.

If g and λ are small, β remains essentially constant (and positive) during inflation. Then the results of Section 4.2.1 apply. In particular $n < 1$, with a slight running $\mathrm{d}n/\mathrm{d}\ln k < 0$, as given by equations (4.15), (4.20) and (4.21). According to that discussion, it is not possible in this regime to achieve condition *iii)*, i.e. a running spectral index crossing through $n = 1$. In consequence we will focus for the rest of this section in the case of more sizable coupling constants.

Let us first verify that the slow–roll conditions are satisfied using equations (4.8) and (4.9). Taking into account that α is of order 1 and that $\dot{\beta}$ is at most of the order of β, it is clear that $\eta \simeq M_p^2\beta/\rho\phi^2$ and $\epsilon \simeq \eta\beta/\rho$. Therefore both ϵ and $|\eta|$ will be much smaller than 1 as long as

$$\frac{\beta}{\rho} \ll \frac{\phi^2}{M_p^2} \,, \tag{4.40}$$

which naturally leads to $\beta \ll \rho$ because inflation will normally happen below M_p. A simple way of guaranteeing the slow–rolling of the inflaton is taking

$$\frac{g^2}{\lambda^2} \ll \frac{\mu^4}{g^2\xi_D^2} \ll \frac{1}{2} \,, \tag{4.41}$$

which means that β is dominated by the Yukawa contribution:

$$\beta \approx \frac{\lambda^2\mu^4}{8\pi^2} \,, \tag{4.42}$$

and ρ is dominated by the D–term (Fayet-Iliopoulos) contribution:

$$\rho \approx \frac{1}{2}g^2\xi_D^2 \,. \tag{4.43}$$

Imposing (4.41) is by no means the only way of satisfying the slow–roll conditions, but it is particularly simple and useful for a clear analytic discussion. We have checked that reversing the inequalities in (4.41) would also provide slow–roll but this does not allow to get an initial spectral index above 1. Actually, it is important to note that once global supersymmetry is promoted to supergravity, requiring the second inequality of (4.41) is mandatory for almost any form of the Kähler potential. The reason is the well known $\eta-$problem, i.e. the appearance of a mass term for the inflaton of the order of H^2 (making η of order 1) if $V \simeq V_F$. However, it is remarkable that for the superpotential of this model (4.24) and a minimal Kähler potential, $K = |\Phi|^2$, no such mass term is generated due to an amusing cancellation of contributions.

Using this dominance of the Yukawa coupling, we can evaluate ϵ and η from equations (4.8) and (4.9):

$$\begin{aligned} \epsilon &= \frac{1}{2}\alpha^2\frac{M_p^2}{\phi^2}\left(\frac{\beta}{\rho}\right)^2 \,, \\ \eta &= \alpha\frac{M_p^2}{\phi^2}\frac{\beta}{\rho}\left[-1+\frac{\lambda^2}{2\pi^2}\left(\alpha+\frac{9}{32}\frac{\lambda^2}{2\pi^2}\alpha^2\right)\right] \,, \end{aligned} \tag{4.44}$$

with

$$\frac{1}{\alpha} = 1 - \frac{\beta_\lambda}{\lambda} = 1 - \frac{3\lambda^2}{16\pi^2} \,. \tag{4.45}$$

As announced in the previous section, there is a scale, say Q_0, at which $\eta \simeq 0$ and $n-1$ changes from positive to negative. Using (4.44), the corresponding value of

λ, that we denote $\lambda_0 \equiv \lambda(Q_0)$, turns out to be independent of the other parameters of the model, namely

$$\frac{\lambda_0^2}{(4\pi)^2} = \frac{1}{15}(7 - \sqrt{34}) \simeq 0.078 \ . \tag{4.46}$$

The coupling λ_0 is quite sizable ($\lambda_0 \simeq 3.51$), but well within the perturbative range since $\lambda_0^2/(4\pi)^2 \ll 1$. It is perfectly possible that Q_0 is crossed during the first few efolds after the beginning of inflation at $t_\star$ (recall $Q = \lambda\phi/\sqrt{2}$), so that this hybrid inflation model (and in principle any tree level flat inflationary model as well) is able to implement the crossing of the spectral index through $n = 1$ at small k. However, to reproduce the suggested value of $\mathrm{d}n/\mathrm{d}\ln k$ *and* a sufficient number of efolds at the same time is not that easy, as we show next.

From (3.159), the number of efolds between Q_0 and the end of inflation can be written as

$$\begin{aligned} N_e^0 &= \frac{1}{M_p^2}\int_{Q^2_{\rm end}}^{Q_0^2} \frac{1}{\alpha^2\lambda^2}\frac{\rho}{\beta} dQ^2 \\ &\simeq -\frac{64\pi^4}{3}\vartheta_0\lambda_0^{2/3}\exp\left[\frac{16\pi^2}{3\lambda_0^2}\right]\int_{1/\lambda^2_{\rm end}}^{1/\lambda_0^2} x^{7/3}\left(1 - \frac{3}{16\pi^2 x}\right)^2 \exp\left[-\frac{16\pi^2 x}{3}\right] dx \\ &\simeq 0.303\ \vartheta_0 = 1.818\ \frac{Q_0^2 H^2}{\mu_0^4}\,, \end{aligned} \tag{4.47}$$

with

$$\vartheta_0 \equiv \left[\frac{Q_0^2}{M_p^2}\frac{g^2\xi_D^2}{\mu_0^4}\right] \ ; \tag{4.48}$$

and $\mu_0 = \mu(Q_0)$. In the first line we have performed a change of variable $\phi \to Q^2$ with respect to the expression (3.159). In the second line we have changed variables once more, $Q^2 \to x = 1/\lambda^2$, neglecting the contributions to the RGEs of λ and g^2 that are proportional to g^2 as well as the μ^4 contribution to ρ, according to the assumption (4.43). Finally, in the last line we have taken into account that the contribution to the integral coming from small values of λ is negligible, so we have imposed $\lambda_{\rm end} = 0$. Substituting λ_0 by the value quoted in (4.46) and evaluating the integral numerically the final result turns out to be a very good approximation, provided (4.41) is fulfiled. Notice that, since the point Q_0 (i.e. where $n = 1$) should be crossed after the first few efolds of inflation, N_e^0 should be roughly 50 (unless there are subsequent episodes of inflation, in which case it could be much smaller).

The running $\mathrm{d}n/\mathrm{d}\ln k$ can be directly computed using (3.224). It gets a particularly simple form when evaluated at the scale Q_0, where $\eta = 0$ and $n \simeq 1$:

$$\begin{aligned} \left.\frac{dn}{d\ln k}\right|_{Q_0} &= -\frac{3}{4}\lambda_0^4\alpha_0^5(3\alpha_0 - 1)\left(\frac{\lambda_0^2}{4\pi^2}\right)^4 \vartheta_0^{-2} \\ &\simeq -11.85\,\vartheta_0^{-2} = -0.33\left(\frac{Q_0^2H^2}{\mu_0^4}\right)^{-2}\,, \end{aligned} \tag{4.49}$$

where we have used (4.46) for the numerical estimate.

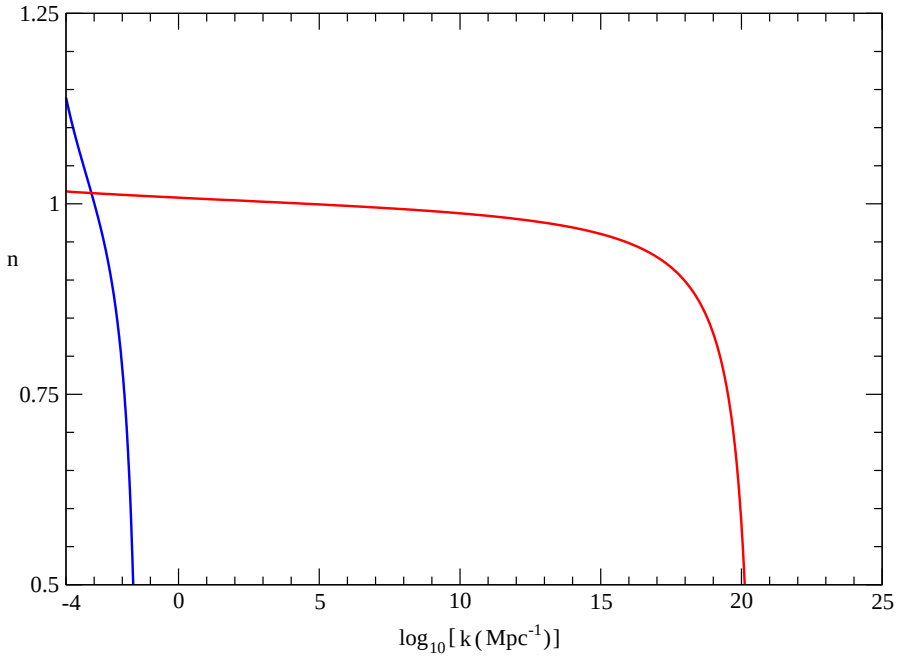

Figure 4.3: Scalar spectral index as a function of $\log_{10}[k(\mathrm{Mpc}^{-1})]$ for the inflaton potential of equations (4.30) and (4.31) for two different choices of parameters: one to get right N_e and the other to get right $\mathrm{d}n/\mathrm{d}\ln k$.

Clearly, N_e^0 and $dn/d\ln k|_{Q_0}$ depend on the same combination of parameters, namely ϑ_0, and it turns out that the product $(N_e^0)^2(dn/d\ln k|_{Q_0})$ is independent of them

$$-(N_e^0)^2 \left.\frac{dn}{d\ln k}\right|_{Q_0} \simeq 1.1 \ . \tag{4.50}$$

This constraint makes it impossible to satisfy $-dn/d\ln k|_{Q_0} \simeq 0.05$ and $N_e^0 \simeq 50$ simultaneously. However $N_e^0 \simeq 5$ is perfectly possible, which means that the model can account for the WMAP indications in favour of a running, provided there exist subsequent episodes of inflation.

The previous behaviour is illustrated in Figure 4.3 which gives the spectral index n as a function of the scale wavenumber k. The flat red curve (corresponding to $g_\star = 0.02$, $\lambda_\star = 4$, $\mu_\star^2 = (3.6 \times 10^{-4} M_p)^2$, $\xi_D = (1.2 \times 10^{-2} M_p)^2$, $\phi_\star = 0.28 M_p$) is able to accommodate a large $N_e \simeq 57$ but has very small running. The steep blue curve instead (with the same parameters except for $\mu_\star^2 = (1.9 \times 10^{-3} M_p)^2$ and $\xi_D = (3.6 \times 10^{-2} M_p)^2$) has a sizable $\mathrm{d}n/\mathrm{d}\ln k|_\star \simeq -0.075$ but fails to give enough efolds: $N_e \simeq 7$. There is no problem to obtain the amplitude of the observed scalar power spectrum.

From Equation (3.219) we find:

$$\Delta^2_{\mathcal{R}}\big|_{Q_0} = \frac{4\pi^2}{3}\frac{1}{\alpha_0^2\lambda_0^6}\frac{(g^2\xi_D^2)^2}{M_p^4\mu_0^4}\vartheta_0$$
$$\simeq 4.14\times 10^{-4}\frac{(g^2\xi_D^2)^2}{M_p^4\mu_0^4}\vartheta_0 = 0.089\frac{H^4}{\mu_0^4}\left(\frac{Q_0^2H^2}{\mu_0^4}\right). \qquad (4.51)$$

If we fix ϑ_0 in order to get the running or the number of efolds conveniently, it is always possible to vary the parameters of the model so that the prefactor of (4.51) changes to fit the observed amplitude of the power spectrum at Q_0.

It is worth mentioning that the fiducial scale in [218], $k_0 = 0.002$ Mpc^{-1} (which corresponds to roughly 3 efolds after the beginning of inflation) approximately coincides with the stage at which $n \simeq 1$ (i.e. when $Q = Q_0$). This is a fortunate circumstance to perform rough estimates.

In summary, the simple hybrid inflation model of [254], in the small–coupling regime, produces the general results shown in Section 4.2.1, with very clean predictions, in particular $n < 1$ with a mild $\mathrm{d}n/\mathrm{d}\ln k < 0$ running. In the regime of sizable couplings, the model can account for the scalar power spectrum at the fiducial scale and a running spectral index crossing $n = 1$ at a suitable scale with the suggested slope, $\mathrm{d}n/\mathrm{d}\ln k \simeq -0.05$; *or* an adequate number of efolds. Choosing to fit properly the running of the spectral index means that the corresponding number of efolds is rather small, so this model would require other inflationary episodes.

This analysis can be generalized for an arbitrary number of pairs of $H_\pm$ fields, using the formulas given in Section 4.4. The results do not change much, except for the fact that the value of λ_0 scales as $1/\sqrt{N}$. Also, the right hand side of equation (4.50) depends slightly on the value of N but is always $\lesssim 1.1$.

One cannot exclude the possibility that other flat tree level models were able to reproduce a large running of the spectral index without the above limitation for the number of efolds. To achieve this it would be required a sizable η at a high scale, so that the spectral index ran appreciably in the first stages of inflation, *and* small ϵ at lower scales, so that a sufficient number of efolds is produced. This implies that β (and thus the relevant coupling constants) should evolve from sizable values at high scale to substantially smaller values at lower scales. The faster such evolution, the easier to accomplish both requirements. Since this evolution is a result of the renormalization group running, one can imagine scenarios where it is speeded up. For example, if some threshold of new physics is crossed in the inflationary course, the β–functions may suffer quick changes, as desired. However the analysis has to be done carefully to eliminate spurious effects, as we shall see. On the other hand, the existence of new physics can have even more interesting implications. In forthcoming sections we analyze the various effects of thresholds of new physics in the inflationary process.

4.4 Adding flavours in D–term inflation

We consider here the same hybrid-inflation model of Section 4.3, with $N+1$ pairs of $H_\pm$ fields, instead of the unique pair of the original model. The results have interest

on their own (e.g. they illustrate how the values of the coupling constants and the speed of running are affected by the number of flavours), but they are also useful to illustrate the threshold-crossing procedure discussed in Section 4.5.

The superpotential reads now

$$W = \Phi \left(\sum_{a=1}^{N+1} \lambda_a H_+^a H_-^a - \mu^2 \right) \ , \tag{4.52}$$

where λ_a are the $N+1$ Yukawa couplings. As in the $N=0$ case, $H_\pm^a$ have charges ± 1 with respect to the $U(1)$ gauge group with gauge coupling g and Fayet-Iliopoulos term ξ_D. The tree level scalar potential is given by $V_0 = V_F + V_D$, with

$$\begin{aligned} V_F &= \left| \sum_a \lambda_a H_+^a H_-^a - \mu^2 \right|^2 + \sum_a \lambda_a^2 \left(|H_-|^2 + |H_+|^2 \right) |\Phi|^2 \ , \\ V_D &= \frac{g^2}{2} \left[\sum_a \left(\left|H_+^a\right|^2 - \left|H_-^a\right|^2 \right) + \xi_D \right]^2 \ . \end{aligned} \tag{4.53}$$

Again, the global minimum of the potential is supersymmetric ($V_F = 0$, $V_D = 0$), but for large enough $|\Phi|$ the potential has a minimum at $H_\pm^a = 0$ and is flat in ϕ. The tree level potential in this region is

$$\rho = \mu^4 + \frac{1}{2} g^2 \xi_D^2 \ . \tag{4.54}$$

The β–functions, defined as derivatives with respect to $\ln Q$, are given by the following set of formulas

$$\beta_g = \frac{1}{8\pi^2} (N+1) g^3 \, , \tag{4.55}$$

$$\beta_{\lambda_a} = \frac{1}{16\pi^2} \lambda_a \left[3\lambda_a^2 + \sum_{b \neq a} \lambda_b^2 - 4g^2 \right] \ , \tag{4.56}$$

$$\beta_{\mu^2} = \frac{1}{16\pi^2} \sum_{a=1}^{N+1} \lambda_a^2 \mu^2 \, , \tag{4.57}$$

$$\beta_\rho = \frac{1}{8\pi^2} \left[(N+1) g^4 \xi_D^2 + \sum_{a=1}^{N+1} \lambda_a^2 \mu^4 \right] \ , \tag{4.58}$$

$$\beta_{\xi_D} = 0 \, . \tag{4.59}$$

For simplicity we can take the same Yukawa coupling $\lambda_a = \lambda$ for all $\{H_+^a, H_-^a\}$ pairs, which is a stable condition under renormalization group evolution.

4.5 Thresholds crossed in the inflationary process

Let us suppose that the inflaton potential is flat at tree level and the 1–loop radiative correction, ΔV_1, contains contributions from states with different masses. This

generalizes the situation discussed in Section 4.2. To be concrete, consider two types of particles with masses $m(\phi)$ and $M(\phi)$ satisfying $m(\phi) \ll M(\phi)$. The 1–loop effective potential reads

$$V(\phi) = \rho(Q) + \beta_l \ln \frac{m(\phi)}{Q} + (\beta_h - \beta_l) \ln \frac{M(\phi)}{Q} \ . \tag{4.60}$$

As always, the tree level potential depends implicitly on Q through its RGE. The definition of β_h is such that it represents the running of ρ in the full theory, while β_l is the corresponding $\beta-$function when only the light particles are present. Generically,

$$m^2(\phi) = m^2 + c^2\phi^2 \,, \tag{4.61}$$
$$M^2(\phi) = M^2 + C^2\phi^2 \,, \tag{4.62}$$

where m and M do not depend on ϕ, and c and C are coupling constants.

This kind of potential allows us to focus on the interesting situation in which the scale of inflation crosses the threshold M where the heavier particles decouple. In this case one needs a reliable prescription to evaluate $V(\phi)$ above and below the threshold. In particular one should take care of potentially large logarithms in (4.60) and higher order corrections to it. In the case of just one type of mass, say $m(\phi)$, this can be achieved by choosing $Q = m(\phi)$, so that the unique logarithm in the radiative correction cancels and $V(\phi) = \rho[Q(\phi)]$. This corresponds to summing up the leading–log contributions in V to all loops. This simple procedure is not possible here because of the two different logs in (4.60).

A convenient approach is to perform the integration of the RGEs in an effective theory framework. To this end, we consider two different regions for the potential. In the high energy region, when $\{Q, m(\phi)\} \geq M$, the potential, V_{high}, is as written in (4.60), with RGEs including the virtual effects of the heavy states. In the low energy region, defined by $\{Q, m(\phi)\} \leq M$, the potential, V_{low}, is defined by dropping the contribution from the heavy multiplets to the potential and to all RGEs. For this procedure to be consistent we have to match the high and low energy potentials, i.e. we have to add a piece $\delta_{th}V_{low}(\phi)$ to V_{low} to guarantee $V_{low} = V_{high}$ at $Q = M$. In this way one gets

$$V_{low}(\phi) = \rho(Q) + \beta_l \ln \frac{m(\phi)}{Q} \ + \ \delta_{th}V_{low}(\phi), \tag{4.63}$$

where ρ runs with the low energy RGE, i.e. with β_l, and

$$\delta_{th}V_{low}(\phi) = \left.(\beta_h - \beta_l)\right|_M \ln \frac{M(\phi)}{M} \ , \tag{4.64}$$

where the subscript M means that the quantity within the parenthesis is evaluated at $Q = M$.

The additional piece $\delta_{th}V_{low}(\phi)$ could be expanded in powers of ϕ/M if desired: one would get ϕ operators suppressed by inverse powers of M, which is the reason why one can discard such high energy remnants when interested in low energy physics well below the threshold. However we keep here the whole expression as we are also interested in the potential for values of ϕ in the neighbourhood of the threshold.

Actually a correct treatment of that region is crucial for a reliable analysis. Notice for instance that since ϵ goes as $1/\phi$ most of the efolds in the energy region below $Q = M$ are produced precisely near that threshold. The inclusion of the $\delta_{th}V_{low}(\phi)$ contribution usually increases ϵ, therefore decreasing (importantly) the number of low–energy efolds, and should not be neglected.

The next step is to make a judicious choice of the renormalization scale Q. The simplest option is to take $Q(\phi) = m(\phi)$, which works well in both energy regimes (meaning that the explicit logarithms are never large). After doing that we get the following expressions for the potential in the two regions:

$$\begin{aligned} V_{high}(\phi) &= \rho[Q(\phi)] + (\beta_h - \beta_l) \ln \frac{M(\phi)}{m(\phi)} \ , \\ V_{low}(\phi) &= \rho[Q(\phi)] + (\beta_h - \beta_l)|_M \ln \frac{M(\phi)}{M} \ . \end{aligned} \tag{4.65}$$

As a matter of fact, the previous approximation may not be as good as we wish in some cases, for example when the coupling constants involved are not small enough. In particular, although V in (4.65) is continuous across the threshold by construction, the derivatives V', V'' (and thus ϵ and η) are not. This is an spurious effect which is conveniently smeared out when the approximation is improved. This can be done by including higher–loop corrections to the effective potential. Indeed, without any further calculations, one can obtain the leading–log corrections at arbitrary loop order by using the Q–invariance of the potential. In particular, at two–loop leading–log (2LL) the potential reads

$$\begin{aligned} V^{2LL}(\phi) &= \rho(Q) + \beta_l \ln \frac{m(\phi)}{Q} + (\beta_h - \beta_l) \ln \frac{M(\phi)}{Q} \\ &+ \frac{1}{2}\dot{\beta}_l \left[\ln \frac{m(\phi)}{Q}\right]^2 + \frac{1}{2}\left(\overset{\circ}{\beta}_h - 2\,\overset{\circ}{\beta}_l + \dot{\beta}_l\right)\left[\ln \frac{M(\phi)}{Q}\right]^2 \\ &+ \left(\overset{\circ}{\beta}_l - \dot{\beta}_l\right) \ln \frac{m(\phi)}{Q} \ln \frac{M(\phi)}{Q} \ , \end{aligned} \tag{4.66}$$

where the circle (dot) indicates $\mathrm{d}/\mathrm{d}\ln Q$ in the high (low) energy region.

Redoing the decoupling and matching procedure at the same scale $Q = M$, the corresponding expressions for V^{2LL} in the high and low energy regions read

$$\begin{aligned} V^{2LL}_{high}(\phi) &= \rho[Q(\phi)] + (\beta_h - \beta_l) \ln \frac{M(\phi)}{m(\phi)} + \frac{1}{2}\left(\overset{\circ}{\beta}_h - 2\,\overset{\circ}{\beta}_l + \dot{\beta}_l\right)\left[\ln \frac{M(\phi)}{m(\phi)}\right]^2 \ , \\ V^{2LL}_{low}(\phi) &= \rho[Q(\phi)] + (\beta_h - \beta_l)|_M \ln \frac{M(\phi)}{M} + \frac{1}{2}\left(\overset{\circ}{\beta}_h - 2\,\overset{\circ}{\beta}_l + \dot{\beta}_l\right)\Big|_M \left[\ln \frac{M(\phi)}{M}\right]^2 \\ &+ \left(\overset{\circ}{\beta}_l - \dot{\beta}_l\right)\Big|_M \ln \frac{m(\phi)}{M} \ln \frac{M(\phi)}{M} \ . \end{aligned} \tag{4.67}$$

The V', V'' derivatives are straightforward to evaluate by taking into account the $\phi-$dependence of the scale.

An alternative procedure, starting with the one–loop initial potential (4.60), to incorporate the leading-log corrections at arbitrary order is to perform the decoupling at the $\phi-$dependent scale $M(\phi)$ (which leaves no threshold corrections) and

then evaluate the potential at the $m(\phi)$ scale. In this way one obtains expressions for the potential in the high and low energy regions which coincide with those of the previous procedure. Concretely, collecting the 2–loop leading–log contributions one exactly recovers the result (4.67).

To illustrate this general scheme of constructing the effective potential across thresholds of new particles, let us consider again the simple hybrid inflation model of Section 4.3, but now with N additional pairs of $\{H_+, H_-\}$ fields with invariant mass M as described in Section 4.4 . The superpotential of the full (high–energy) theory reads

$$W = \Phi\left(\sum_{a=1}^{N+1} \lambda H_+^a H_-^a - \mu^2\right) \; + \; \sum_{a=2}^{N+1} M H_+^a H_-^a \; , \tag{4.68}$$

where, for simplicity, we have taken equal Yukawa couplings for all the $\{H_+, H_-\}$ pairs. For large enough $|\Phi|$ the tree level potential is flat, having the same form as in equation (4.30)

$$V_0 \equiv \rho = \mu^2 + \frac{1}{2} g^2 \xi_D^2 \; . \tag{4.69}$$

The 1–loop effective potential has the form (4.60) up to suppressed corrections with

$$m^2(\phi) = \frac{1}{2}\lambda^2\phi^2 \; , \qquad M^2(\phi) = M^2 + \frac{1}{2}\lambda^2\phi^2, \tag{4.70}$$

where $\phi = \sqrt{2}\,\mathrm{Re}\;\Phi$ and

$$\beta_l = \frac{1}{8\pi^2}\Delta^2 \; , \qquad \beta_h = \frac{1}{8\pi^2}(N+1)\Delta^2 \; , \tag{4.71}$$

with

$$\Delta = \sqrt{g^4\xi_D^2 + \lambda^2\mu^4}\,. \tag{4.72}$$

Using the above RGEs, we can also include the two–loop leading-log corrections, simply making use of the general expressions (4.60) and (4.66):

$$\begin{aligned} V(\phi) \;&=\; \rho(Q) + \frac{1}{8\pi^2}\Delta^2(L_m + N L_M) \\ &+\; \frac{1}{(8\pi^2)^2}\left\{\lambda^4\mu^4\left[2L_m^2 + 2N L_M L_m + N(N+1)L_M^2\right] - 2\lambda^2 g^2\mu^4(L_m^2 + N L_M^2)\right. \\ &\qquad \left. + \; g^6\xi_D^2(2L_m^2 + N L_m L_M + N^2 L_M^2)\right\} \; , \end{aligned} \tag{4.73}$$

where we have used the shorthand notation $L_m = \ln[m(\phi)/Q]$ and $L_M = \ln[M(\phi)/Q]$. We have explicitly checked that this potential agrees with the one obtained by using the expressions for the two–loop potential of generic supersymmetry given in [260], which can also be used to add subleading logs and finite corrections.

The expressions for the potential above and below the threshold M can be easily obtained following the effective approach described above. More precisely, one can write the potential in the high and low energy regions up to 1–loop or 2–loop leading

log order using equations (4.65) and (4.67) respectively. The $\dot{\beta}_{l,h}$ and $\overset{\circ}{\beta}_{l,h}$ derivatives for the latter can be easily extracted from (4.73) (by comparison with (4.66)), or calculated using the β–functions for the various parameters of the model involved in the expressions (4.71), which are given by equations (4.35–4.37) for the low–energy region and by equations (4.55–4.57) for the high–energy one.

The results are somewhat better than in the case without thresholds analyzed in Section 4.3 . Nevertheless the conclusions are basically the same: The number of efolds and the slope of the spectral index are correlated by an equation similar to (4.50), so it is not possible to get $\mathrm{d}n/\mathrm{d}\ln k \simeq (-0.05)$ and $N_e \simeq 60$ at the same time. It is worth remarking that this happens in spite of the fact that the β functions undergo quick changes in the threshold region, as desired. The corrected potential as given in Equation (4.67) softens these effects and the net impact in N_e and $\mathrm{d}n/\mathrm{d}\ln k$ gets much reduced.

4.6 New physics above the inflationary scale

We consider now a scale of new physics, M , higher than the scales at which inflation takes place. The new physics will show up in the effective theory at lower scales as non–renormalizable operators (NROs) of the light fields, suppressed by inverse powers of M . Therefore, this scale will in general affect the inflaton potential through NROs of the inflaton field that lift the flat direction along which the inflaton rolls. It might seem that these operators should have a negligible impact on inflation whenever they can be reliably taken into account (i.e. $\phi^2/M^2 \ll 1$) but we will show that in reality that is not the case. It is true that typically, due to the suppression scale factor, the impact of the NROs in the physics at low scales is usually very small. However, if the NRO has characteristics not shared by the low energy physics, its effect may be significant. This is what happens, for instance, with high dimension operators that mediate proton decay or give a Majorana mass to neutrinos. For a discussion of non–renormalizable physics in the context of inflation see [145]. In our case, the new physics does not need to respect the accidental flat directions of the effective theory. In fact, making use of such effects we are able to give a simple and complete potential that satisfies all three goals [*i)-iii)*] listed in section (4.3). Moreover, the analysis can be carried out in a very model independent way if we focus on the small–coupling regime.

Let us start directly with an inflaton potential that reads

$$V(\phi) = \rho + \beta \ln \frac{m(\phi)}{Q} + \phi^4 \frac{\phi^{2N}}{M^{2N}} \ . \tag{4.74}$$

The first two terms correspond to the generic one–loop potential we have discussed in previous sections. In the small–coupling regime, we can take β as a constant. As we have just explained, the last term in (4.74) is a non–renormalizable operator left in the low–energy theory after integrating out some unspecified physics at the high scale M . This scale has been defined in such a way that it absorbs any possible coupling in front of the operator. We assume that the NRO shown in Equation (4.74) is the lowest order one that can appear. If there are operators of higher

order they will have a negligible impact compared to the lowest order one provided they are suppressed by the same mass scale M. The sign and exponent we have assumed for the NRO are convenient to guarantee the stability of the potential. Let us note that an even power for this operator is what one expects generically in supersymmetric theories. In fact, the question of whether such a potential can have a supersymmetric origin is an interesting one and we are going to postpone its discussion for later analysis.

It takes next to no time to write the first derivatives with respect to ϕ of the inflaton potential (4.74):

$$V'(\phi) = \frac{\beta}{\phi} + 2(N+2)\phi^3 \frac{\phi^{2N}}{M^{2N}} , \tag{4.75}$$

$$V''(\phi) = -\frac{\beta}{\phi^2} + 2(N+2)(2N+3)\phi^2 \frac{\phi^{2N}}{M^{2N}} , \tag{4.76}$$

$$V'''(\phi) = 2\frac{\beta}{\phi^3} + 4(N+2)(2N+3)(N+1)\phi \frac{\phi^{2N}}{M^{2N}} . \tag{4.77}$$

From these expressions, and taking into account the definitions of the potential slow–roll parameters, we realize that the effect of the NRO will have a significant impact on any quantity that can be expressed in terms of a slow–roll expansion when the small number $(\phi/M)^{2N}$ is comparable in size to β/ϕ^4 (which is also naturally small). Even for $\phi^2 \ll M^2$, the NRO can have an important effect because it gives a correction to a potential which is almost flat.

It is also immediate to realize from (4.75)–(4.77) that, for sufficiently large ϕ, the higher derivatives V'', V''' (and thus η and ξ) can receive a large contribution from the NRO term while the contribution to V' (and so ϵ) remains small, thanks to the additional $(2N+3)$ and $(2N+3)(2N+2)$ factors in V'', V'''. This means that the effect of the NRO on the inflationary process will be particularly important at the beginning of inflation, when ϕ takes its highest values. As ϕ rolls down its potential, the effect of the NRO quickly dies away and inflation proceeds as discussed in section 4.2. However, in the early stages of inflation the running of n can get important modifications from the NRO corrections, even though the values of V and (to some extent) V' are scarcely modified. We will examine this in more quantitative terms.

The slow–roll parameters can be readily found as a function of ϕ from the derivatives of the potential (4.75)–(4.77). The ϵ parameter is much smaller than η and ξ, so $n \simeq 1 + 2\eta$ and $\mathrm{d}n/\mathrm{d}\ln k \simeq -2\xi$. In this way we obtain

$$\frac{\mathrm{dn}}{\mathrm{d}\ln \mathrm{k}} \simeq -\frac{1}{N_e^2(\phi)} \left[1 + (2N+3)(N+1)p(\phi)\right] \left[1 + p(\phi)\right] , \tag{4.78}$$

where

$$p(\phi) \equiv 2(N+2)\frac{\phi^4}{\beta}\frac{\phi^{2N}}{M^{2N}} , \tag{4.79}$$

and

$$N_e(\phi) = \frac{\rho\phi^2}{2\beta M_p^2} , \tag{4.80}$$

which is approximately the number of efolds from ϕ till the end of inflation, obtained by neglecting the NRO contribution to $V'(\phi)$ in (3.216). Applying Equation (4.78) to

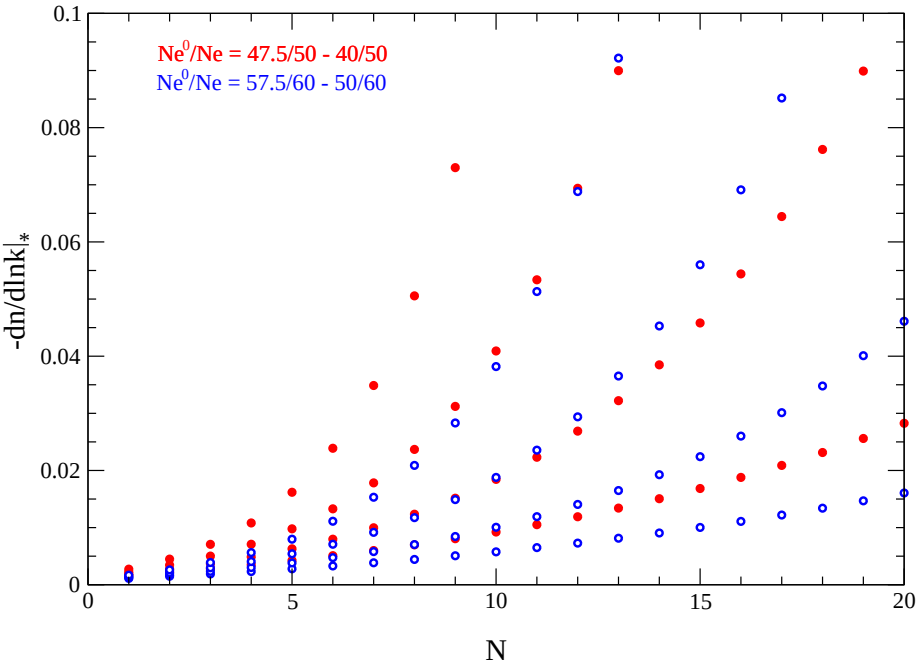

Figure 4.4: Running of the scalar spectral index as a function of N for several values of Ω. The red solid dots correspond to $N_{e\star} = 50$ and $N_{e0} = \{40, 42.5, 45, 47.5\}$. The blue open dots correspond to $N_{e\star} = 60$ and $N_{e0} = \{50, 52.5, 55, 57.5\}$. Larger values N_{e0} give smaller running.

the starting point $\phi_\star$, it looks possible to get $N_e^2(\mathrm{d}n/\mathrm{d}\ln k|_\star) \simeq -125$, as suggested by WMAP data, if N or $p(\phi_\star)$ are not small. Let us see to which extent this is feasible.

We call ϕ_0 the value of the inflaton at the particular point with $n = 1$ [3]. There we should have $V''(\phi_0) \simeq 0$, which implies $p(\phi_0) \simeq 1/(2N+3)$. Using the approximation of Equation (4.80) it is simple to get

$$p(\phi_\star) \simeq \frac{1}{2N+3}\left(\frac{N_e}{N_e^0}\right)^{N+2} , \tag{4.81}$$

where $N_e = N_e(\phi_\star)$ is the total number of efolds, and $N_e^0 = N_e(\phi_0)$; i.e. $n = 1$ after the first $N_e - N_e^0$ efolds. Using Equations (4.78-4.81) we can find out what values of N are required to get enough running for n. This is shown in Figure 4.4, which gives $\mathrm{d}n/\mathrm{d}\ln k|_\star$ as a function of N for different choices of N_e^0/N_e corresponding to $k(\phi_0)$ not far from $10^{-2}\mathrm{Mpc}^{-1}$. From this plot we see that large values of N are required to get a significant running of n, with smaller N_e^0/N_e being preferred. As an example, let us take $N = 9$ and $N_e^0/N_e = 42.5/50$, which gives $\mathrm{d}n/\mathrm{d}\ln k|_\star \simeq -0.03$.

For a fixed value of the scale of new physics, M, the quantities β and ρ are de-

[3] Notice that the meaning of this '$_0$' subscript has nothing to do with the one it had in the previous chapter where it represented today's time

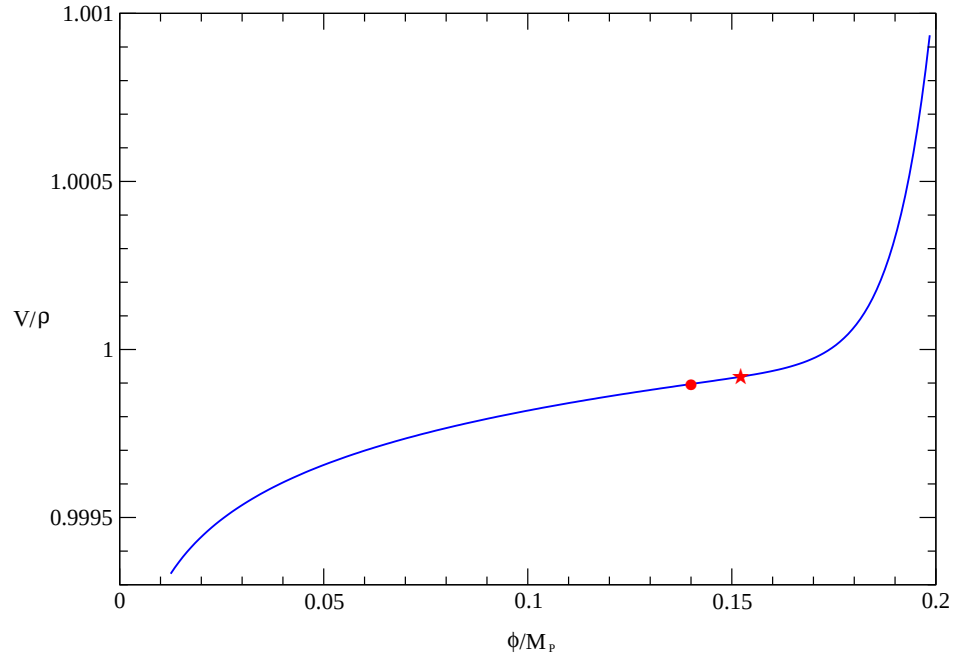

Figure 4.5: Inflaton effective potential with expression (4.74) normalized to ρ for $N = 9$ and parameters as given in the text. The star marks $\phi_\star/M_p$ and the circle, ϕ_0/M_p.

termined by the constraints of P_k and N_e: $\rho \simeq (10^{-3}\sqrt{MM_p})^4$ and $\beta \simeq (10^{-4}M)^4$. Choosing for instance $M \simeq 0.95M_p$ one further gets $\mathrm{d}n/\mathrm{d}\ln k|_\star \simeq -0.03$ for $\phi_\star \simeq 0.15M_p$ while $\phi_0 \simeq 0.142M_p$; the numerical values for the number of efolds are $N_e \simeq 48.8$ and $N_e^0 \simeq 42.4$; and one gets $P_k \simeq 2.36 \times 10^{-9}$. Note that $\phi_\star/M$ is sufficiently small for the effective theory with the NRO to be trustable. Figure 4.5 shows the effective potential as a function of ϕ/M_p, with $\phi_\star$ indicated by a star and ϕ_0 by a circle. Notice how $\phi_\star$ is below the range where the NRO starts to be important for $V'(\phi)$, but not for $V''(\phi)$. The Figure 4.6 shows the slow–roll parameters as a function of ϕ/M_p. Inflation does not continue below $\phi \simeq 0.02M_p$. Finally, Figure 4.7 gives the scalar spectral index as a function of $\log_{10} k$.

4.7 Possible physical origin of the high energy threshold

Now we should wonder how reasonable it is to expect a non–renormalizable operator with $N = 9$ or even larger. Let us recall that, for the previous mechanism to work, such operator should be the leading one. This is not a serious problem because supersymmetric flat directions as the one we are using for inflation can be protected against lifting by additional symmetries. In fact it is common that some of the flat directions of supersymmetric models are only lifted by NROs at very high order. This is well known, for instance in the MSSM [261]. And also very common in the context of D=4 string theories, where string selection rules forbid many operators in

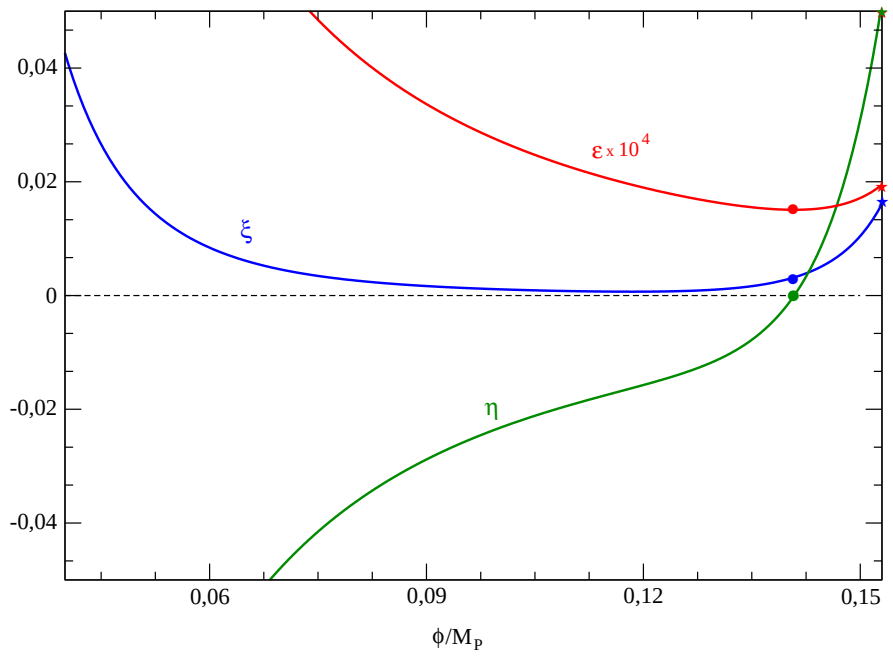

Figure 4.6: Slow–roll parameters for the potential of Figure 4.5. The stars mark $\phi_\star/M_p$ and the circles, ϕ_0/M_p .

the superpotential that would be allowed by gauge invariance. For example, in the popular Z_3-orbifold compactifications of the heterotic string non–renormalizable couplings involving twisted matter fields have the structure Φ^{3+9n} , with $n = 1, 2, ...$ [262, 263].

Concerning the supersymmetric realization of a potential like that in (4.74) the first guess would be to use a superpotential of the form

$$W = \Phi(\lambda H_+ H_- - \mu^2) + \frac{1}{(N+3)}\Phi^3 \frac{\Phi^N}{M^N} \ , \tag{4.82}$$

which is simply the standard superpotential of the D–term inflation model we have used supplemented by a non–renormalizable term for the inflaton. From (4.82), one obtains at tree level the inflaton potential

$$V = V_D + \left| \Phi^2 \frac{\Phi^N}{M^N} - \mu^2 \right|^2 \ . \tag{4.83}$$

This potential has a term of order $\Phi^4 \Phi^{2N}/M^{2N}$ like the one we are after, but also a term of lower order: $2\mu^2 \, \mathrm{Re}(\Phi^2 \Phi^N)/M^N$. For the higher order term to dominate one would need $|\mu^2| \ll \Phi^2 \Phi^N / M^N$ which can in principle be arranged.

In any case, the presence of a non–zero μ poses a different problem. In view of the form of the potential (4.83) it is clear that there will be two series of minima

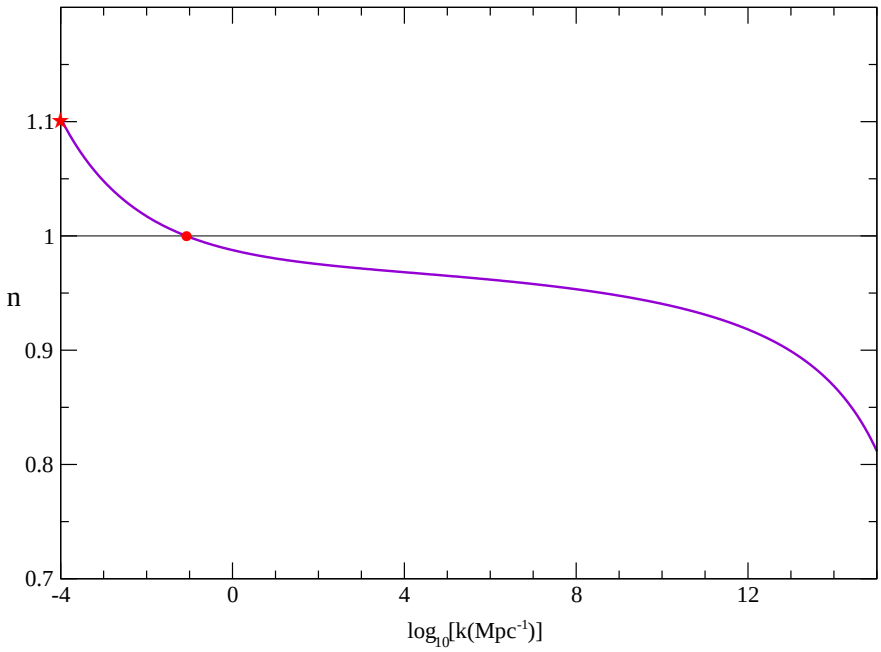

Figure 4.7: Scalar spectral index as a function of the scale for the potential of Figure 4.5.

with $\Phi = \Phi_m \exp[i\pi l/(2+N)]$ where $\Phi_m^{(N+2)} = \text{sign}[\mu^2](-1)^l|\mu^2|M^N$ and $l \in \mathbb{Z}$. The flat potential for Φ is therefore lifted by the NRO along some directions in the complex plane of Φ while along other directions the potential develops minima and this can change qualitatively the evolution of the inflaton. It is interesting that the usual logarithmic one–loop corrections that cause the inflaton to roll in the standard scenario can also cure this problem in the present case, so that the minima are no longer dangerous. In that case one can have the inflaton running in a stable trajectory along which only its real part is non zero.

Nevertheless, the simplest and most obvious solution for the previous problem is to choose $\mu = 0$ which, incidentally, is the choice of the original formulation of the D–term inflation model [254]. In that case one simply gets a potential term of the desired order as in equation (4.74). Notice how, thanks to supersymmetry, the order of the NRO in the superpotential (4.82) has almost doubled in the potential (4.83).

An appealing alternative is to start with

$$W = \lambda \Phi H_+ H_- + \frac{1}{2} m \Psi^2 + \frac{1}{(P+2)} \Psi \Phi^2 \frac{\Phi^P}{M^P} \,, \tag{4.84}$$

where we have introduced an extra field Ψ with mass $m \ll M$ (so that Ψ really belongs in the effective theory below M). Along the flat direction for the inflaton field Φ the coupling to Ψ generates a tadpole for it so that also Ψ develops a VEV. As we are only interested in the evolution of the inflaton field, we can simply eliminate

Ψ by solving its equation of motion in terms of Φ and substituting in the two-field potential $V(\Phi,\Psi)$ to get the final potential for Φ: $V(\Phi) = V(\Phi,\Psi(\Phi))$. In this way one gets the following inflationary potential (along $\phi = \sqrt{2}\,\mathrm{Re}\,\Phi$ and absorbing factors of $\sqrt{2}$ in M)

$$V = V_D + \phi^4 \frac{\phi^2}{m^2}\frac{\phi^{4P}}{M^{4P}}\,, \tag{4.85}$$

where again V_D is the Fayet–Iliopoulos contribution. The advantage of this option is that the NROs are naturally of higher order. For instance, to get $N = 9$ one needs a rather modest $P = 4$ in the superpotential.

4.8 Primordial spectra in the slow–roll approximation

In this section we derive formulas for the primordial spectra of the classes of models that we have introduced. We will work in the small–coupling regime and start with the flat tree level case. Then, we will move on to include the effect of a NRO operator. In the regime that we will be working on we will have no need of specifying the detailed coupling structure of the tree level potentials and their beta functions, which makes our results very general and suitable for the analysis of a wide variety of models. To simplify our notation we will refer to the flat tree level case as LOG. Similarly, we will call LOG+NRO the extended situation where the effect of a threshold of new physics above the inflationary scales will be taken into account.

4.8.1 Small–coupling regime

The first three slow–roll parameters (4.13) can be written as

$$\epsilon \simeq \frac{1}{2}q^2\frac{M_p^2}{\phi^2}\,, \qquad \eta \simeq -q\frac{M_p^2}{\phi^2} \simeq -2\frac{\epsilon}{q}\,, \qquad \xi \simeq 2\eta^2\,, \tag{4.86}$$

where we have introduced the quantity

$$q \equiv \frac{\beta}{\rho_0}\,, \tag{4.87}$$

which will be positive if we assume that $\beta > 0$ as it is usually the case. The subscript for ρ comes from the fact that we are working in the small–coupling regime and therefore we can write the potential at one–loop with the tree level part evaluated at ϕ_0 as in (4.17). Let us recall that within this framework the β–function of the potential can be treated as a constant. We already explained in section 4.2.1 that satisfying the slow–roll condition $\epsilon \ll 1$, requires $q \ll 1$ for $\phi < M_p$. This implies in turn $\epsilon \ll |\eta|$.

The number of efolds between time t_0 (i.e. the time when $\phi = \phi_0$) and the end of inflation, t_e, can be easily computed using ϵ, and we found it to be (4.19), which we can express as

$$N_e(t_0 \to t_e) \simeq \frac{1}{2}\frac{\phi_0^2}{qM_p^2} \equiv N_e^0\,, \tag{4.88}$$

and from now on we will use this notation. We will see that N_e^0, besides from giving an excellent approximation to $N_e(t_0 \to t_e)$, will play a relevant role when performing the fits to the data. Let us remind that (4.88) is based on the assumption that inflation ends because $|\eta|$ becomes of order unity. This gives us an upper bound in the number of efolds that can be produced, since inflation might terminate earlier due to other mechanisms, like the effect of a waterfall field in hybrid models.

Now the derivative relation between ϕ and k, Equation (3.217), can be integrated at first order in q, giving

$$\frac{\phi^2}{\phi_0^2} = 1 - \frac{1}{N_e^0} \ln \frac{k}{k_0} \,, \tag{4.89}$$

where we have used (4.88). Note that increasing ϕ corresponds to decreasing k so that the scales probed by WMAP correspond to the highest values of ϕ during its slow–roll towards the origin. We can now obtain $P_s(k)$ from equation (3.219). For the purpose of comparing the model with the data, it is convenient to write P_s in terms of $P_s^0 \equiv P_s(k_0)$ using the general expression

$$\ln P_s = \ln P_s^0 + 3 \ln \frac{V(\phi)}{V(\phi_0)} - 2 \ln \frac{V'(\phi)}{V'(\phi_0)} \,, \tag{4.90}$$

valid in slow–roll. Using equations (4.17) and (4.89) and expanding in q we find, at first order,

$$\ln P_s(k) = \ln P_s^0 + \left(1 + \frac{3}{2} q\right) \ln \left(1 - \frac{1}{N_e^0} \ln \frac{k}{k_0}\right) \,, \tag{4.91}$$

where, from equation (3.219),

$$P_s^0 = \frac{1}{12\pi^2} \frac{\rho_0^3 \phi_0^2}{M_p^6 \beta^2} \,. \tag{4.92}$$

The same result can be obtained by integrating the slow–roll equation for the scalar spectral index, which gave us (4.22). Let us remark that (4.22) is the prediction for the spectral index in scenarios with flat tree level potential in the regime of small coupling. It can be compared with the $n =$ constant or $\mathrm{d}n/\mathrm{d}\ln k =$ constant assumptions made in standard analyses. In that expression N_e^0 is the only independent parameter and has a precise physical meaning.

Similarly, the spectrum of tensor perturbations, $P_t(k)$, can be obtained from equation (3.220)

$$P_t(k) \simeq \frac{4 q P_s^0}{N_e^0} \left[1 + \frac{q}{2} \ln \left(1 - \frac{1}{N_e^0} \ln \frac{k}{k_0}\right)\right] \,. \tag{4.93}$$

At the same level of approximation, the tensor to scalar ratio (3.221) reads

$$r(k) \simeq \frac{4q}{N_e^0} \left(1 - \frac{1}{N_e^0} \ln \frac{k}{k_0}\right)^{-1} \,. \tag{4.94}$$

Let us now count the number of independent parameters. The power spectra, $P_s(k)$ and $P_t(k)$, contain three independent parameters, $\{P_s^0\,,\ q\,,\ N_e^0\}$, which are

combinations of the initial parameters $\{\phi_0\,,\,\rho_0\,,\,\beta\}$. Incidentally note that the scalar potential (4.17) is a function of just two combinations of parameters, but a third one appears in the conversion of ϕ into k through equation (4.89). Actually, the q term in (4.91) is subdominant because $q \ll 1$. Removing it from the expression is a good approximation and eliminates one parameter. So the expression of $P_s(k)$ contains basically two parameters. This is to be compared with the three parameters (two if the running of n is set to zero) of the simple standard parameterization (3.229). As a consequence this LOG scenario is highly predictive. On the other hand, the fits to WMAP data prefer $P_t(k) \ll P_s(k)$, which means that P_t turns out to be scarcely important in the fit, and so the number of relevant parameters continues to be two. Indeed, from equation (4.94) and $q \ll 1$, we do expect by construction $P_t(k) \ll P_s(k)$, something that cannot be postulated from the simple parameterizations (3.229) and (3.230) (unless slow–roll is assumed), which contain the additional parameter $P_t(k_0)$ or, equivalently, r (unless r is set to zero by hand).

According to Equation (4.15) the dependence of n on the scale is weak, and therefore $n \simeq$ constant, we can expect a fit similar to the one obtained by using the standard parameterization of equation (3.229) with $\mathrm{d}n/\mathrm{d}\ln k = 0$, leading to $n_0 \simeq 0.95$. We will later see that this is indeed the case.

4.8.2 Small–coupling regime and non–renormalizable operator

In this scenario the derivatives of the potential $V(\phi)$ [equation (4.74)] with respect to ϕ are (4.75)–(4.77). The corresponding expressions for the first order slow–roll parameters ϵ and η are:

$$\epsilon = \frac{1}{4qN_e^0\,\Phi}\left[\frac{1+(A\,\Phi)^M}{\frac{1}{q}+\frac{1}{2M}(A\,\Phi)^M+\frac{1}{2}\ln\Phi}\right]^2 , \tag{4.95}$$

$$\eta = \frac{1}{2qN_e^0\,\Phi}\left[\frac{(2M-1)(A\,\Phi)^M-1}{\frac{1}{q}+\frac{1}{2M}(A\,\Phi)^M+\frac{1}{2}\ln\Phi}\right] , \tag{4.96}$$

where we have defined

$$\Phi \equiv \left(\frac{\phi}{\phi_0}\right)^2 , \tag{4.97}$$

to simplify the notation. In the limit of the NRO going to zero we recover the formulas (4.86).

As we already commented in Section 4.6 the NRO can have a significant impact on inflation when the small number $(\phi/M)^{2N}$ is comparable in size to β/ϕ^4. Significant modifications of the spectral index, n, and its running, $\mathrm{d}n/\mathrm{d}\ln k$, can be expected because they depend on η and ξ, especially at the initial scales (very small k and thus large ϕ). However, much smaller changes can be foreseen in the number of efolds which is a function on ϵ.

Let us now calculate the expression of the power spectrum $P_s(k)$ in this scenario. As in the previous subsection, we start with the general expression (4.90) where $V(\phi)$

and $V'(\phi)$ are given now by equations (4.74) and (4.75) respectively, and

$$P_s^0 = \frac{1}{12\pi^2}\frac{[V(\phi_0)]^3}{M_p^2[V'(\phi_0)]^2}\ . \tag{4.98}$$

Next we have to convert ϕ into k by integrating equation (3.217).

Applying the following two identities of hypergeometric functions [198]:

$$\begin{aligned} {}_2F_1(a,b;c;z) &= {}_2F_1(b,a;c;z) \\ {}_3F_2(a,b,c;a+1,b+1;z) &= \frac{1}{b-a}\left[b\,{}_2F_1(a,c;a+1;z) - a\,{}_2F_1(b,c;b+1;z)\right] \end{aligned}$$

one can see, integrating equation (3.217), that

$$\begin{aligned} \ln\frac{k}{k_0} &\simeq -\frac{q}{2}N_e^0\varphi\left\{\frac{1}{N+2} + \left(\frac{2}{q} - \frac{1}{N+2} + \ln\varphi\right){}_2F_1\left(\frac{1}{N+2},1;\frac{N+3}{N+2};-(A\varphi)^{N+2}\right)\right. \\ &+ \frac{N+2}{(N+1)^2}\left[(A\varphi)^{-N-2}\left(1-(A\varphi)^{N+2}\right)^{-\frac{1}{N+2}} + \left(1-(A\varphi)^{N+2}\right)^{-\frac{1}{N+2}}\right. \\ &- \left.\left.(A\varphi)^{-N-2} - (N+1){}_2F_1\left(\frac{1}{N+2},\frac{1}{N+2};\frac{N+3}{N+2};-(A\varphi)^{N+2}\right)\right]\right\}\Bigg|_{\varphi=1}^{\phi^2/\phi_0^2} \end{aligned} \tag{4.99}$$

where φ is just a dummy variable and

$$A^{N+2} \equiv 2(N+2)\frac{\phi_0^4}{\beta}\frac{\phi_0^{2N}}{M^{2N}}\,. \tag{4.100}$$

The slow–roll approximation is the only reason for the symbol of approximate equality in (4.99). This cumbersome expression is not what we will later use to make numerical fits. Instead, using $|q| \ll 1$, we can write the much simpler but extremely accurate expression in that regime:

$$\ln\frac{k}{k_0} \simeq -\varphi N_e^0\ {}_2F_1\left[\frac{1}{N+2},1;\frac{N+3}{N+2};-(A\varphi)^{N+2}\right]\Bigg|_{\varphi=1}^{\phi^2/\phi_0^2}\,, \tag{4.101}$$

which comes from (4.99) neglecting the irrelevant addends, i.e. all but the one that is not proportional to the small parameter q.

Note that N_e^0 is still defined as in equation (4.88) and gives a good estimate of the number of efolds $N_e(t_0 \to t_e)$. It is possible to invert (4.101) numerically to get $\phi = \phi(k)$. Plugging $\phi(k)$ into equation (4.90) we obtain $P_s(k)$. This is the procedure we have followed in doing the fits. Using $\phi(k)$ we can also obtain other quantities of interest as functions of k, e.g. the spectral index $n \simeq 1 + 2\eta - 6\epsilon$ or the tensor to scalar ratio $r \simeq 16\epsilon$.

In order to get some intuition about the shapes of $P_s(k)$ and $n(k)$ it is convenient to derive an analytical approximation to the previous numerical procedure. Actually, the numerical part just comes from the ϕ to k conversion, i.e. the integration of equation (3.217). This equation depends on ϵ (on V and V') but not on higher derivatives of V, which are the ones most affected by the presence of the NRO, as

discussed after Equations (4.75)–(4.77). Therefore it is sensible to use here the value of ϵ when the NRO is switched off, i.e. that of Equation (4.86). Then the ϕ to k relation is still given by equation (4.89). Substituting this in the general expression for $P_s(\phi)$, equation (4.90), and expanding at first order in the NRO contributions, one gets[4]

$$\ln \frac{P_s(k)}{P_s^0} \simeq \left(1+\frac{3}{2}q\right)\ln\left(1-\frac{1}{N_e^0}\ln\frac{k}{k_0}\right)+\frac{\gamma N_e^0}{N+2}\left[1-\left(1-\frac{1}{N_e^0}\ln\frac{k}{k_0}\right)^{N+2}\right] \quad (4.102)$$

where

$$\gamma \equiv \left\{2N+3+\left[\frac{1}{2(N+2)}-3\right]q+\frac{3}{2(N+2)}q^2\right\}\frac{A^{N+2}}{N_e^0} \quad (4.103)$$

$$\approx (2N+3)\frac{A^{N+2}}{N_e^0}\,. \quad (4.104)$$

The approximate equality in the last expression is justified by the smallness of q. Alternatively, one can expand $n-1 \simeq 2\eta - 6\epsilon$ at first order in the NRO and approximate again the ϕ to k conversion by equation (4.89). One obtains

$$n(k)-1 \simeq -\left(1+\frac{3}{2}q\right)\frac{1}{N_e^0}\left(1-\frac{1}{N_e^0}\ln\frac{k}{k_0}\right)^{-1}+\gamma\left(1-\frac{1}{N_e^0}\ln\frac{k}{k_0}\right)^{N+1}\,. \quad (4.105)$$

Then, the direct integration of (4.105) gives back expression (4.102). Equation (4.105) corresponds to a running $n(k)$ with *non*–constant slope, departing from the assumption of analyses done using the standard parameterization. Unlike in the LOG scenario, in this case the running is not constrained to be very small.

It is also worth mentioning that, due to the positivity of $1-(1/N_e^0)\ln k/k_0$, the sign of the LOG and the NRO contributions to $\{n(k)-1,\ \mathrm{d}n/d\ln k,\ \mathrm{d}^2n/\mathrm{d}\ln^2 k\}$ are $\{-,\ -,\ -\}$ and $\{+,\ -,\ +\}$ respectively (see equation(4.105)). Since a sizable running at low k requires a dominant NRO contribution, we can conclude from equation (4.105) that in that case the sign of the second derivative will be positive, although for large enough k it will turn to negative as the LOG part becomes dominant.

In a similar way one can obtain expressions for $P_t(k)$ or equivalently $r(k)$ starting with the general equations (3.220) or (3.221). In particular, the previous analytical approximation gives in this case

$$r(k) \simeq \frac{4q}{N_e^0}\left(1-\frac{1}{N_e^0}\ln\frac{k}{k_0}\right)^{-1}+\frac{8qA^{N+2}}{N_e^0}\left(1-\frac{q}{2N+4}\right)\left(1-\frac{1}{N_e^0}\ln\frac{k}{k_0}\right)^{N+1}\,. \quad (4.106)$$

Let us finally count the number of independent parameters. From expressions (4.102) and (4.106) we see that the spectrum of primordial perturbations depends upon five parameters $\{P_s^0\,,\,N_e^0\,,\,q\,,\,A\,,\,N\}$, which are combinations of the five parameters $\{\rho_0,\beta,\phi_0,M,N\}$ appearing in the scalar potential (4.74). Thus, the LOG+NRO

[4]This approximate formula gives $P_s(k)$ with a maximum error of $\lesssim 13\%$ in the most extreme cases although typically is much better. Anyway, we remark that in the fit we evaluate $P_s(k)$ numerically using equation (4.101).

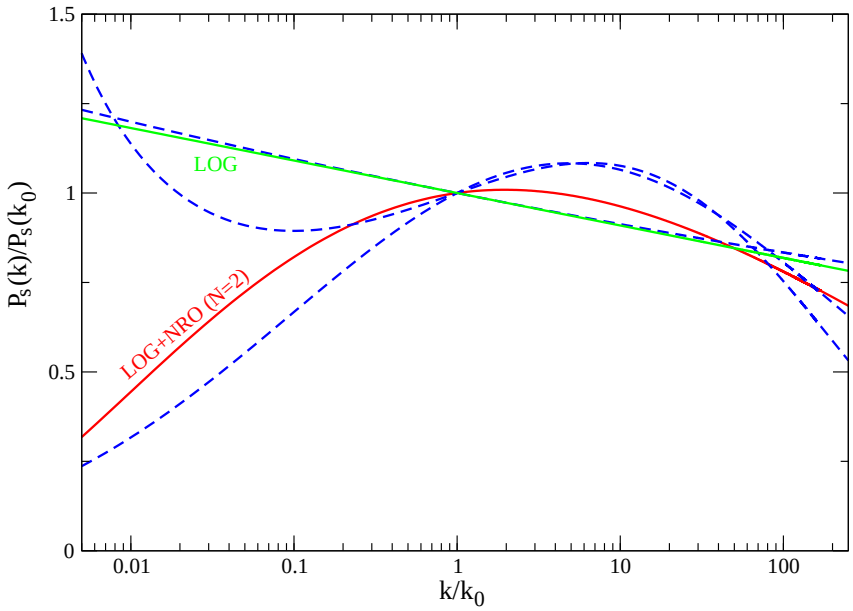

Figure 4.8: Primordial power spectra in the standard parameterization (blue dashed lines) with Taylor expansion up to second order, i.e. running of running and as predicted by the LOG (green) and LOG+NRO (red) ($N = 2$) scenarios. The parameters chosen for each case are the best–fit ones (given in Tables 4.7, 4.8 and 4.9).

has two more parameters than the LOG model. Again, as in the LOG case, the smallness of q implies that $P_s(k)$ is nearly independent of q and, besides, the tensor spectrum is much less important than its scalar counterpart. Hence, q will be irrelevant for a broad range of values in the fit to the data. In practice, the primordial spectrum depends essentially on four parameters which become just three if we consider N to be a fixed integer. Again, this is to be compared with the four parameters of the simplest standard parameterizations (3.229) and (3.230). In consequence, the LOG+NRO scenario is still highly predictive.

To illustrate the shapes of the scalar power spectrum in the different parameterizations we plot $P_s(k)$ from in Figure 4.8. The parameters for the models are chosen to be the best–fit values given in Section 4.10 and discussed later in the text.

4.9 Data analysis procedure

In order to constrain the parameters of the two scenarios introduced above, by comparing their predictions with CMB and LSS data, we use a modified version of the `cosmomc` package [264] with a suitable parameterization of the expressions for $P_s(k)$ and $P_t(k)$. In the next two subsections we describe the detailed procedure for each case separately. We ran six chains for each model, gathering 3×10^5 samples per chain, using the default Metropolis algorithm to sample the parameter space. We discard a burn–in period encompassing the first 10^3 samples in each chain and

we employ the usual Raftery and Lewis mixing criterion [265], requiring $R-1<0.1$ for the merged chains.

We consider a flat cosmology, taking flat priors on the cosmological parameters $\Omega_b h^2$, $\Omega_c h^2$ (the baryon and CDM density, respectively), Θ_* (the ratio of the distance to the last scattering surface to the sound horizon) and τ (the optical depth to reionization). We assume dark energy in the form of a cosmological constant and 3 species of massless neutrinos. The parameterizations of the primordial power spectrum are discussed in detail below.

We used a combination of CMB and LSS data to constrain the parameters of the models. The main reason for doing so is that it helps to break parameter degeneracies [266]. In particular, we used the WMAP3 data [267], ACBAR [248], CBI [268] and BOOMERANG [236] CMB data set releases and the results from the SDSS galaxy survey [269]. We also added the Hubble Space Telescope measurement of the Hubble constant $H_0 = 72 \pm 8$ km/s/Mpc [270].

4.9.1 Small–coupling regime

As discussed in Section 4.8.1, the LOG scenario is described by the three independent parameters $\{\rho, \beta, \phi_0\}$, appearing in the scalar potential (4.17). However, for the purpose of comparing the model with data, it is more appropriate to use the following set:

$$\mathbb{P}_{\rm LOG} \equiv \{ \ln P_s^0, N_e^0, q \} , \tag{4.107}$$

which are related to the potential parameters by the relations (4.87), (4.88) and (4.92). The inverse transformations are given by

$$\begin{aligned} \phi_0 &= \sqrt{2qN_e^0}\, M_p \ , \\ \rho_0 &= \frac{6\pi^2 q P_s^0}{N_e} M_p^4 \ , \\ \beta &= q\frac{6\pi^2 q P_s^0}{N_e} M_p^4 . \end{aligned} \tag{4.108}$$

The reasons for preferring the set (4.107) over the original potential parameters are the following. First, the fit to WMAP data is very sensitive to the value of $\ln P_s$ at the fiducial scale, which makes it very convenient to use $\ln P_s^0$ as one of the parameters. Second, N_e^0 appears explicitly in the expressions of $P_s(k)$ and $P_t(k)$ (see equations (4.91) and (4.93)). In addition, N_e^0 has a clear physical meaning, since for small q it simply expresses the number of efolds since the time when k_0 crosses out the horizon until the end of inflation. This also makes possible to impose on it a physically motivated prior for the number of efolds, as required to solve the homogeneity and flatness problems. Furthermore, we note from Equation (4.21) that N_e^0 and the spectral index at k_0 are simply related,

$$n_0 \simeq 1 - \frac{1}{N_e^0} , \tag{4.109}$$

in analogy to (4.20). Finally, the third parameter, q , does also appear explicitly in the expressions for the spectra. As argued before, in Section 4.8.1, we expect

$q \ll 1$, implying that the scalar primordial spectrum depends essentially only on $\ln P_s^0$ and N_e^0, while the tensor spectrum $P_t(k) \simeq 16\epsilon P_s(k)$ is suppressed (and much less important for the fit). Therefore it is convenient to choose q as a parameter for the fit in order to single out this effect. From the above discussion, $\ln P_s^0$ and N_e^0 will be well determined by the observable properties of the power spectrum, and therefore it is appropriate to impose flat priors on them, which corresponds to the assumption that they are location parameters.

The relations between $\mathbb{P}_{\rm LOG}$ and the potential parameters are non–linear and so one expects volume effects coming from the Jacobian of the transformation that will in general make the marginalized constraints on the potential parameters sensitive to the choice of priors. Furthermore, as argued above, only two combinations of parameters of the potential are going to be well determined by the data. The constraints on these 'principal directions' in the potential parameter space are however essentially prior–independent, as we discuss in detail in Section 4.10.2

Let us now focus on the physical constraints on the parameter space spanned by $\mathbb{P}_{\rm LOG}$. The evolution equations of the classical value of the field are based on General Relativity. To prevent effects of quantum gravity from becoming important, we conservatively require the energy density to satisfy

$$\rho < M_p^4 \,. \tag{4.110}$$

Similarly, it is sensible to keep the inflaton field below the Planck scale. Note in particular that, at least in this framework, the renormalization scale Q is to be identified with the value of the inflaton, in order to maintain the radiative corrections under control, and obviously the RGE are only reliable for Q below the Planck scale. Thus we also require, conservatively,

$$\phi_0 < M_p \,. \tag{4.111}$$

Notice that, since the inflaton rolls towards zero, if the above condition is satisfied for ϕ_0 it will automatically be satisfied for smaller values of ϕ, as well. For larger values of ϕ, imposing equation (4.111) easily guarantees that they are well below M_p, since there are very few efolds before k_0, and they correspond to a short range of ϕ–values.

Moreover, one must ensure that the slow–roll approximation is fulfilled, which means that we require

$$\epsilon < 1 \,, \tag{4.112}$$

$$|\eta| < 1 \,. \tag{4.113}$$

For simplicity we impose these conditions at k_0 and this automatically ensures that the slow–roll is not violated for smaller values of k, which means greater values of ϕ. Therefore, the slow–roll will be guaranteed at the scale $k_{\rm obs} \equiv 10^{-4}{\rm Mpc}^{-1}$, which roughly gives us the size of the observable universe. On the other hand, larger values of k are probed and the slow–roll parameters grow as ϕ goes to zero. Taking into account that the largest relevant multipole is about 3000, one gets a maximum k around $k_{max} \equiv 0.1$ Mpc^{-1} [271]. Using Equation (4.89), we have checked that the

slow–roll for such large value of k is indeed satisfied by the samples in our Markov chains. The slow–roll condition on η is equivalent to

$$2N_e^0 > 1\,, \tag{4.114}$$

while the one on ϵ leads to

$$4N_e^0 > q. \tag{4.115}$$

On the other hand, the inequality (4.111) implies

$$2qN_e^0 < 1\,, \tag{4.116}$$

which together with equation (4.114) implies

$$q < 1\,, \tag{4.117}$$

as anticipated in Section 4.8.1.

We found that samples in the Markov chains that fulfil the condition (4.116), automatically satisfy also conditions (4.114), (4.117) and (4.110). This can be understood as follows. We expect a value for $n_0 \simeq 0.95$, similar to the one obtained with the simplest parameterization. Then Equation (4.109) implies (4.114). Moreover, the value of n, coupled with the physical prior (4.111), translates into an upper bound on q: since $n-1 \simeq -2\eta \simeq 2q(M_p/\phi_0)^2$, for $\phi_0 \leq M_p$ one gets $q \leq (1-n)/2$, and therefore the condition (4.117) holds. Incidentally, this upper bound on q implies that the contribution of the tensor part of the power spectrum must be necessarily small: $r = 16\epsilon \leq 2(1-n)^2$. Finally, (4.110) is granted by the smallness of P_s^0. Notice also that the condition (4.112) on ϵ is, in practice, irrelevant because (4.117) ensures that $\epsilon < |\eta|$, as can also be read off directly from (4.86). In consequence, the condition (4.116) remains the only non–trivial constraint.

In summary, we take $\mathbb{P}_{\rm LOG}$ as the set of independent parameters, imposing flat priors on them and enforcing the constraint (4.116). We then compute the scalar and tensor contributions to the primordial spectrum via the expressions (4.91) and (4.93).

As mentioned above, one of the reasons for choosing N_e^0 as an independent parameter is its direct physical interpretation as the number of efolds. In fact, we have a strong theoretical prejudice about its value, which should be[5] about 50 or 60. We have taken into account this fact by performing two different analyses. The first one imposes a flat prior on N_e^0, therefore assuming no prejudice about its value and leaving the data to constrain it. In the second case we enforce the theoretical requirement by imposing a Gaussian prior on N_e^0 centered on 50 with a standard deviation of 5 efolds. The details of these two fits and the results are discussed below, in Section 4.10.2.

[5]Recall however that its value could be less than 50 if there are subsequent episodes of inflation. See discussion after Equation (4.50). On the other hand, the parameter N_e^0 could be larger than 50 or 60 if inflation is interrupted by a waterfall condition in hybrid models, as we explained after (4.88).

4.9.2 Small–coupling regime and non–renormalizable operator

Concerning the LOG+NRO scenario, for practical reasons it is convenient to work with the set of independent parameters

$$\mathbb{P}_{\rm LOG+NRO} \equiv \{\, \ln P_s^0, N_e^0, q\,, A\,, N\,\}\,, \tag{4.118}$$

where A was defined in equation (4.100), instead of the parameters $\{\rho, \beta, \phi_0, M, N\}$ of the scalar potential (4.17). The relation between $\mathbb{P}_{\rm LOG+NRO}$ and the physical parameters of the potential are given by:

$$\phi_0/M_p = \sqrt{2qN_e^0}\,, \tag{4.119}$$

$$\rho/M_p^4 = 48\pi^2 q(N+2)^3 \frac{P_s^0}{N_e^0} \frac{\left(1+A^{N+2}\right)^2}{\left[2(N+2)+qA^{N+2}\right]^3}\,, \tag{4.120}$$

$$\beta/M_p^4 = 48\pi^2 q^2(N+2)^3 \frac{P_s^0}{N_e^0} \frac{\left(1+A^{N+2}\right)^2}{\left[2(N+2)+qA^{N+2}\right]^3}\,, \tag{4.121}$$

$$M/M_p = \sqrt{2qN_e^0}\left\{6\pi^2(N+2)^2 \frac{P_s^0}{{N_e^0}^3} \frac{A^{N+2}\left(1+A^{N+2}\right)^2}{\left[2(N+2)+qA^{N+2}\right]^3}\right\}^{-\frac{1}{2N}}. \tag{4.122}$$

The convenience and significance of the first three parameters in $\mathbb{P}_{\rm LOG+NRO}$ are the same as in the LOG scenario. However, the interpretation of N_e^0 as the number of efolds between k_0 and the end of inflation is now less accurate since there are NRO corrections, although it is still a good approximation. This is also true for the connection between N_e^0 and the spectral index n_0: the relation (4.109) becomes now

$$n_0 \simeq 1 - \left(1+\frac{3}{2}q\right)\frac{1}{N_e^0} + \gamma \simeq 1 - \frac{1}{N_e^0} + (2N+3)\frac{A^{N+2}}{N_e^0}\,. \tag{4.123}$$

This expression tells us that for not too large N_e^0 we should expect A to be bounded from above by some number close to unity because otherwise n_0 can become substantially different from 1 (especially for high values of N), thus violating the slow–roll conditions. This is also illustrated in Figure 4.9 which shows contour plots for the scalar spectral index and its running at k_0 at lowest order in slow–roll as functions of A and N_e^0 for $N = 2$ and $N = 10$. It is worth remarking here that since we are dealing with scale dependent quantities the appearance of these graphs would change if we made them at a different k. Figure 4.9 allows to realize that, in the context of the LOG+NRO scenario, it is possible to have simultaneously a sizable running and a reasonable number of efolds.

Concerning the physical limits in parameter space, we must take into account the presence of the scale of new physics M. The role played by the Planck mass in the LOG scenario corresponds now to M. To keep the validity of the effective potential (4.74) the inflaton must evolve well below that scale, which should be itself smaller than the Planck scale. Thus, we impose the following conservative limits:

$$2\phi_{\rm obs} < M \leq M_p\,, \tag{4.124}$$

$$\rho < M^4\,. \tag{4.125}$$

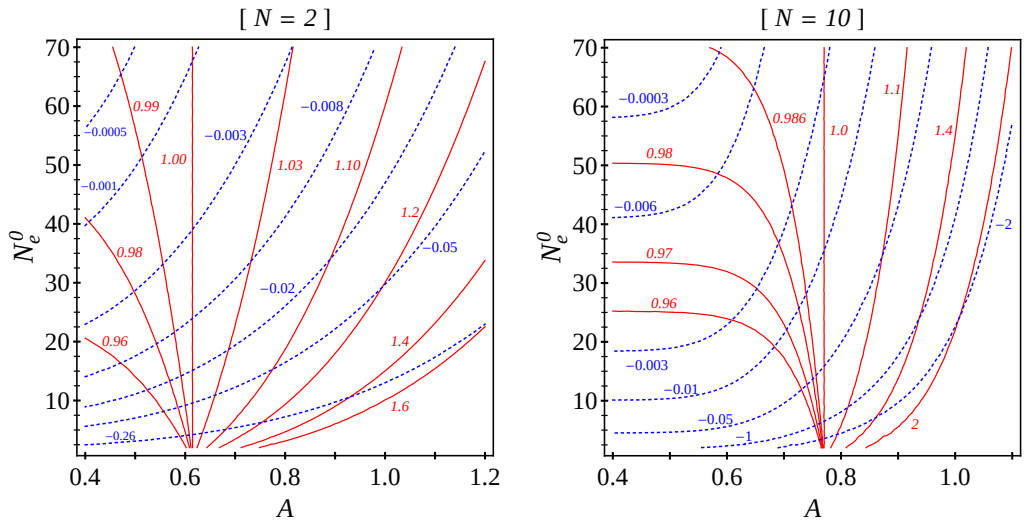

Figure 4.9: Values of the scalar spectral index (red lines) and its running (blue dashed lines) at k_0 computed at lowest order in slow–roll for the LOG+NRO class of models with N as indicated.

Notice that we set the first constraint at $\phi_{\rm obs} \equiv \phi(k_{\rm obs})$ in order to ensure it for any value of ϕ in the observable range.

As in the LOG scenario, $|\eta| \gg \epsilon$, and so η is the relevant parameter for the breakdown of slow–roll. However, unlike in the LOG case, due to the NRO, the absolute value of η grows with sufficiently large ϕ. Therefore, we must ensure the fulfilment of slow–roll not only at k_{max} but also at $k_{\rm obs}$. This guarantees that any point in between will satisfy the slow–roll conditions as well. So, we reject in the Monte Carlo process those points such that

$$|\eta(k_{\rm obs})| > \eta_{\rm lim} \ , \tag{4.126}$$

or

$$\eta(k_{max}) > \eta_{\rm lim} \, , \tag{4.127}$$

being $\eta_{\rm lim}$ a limiting value (smaller than 1) that we set at the beginning of the run. At the end we check that $\eta_{\rm lim}$ was indeed well chosen to ensure the validity of the slow–roll approximation. In practice we work with $\eta_{\rm lim} = 0.2$ which is a rather conservative value. We have checked that the change in the results is negligible if instead we use $\eta_{\rm lim} = 0.5$.

On the other hand, we expect theoretically that the parameter N should be in the range from 1 to $\mathcal{O}(10)$. As we commented in Section 4.7, it is very common that flat directions in supersymmetric models are only lifted by NROs at very high order (for instance in the case of the MSSM [261, 272]). This is also very common in D=4 string compactifications due to stringy selection rules [262, 263]. In Section 4.10 we discuss in detail two representative cases, which reasonably encompass the range of values for N ($N = 2$ and $N = 10$), and we comment on the qualitative behaviour for values of N between them.

As for the LOG scenario, we can consider N_e^0 as a free parameter with a flat

prior on it or we can alternatively constrain it to be around 50. We have performed the two types of fit.

Finally, we can anticipate theoretically the appearance of some strong bounds on the parameters of the model when performing the fits. First note that the observed power spectrum normalization $P_s^0 \simeq 2\times 10^{-9}$ implies through Equation (3.219) the smallness of ρ_0/M_p^4. More precisely

$$\frac{\rho_0}{M_p^4} \simeq 5\times 10^{-7}\epsilon_0 \ , \tag{4.128}$$

where the subscript on ϵ indicates evaluation at the fiducial scale. On the other hand, from Equations (4.95) and (4.96) we note that the smallness of $|\eta|$ (to preserve the slow–roll) implies that the two contributions within the square brackets (i.e. the LOG and the NRO contributions) must be small separately. Otherwise one should require an unjustified fine–tuned cancellation between them. Actually, even with fine–tuning, one could arrange the parameters to produce the cancellation only at a particular ϕ (and thus k): since the $\phi-$dependence of the two terms is very different, at another (not too distant) value of ϕ the cancellation would not work, spoiling the slow–roll. Consequently, the smallness of $|\eta|$ implies

$$\frac{\beta}{\rho_0} \lesssim \eta_0\left(\frac{\phi_0}{M_p}\right)^2 \ , \tag{4.129}$$

$$\left(\frac{\phi}{M_p}\right)^{2N+2} \lesssim \frac{|\eta_0|}{2(N+2)(2N+3)}\frac{\rho_0}{M_p^4} \simeq \frac{5\times 10^{-7}\epsilon_0|\eta_0|}{2(N+2)(2N+3)} \ , \tag{4.130}$$

In the second equation we have used $M \leq M_p$ and equation (4.128). On the other hand, comparing the two equations (4.95) and (4.96), and recalling that there cannot be fine–tuned cancellations in η, it is clear that

$$\epsilon_0 \lesssim \frac{1}{2}\left(\frac{\phi_0}{M_p}\right)^2 \eta_0^2 \ . \tag{4.131}$$

Using this relation in (4.130) we get

$$\left(\frac{\phi}{M_p}\right)^{2N} \lesssim \frac{5\times 10^{-7}|\eta_0|^3}{4(N+2)(2N+3)} \ , \tag{4.132}$$

which, substituted into (4.129), gives

$$q = \frac{\beta}{\rho_0} \lesssim |\eta_0|^{1+\frac{3}{N}}\left[\frac{5\times 10^{-7}}{4(N+2)(2N+3)}\right]^{\frac{1}{N}} \ . \tag{4.133}$$

This shows that q is typically small: for $N=2$ ($N=10$) one obtains $q \lesssim 1.7\times 10^{-6}$ ($q \lesssim 1.4\times 10^{-2}$), a conservative estimate obtained by replacing $\eta_0 \to \eta_{\rm lim} = 0.2$. In practice η is substantially smaller since the bound $\eta \leq \eta_{\rm lim}$ is to be fulfiled at all k, not just at the fiducial scale. Similar bounds on q can be obtained using our priors together with the constraint $M \leq M_p$. We have checked numerically that the values obtained agree with the ones derived above.

4.10 Results of the numerical analysis

4.10.1 Standard parameterization

The results obtained using the standard parameterization for the primordial spectra, Equations (3.229) and (3.230), are summarized for easy reference in Table 4.7 both with and without a running spectral index. For later reference, we have also considered the next term in the Taylor expansion (3.229), which has been denoted as 'running of the running', in the last two numerical columns of Table 4.7. The table shows the best–fit parameter values, the posterior values and 68% 1-dimensional posterior intervals for the parameters. We also give the best–fit values for the log–likelihood, normalized with respect to the model with only a constant tilt included[6]. Let us recall that the quantities describing the primordial spectrum are defined at the fiducial scale $k_0 = 0.002\,\mathrm{Mpc}^{-1}$. These results will be useful later on to interpret the outcomes for the LOG and LOG+NRO models and for the comparison with them. For the moment we can go back to the Table 4.4 which summarizes the results from the WMAP team that are comparable with the second column of 4.7. The main difference between the two analyses is that we used the SDSS large scale structure information in conjunction with four different CMB data sets, while in the WMAP case only their own data together with SDSS data were considered. This is the reason of the discrepancy in the running that is apparent. The effect of adding more extra CMB data sets enhances the relevance of the running in the fit.

It is interesting to note that using the standard parameterization up to second order a large and negative running of the running is preferred [6], which increases the power on large scales (see bottom panel of Figure 4.11), even though the fit is only marginally better than the case with constant running, according to Table 4.7. This is somewhat surprising: since in the slow–roll approximation $n = 1 + 2\eta - 6\epsilon$, if n departs from scale–invariance too quickly then η, ϵ or both grow up to order 1 values, prompting the end of slow–roll and the inflationary process at quite small k. However, in order to solve the horizon problem, we need about 50 or 60 efolds of inflation, which corresponds to the same interval in $\ln k$. This requires the (large and negative) $\mathrm{d}n/\mathrm{d}\ln k$ to get suppressed at some point, suggesting a positive second derivative (unlike the result of the fit). This contradiction could only be avoided if the $n(k)$ function changes abruptly at some point (or, maybe, if there are subsequent episodes of inflation). In any case, it seems clear that the current preference for a negative second derivative is strongly driven by the (possibly anomalous) low power of the large–scale multipoles. This could easily change if observations by Planck do not confirm the lack of large scale power observed by COBE and WMAP. However, we notice that from a model selection perspective even present data do not require a non–zero running of the running, as discussed in section 4.1.2. The previous discussion will be useful later to interpret the outcomes for the LOG and LOG+NRO models and for the comparison with them.

[6]The absolute value of the log–likelihood is of little interest here and in the following. For completeness, we have computed the likelihood values using the WMAP3 likelihood code version v2p2 with the default settings regarding the offset for the log–likelihood. The best–fit value for the constant tilt model is $-2\ln\mathcal{L} = 3614.0$.

Table 4.7: 1-dimensional marginalized 68% region and best fit values results for the standard parameterizations (3.229), (3.230) with $n = \text{constant}$, $dn/\ln k = \text{constant}$ and $d^2n/\ln^2 k = \text{constant}$, from left to right.

Model	no running		with running		running of running	
$-2\Delta\ln\mathcal{L}$	0.0		-3.4		-4.4	
	1D 68%	Best fit	1D 68%	Best fit	1D 68%	Best fit
Cosmological parameters						
$\Omega_b h^2 \times 10^2$	2.23 ± 0.07	2.25	$2.20^{+0.09}_{-0.08}$	2.18	2.22 ± 0.08	2.18
$\Omega_c h^2$	0.106 ± 0.004	0.107	0.107 ± 0.004	0.109	0.107 ± 0.004	0.107
Θ_*	1.043 ± 0.003	1.042	1.043 ± 0.003	1.043	1.044 ± 0.004	1.043
τ	0.084 ± 0.029	0.087	0.114 ± 0.035	0.113	0.106 ± 0.033	0.109
H_0[Km/s/Mpc]	74.3 ± 2.1	73.1	73.1 ± 2.3	72.0	73.6 ± 2.4	72.8
Power spectra parameters						
$\ln(P_s^0 \times 10^{10})$	3.11 ± 0.07	3.15	3.00 ± 0.10	3.09	$2.99^{+0.10}_{-0.11}$	3.06
n_0	0.973 ± 0.019	0.961	$1.141^{+0.083}_{-0.082}$	1.085	$1.111^{+0.096}_{-0.091}$	1.069
$\mathrm{d}n/\mathrm{d}\ln k\big\vert_{k_0}$	—	—	-0.07 ± 0.03	-0.06	-0.03 ± 0.07	-0.01
$\mathrm{d}^2n/\mathrm{d}\ln^2 k\big\vert_{k_0}$	—	—	—	—	-0.021 ± 0.032	-0.032
r_0	< 0.22	0.003	< 0.59	0.15	< 0.63	0.22

4.10.2 Small–coupling regime

We denote the choice of flat prior on N_e^0 by LOG$\mathcal{F}$, where the top–hat distribution is taken in the interval $2 \leq N_e^0 \leq 1000$. In the second case, denoted by LOG$\mathcal{G}$, we impose a Gaussian prior on N_e^0, with mean 50 and 5 efolds of standard deviation. Let us remind here that N_e^0 approximates the number of efolds since the time when the scale associated with k_0 first crossed the horizon till the end of inflation. Thus the total number of efolds since the time when the largest observable scale, $k_{\rm obs}$, crossed the horizon is $\simeq N_e^0 + 3$. This prior choice incorporates the theoretical prejudice that the total number of efolds should be in the 50–60 range.

The results of the Monte Carlo Markov chain (MCMC) analysis for the LOG$\mathcal{F}$ and LOG$\mathcal{G}$ cases are given in Figure 4.10 and are summarized in Table 4.8. We give 1–dimensional regions encompassing 68% of probability for well–determined parameters; robust upper bounds for parameters whose detailed constraints are parameterization–dependent; and best–fit values. The Table also gives posterior ranges and best–fit values for the corresponding expressions for the tilt, running and tensor–to–scalar ratio at the fiducial scale: n_0, $\mathrm{d}n/\mathrm{d}\ln k|_0$ and r_0, respectively. These have been obtained by using lowest order expressions in terms of the slow–roll

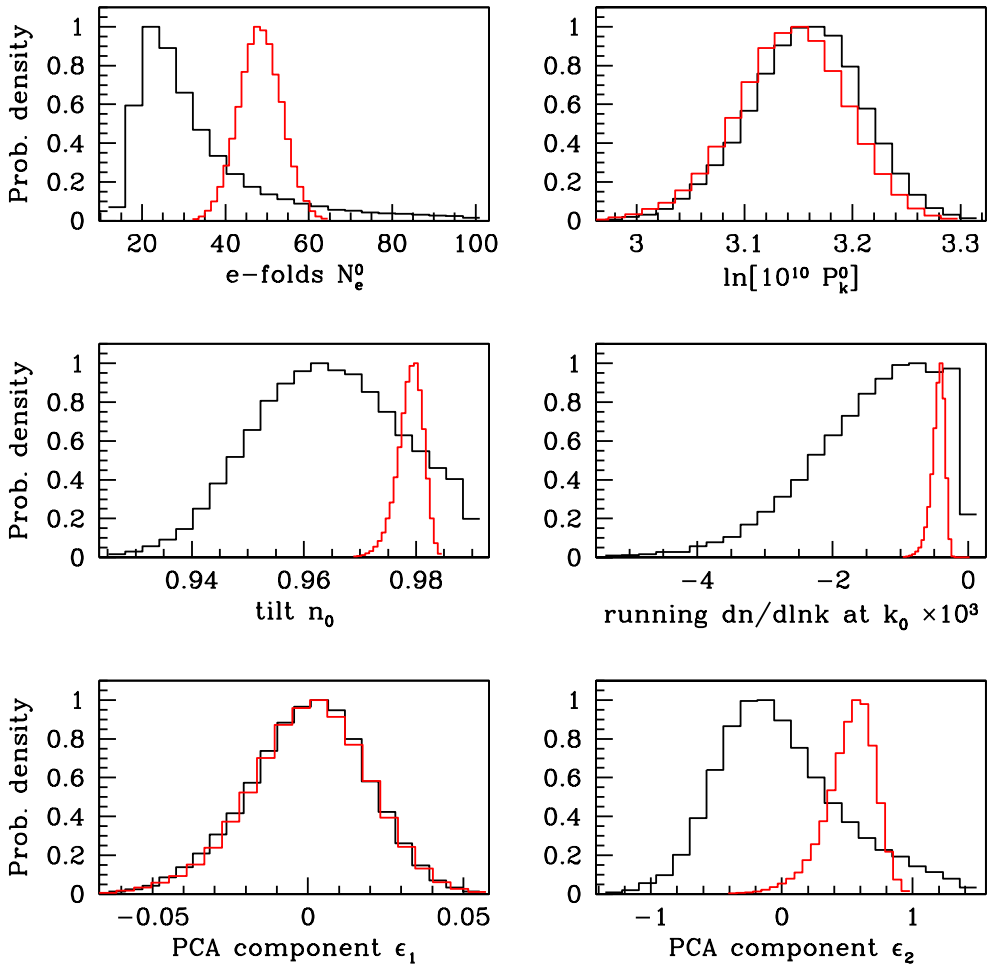

Figure 4.10: 1D marginalized probability distributions for the well–constrained parameters in the LOG scenario (compare Table 4.8). Black curves are for the case with a flat prior on N_e^0, while red is for the case where a Gaussian prior around $N_e^0 = 50$ has been enforced.

parameters, equations (3.221), (3.223) and (3.224).

As anticipated, constraints on N_e^0 and $\ln P_s^0$ are quite tight, and we have checked that they are almost independent of the choice of prior by performing a run with priors flat in $\{\ln N_e^0, \ln q, \ln P_s^0\}$ instead. It is interesting to notice that in the LOG$\mathcal{F}$ case the 1D 68% (95%) posterior region (2–tails) is approximately $21 < N_e^0 < 46$ ($16 < N_e^0 < 81$), even though the mean is somewhat lower, at around 33 efolds, and the best fit is around 26 efolds. This result is close to the theoretical prejudice $N_e^0 \simeq 50$, required to solve the horizon and flatness problems. Hence, assuming a flat tree level potential for the inflaton, the observed shape of the power spectrum appears to automatically point to model parameters giving a very sensible number of efolds, in particular given the heavy tail of the probability distribution function (pdf) for large N_e^0. This is not a triviality, in principle any value for N_e^0 could have

Table 4.8: Marginalized 68% regions and best–fit values for the class of models LOG (small–coupling regime) for quantities that are well–determined and essentially prior/parameterization independent. For q and the tensor–to–scalar ratio at the fiducial scale, r_0, we give absolute upper limits that are a consequence of the spectral tilt and of physical priors on the potential parameter space, Equation (4.111). These bounds have no confidence level attached as the precise numerical value would depend on the prior/parameterization choice, a consequence of the PCA component ε_3 being an unconstrained, degenerate direction in parameter space (see text for details).

Model	$\boxed{\text{LOG}\mathcal{G}}$		$\boxed{\text{LOG}\mathcal{F}}$	
$-2\Delta\ln\mathcal{L}$	2.1		-0.4	
	1D 68%	Best fit	1D 68%	Best fit
Cosmological parameters				
$\Omega_b h^2 \times 10^2$	2.30 ± 0.04	2.30	2.24 ± 0.07	2.23
$\Omega_c h^2$	0.107 ± 0.004	0.1058	0.107 ± 0.004	1.071
Θ_*	1.044 ± 0.003	1.044	1.042 ± 0.003	1.041
τ	0.103 ± 0.026	0.107	$0.089^{+0.028}_{-0.030}$	0.089
H_0 [Km s^{-1}Mpc^{-1}]	74.5 ± 1.5	74.9	73.2 ± 1.9	72.9
Power spectra parameters				
$\ln(P_s^0 \times 10^{10})$	3.14 ± 0.05	3.14	$3.16^{+0.05}_{-0.06}$	3.17
N_e^0	48.3 ± 5.1	48.5	$33.4^{+12.3}_{-12.5}$	25.6
q	< 0.04 for any parameterization			
Derived power spectra parameters				
n_0	0.979 ± 0.002	0.979	$0.964^{+0.016}_{-0.013}$	0.961
$\mathrm{d}n/\mathrm{d}\ln k\big\vert_{k_0} \times 10^3$	-0.45 ± 0.09	-0.43	-1.42 ± 0.94	-1.54
r_0	$< 4 \times 10^{-3}$ for any parameterization			
Potential parameters and PCA components				
ρ/M_p^4	$< 4 \times 10^{-10}$ for any parameterization			
β/M_p^4	$< 1 \times 10^{-12}$ for any parameterization			
ϕ_0/M_p	< 1 (from prior, Equation (4.111))			
ε_1	0.00 ± 0.02	0.01	0.00 ± 0.02	0.00
ε_2	0.52 ± 0.18	0.67	0.00 ± 0.48	-0.20
ε_3	essentially unconstrained			

emerged from the analysis.

The values of the spectral index and its running at the fiducial scale are easily derived from the parameters of the fit and are also given in Table 4.8. Note that $\mathrm{d}n/\mathrm{d}\ln k|_0$ is very small (of order 10^{-3}), as expected from the relation (4.15). So the LOG scenario is indeed close to the constant $n =$ limit. The value of n at the fiducial scale, n_0, is directly related to the value of N_e^0 by equation (4.109), leading to the values of n_0 quoted in the Table. The LOG$\mathcal{F}$ best fit value $n_0 = 0.961$, that corresponds to $N_e^0 = 25.6$, coincides with the value obtained assuming constant n and negligible running, as indicated in Table 1. It is interesting to note that although the LOG$\mathcal{F}$ and constant n fits are very similar, they are not identical, and indeed LOG$\mathcal{F}$ gives a slightly better fit, as can be checked by comparing the best fit likelihood values (also compare Figure 4.11). Furthermore, if future CMB and LSS data favour a value of n_0 closer to 0.98, the value of N_e^0 will come out even closer to the theoretically preferred value, $N_e^0 \simeq 50$. The upper bound on q is a consequence of the measured tilt and of the physical boundaries imposed on the potential parameters. Let us recall from the discussion after equation (4.117) that we expect $q \leq (1-n)/2$. For the reasons explained below, the pdf for q depends on the prior chosen, and therefore we do not show it in Figure 4.10. However the upper bound is robust with respect to a change of priors, and therefore we chose to report only this value. The tensor contribution remains negligible, below the level of 10^{-3}, since from (4.94) the value of the tensor to scalar ratio at the fiducial scale is

$$r_0 \simeq 4\frac{q}{N_e^0} \,. \tag{4.134}$$

Consequently the upper bound on q corresponds to an order of magnitude smaller bound on r_0.

The fact that we can extract two measured quantities in this scenario (the tilt and normalization) from three model parameters (either (4.107) or (4.108)) means that we expect a strongly degenerate direction in the primordial power spectrum parameter space. In fact, the constraints coming from the data define a region shaped as a long solid cylinder in the 3D subspace spanned by (4.108). Since this cylinder is not aligned with the potential parameters direction, if one tries to convert limits on (4.107) into limits on the potential parameters (4.108) one unavoidably picks up the degenerate direction along the axis of the cylinder. This means that while in the set (4.107) the constraints on N_e^0 and $\ln P_s^0$ are robust with respect to a change in the parameterization of the problem (since all the parameterization dependency is dumped into q), it is not possible to translate these into completely parameterization independent results for the potential parameters (4.108).

However, one can still define well constrained parameterization independent directions in the subspace spanned by (4.108) by performing a Principal Component Analysis (PCA), i.e. by changing into a new coordinate system aligned with the degenerate direction. We therefore consider the covariance matrix C in the subspace spanned by the reduced variables $\zeta = (\ln\hat{\rho}_0, \ln\hat{q}, \ln\hat{\phi}_0)$, where hats indicate that the variables have been shifted by their posterior mean and normalized to their posterior standard deviation. Then the PCA vector ε is given by

$$\varepsilon = U\zeta \,, \tag{4.135}$$

where U is the 3D matrix that diagonalizes C:

$$\zeta^t C \zeta = \varepsilon^t \Lambda \varepsilon \ , \tag{4.136}$$

and $\Lambda = \mathrm{diag}(\lambda_1, \lambda_2, \lambda_3)$ is the matrix of eigenvalues, whose square roots give the error along the directions defined by ε. The matrix U is numerically given by

$$U = \begin{pmatrix} 0.46 & -0.68 & 0.57 \\ 0.80 & 0.05 & -0.60 \\ 0.38 & 0.73 & 0.56 \end{pmatrix} \ , \tag{4.137}$$

and $\sqrt{\lambda_1} = 0.02$, $\sqrt{\lambda_2} = 0.48$ while $\sqrt{\lambda_3} \gg 1$, showing that ε_3 is indeed the degenerate direction. We have checked that the constraints on $(\varepsilon_1, \varepsilon_2)$ are largely independent on the chosen parameterization.

The 1–dimensional marginalized probability distributions for the well constrained parameters in the problem are shown in Figure 4.10. We do not show the probability distributions for the non–primordial cosmological parameters as they are mostly very similar to the standard scenario, nor do we plot the pdfs for the parameters for which we have only upper limits (q, r_0, ε_3) since their distribution depends on the parameterization employed.

Turning now to the LOG$\mathcal{G}$ case, which imposes a theoretically motivated prior on the number of efolds, we want to point out that the prior enforces $N_e^0 \simeq 50$. This means that the model essentially loses one parameter, and therefore the best fit log–likelihood is slightly worse (see Table 4.8). In fact, the LOG$\mathcal{G}$ fit has basically just one free parameter for the power spectrum (namely the normalization $\ln P_s^0$), since q is almost irrelevant. Still, it gives an excellent best fit to the observational data. Also, enforcing 50 efolds results in a very strong prediction for the tilt to be $n_0 \simeq 0.98$: compare Figure 4.10 and the tightness of the posterior probability for n_0 (red curve); while both the tensor contribution and the running are predicted to be very small.

In Figure 4.11 we plot the CMB temperature power spectrum for the best fit models discussed here along with the compilation of the data used.

4.10.3 Small–coupling and non–renormalizable operator

In this scenario the five parameters we use to describe the primordial spectrum are

$$\mathbb{P}_{\mathrm{LOG+NRO}} \equiv \{\ln P_s^0, N_e^0, q\,, A\,, N\}. \tag{4.138}$$

We discussed in Section 4.9.2, the meaning of the first three ones is similar to those of the LOG case, and we impose flat priors on $\ln P_s^0$ and q. As we did in the previous section, we consider two types of fits: LOG+NRO$\mathcal{F}$ (with a flat prior on N_e^0) and LOG+NRO$\mathcal{G}$ (with a Gaussian prior centered at $N_e^0 = 50$ with standard deviation of 5). Since A is expected to be of order unity or less according to the discussion above, it is appropriate to use a flat prior on A between 0 and 1.

Let us recall that N determines the order of the NRO. As argued in Section 4.9.2, we expect it to be within 1 to $\mathcal{O}(10)$. One could imagine treating N as a free

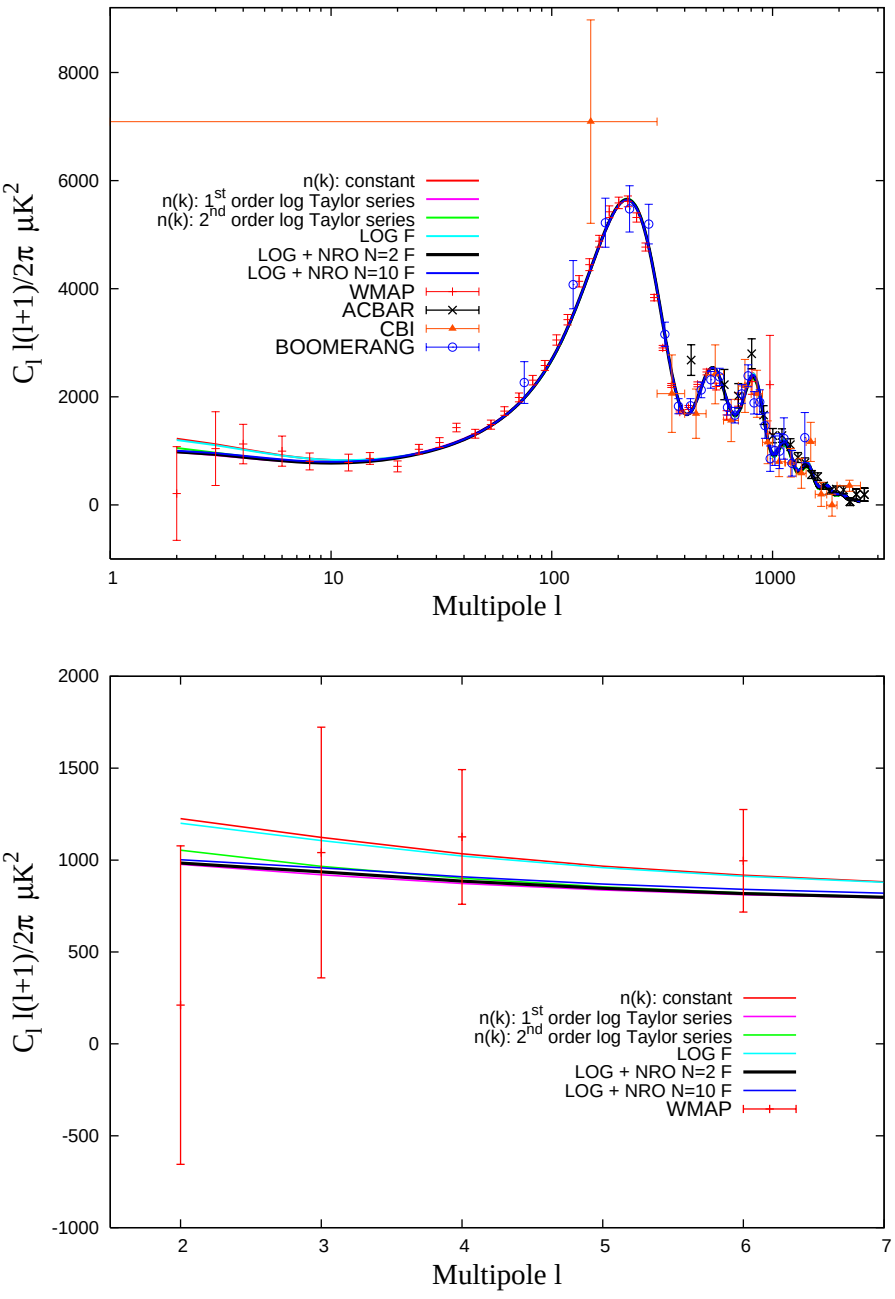

Figure 4.11: CMB temperature power spectrum for the best–fit model parameters for the standard parameterization, the LOG and the LOG+NRO scenarios. The bottom panel shows the details of the large–scale region.

parameter and trying to derive a posterior bound on it from the data. However it is technically difficult to ensure that the MCMC is correctly performed across disjoint regions of the parameter space. Since N is an integer, using it as a free parameter effectively gives N separated patches across which it is very difficult to sample. Furthermore, NROs with different values of N are better considered as different models, since the underlying physics is likely to be different. Therefore distinguishing between values of N can be regarded as a model selection task, rather than a parameter constraint exercise. For this reason it is more instructive to consider two separate cases which are representative of the general behaviour at low ($N = 2$) and large ($N = 10$) values of N. Parameter constraints from CMB and LSS data, which are discussed next, are summarized in Table 4.9 for the $N = 2$ case and in Table 4.10 for the $N = 10$ case.

Starting from the $N = 2$ case, we find a strong upper bound on q, which reflects the theoretical considerations exposed above and is a consequence of the physically motivated prior (4.124). As a consequence, the tensor contribution is always negligible. The number of efolds for the LOG+NRO$\mathcal{F}$ case ($N = 2$) is $N_e^0 = 14.5 \pm 3.5$ at 68%, becoming $10.1 \leq N_e^0 \leq 25.8$ at 95%, which is too small to solve the horizon problem. Meanwhile, the parameter A is rather tightly constrained, $A = 0.60^{+0.08}_{-0.09}$. These results can be intuitively understood in the following way. As we explained when we introduced the classes of models, the presence of the NRO increases $\mathrm{d}n/\mathrm{d}\ln k$. This effect is maximal at low k. The lower N is, the more gradual is the decrease of $\mathrm{d}n/\mathrm{d}\ln k$ with the wavenumber. In the $N = 2$ case the value of the running of the spectral index is fairly constant in the region of k accessible to observations. Therefore, the model (for not too small A, which would lead back to the LOG scenario) could be reasonably well approximated by the constant $\mathrm{d}n/\mathrm{d}\ln k$ standard parameterization. We know from the data analyses that for this standard parameterization the value of n at $k = k_0$ cannot be very far from $n = 1$. This implies from Equations. (4.105), (4.103) and the smallness of q that A cannot be far from $A \sim (2N + 3)^{-1/(N+2)}$, which explains the value $A \simeq 0.6$. The running $\mathrm{d}n/\mathrm{d}\ln k$ is then determined by N_e^0 (see Equation (4.105)). Not surprisingly, the preferred value for the running turns out to be consistent with the one from the standard parameterization (compare Tables 4.7 and 4.9), which corresponds to the value of N_e^0 quoted above. This is also consistent with our discussion of the (too small) number of efolds in the standard parameterization. Some of these features are illustrated in Figure 4.12 (left panel), which shows the interplay of N_e^0 and A and their impact on the spectral index; and Figure 4.13, which shows the best–fit $n(k)$ (left panel) and the curve corresponding to the posterior mean, alongside with the favoured 95% posterior region of $n(k)$ for $N = 2$. The corresponding $P_s(k)$ is shown in the right panel.

Note that the number of free parameters is essentially the same for both the LOG+NRO case and the constant running parameterization: 4 for the latter (3 if r is set to zero) and 5 for LOG+NRO$\mathcal{F}$ (among which q is almost irrelevant and N has been fixed), and their best fit log–likelihoods are similar. We comment further on this in the next section.

Further enforcing a sufficient number of efolds by imposing a Gaussian prior on N_e^0 (LOG+NRO$\mathcal{G}$ case in Table 4.9) results in a worsening of the quality of fit (an

Table 4.9: As in Table 4.7, but for the class of models referred in the text as LOG+NRO, for $N = 2$. Upper or lower bounds at the specified confidence level are understood to be 1–tail limits.

Model	LOG+NRO$\mathcal{G}$		LOG+NRO$\mathcal{F}$	
$-2\Delta \ln \mathcal{L}$	2.4		-2.7	
	1D 68%	Best fit	1D 68%	Best fit
Cosmological parameters				
$\Omega_b\, h^2 \times 10^2$	2.32 ± 0.05	2.31	2.18 ± 0.07	2.16
$\Omega_c\, h^2$	0.107 ± 0.004	0.107	0.108 ± 0.004	0.109
Θ_*	$1.044^{+0.003}_{-0.002}$	1.044	1.041 ± 0.003	1.042
τ	0.112 ± 0.026	0.010	0.095 ± 0.030	0.102
H_0 [Km s^{-1}Mpc^{-1}]	$74.7^{+1.6}_{-1.5}$	75.0	$73.3^{+1.9}_{-2.0}$	71.6
Power spectra parameters				
$\ln(P_s^0 \times 10^{10})$	3.14 ± 0.05	3.13	3.15 ± 0.05	3.15
N_e^0	47.0 ± 5.1	49.6	14.5 ± 3.5	11.7
A	0.46 ± 0.11	0.27	$0.60^{+0.08}_{-0.09}$	0.66
q	$< 5 \times 10^{-6}$ for any parameterization			
Derived power spectra parameters				
n_0	0.987 ± 0.007	0.981	$1.001^{+0.016}_{-0.048}$	1.027
$\mathrm{d}n/\mathrm{d}\ln k\big\vert_{k_0} \times 10^2$	$-0.11^{+0.11}_{-0.05}$	-0.45	$> -6.1\,(95\%)$	-4.28
$\mathrm{d}^2n/\mathrm{d}\ln^2 k\big\vert_{k_0} \times 10^3$	0.02 ± 0.02	-0.05	$< 14.2\,(95\%)$	7.93
r_0	$< 3 \times 10^{-8}$ for any parameterization			
Potential parameters and PCA components				
ρ/M_p^4	$< 1 \times 10^{-10}$ for any parameterization			
β/M_p^4	$< 7 \times 10^{-13}$ for any parameterization			
ϕ_0/M_p	$< 1 \times 10^{-3}$ for any parameterization			
M/M_p	< 1 (from prior, Equation (4.124))			
ε_1	0.04 ± 0.02	0.06	0.00 ± 0.02	0.00
ε_2	0.28 ± 0.13	0.05	0.01 ± 0.08	-0.02
ε_3	-2.3 ± 0.4	-3.1	0.01 ± 0.72	0.87
ε_4	essentially unconstrained			

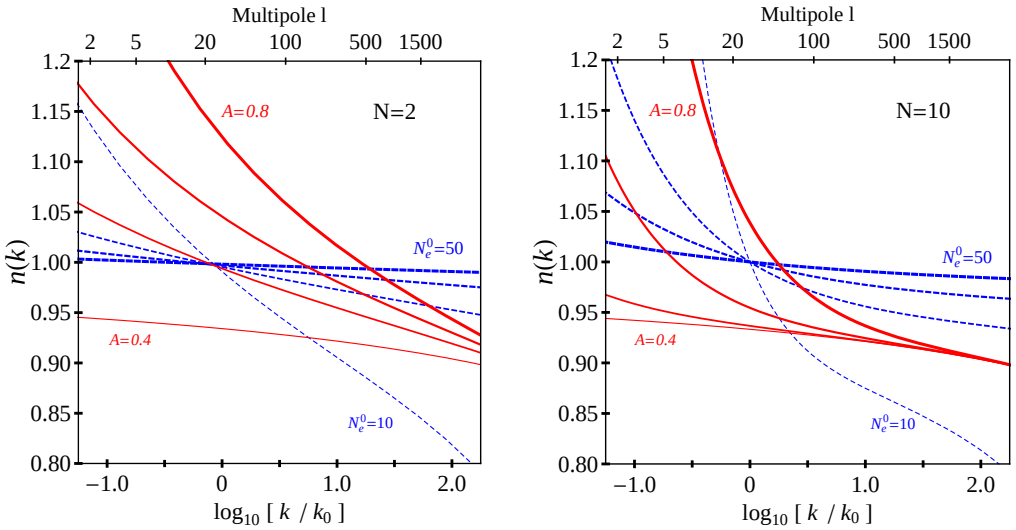

Figure 4.12: Dependence of $n(k)$ on the parameters N_e^0 (blue, from thin to thick $N_e^0 = 10, 20, 30, 50$, for fixed $A = 0.6$ in the $N = 2$ case, left, and for fixed $A = 0.77$ in the $N = 10$ case, right) and on A (red, from thin to thick $A = 0.2, 0.4, 0.6, 0.8$, for fixed $N_e^0 = 15$ in both panels) in the LOG+NRO scenario with N as indicated.

increase of minus twice the best fit log–likelihood by 2.1 with respect to the standard power–law case). This is because a larger N_e^0 for a given A implies a spectrum closer to scale–invariance, which is not favoured by the data if this freedom is allowed. For example, [191] reports an evidence of 17:1 against a scale invariant spectrum using WMAP3 data. However, see [148] and (more recently) [5] for a different analysis reaching a very different conclusion on this matter.

As observed in the LOG case, also in the LOG+NRO situation the strong degeneracy among the potential parameters makes it impossible to robustly translate the constraints on $\mathbb{P}_{\rm LOG+NRO}$ into prior independent constraint for the potential parameters, (4.17). As we have done above, we can still define well constrained directions in the subspace spanned by the parameters $\zeta = (\ln\hat{\rho}_0, \ln\hat{q}, \ln\hat{\phi}_0, \ln\hat{M})$, where the hats indicate that the variables have been shifted by their posterior mean and normalized to their posterior standard deviation. The eigenvalues of the 3 well constrained directions are now $\sqrt{\lambda_1} = 0.02$, $\sqrt{\lambda_2} = 0.08$, $\sqrt{\lambda_3} = 0.72$ while $\sqrt{\lambda_4} \gg 1$, and the corresponding rotation matrix is

$$U = \begin{pmatrix} 0.49 & -0.56 & 0.43 & 0.51 \\ -0.84 & -0.05 & 0.23 & 0.53 \\ 0.31 & 0.79 & 0.04 & 0.54 \\ 0.04 & -0.26 & -0.87 & 0.42 \end{pmatrix} . \tag{4.139}$$

Figure 4.14 shows marginalized 1–dimensional posterior distributions for some of the well constrained parameters in the LOG+NRO ($N = 2$) scenario. Since the value of the tilt, running and running of the running at the fiducial scale are not really representative of the functional form of $n(k)$ in this case, we do not show pdfs for those quantities (even though their constraints are reported for completeness in Table 4.9). A more faithful representation is actually given in Figure 4.13.

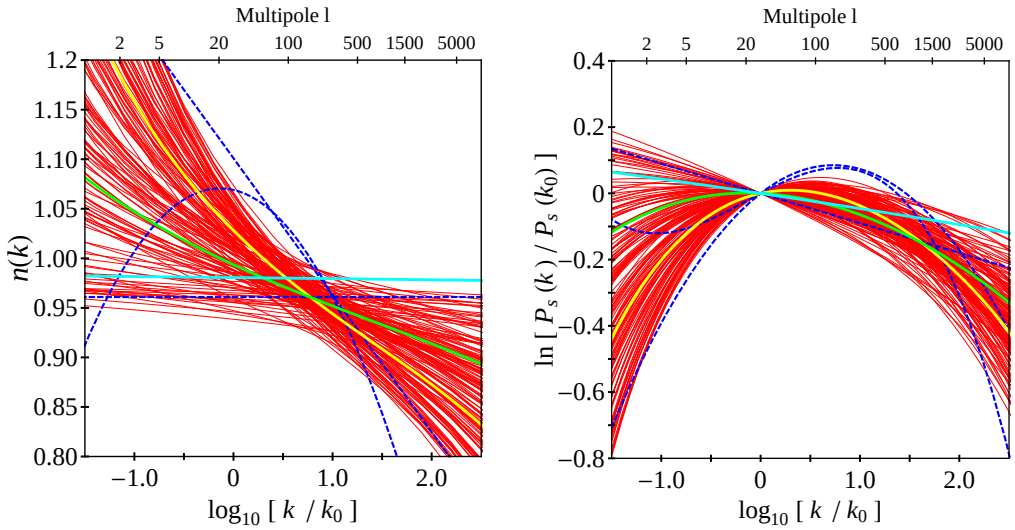

Figure 4.13: Preferred shape of the spectral index $n(k)$ (left) and the corresponding power spectrum (right) from CMB and LSS data (at 95%, red curves) in the LOG+NRO scenario for $N = 2$. The yellow line shows the best–fit value, the green line the posterior mean while the cyan line is the best–fit further imposing a Gaussian prior on the number of efolds (LOG+NRO$\mathcal{G}$ scenario). The dotted blue lines represent for reference the best–fit power spectra in the standard parameterization with tilt only, with running and with running of the running (from top to bottom on the right–hand side of the $n(k)$ panel, from top to bottom on the left–hand side of the $P_s(k)$ panel, compare Table 4.7).

Let us now turn to the $N = 10$ case. The main difference with the previous case is that the effect of the NRO is much more pronounced on large scales. In particular the running $\mathrm{d}n/\mathrm{d}\ln k$ can be quite large now at very low k and decrease very quickly, converging to the LOG scenario. Thus, the scenario is qualitatively different from the constant running standard parameterization. As for $N = 2$, the value of q is small and below the theoretically expected bound given by equation (4.133), which translates again into a negligible tensor contribution ($r_0 < 3 \times 10^{-4}$). The preferred value of A is still approximately determined by the observational empirical condition $n_0 \simeq 1$. From Equations (4.105) and (4.103), this translates into $A \simeq (2N+3)^{-1/(N+2)} \simeq 0.77$. The fact that the model rapidly converges to the LOG scenario allows to increase the number of efolds to values similar to those of the LOG$\mathcal{F}$ case. More precisely, in the LOG+NRO$\mathcal{F}$ case, the probability distribution for the number of efolds has a heavier tail for large values of N_e^0, and the 2–tails posterior 68% (95%) region is given by $18.8 < N_e^0 < 37.1$ ($15.8 < N_e^0 < 69.5$), which means that the horizon and flatness problems are solved at the 2σ level.

Some of these features are illustrated in Figure 4.15. Note in particular that the running of running for the best fit (yellow line in Figure 4.15) is positive and sizable. The quality of the fit is similar to the constant running case for the standard parameterization, though the actual shape of the spectrum is quite different, but slightly worse. This is not surprising. We know that data prefer a negative second derivative, which cannot be achieved in the LOG+NRO scenario at low k. Remember the discussion after equation (4.105). However, as explained there, if the spectral

Table 4.10: As in Table 4.9 but for $N = 10$ in the LOG+NRO scenario. We did not perform in this case a Principal Component Analysis as for $N = 2$.

Model	LOG+NRO$\mathcal{G}$		LOG+NRO$\mathcal{F}$	
$-2\Delta \ln \mathcal{L}$	2.1		-1.8	
	1D 68%	Best fit	1D 68%	Best fit
Cosmological parameters				
$\Omega_b\, h^2 \times 10^2$	2.31 ± 0.05	2.30	2.23 ± 0.07	2.19
$\Omega_c\, h^2$	0.107 ± 0.004	0.107	0.107 ± 0.004	0.108
Θ_*	$1.044^{+0.003}_{-0.002}$	1.044	1.041 ± 0.003	1.041
τ	0.105 ± 0.026	0.104	$0.089^{+0.014}_{-0.030}$	0.93
H_0 [Km s^{-1}Mpc^{-1}]	74.6 ± 1.6	74.5	73.1 ± 1.8	72.1
Power spectra parameters				
$\ln(P_s^0 \times 10^{10})$	3.14 ± 0.05	3.14	3.15 ± 0.05	3.16
N_e^0	48.2 ± 5.1	48.7	$28.5^{+8.6}_{-9.6}$	17.5
A	$0.52^{+0.19}_{-0.16}$	0.54	$0.57^{+0.17}_{-0.20}$	0.77
q	$< 2 \times 10^{-3}$ for any parameterization			
Derived power spectra parameters				
n_0	$0.982^{+0.002}_{-0.004}$	0.980	0.971 ± 0.016	1.002
$\mathrm{d}n/\mathrm{d}\ln k\big\vert_{k_0} \times 10^2$	$-0.11^{+0.09}_{-0.06}$	-0.05	$> -3.4\,(95\%)$	-4.17
$\mathrm{d}^2n/\mathrm{d}\ln^2 k\big\vert_{k_0} \times 10^3$	$0.13^{+0.11}_{-0.18}$	-0.03	$< 17.8\,(95\%)$	23.7
r_0	$< 3 \times 10^{-4}$ for any parameterization			
Potential parameters				
ρ/M_p^4	$< 1 \times 10^{-11}$ for any parameterization			
β/M_p^4	$< 1 \times 10^{-14}$ for any parameterization			
ϕ_0/M_p	< 0.2 for any parameterization			
M/M_p	< 1 (from prior, Equation (4.124))			

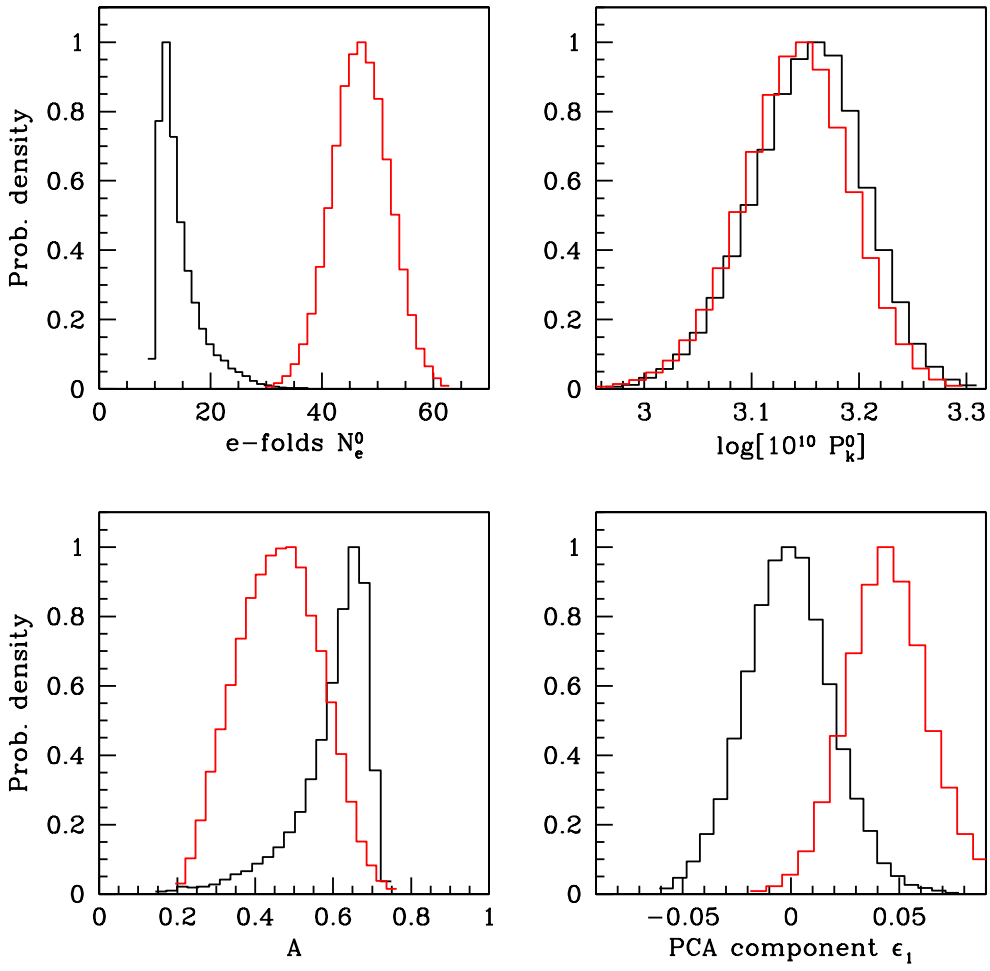

Figure 4.14: 1D marginalized probability distributions for some well–constrained parameters in the LOG+NRO scenario, for $N = 2$ (compare Table 4.9). Black curves are for the case with a flat prior on N_e^0, while red is for the case where a Gaussian prior around $N_e^0 = 50$.

index really runs, a positive second derivative can be much more satisfactory from the physical point of view, in particular to produce a reasonable number of efolds. This is precisely the case here.

If one enforces a Gaussian prior around $N_e^0 = 50$ (as in the LOG+NRO$\mathcal{G}$ case), then the best fit spectrum becomes again featureless (light blue, solid line in Figure 4.15) but with a smaller tilt than the standard parameterization ($n_0 = 0.980$ for the $N = 10$ LOG+NRO$\mathcal{G}$ case), which in turn means that the goodness of fit becomes worse than the standard case (see Table 4.10). Indeed, the model becomes in this case quite similar to the simpler LOG$\mathcal{G}$ scenario.

Finally, for values of N between 2 and 10 we have found that the behaviour is intermediate between the cases discussed in the text as one could have naively expected.

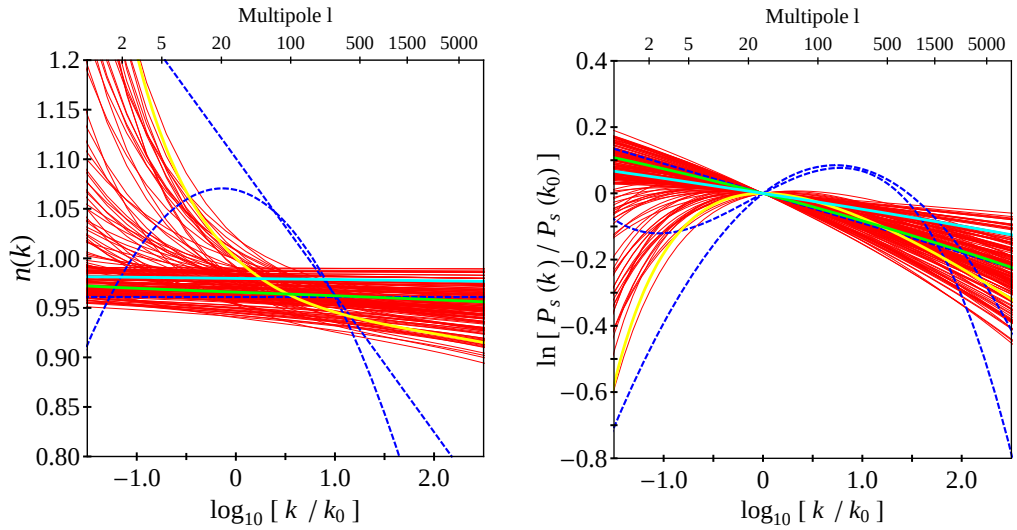

Figure 4.15: As in Figure 4.13 but for the LOG+NRO scenario with $N = 10$.

The above discussion shows that there are cases where the standard Taylor expansion of $n(k)$ fails to capture the physics of the models. Generally, the LOG+NRO scenario predicts a running of n which is stronger on large scales. This can only be recovered with several terms in the Taylor expansion, which results in a higher number of free parameters in the fit. On the other hand, the functional form of $n(k)$ in the LOG+NRO scenario implies the positiveness of the second derivative in most of the parameter space, unlike the standard fit. These facts make it impossible to use the results of the standard fits to constrain the LOG+NRO scenario: a direct comparison of the model with the data becomes necessary (as we have done here). This situation could easily apply to other theoretical models as well; and therefore great caution is necessary when interpreting generic constraints on the coefficient of the standard Taylor expansion in terms of specific physical models.

4.11 Model comparison

In the previous section we have presented parameter constraints for each class of models, namely the standard parameterization and the more physically motivated LOG and LOG+NRO scenarios. Assessing the relative performance of the three models is a model comparison question, to which we now turn our attention.

In the traditional frequentist approach to statistics, model comparison is tackled in terms of hypothesis testing: for example, we might ask whether the improvement in the best–fit likelihood in terms of the effective $\Delta\chi^2 = -2\Delta \ln \mathcal{L}$ when adding a running to the tilt is significant enough to warrant the inclusion of a non–zero running. There are however several reasons why answering this question is far from trivial. A technical reason is that the usual rule of thumb of "$\Delta\chi^2$ per extra degree of freedom" can only be applied if certain regularity conditions are met, and in particular only if the extra parameter for nested model does not lie on the boundary of the parameter space. See [273] for an astrophysical example and references therein.

For example, the $\Delta\chi^2$ criterion could not be applied to compare the quality of fit of the LOG model with that of LOG+NRO, since the former is obtained from the latter by setting $A = 0$, and $A < 0$ is not allowed.

Another aspect, more fundamental, has to do with the meaning and interpretation of frequentist hypothesis testing. As discussed in detail in [190], frequentist likelihood ratio tests *assume* the hypothesis *Hyp* is true and give the probability of observing data d as extreme or more extreme than what has actually been measured. This is a statement on the probability of the data assuming a hypothesis *Hyp* to be true (which in Bayesian terms amounts to the choice of a model, $\mathcal{M}$), i.e. frequentist hypothesis testing gives $P(d \mid Hyp)$. But this is not the quantity one is usually interested in, which is actually $P(\mathcal{M}|d)$, the probability of the model $\mathcal{M}$ given the observations, which can only be obtained by using Bayes theorem to invert the order of conditioning. For this reason, model selection is an inherently Bayesian question [191].

Bayesian model selection is based on the computation of the model likelihood

$$P(d|\mathcal{M}) \equiv \mathcal{E}(\mathcal{M}), \tag{4.140}$$

also called 'evidence', which is the normalization constant in the denominator of Bayes theorem (see [191,274] for details) obtained by averaging the likelihood $P(d|\theta, \mathcal{M})$ over the prior $P(\theta|\mathcal{M})$ in the parameter space θ of the model

$$\mathcal{E}(\mathcal{M}) = \int P(d|\theta, \mathcal{M}) P(\theta|\mathcal{M}) d\theta. \tag{4.141}$$

From the model likelihood one obtains the model probability given the data by using once more Bayes theorem, $P(\mathcal{M}|d) \propto P(\mathcal{M})\mathcal{E}(\mathcal{M})$, where $P(\mathcal{M})$ is the prior probability assigned to the model (often taken to be noncommittal if there is no underlying particular physical or otherwise motivation; and equal to $1/N_m$ if one considers N_m different models). When comparing two models one usually computes the Bayes factor B_{12}, given by the ratio of the evidences between the two models:

$$\ln B_{12} = \ln \mathcal{E}(\mathcal{M}_1) - \ln \mathcal{E}(\mathcal{M}_2). \tag{4.142}$$

The Bayes factor thus gives the factor by which the relative odds among two models have changed after the arrival of the data. As a simple calculation shows for the case of Gaussian likelihood and prior, Equation (4.141) contains both a likelihood ratio term which rewards better fitting, and an "Occam's razor" term that disfavours unnecessary model complexity, defined in terms of useless parameters (see [275] for a discussion of model complexity). The "best" model is one that combines good fitting with a good capacity of making predictions. Bayes factors are usually interpreted against the Jeffreys' scale for the strength of evidence, which we qualify as follows: "weak evidence" for $|\ln B| < 2.5$, "moderate evidence" for $2.5 < |\ln B| < 5.0$ and "strong evidence" for $|\ln B| > 5.0$. The computation of the model likelihood is in general a numerically difficult task, as it involves a multi–dimensional integration over the whole of parameter space. Furthermore, a prior dependence is (correctly) built into the method, as the Occam's razor term depends on the ratio of the prior to posterior volume, which gives the amount of "wasted" parameter space of the model.

Therefore it is problematic to evaluate the Bayes factor unless one has a physically motivated way of setting the prior volume.

The difficulty of using a fully Bayesian approach to the comparison of the standard Taylor series parameterization with either the LOG or the LOG+NRO scenario is that the former represents a purely phenomenological fit to the data, while the LOG and LOG+NRO models are physically motivated. In particular, setting a prior on the potential parameters of the LOG and LOG+NRO models is not comparable to setting a strictly phenomenological prior on the quantities of direct relevance for the fit, i.e. the spectral tilt, the running, etc. in the standard parameterization. The Occam's razor effect which rewards highly predictive models does not work properly if we do not compare like with like, i.e. if we are unable to set priors on the parameter space of the phenomenological parameterizations used for the fit. Since the standard parameterization is by construction phenomenological, it cannot be directly compared to the LOG and LOG+NRO scenarios using the Bayesian evidence.

However, we can still draw some interesting, partial conclusion from a Bayesian approach. In [190], a method was presented to derive upper bounds on the Bayesian evidence for nested models, called "Bayesian calibrated p–values", that is useful in cases such as this where there is only a very loose physical basis to assign priors to phenomenological quantities in the fit (here, the various terms in the expansion of the potential). This allows to assess whether extra parameters are unnecessary within the framework of nested models, as it gives the Bayes factor which (under mild assumptions) maximizes the evidence in favour of the more complex model (i.e., with more terms in the Taylor expansion). If this turns out to be not very strong, then one can confidently conclude that the extra parameters are not needed.

Table 4.11 summarizes some relevant model comparison statistics. Focusing first on the standard parameterization section, we have employed the method of [190] to derive a prior independent upper bound on the Bayesian evidence in favour of extra terms in the Taylor expansion. The maximum Bayesian evidence in favour of a running is only $\ln \bar{B}_{21} = 0.7$ (compared to a model with just a spectral tilt), which falls short of even the "weak evidence" threshold. The maximum evidence in favour of a third term in the Taylor expansion is even weaker. We can therefore conclude that, for the standard parameterization, present data do not require any higher order terms than a spectral tilt (for which [190] found a maximum evidence of $\ln \bar{B} = 2.9$ compared to a scale–invariant spectrum). Notice that in this phenomenological approach the number of efolds has to be added by hand as an extra parameter of the model, indicated as (+1) in the column giving an approximate value of the effective number of parameters in the model.

Regarding the LOG class of models, the goodness of fit of the LOG$\mathcal{F}$ case is similar to the one of the simple tilt model. Although the number of free parameters of the LOG scenario is 3, the parameter q is irrelevant to the fit and therefore the effective number of parameters is closer to 2. A more precise counting of the effective parameters could be achieved using the notion of Bayesian complexity [275], but this is not required in the context of the present discussion. It is interesting to notice that the LOG scenario also solves the horizon problem (within 2σ of the posterior

Table 4.11: Summary of model comparison statistics. Wherever the Bayes factor is given, the notation $\ln B_{ij}$ indicated the Bayes factor between model i and model j (with $\ln B_{ij} > 0$ favouring model i). An overbar indicates a prior–independent upper limit obtained using the Bayesian calibrated p–values method. The quantity n gives the number of effective parameters in the model.

Model	$\Delta\chi^2$	n	> 50 efolds?	Bayes factor	Notes
Standard parameterization					
no running	0.0	3(+1)	ad hoc	—	
running	-3.4	4(+1)	ad hoc	$\ln \bar{B}_{21} = 0.7$	No evidence
running of running	-4.4	5(+1)	ad hoc	$\ln \bar{B}_{32} = 0.0$	No evidence
				$\ln \bar{B}_{31} = 0.4$	No evidence
LOG models					
LOG$\mathcal{F}$	-0.4	~ 2	yes (at 2σ)	—	
LOG$\mathcal{G}$	$+2.1$	~ 1	yes	$\ln \bar{B}_{45} = 0.4$	
LOG+NRO models					
+NRO$\mathcal{F}$ $N = 2$	-2.7	~ 3	no	—	Excluded
+NRO$\mathcal{G}$ $N = 2$	$+2.4$	~ 2	yes	—	Disfavoured
+NRO$\mathcal{F}$ $N = 10$	-1.8	~ 3	yes (at 2σ)	$\ln B_{84} \sim 0.0$	Au par LOG$\mathcal{F}$
+NRO$\mathcal{G}$ $N = 10$	$+2.1$	~ 2	yes	$\ln B_{95} < -2.3$	Disfavoured

mean) with an extreme economy of free parameters. The LOG$\mathcal{G}$ case dispenses with one further parameter (as N_e^0 becomes almost fixed to $N_e^0 \simeq 50$) and the upper bound on the Bayesian evidence in favour of LOG$\mathcal{F}$ indicates that the difference of $\Delta\chi^2 = 2.5$ between the flat and Gaussian prior on N_e^0 is not strongly significant.

The LOG model can be considered nested within the LOG+NRO class of models, with the former formally obtained from the latter by setting $A = 0$. For $N = 2$, the LOG+NRO$\mathcal{F}$ model falls short of achieving the necessary number of efolds, and for this reason it must be excluded, even though its quality of fit is comparable to the standard case with constant running. The LOG+NRO$\mathcal{G}$ case has one extra parameter (for fixed N) than LOG$\mathcal{G}$, and a best–fit value which is actually slightly worse, a consequence of the Gaussian prior forcing the posterior distribution around a value of N_e^0 which is not strongly favoured by the data. Hence we can conclude that LOG+NRO$\mathcal{G}$ ($N = 2$) is disfavoured with respect to LOG$\mathcal{G}$ and LOG$\mathcal{F}$ since it is unable to achieve a better fit even with one extra parameter.

The LOG+NRO$\mathcal{F}$ with $N = 10$ has a better fit than the LOG scenario and it achieves a sufficient number of efolds within 2σ. The method of Bayesian calibrated p–values cannot be used to compare the two models because the LOG model (obtained by setting $A = 0$ in the LOG+NRO model) lies at the boundary of parameter

space. However, we can still roughly estimate the Bayes factor between LOG$\mathcal{F}$ and LOG+NRO$\mathcal{F}$ by taking a prior width on the extra parameter A of order unity (as motivated by the theoretical expectations presented in Section 4.9.2) and using that, for nested models, the Bayes factor in favour of the simpler model is approximately (see equation (9) in [191])

$$\ln B \sim I - \lambda^2/2\,, \tag{4.143}$$

where I is the logarithm of the ratio of the prior to posterior volume (the information gain) for the extra parameter and λ is the number of sigmas discrepancy between the likelihood peak and the value of the extra parameter under the nested model (here, $A = 0$). Using the values in Table 4.10 one obtains $\lambda \sim 2.8$ and $I \sim 1.6$ and thus $\ln B \sim -2.3$, which would weakly favour the LOG+NRO$\mathcal{F}$ model. However, one has to bear in mind that the parameter N has been fixed to a value picked among a range of order 10 possible values, and so one has to factor in an extra Occam's razor effect coming from the fact that $N = 10$ is one of about 10 possible choices for N. Hence $\ln B$ has to be increased by about a factor $\ln 10 = 2.3$, which brings the final odds between LOG+NRO$\mathcal{F}$ and LOG$\mathcal{F}$ to unity (i.e., $\ln B \sim 0$). Finally, the LOG+NRO$\mathcal{G}$ case has the same quality of fit of the LOG$\mathcal{G}$ case and one extra parameter. The Occam's razor term from the choice of N alone would disfavour LOG+NRO$\mathcal{G}$ by a factor $\ln B = 2.3$ with respect to LOG$\mathcal{G}$, so even without computing the precise Bayes factor we can conclude that this scenario is disfavoured.

In conclusion, a model comparison approach singles out the LOG scenario and the LOG+NRO$\mathcal{F}$ ($N = 10$) model as the most viable cases in light of the present data. This kind of considerations could be extended to compare these classes of models with other inflationary scenarios, once they have been suitably parametrized in terms of fundamental variables. However, a direct comparison with a phenomenological approach such as the standard Taylor expansion of the spectrum is not feasible due to the lack of predictivity of the latter. The Bayesian evidence still concludes that no higher order term than the tilt is presently required in the series.

Finally, we emphasize that the LOG and LOG+NRO models predict tensor contributions that are generally very small and will be largely undetectable. The most optimistic case is the LOG, where the upper bound is of order $r_0 \simeq 10^{-3}$, which might be just within reach of future B–mode observations. Conversely, a detection of tensor modes clearly above 10^{-3} would disprove the scenario of flat tree level inflationary potentials.

Chapter 5

Dark energy perturbations and the growth of structure

5.1 Introduction

As we have explained earlier, current observations of Type Ia supernovae luminosity distances indicate that our universe is in a phase of accelerated expansion [2, 3]. Various proposals have been put forward to explain the present acceleration of the universe. One can roughly distinguish two classes. On the one hand, the acceleration might be caused by the presence of dark energy, a fluid with negative equation of state w . This may be provided by a tiny cosmological constant which is characterized by $w = -1$ or by some ultralight scalar field whose potential is presently dominating the energy density of the universe. This is usually dubbed quintessence (see [65] for a comprehensive review). On the other hand, the acceleration might be due to a modification of standard gravity at large distances. This happens in $f(R)$ theories [91] and in extra–dimension inspired models, like DGP [96]. Understanding which class of models nature has chosen will represent not only a breakthrough in cosmology, but also in the field of high energy physics.

Mapping the expansion of cosmic scales and the growth of large scale structure in tandem can provide insights to distinguish between the two possible origins of the present acceleration. For such reason, there has been increasing interest in analysing the time evolution of the dark matter perturbation. Several recent works deal with characterizing the growth of dark matter perturbations in different frameworks [11, 13, 103, 276–287].

The evolution of the growth function of dark matter perturbations $g = \delta_m/a$, which is the ratio between the perturbation δ_m and the scale factor of the universe a , can be parameterized in a useful way using the growth index γ [12]. In a pure matter–dominated universe, g does not evolve in time (remains equal to one) and γ is zero. However, in the presence of a dark energy background, g changes in time, γ is different from zero and its value can be approximated by

$$\gamma = 0.55 + 0.05\,[1 + w(z = 1)]\,, \tag{5.1}$$

which provides a fit to the evolution of g to better than 0.2% for $-1 \lesssim w$ and a broad

range of initial conditions for the dark matter abundance [12]. Typically, the growth index in modified gravity models turns out to be significantly different (for instance $\gamma \simeq 0.68$ for DGP [12]) and therefore it is in principle distinguishable from the one predicted for dark energy models[1]. The available data on the growth of structures are still poor and there is a long way to go before we can talk about precision cosmology in this respect. The methods developed to study the growth of structure involve baryon acoustic oscillations, weak lensing, observations of X–ray luminous clusters, large scale galaxy surveys, Lyman α power spectra and the integrated Sachs–Wolfe effect on the cosmic microwave background. There are however various works that use these kind of techniques to place constraints on the growth index (and some also on the equation of state of dark energy) as well as forecasts for its determination based on future observations [142, 288–296]. In particular, it is found in [142] using Bayesian methods that a next generation weak lensing survey like DUNE [297] can strongly distinguish between two values of γ that differ by approximately 0.05. The authors of [289] made a forecast for the same kind of satellite proposal and concluded that it will be possible to measure the growth index with an absolute error of about 0.04 at 68% confidence level. In [290] a slightly bigger error of 0.06 at the same confidence level is given for a forecast based on baryon acoustic oscillations. Finally, for a combination of weak lensing, supernovae and cosmic microwave background data an error of about 0.04 is estimated in [288] after marginalizing over the other cosmological parameters. Since the growth index is approximately equal to 0.55, the nearest future observations should be able to determine it with a relative error of around 8%.

While much effort has been put into determining the value of the growth index in dark energy and in modified gravity models, less attention has been devoted to the possible effect on γ of non vanishing dark energy perturbations. The latter do not affect the background evolution, but are fundamental in determining the dark energy clustering properties. They will have an effect on the evolution of fluctuations in the matter distribution and, consequently, on γ. While minimally coupled scalar field (quintessence) models commonly have a non–adiabatic speed of sound close or equal to unity, and therefore dark energy perturbations can be neglected for them; other non–minimal models, for instance the adiabatic Chaplygin gas model, motivated by a rolling tachyon [83], have a speed of sound which is approximately zero. Observational implications of dark energy perturbations with a small speed of sound in a variety of dark energy models have been recently discussed in k–essence [133, 298], condensation of dark matter [299] and the Chaplygin gas, in terms of the matter power spectrum [300, 301] and combined full CMB and large scale structure measurements [132, 302]. Let us also emphasize that dark energy perturbations may not be consistently set to zero in perturbation theory [303] even if $w \neq -1$. Indeed, it is unavoidable that dark energy perturbations are generated, even if set to zero on some initial hypersurface, due to the presence of a non vanishing gravitational potential. Therefore, the expression (5.1) rigorously holds only in the physical limit in which the speed of sound is very close to unity (if $w \neq -1$) so that dark energy perturbations are sufficiently suppressed.

We study the effect of dark energy perturbations on the growth index γ. Our

[1] However, see [11] and [13].

main motivation is to understand if the new degrees of freedom introduced by dark energy perturbations imply changes in γ large compared to the forecasted errors $\Delta\gamma \simeq \mathcal{O}(0.04)$ (at 68% confidence level). Following the common lore, see for instance [132], and to simplify the analysis, we will assume that the speed of sound associated with the dark energy perturbations and the equation of state do not change appreciably in the proper time range and that the dark energy perturbations have no shear. This is a good approximation in linear perturbation theory for dark energy models with a scalar field. Under these assumptions, we provide an analytical formula for the growth index γ as a function of the speed of sound, the equation of state w, the dark matter abundance and the comoving scale. As we will see, in the presence of dark energy perturbations, the growth index differs from the corresponding value without dark energy perturbations by an amount which is comparable to the realistic forecasted errors, especially for small speed of sound and w significantly different from -1. This opens up the possibility that the presence of dark energy perturbations may leave a relevant imprint on the growth function of dark matter perturbations.

5.2 The evolution equations

Let us consider a flat FLRW universe, with metric (3.82), filled with cold dark matter and dark energy characterized by an equation of state w. The background equations (3.15) and (3.16) are simply

$$3\mathcal{H}^2 = 8\pi G a^2 \bar{\rho}\,, \tag{5.2}$$

$$2\mathcal{H}' = -\mathcal{H}^2\left(1+3w\Omega_x\right)\,, \tag{5.3}$$

where $\bar{\rho} = \bar{\rho}_m + \bar{\rho}_x$ is the total energy density and the flatness of space means that the time varying relative dark energy density is $\Omega_x = \bar{\rho}_x/\bar{\rho}$. The bars indicate homogeneous background quantities and the subindexes '$_m$' and '$_x$' refer to dark matter and dark energy respectively. We assume that the equation of state of dark energy is a constant and that the dark energy and the dark matter do not interact. Combining (3.93) and (3.95) we obtain

$$h'' + \mathcal{H}' h = 8\pi G a^2 \left(\delta T^i{}_i + \delta T^0{}_0\right)\,. \tag{5.4}$$

The divergence of the dark matter velocity in its own rest frame is zero by definition and therefore, from (3.102), in Fourier space we have

$$\delta_m' + \frac{1}{2}h' = 0\,, \tag{5.5}$$

where we have taken into account that the equation of state of dark matter and its pressure perturbation are zero; and we denote by

$$\delta\rho_m \equiv \bar{\rho}_m\,\delta_m\,, \tag{5.6}$$

the energy density perturbation of dark matter. Differentiating (5.5) with respect to conformal time we can write (5.4) as

$$\delta_m'' + \mathcal{H}\delta_m' = 4\pi G a^2\left(\delta\rho_m + \delta\rho_x + 3\delta P_x\right)\,. \tag{5.7}$$

Then, using (3.150) to express the pressure perturbation of the dark energy component in the rest frame of dark matter in terms of the dark energy rest frame speed of sound $\hat{c}_s$; and taking into account the background evolution (3.15) we arrive to

$$\delta_m'' + \mathcal{H}\delta_m' - \frac{3}{2}\mathcal{H}^2\Omega_m\delta_m = \frac{3}{2}\mathcal{H}^2\Omega_x\left[\left(1+3\hat{c}_s^2\right)\delta_x + 9\left(1+w\right)\mathcal{H}\left(\hat{c}_s^2 - w\right)\frac{\theta_x}{k^2}\right] . \quad (5.8)$$

Similarly, making use of (3.150) into (3.102) and (3.103) we obtain the following two equations:

$$\delta_x' = -(1+w)\left\{\left[k^2 + 9\left(\hat{c}_s^2 - w\right)\mathcal{H}^2\right]\frac{\theta_x}{k^2} - \delta_m'\right\} - 3\mathcal{H}(\hat{c}_s^2 - w)\delta_x , \quad (5.9)$$

$$\frac{\theta_x'}{k^2} = -\left(1-3\hat{c}_s^2\right)\mathcal{H}\frac{\theta_x}{k^2} + \frac{\hat{c}_s^2}{1+w}\delta_x . \quad (5.10)$$

Differentiating (5.9) with respect to τ and express θ_x' in the result using (5.10) we get

$$\begin{aligned}\delta_x'' &= -(1+w)\left[k^2 + 9\mathcal{H}^2\left(\hat{c}_s^2 - w\right)\right]\left[\frac{\hat{c}_s^2}{1+w}\delta_x - \mathcal{H}\left(1-3\hat{c}_s^2\right)\frac{\theta_x}{k^2}\right] \\ &- 3\left(\hat{c}_s^2 - w\right)\left[6\mathcal{H}\mathcal{H}'\frac{\theta_x}{k^2} + \left(\mathcal{H}\delta_x\right)'\right] + (1+w)\delta_m'' \end{aligned} \quad (5.11)$$

Now, we eliminate θ_x in (5.11) by means of (5.9) and take into account (3.16) to write $\mathcal{H}'$ in terms of $\mathcal{H}$, arriving finally to the equation:

$$\begin{aligned}\delta_x'' &+ \left[3\left(\hat{c}_s^2 - w\right)\mathcal{H} - \mathcal{F}\right]\delta_x' \\ &+ \left\{\hat{c}_s^2 k^2 - \frac{3}{2}\left(\hat{c}_s^2 - w\right)\mathcal{H}\left[\left(1+3w\Omega_x - 6\hat{c}_s^2\right)\mathcal{H} + 2\mathcal{F}\right]\right\}\delta_x \\ &= (1+w)\delta_m'' - (1+w)\mathcal{F}\delta_m' , \end{aligned} \quad (5.12)$$

where

$$\mathcal{F} \equiv -9\left(1+3w\Omega_x\right)\frac{\hat{c}_s^2 - w}{k^2 + 9\left(\hat{c}_s^2 - w\right)\mathcal{H}^2}\mathcal{H}^3 - \left(1-3\hat{c}_s^2\right)\mathcal{H} . \quad (5.13)$$

The expressions (5.8), (5.9), (5.12) and (5.13) constitute a system of two second order differential equations that allow us to describe the evolution of linear perturbations of dark matter and dark energy as functions of conformal time in a FLRW background.

5.3 The growth index

The growth of matter perturbations has been studied neglecting the effect of dark energy perturbations through the behaviour of the growth function [304]

$$g \equiv \frac{\delta_m}{a} , \quad (5.14)$$

as a function of the natural logarithm of the scale factor. It is possible to fit g using a simple parameterization that defines the growth index γ and depends on the relative energy density of dark matter

$$g(a) = g(a_i)\exp\int_{a_i}^{a}\left(\Omega_m(\hat{a})^\gamma - 1\right)\frac{\mathrm{d}\hat{a}}{\hat{a}} . \quad (5.15)$$

The growth function can be normalized to unity for some value of the scale factor bigger than the one at matter–radiation equality: $a_i > a_{(mr)}$; in other words, deep in the matter dominated epoch where, $\delta_m \sim a$. The growth index γ is normally taken to be a (model dependent) number whose best fitting value for standard gravity and no dark energy perturbations is around 0.55, see equation (5.1). This result is obtained from the evolution of dark matter perturbations using the equation

$$\delta_m'' + \mathcal{H}\delta_m' - \frac{3}{2}\mathcal{H}^2\Omega_m\delta_m = 0\,, \tag{5.16}$$

with no dark energy perturbations, instead of the system of second order differential equations that includes δ_x .

It is important to remark that it is not possible to reduce the system (5.8), (5.9), (5.12) and (5.13) to (5.16) by setting $\delta_x = 0$ or with any particular choice of the parameters. Those equations show that even if the dark energy perturbation is set to zero initially it will be generated at later times. The effect of dark energy perturbations should be included in the analysis of the growth history for consistency. The growth of dark matter perturbations depends not only on w (which already enters in (5.16) through Ω_m and $\mathcal{H}$) but also on the other two parameters appearing explicitly in the differential equations that control the evolution of the perturbations, i.e. k and $\hat{c}_s^2$. The reason for the dependence of the dark matter perturbations on the sound speed of dark energy is clear from the previous discussion and the definition (3.146). In contrast to equation (5.16), the dependence on the comoving momentum now appears explicitly as an effect of a non vanishing speed of sound.

Given a numerical solution for the dark matter perturbation evolution, the definition (5.15) of the growth index can be used to compute γ exactly:

$$\gamma = (\ln\Omega_m)^{-1}\ln\left(\frac{a}{\delta_m}\frac{\mathrm{d}\delta_m}{\mathrm{d}a}\right)\,. \tag{5.17}$$

We will use this equation together with (5.8), (5.9), (5.12) and (5.13) for obtaining our results. Obviously γ will be a function of a and it will depend on k , $\hat{c}_s^2$, w and Ω_m^0 as well.

5.4 The solution of the evolution equations

In our analysis we consider w in the reasonably broad range $[-1, -0.7]$. We choose not to allow the possibility that the equation of state of dark energy can be smaller than -1 . As for k , the values of interest are the ones for which there are large scale structure data on the matter power spectrum [269]. This goes approximately from $0.01h$ Mpc^{-1} to $0.2h$ Mpc^{-1} , including the nonlinear part of the spectrum, which becomes so at roughly $0.09h$ Mpc^{-1} . The scale that corresponds to the Hubble size today is 2.4 10^{-4} Mpc^{-1} and, if we normalize it to $\mathcal{H}_0 = 1$, the range of k we will focus on (discarding the nonlinear part of the spectrum) is approximately $[30, 270]$ in units of $\mathcal{H}_0$. It is worth noticing that the lower k value roughly gives the position of the baryon acoustic oscillation peak that can be used for constraining the growth index [290]. Finally, as we already commented regarding the sound speed of dark

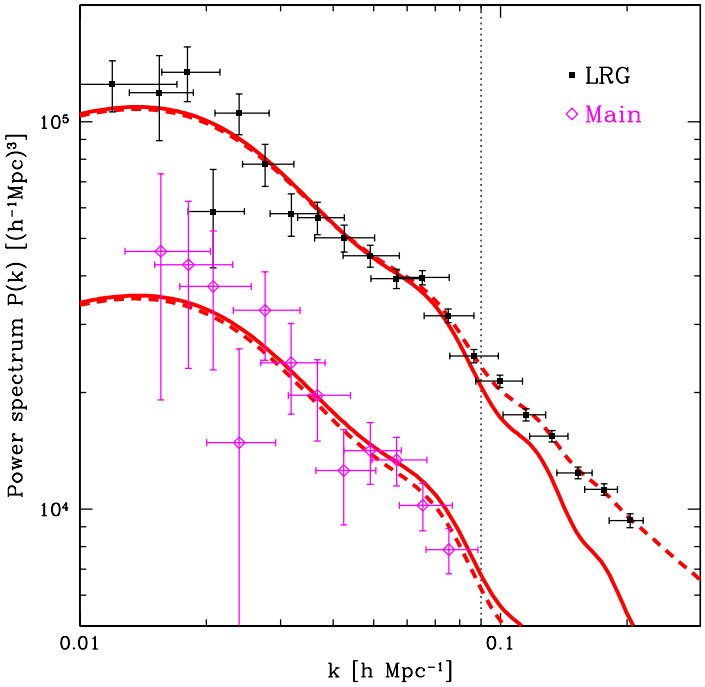

Figure 5.1: Measured power spectra for the full luminous red galaxies in the Sloan Digital Sky Survey (SDSS) and main galaxy samples from [269]. The dashed curves include a nonlinear correction of [238]. The onset of the nonlinearities is visible in the figure and marked at $k \gtrsim 0.09h\mathrm{Mpc}^{-1}$ with a vertical dotted line

energy, we restrict $\hat{c}_s^2$ to be positive and smaller than unity as currently its value is essentially unconstrained.

To solve the set of equations (5.8), (5.9), (5.12) and (5.13) we impose initial conditions at the redshift $z_{mr} = 3200$, which approximately corresponds to the time equality between matter and radiation. Since we consider non interacting fluids to describe the dark matter and dark energy, their energy densities satisfy:

$$\bar{\rho_m}' + 3\mathcal{H}\bar{\rho_m} = 0 \,, \tag{5.18}$$

$$\bar{\rho_x}' + 3(1+w)\mathcal{H}\bar{\rho_x} = 0. \tag{5.19}$$

We choose adiabatic initial conditions at matter radiation equality:

$$\frac{\delta\rho_m}{\bar{\rho_m}'} = \frac{\delta\rho_x}{\bar{\rho_x}'} \,, \tag{5.20}$$

which means

$$\delta_{x(mr)} = (1+w)\delta_{c(mr)} \,. \tag{5.21}$$

Furthermore, we assume zero initial time derivatives of the dark matter and dark energy perturbations. This is consistent with the fact that at early times (in the beginning of the matter dominated period) the equations of the perturbations admit

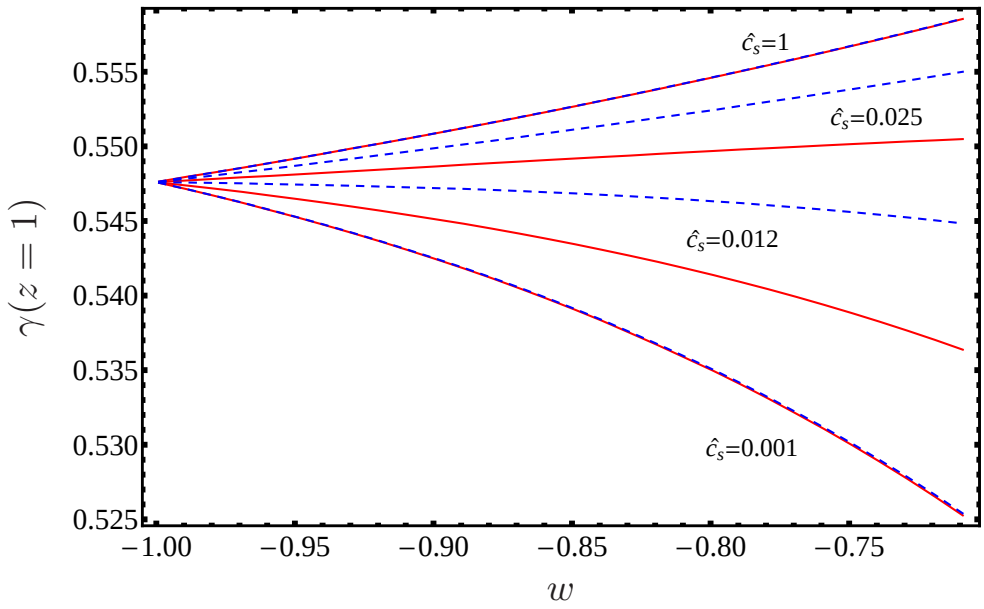

Figure 5.2: $\gamma(z=1)$ as a function of w is shown for four values of $\hat{c}_s$. Red curves correspond to $k = 0.050\,h\mathrm{Mpc}^{-1}$ and blue dashed ones to $k = 0.078\,h\mathrm{Mpc}^{-1}$.

the solution $\delta_x \propto (1+w)\delta_m \propto \tau^2$ [132] as it can be easily checked with (5.8), (5.9), (5.12) and (5.13). In fact, we can even use non zero initial velocities and consider non adiabatic initial conditions; our results on the growth index are robust under these modifications. For the background we consider the present (i.e. at $z_0 = 0, a_0 \equiv 1$) value of the relative energy density of dark matter in the range $[0.25, 0.30]$ and $\Omega_x^0 = 1 - \Omega_m^0$. In our computations we do not include a specific baryon component. We have estimated (by varying the matter content) that the effect of adding baryons on the growth index can be at most as big as 0.2%, which is much smaller than the 8% accuracy forecasted for the near future experiments.

In Figure 5.2 we plot the growth index at $z = 1$ versus w for several values of the speed of sound of dark energy and two different scales. The curves for the two different values of the comoving momenta coincide for $\hat{c}_s = 1$ and in the limit of very small speed of sound. The figure indicates that the dark energy speed of sound and the scale determine whether γ grows or decreases as a function of w at a given redshift. This is one of the reasons why having a more complete parameterization than (5.1) is important. Choosing another redshift would have the effect of an overall shift of the merging point at $w = -1$ together with modifications in the curvatures of the lines.

To gain some insight on the change of the value of γ from $\hat{c}_s^2 = 1$ to $\hat{c}_s^2 \ll 1$, we observe that, in the limit $\hat{c}_s^2 \simeq 0$ and from Equation (5.10), the dark energy velocity perturbation promptly decays in time. One is left with the following solution for δ_x

$$\delta_x(a) = \delta_{x(mr)} \left(\frac{a}{a_{(mr)}} \right)^{3w} + (1+w) a^{3w} \int \hat{a}^{-3w-1}\, \dot{\delta}_m \left(\hat{c}_s^2 = 1 \right) \mathrm{d}\hat{a}\,, \qquad (5.22)$$

where the dot stands for differentiation with respect to $\ln a$. As a first approx-

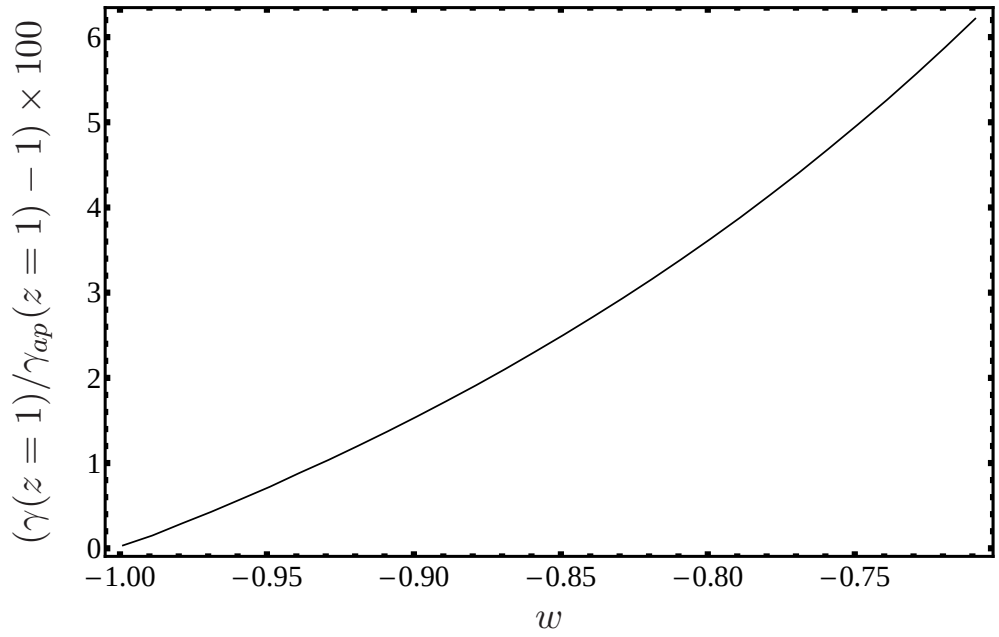

Figure 5.3: Relative error as a function of w between the exact numerical result for $\gamma(z=1)$ with very small dark energy speed of sound and the approximation γ_{ap} at the same redshift based on Equations (5.22) and (5.8) with zero θ_x. The figure has been done for $\hat{c}_s^2 = 10^{-6}$, $\Omega_m^0 = 0.30$ and $k = 0.050\,h\mathrm{Mpc}^{-1}$.

imation, we can solve Equation (5.22) plugging in the dark matter perturbation $\delta_m\left(\hat{c}_s^2 = 1\right)$ obtained taking $\hat{c}_s^2 = 1$, which for this purpose corresponds to the case in which no dark energy perturbations are present. From Equation (5.8), it is clear that the dark energy perturbations provide an extra source for the dark matter pertrubation growth. We then solve numerically Equation (5.8) with this new known source and $\theta_x = 0$. The difference between the true value of γ and the one obtained with such an approximation is plotted in Figure 5.3.

In Figure 5.4 we show the growth index at $z = 1$ versus $\log_{10}\hat{c}_s$ for different values of the equation of state of dark energy and two scales k. From this plot it is clear that the effect of changing the scale is an overall shift along the $\log_{10}\hat{c}_s$ axis. Notice that the intersecting points for the two sets of lines have the same value of the growth index, $\gamma \simeq 0.547$, which corresponds to the merging point in Figure 5.2.

The redshift dependence of the growth index has already been studied without taking into account dark energy perturbations [305] concluding that $\mathrm{d}\gamma/\mathrm{d}z \sim -0.02$ at $z = 0$; being this value nearly independent of z for a given Ω_m^0. However, including dark energy perturbations, we find that it is actually the derivative of γ with respect to the scale factor a which is constant. Therefore the redshift dependence of the growth index can be better modeled with a $1/z$ term plus a constant term. We will later see that the growth index actually has an almost constant slope as a function of the scale factor when dark energy perturbations are taken into account.

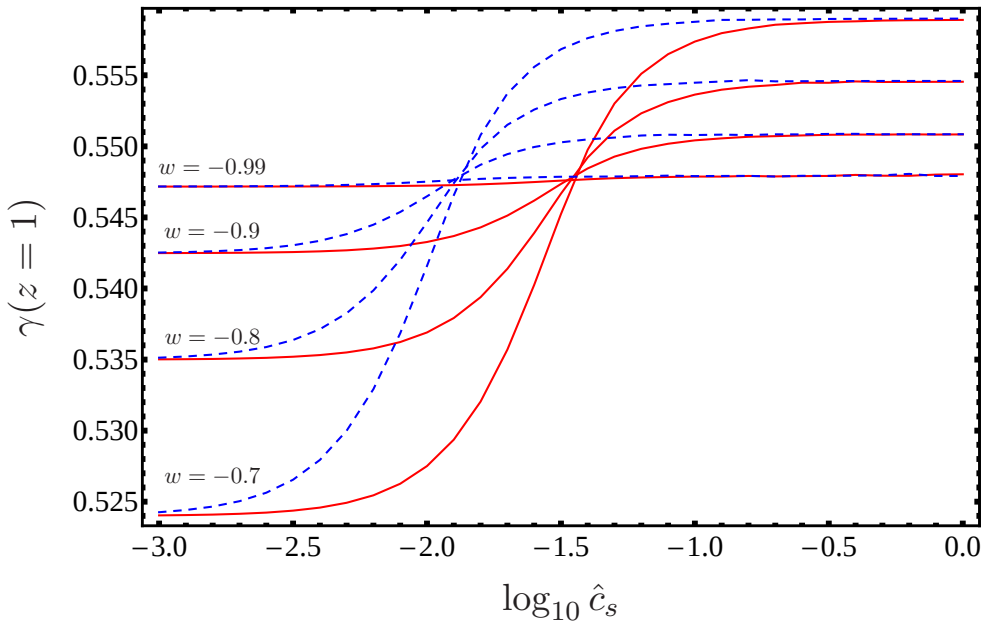

Figure 5.4: $\gamma(z=1)$ as a function of $\log_{10}\hat{c}_s$ is shown for four values of w. Red curves correspond to $k=0.03\,h\,\mathrm{Mpc}^{-1}$ and blue dashed ones to $k=0.08\,h\,\mathrm{Mpc}^{-1}$.

5.5 A parameterization of the effects of dark energy perturbations on the growth of structures

In this section we obtain an analytical parameterization of the growth index as a function of the relevant cosmological variables and perform a fit to our numerical results. We start with the following generic ansatz:

$$\gamma\left(\Omega_m^0,\hat{c}_s,k,w,a\right)=\gamma_{eq}\left(\Omega_m^0,\hat{c}_s,k,w\right)+\zeta\left(\Omega_m^0,\hat{c}_s,k,w\right)\left[a-a_{eq}\left(\Omega_m^0,w\right)\right]\ , \quad (5.23)$$

where a_{eq} is the value of the scale factor at which "dark equality" ($\Omega_m=\Omega_x=1/2$) takes place:

$$a_{eq}=\left(\frac{1}{\Omega_m^0}-1\right)^{-3w}\ . \quad (5.24)$$

We want to fit the growth index for a in the interval $[a_{eq},1]$ which approximately corresponds to a redshift $z\in[0,0.55]$ for the ranges of the equation of state of dark energy and its relative energy density that we consider. Ideally, one would wish to be able to use (5.17) and the equations for the perturbations to infer completely the analytical dependence of $\gamma_{eq}\left(\Omega_m^0,\hat{c}_s,k,w\right)$ and $\zeta\left(\Omega_m^0,\hat{c}_s,k,w\right)$ in their variables. This turns out to be difficult and we find it efficient to make a numerical fit directly. The generic form (5.23), which can be viewed as a first order Taylor expansion in the scale factor, is motivated by the nearly zero variation of $\mathrm{d}\gamma/\mathrm{d}a$. The choice of a_{eq} as the point around which we make the expansion is a convenient one, but the fit could in principle be done taking a model independent value of a as the fiducial point. We use the same ansatz to fit γ_{eq} and γ_0, which is the growth index at $a_0=1$, and

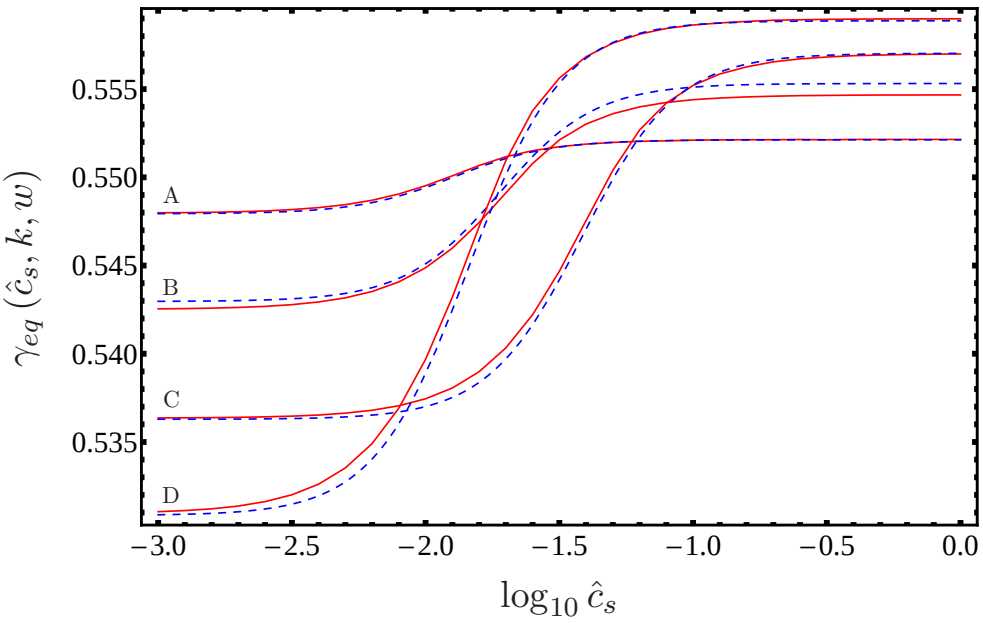

Figure 5.5: $\gamma_{eq}\,(\hat{c}_s, k, w)$ versus $\log_{10}\hat{c}_s$ for different combinations of the pair $\{k, w\}$: A $= \{0.08\,h\,\mathrm{Mpc}^{-1}, -0.95\}$, B $= \{0.02\,h\,\mathrm{Mpc}^{-1}, -0.7\}$, C $= \{0.04\,h\,\mathrm{Mpc}^{-1}, -0.87\}$ and D $= \{0.06\,h\,\mathrm{Mpc}^{-1}, -0.75\}$. Red lines are the exact numerical result and blue dashed ones the corresponding fits.

doing so we directly obtain the slope ζ from (5.23):

$$\zeta\left(\Omega_m^0, \hat{c}_s, k, w\right) = \frac{\gamma_0 - \gamma_{eq}}{1 - a_{eq}}\,. \tag{5.25}$$

In particular, we assume the following parameterization for γ_{eq} and γ_0:

$$\gamma_j\,(\hat{c}_s, k, w) = h_j(w)\tanh\left[\left(\log_{10}\hat{c}_s - g_j(k)\right)\frac{r_j(w)}{h_j(w)}\right] + f_j(w)\;,\; j = \{eq, 0\}\,. \tag{5.26}$$

We have taken γ_{eq} and γ_0 to be independent of Ω_m^0 and we incorporate this assumption in our notation, so we will refer to $\gamma_j\,(\hat{c}_s, k, w)$ from now on. The functions $f_j(w)$, $g_j(k)$, $h_j(w)$ and $r_j(w)$ are polynomials in their variables. It turns out that the fit obtained with this procedure can be importantly improved with the addition of a polynomial correction to ζ that depends on Ω_m^0, so finally:

$$\begin{aligned}\gamma\left(\Omega_m^0, \hat{c}_s, k, w, a\right) &= \gamma_{eq}\,(\hat{c}_s, k, w) \\ &\quad + \left[\zeta\left(\Omega_m^0, \hat{c}_s, k, w\right) + \eta\left(\Omega_m^0\right)\right]\left[a - a_{eq}\left(\Omega_m^0, w\right)\right]\,.\end{aligned} \tag{5.27}$$

The set of equations (5.25), (5.26) and (5.27) constitute the full fitting formula for the growth index. The resulting nine polynomials through which the fit can be expressed are the following:

$$\begin{aligned} f_{eq}(w) &= 4.498\cdot 10^{-1} - 2.176\cdot 10^{-1}\,w - 1.041\cdot 10^{-1}\,w^2 + 5.287\cdot 10^{-2}\,w^3 \\ &+ 4.030\cdot 10^{-2}\,w^4\,, \end{aligned} \tag{5.28}$$

$$\begin{aligned} f_0(w) &= 4.264\cdot 10^{-1} - 3.217\cdot 10^{-1}\,w - 2.581\cdot 10^{-1}\,w^2 - 5.512\cdot 10^{-2}\,w^3 \\ &+ 1.054\cdot 10^{-2}\,w^4\,, \end{aligned} \tag{5.29}$$

$$
\begin{aligned}
g_{eq}(k) &= -5.879\cdot 10^{-1} - 2.296\cdot 10^{-2}\,k + 2.125\cdot 10^{-4}\,k^2 - 1.177\cdot 10^{-6}\,k^3 \\
&+ 3.357\cdot 10^{-10}\,k^4 - 3.801\cdot 10^{-12}k^5\,, \qquad (5.30)\\
g_0(k) &= -6.401\cdot 10^{-1} - 2.291\cdot 10^{-2}\,k + 2.119\cdot 10^{-4}\,k^2 - 1.173\cdot 10^{-6}\,k^3 \\
&+ 3.344\cdot 10^{-10}\,k^4 - 3.787\cdot 10^{-12}k^5\,, \qquad (5.31)
\end{aligned}
$$

$$
\begin{aligned}
h_{eq}(w) &= 1.759\cdot 10^{-1} + 4.066\cdot 10^{-1}\,w + 3.254\cdot 10^{-1}\,w^2 + 9.470\cdot 10^{-2}\,w^3\,, \qquad (5.32)\\
h_{eq}(w) &= 2.008\cdot 10^{-1} + 4.644\cdot 10^{-1}\,w + 3.713\cdot 10^{-1}\,w^2 + 1.076\cdot 10^{-1}\,w^3\,, \qquad (5.33)
\end{aligned}
$$

$$
\begin{aligned}
r_{eq}(w) &= 5.158\cdot 10^{-1} + 1.203w + 9.697\cdot 10^{-1}\,w^2 + 2.827\cdot 10^{-1}\,w^3\,, \qquad (5.34)\\
r_0(w) &= 6.093\cdot 10^{-1} + 1.435w + 1.1668w^2 + 3.412\cdot 10^{-1}\,w^3\,, \qquad (5.35)
\end{aligned}
$$

$$
\eta(\Omega_m^0) = 8.037\cdot 10^{-3} + 4.676\cdot 10^{-2}\,\Omega_m^0 - 2.829\cdot 10^{-1}\left(\Omega_m^0\right)^2\,. \qquad (5.36)
$$

The truncation of the coefficients above has been done in such a way that the figures in the paper can be reproduced and that the maximum relative error between the numerical value of γ and the fitting formula does not exceed 0.2% for any combination of the parameters. In fact, this error turns out to be much smaller for generic choices of the parameters. It is worth to remark at this point that we do not make any claim about the goodness of fit of this parameterizaton in comparison to other possible ones. It could be that other choices for the fitting function were able to provide a better adjustment to the numerical results than the one that we have obtained. Moreover, one cannot discard the possibility that even keeping the ansatz that we have taken here there may be other combinations of the coefficients of the polynomials that would improve the fit, altough we believe that such a hypothetical improvement would be smaller than the accuracy of future data.

In Figure 5.5 we show $\gamma_{eq}\left(\hat{c}_s, k, w\right)$ versus the decimal logarithm of $\hat{c}_s$ for several combinations of k and w. The red curves represent the exact numerical growth index and the blue dashed lines are the corresponding fits. In Figures 5.6, 5.7 and 5.8 we show $\gamma\left(\Omega_m^0, \hat{c}_s, k, w, a\right)$ versus the scale factor for several values of w, Ω_m^0 and k respectively, as explained in the captions. The other parameters are kept fixed. The colour code, as in Figure 5.5, is that the red curves represent the exact numerical growth index and the blue dashed lines are the corresponding fits. These figures are meant to illustrate the goodness of fit for several choices of the parameters.

The formulas we have obtained offer an analytical expression for the growth index in terms of the relevant cosmological parameters in the case in which dark energy perturbations are present. The case without dark energy perturbations is reproduced by assuming $\hat{c}_s^2 = 1$. The analytical parameterization fits the numerical results in the assumed range of parameters to a precision of 0.2% (in the worst cases) or better for the growth index.

Our findings show that γ can vary from 0.55 by an amount $\Delta\gamma$ as large as ~ 0.03. We have checked that this result holds for any redshift between z_{eq} (at the time of dark equality) and $z = 1$. This difference is of the same order of magnitude of the 68% c.l. forecasted error band. The predicted value of γ may differ by this amount from the value without dark energy perturbations if the speed of sound is tiny and if the equation of state substantially deviates from -1. This opens up the possibility that a detailed future measurement of the growth factor might help in revealing the

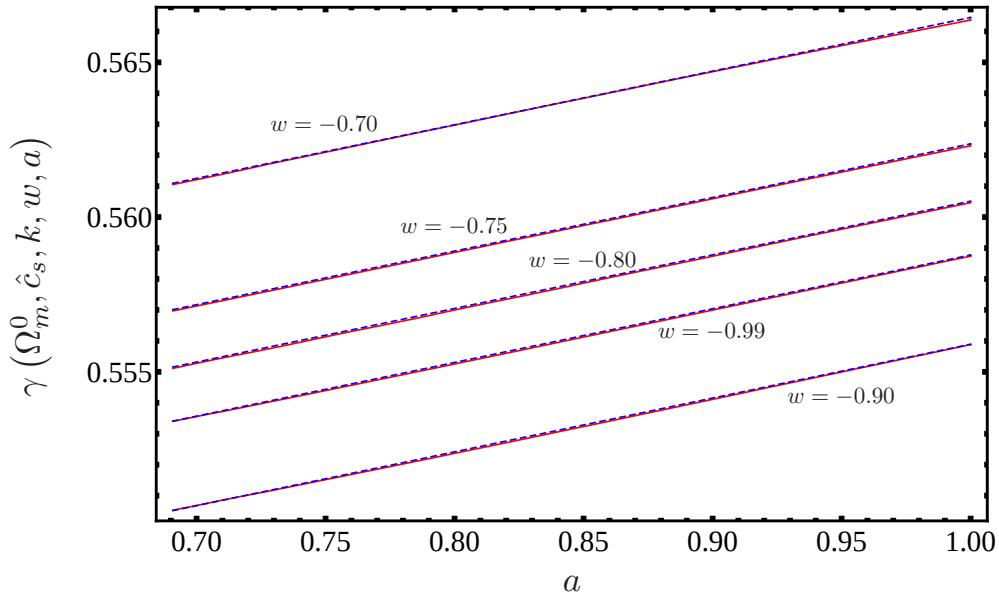

Figure 5.6: $\gamma\left(\Omega_m^0, \hat{c}_s, k, w, a\right)$ versus a for $k = 0.033\,h\,\mathrm{Mpc}^{-1}$, $\Omega_m^0 = 0.27$ and $\hat{c}_s^2 = 0.01$. Different values of w are chosen as shown in the figure. The red lines are the numerical results from the differential equations and the blue dashed ones are the fits to them.

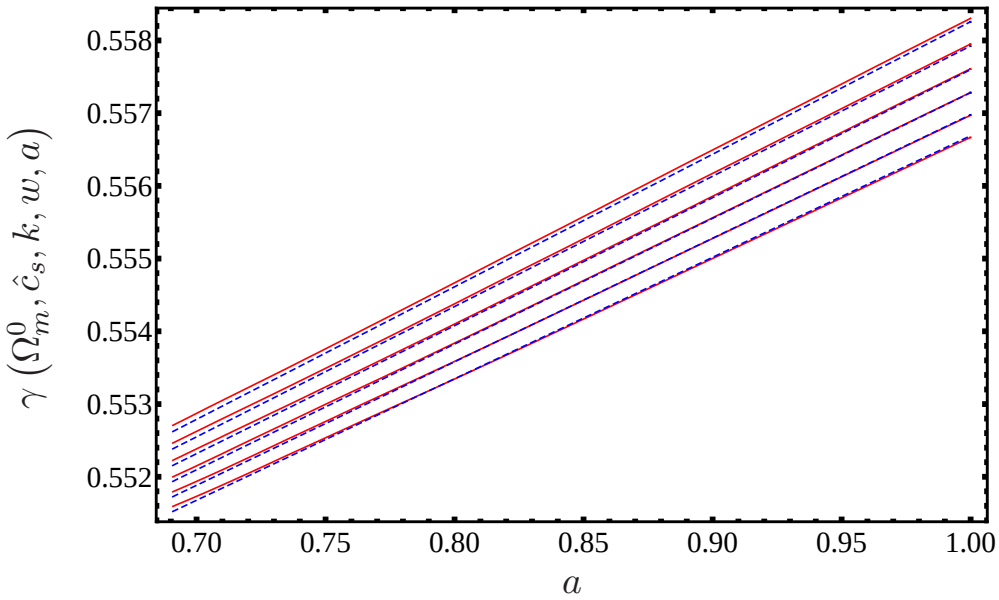

Figure 5.7: $\gamma\left(\Omega_m^0, \hat{c}_s, k, w, a\right)$ versus a for $k = 0.03\,h\,\mathrm{Mpc}^{-1}$, $w = -0.92$ and $\hat{c}_s^2 = 0.0036$. The value of Ω_m^0 runs between 0.25 and 0.30 in steps of 0.01 from top to bottom of the figure. The red lines are the numerical results from the differential equations and the blue dashed ones are the fits to them.

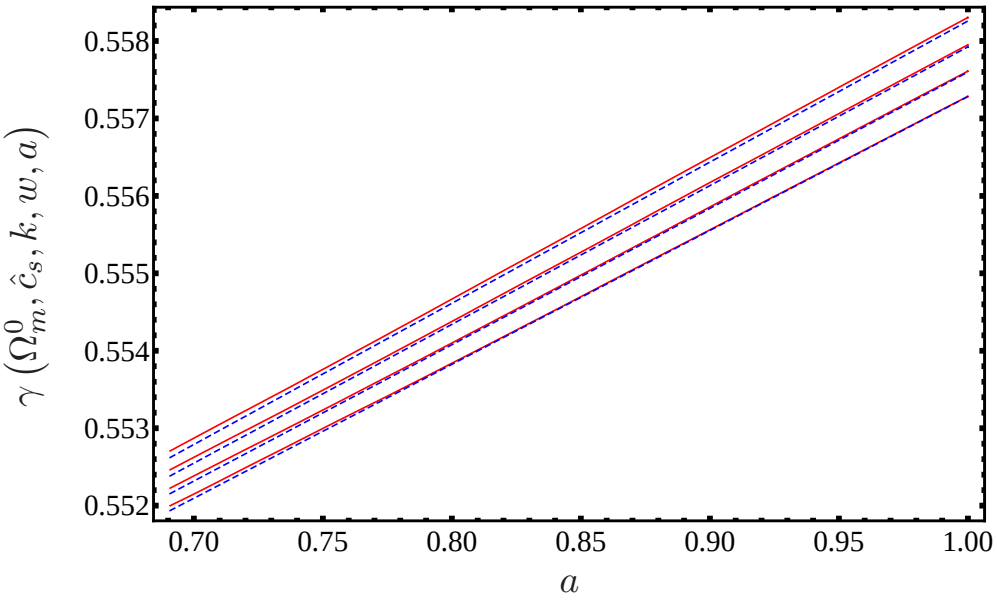

Figure 5.8: $\gamma\left(\Omega_m^0, \hat{c}_s, k, w, a\right)$ versus a for $w = -0.80$, $\hat{c}_s^2 = 0.01$ and $\Omega_m^0 = 0.27$. The scale k in units of $h\,\mathrm{Mpc}^{-1}$ takes the values $\{0.023, 0.027, 0.037, 0.067\}$ from bottom to top of the figure. The red lines are the numerical results from the differential equations and the blue dashed ones are the fits to them.

presence of dark energy perturbations. Finally, let us reiterate that our results have been obtained under the assumption that $\hat{c}_s^2$ and w do not evolve in time, at least for mild values of the redshift. Furthermore, we have assumed that the dark energy perturbations have no shear.

5.6 The origin of the fit

The ansatz we have chosen to perform the fit may seem rather peculiar and it can be helpful to provide an explanation of its motivation. As we have already said, the starting point, Equation (5.23), comes from studying the numerical solution of the equations for the scales we are interested in. The Figures 5.6, 5.7 and 5.8 clearly show that the growth index as a function of the scale factor can be very well approximated by a straight line whose coefficients will depend on the parameters that enter in the differential equations. The problem of finding an approximate dependence for a function of four variables which is given in a numerical form is in general a complicated one. There are several strategies that can be attempted to solve it. For instance, if one knows some generating equations for the function, as in our case, one can try to infer the functional dependence inspecting those equations and using analytic arguments and physical intuition. Another possibility, which can work well when the number of variables is small, consists of plotting sections of the function to guess the behaviour under some of the variables. Then, using that knowledge one can reduce the problem to another with a lower number of degrees of freedom. In practice, this turns out to be generally difficult for more than two

variables unless the function has some symmetries that simplify the problem. In our case, plotting $\gamma_{eq}\left(\Omega_m^0, \hat{c}_s, k, w\right)$ versus its arguments, we find that Ω_m^0 is almost irrelevant. We also see that the dependence on k (keeping the other parameters fixed) is approximately that of a constant and that $\gamma_{eq}\left(\Omega_m^0, \hat{c}_s, k, w\right)$ as a function of w is a straight line. The most complicated dependence of $\gamma_{eq}\left(\Omega_m^0, \hat{c}_s, k, w\right)$ is on the speed of sound of dark energy. The Figure 5.4 shows that this dependence looks very much like a hyperbolic tangent of the logarithm of the speed of sound. All this holds equally for $\gamma_0\left(\Omega_m^0, \hat{c}_s, k, w\right)$. Therefore we try to make a fit using

$$\gamma_j\left(\hat{c}_s, k, w\right) = A_j\left(k, w\right) \tanh\left[B_j\left(k, w\right) \log_{10} \hat{c}_s - C_j\left(k, w\right)\right] + D_j\left(k, w\right) , \qquad (5.37)$$

with $j = \{eq, 0\}$. From now on we will drop this subindex to simplify the notation since it plays no role in the arguments. The expression (5.37) is the most general hyperbolic tangent that we can write with coefficients that depend on k and w. We define $l_s \equiv \log_{10} \hat{c}_s$ and

$$\chi_{\{k,w\}}(l_s) \equiv \gamma\left(10^{l_s}, k, w\right) . \qquad (5.38)$$

In order to go from (5.37) to (5.26) we find out how the characteristic geometrical features of the hyperbolic tangent (5.38) are determined by its parameters k and w. In order to do this it is convenient to express these properties in terms of coordinate independent quantities. In particular we start focusing on the inflection point, which is the point $l_{s0}(k, w)$ at which the second derivative

$$\chi''_{\{k,w\}}(l_s) \equiv \frac{\mathrm{d}^2 \chi_{\{k,w\}}(l_s)}{\mathrm{d}l_s^2} , \qquad (5.39)$$

vanishes. It is straightforward to check that

$$\chi_{\{k,w\}}(l_{s0}(k, w)) = D\left(k, w\right) \qquad (5.40)$$

and the height of the hyperbolic tangent, which is the vertical distance between this point and the asymptotic value $\chi_{\{k,w\}}(l_s \to \infty)$ is

$$h\left(k, w\right) = A\left(k, w\right) + D\left(k, w\right) . \qquad (5.41)$$

The coefficients $B\left(k, w\right)$ and $C\left(k, w\right)$ can be obtained as

$$B\left(k, w\right) = \frac{1}{A\left(k, w\right)} \chi'_{\{k,w\}}(l_{s0}(k, w)), \qquad (5.42)$$

$$C\left(k, w\right) = \frac{l_{s0}(k, w)}{A\left(k, w\right)} \chi'_{\{k,w\}}(l_{s0}(k, w)) . \qquad (5.43)$$

One can check graphically and numerically that it is a very good approximation to consider that $l_{s0}(k, w)$ depends only k; and $h(k, w)$, $A\left(k, w\right)$ and $B\left(k, w\right)$ are functions of w exclusively. Therefore we have:

$$\chi_{\{k,w\}}(l_s) = \left[h\left(w\right) - \chi_0(w)\right] \tanh\left[\frac{l_s - l_{s0}(k)}{h\left(w\right) - \chi_0(w)} \hat{\chi}_0(w)\right] + \chi_0(w) , \qquad (5.44)$$

where

$$\chi_0(w) = \chi_{\{k,w\}}(l_{s0}(k)) , \qquad (5.45)$$

$$\hat{\chi}_0(w) = \chi'_{\{k,w\}}(l_{s0}(k)) , \qquad (5.46)$$

are functions of w. It is clear that the expression (5.44) is equivalent to (5.26). The first step to obtain the fit is finding $l_{s0}(k)$ by numerically solving $\chi''_{\{k,w\}}(l_s) = 0$ and fitting the solution to a polynomial in k. Having done that (for any fixed w) we can directly make a fit to (5.45) and (5.46) obtaining $\chi_0(w)$ and $\tilde{\chi}_0(w)$. Similarly, we use the geometrical definition of the height to get $h(w)$ as another polynomial. Combining these four fitting polynomials into (5.44) we should in principle get the final result. Let us remind that we do this process twice, for the two points we need to reconstruct the slope from (5.25), i.e. $a = a_0$ and $a = a_{eq}$. Comparing the result with the actual numerical solution of the differential equations we find that to reproduce the slope correctly it is necessary to include a correction due to the effect of Ω_m^0, which has been partially hidden so far in our choice of the fiducial point a_{eq}, given by (5.24). The correction $\eta\left(\Omega_m^0\right)$ that gives the final formula (5.27) can be expressed as another polynomial and is obtained by directly fitting the slope as a function of Ω_m^0, keeping the other parameters fixed.

This constructive process leads to a very good fit of the growth index but we cannot assure that it is actually the best possible fit. The procedure that should be followed to achieve the best fit is the direct minimization (for example using a Montecarlo method) of the error committed with the approximation given by (5.25), (5.26) and (5.27). However this is impractical because the number of coefficients in the polynomials is too high for the computation to be efficient. This is the main reason why we make the fit through several steps as we have described above. Since our aim is to get a fit whose accuracy is below the forecasts, our result is completely satisfactory.

Chapter 6

Conclusions

In this thesis we have studied some aspects of the early and present accelerated expansions of the Universe. We have seen how the scale dependence of the spectrum of primordial perturbations may be used to obtain information about physics at very high energies. We have analyzed what is the effect that dark energy fluctuations have on the growth index of dark matter perturbations and how this could help to learn about the properties of dark energy. Since these are clearly two different subjects we decided to explain separately the main conclusions that we have reached studying them.

6.1 Scale dependence of the spectral index

We considered inflationary models that have a flat tree level potential. These models are well motivated from the point of view of particle physics. For instance, supersymmetric theories generally present several accidental flat directions which can in principle be described by the formalism that we have used. In these models there is a one–to–one correspondence between the value of the inflaton field, the comoving inverse distance scale of the primordial perturbations and the associated renormalization scale, in such a way that the running of the inflaton down its potential scans different high energy scales and cosmological distances. We found that one can distinguish between two qualitatively different regimes when radiative corrections are included. If the couplings of the theory are sufficiently small the predictions do not depend on the details of the interaction. In this case, the spectral index can be smaller or greater than unity depending on the sign of the loop corrections. The running turns out to be negative and small, an order of magnitude smaller than the indications of WMAP. On the contrary, when the beta functions of the couplings have a faster variation, it is not possible to extract many model independent conclusions. A general feature of this second case is that the spectral index can change its sign while scanning different scales and therefore this allows a stronger running, which can reproduce the indications that we just mentioned.

We focused on the problem of reproducing the WMAP results concerning a parameterization of the power spectrum with a non–negligible running. The aim

was to find a class of models that would also support enough inflation to solve the flatness and horizon problems. Since a model independent analysis seemed unfeasible in the regime of large couplings, we studied the effect of radiative corrections in a concrete case of D–term hybrid inflation [254]. We showed analytically that there is a tension between a large running of the spectral index and a sufficiently high number of efolds. This appears to be a general feature of models in which inflation is driven by loop corrections to a flat potential. We studied the consequences of mass thresholds crossed by the inflaton during its evolution by generalizing the aforementioned model of D–term inflation. We found that the adequate treatment of the effective potential and matching conditions at the threshold implies that, as it happens in the case without thresholds, it is not possible to get a strong running if we keep the requirement of achieving at least around 50 efolds of inflation. However, we have shown that non–renormalizable operators coming from physics at higher scales than those of inflation have a significant impact in this problem, allowing a solution. In this case, the effect of the new physics on a flat potential is that of making the spectral index strongly scale dependent at the largest energies while the loop corrections help to sustain slow–roll inflation for long enough to solve the horizon and flatness problems. It turns out that this can be achieved with a single extra term in the potential, provided that its coupling is sufficiently negative in mass dimensions. In particular, with a simple estimation, we found that in order to get a running as large as the indications coming from WMAP, it is necessary to have a power of the inflaton in the extra term around 20 . We discussed why this high order non–renormalizable operators are feasible and provide a couple of examples of their possible origin in supersymmetric theories.

Having done this theoretical analysis of the models we moved on to test them against LSS and CMB data. Assuming the regime of small couplings, we studied separately the cases with and without a NRO, obtaining the slow–roll predictions for the spectra of primordial perturbations in these models. We chose to express the results in a base of parameters that provides physical intuition on the features of the models and helps to test them with a MCMC method. It turns out that this choice is a more convenient one than the standard expansion for describing the spectra predicted in these scenarios. In particular, in the case in which we include the NRO, if we had attempted to describe the model using the standard parameterization we would have needed a much higher number of parameters to represent the spectrum reliably.

We find that the results of the fit on the physical parameters of the models depend on the priors that we impose on the variables used to describe the spectrum. Moreover, the best fit values for the total number of efolds, which is a convenient parameter to use in the spectrum because of its clear interpretation and its connection with the spectral index, also depend on the prior chosen. For instance, in the logarithmic case, setting a flat prior on the number of efolds, the data gives a best fit which is relatively close to the amount needed to solve the horizon and flatness problems, but not as good as the one enforced by a Gaussian prior.

The results can be looked at and phrased in the following interesting way: The values for the spectral index that are commonly quoted in the literature rely on the choice of a flat prior on it, and therefore on the assumption that no particular model

is assumed. This is something that should always be taken into account at the time of interpreting classical fits to the data and when drawing from them conclusions concerning any model of inflation. It is not uncommon at all to leave aside the flatness and horizon problems when comparing the data with a given model and this might lead to seemingly paradoxical conclusions. For instance, we could praise a model for having a region of its parameter space that is compatible with the results of fitting the data with the standard parameterization, but this model may not solve the horizon problem in that very same region of its parameters. Possible contradictions such as this one are alleviated by the fact the actual number of efolds that we can probe is just a fraction (roughly 20%, being generous) of the total amount that the solution of those problems requires. Therefore it could be argued that the model would be valid in the observed region and invoke other inflationary periods, driven by different physics, for the solution of the problems that are the motivation for inflation in the first place.

Coming back to the potentials we are interested in, it is remarkable that imposing a gaussian prior around 50 efolds, a flat tree level potential gives an excellent fit to the data, even if this corresponds to a value of the scalar spectral index close to 0.98 slightly away from 0.96 which is the result obtained from the standard parameterization. Moreover, the inclusion of the NRO lead us to realize a couple of points that is worth remarking here. First, the goodness of the fit obtained when a sizable value of the NRO power is chosen is comparable to that of the standard parameterization with constant running of the spectral index. However the shapes of the corresponding two primordial spectra are clearly dissimilar. The explanation is that what we actually fit are the $\mathcal{C}_l$ values, which are defined as integrals of the power spectrum convoluted with some transfer functions. This can be interpreted as a hint that, given the present quality of the data, the shape of the primordial spectrum may not be as important in the fit as it is sometimes assumed. It would seem that a primordial spectrum with sufficiently many degrees of freedom which does not have complicated features can in general provide a good fit to the data. This makes fine detail model comparison a difficult task presently. The other interesting point is that the results of the analysis with the NRO explicitly indicate the need of parameterizing the primordial spectrum with specifically suited functional forms when the scale dependence is significant. The comparison with the fit done using the classical parameterization shows that the number of terms that we would need in the expansion to convey the physics of the NRO is as high as the order of this one. This reinforces our previous conclusion that special care has to be taken in using the standard parameterization to extract conclusions about specific potentials.

The comparison of the performance between different parameterizations also let us extract some conclusions. Mainly, that a strictly Bayesian approach to the problem is very subtle if the models are not nested. This is partly due to the qualitative difference between the priors on the standard parameterization and the one that describes the flat tree level model with NRO. In the first case there is not much physical insight into which kind of prior should be imposed in each parameter; while in the second, the theoretical knowledge about the model helps in the choice. It is fair to say that in a situation like this, with parameterizations of very different motivations, the standard Bayesian model comparison procedure is ill defined. Perhaps

the method could be improved to take into account effectively the role of the physics. Nevertheless, we showed that it is possible to make some statements about how the models compare to each other. For the details we suggest checking Section 4.11 . In summary, the flat tree level class of models in the small coupling regime and the case with a NRO with flat priors on the number of efolds are the preferred descriptions within the models analyzed. This conclusion was obtained using WMAP3 data and not the latest release and it is possible that the result could change with more recent CMB and LSS data. However, we do not expect a modification of it, given the similarities between WMAP3 and WMAP5. Qualitatively, the goodness of the LOG (NRO+LOG$\mathcal{F}$) fits is similar to the standard constant n (constant $\mathrm{d}n/\mathrm{d}\ln k$) parameterization. From Bayesian considerations, the improvement obtained by the inclusion of an extra parameter (as the LOG+NRO scenario implies) is not enough (with WMAP3 data) to require such modification from a purely statistical point of view. Similarly, as regards to the standard parameterization, our analysis indicates that no further terms beyond a constant spectral index are required.

Besides, we would like to remark that:

- Both scenarios, LOG and LOG+NRO, predict rather small tensor fluctuations: $r_0 \lesssim 10^{-3}$ and this is in agreement with the fits.

- In the LOG case there are essentially two parameters: $P_s(k_0)$ and N_e^0 ; and $n(k)$ is approximately constant. If we let N_e to be a free parameter, we get $24 < N_e^0 < 49$ ($16 < N_e^0 < 84$) at 68% (95%) c.l. and the corresponding spectral index is $n_0 = 0.96$. This result is consistent with the theoretical prejudice $N_e^0 \simeq 50 - 60$, which is needed to solve the horizon problem. In the case LOG$\mathcal{G}$, in which we enforce the number of efolds to be around 50, we obtain $n_0 \simeq 0.98$. This fit has just a single parameter but still gives a remarkable fit.

- The LOG+NRO case has two parameters more than LOG. It can produce a sizable running of the spectral index, being consistent with the data, and a reasonable number of efolds, particularly if N is not too small. As we explained above, the effect of the NRO is relevant for small values of k , which corresponds to the first stages in the inflationary process, and then converges to the case that we call LOG.

As a final conclusion for this part, the LOG and LOG+NRO scenarios (based on flat tree–level potentials without or with the presence of extra physics) are not only very well motivated from the physical point of view, but they also fit remarkably well the CMB and LSS data, with very few parameters (being the predictions quite model independent). In addition they are naturally consistent with a reasonable number of efolds. Therefore, they can be considered as a physical class of inflationary models, on a similar footing as monomial potentials.

6.2 Dark energy perturbations

Most of our conclusions on this part are contained in Section 5.5 but it is nevertheless worth it to summarize them here. We have studied what is the effect of dark energy fluctuations on the growth of dark energy perturbations. We have done this by analysing the modifications on the growth index with respect to the smooth dark energy case. We found that the growth of matter perturbations depends on the redshift, the sound speed and the equation of state of dark energy, the comoving scale (as an effect of working in Fourier space) and the present dark matter abundance. We obtained a way of parameterizing these dependences which is highly accurate because the deviation with the exact numerical result does not exceed 0.2% and in general is much smaller than that. We will recall once more that these results assume that the dark energy has no shear and we imposed that the speed of sound and the equation of state are constants.

The first important point to notice is that dark energy perturbations are required for consistency, and so setting them to zero artificially is a biased approach to the problem of structure growth. For some applications the effect of dark energy perturbations can be safely disregarded because it is small for sensible values of the physical parameters. However, dark energy perturbations may have a measurable effect on the growth index of dark matter and therefore they can be relevant for distinguishing between different descriptions of the accelerated expansion. For the same reason they can be useful to gain insight into the properties of dark energy, which was our main motivation in doing this work. The reason why these perturbations cannot be neglected beforehand is Einstein equations. As well as the background energy densities of the two fluids, dark matter and dark energy, are coupled through the scale factor and its first derivative (see (3.15) and (3.16)) the perturbations are coupled through the potentials that we introduced in Section 3.3.1. This feature is hidden in the second order differential Equations (5.9) and (5.12) that govern the evolution of the perturbations because we purposefully wrote them in such a way that the perturbations of the metric do not appear, which is very convenient for the numerical analysis. We were able to do this because we chose to work in the synchronous gauge. What the Equations (5.9) and (5.12) say is that even if we set to zero the dark energy perturbations at some initial instant, they will be dynamically generated at later times. Therefore the motivation for forcing the dark energy perturbation to zero by working with Equation (5.16) seems rather dubious. The parameter that controls the relevance of dark energy perturbation is their sound speed. This is shown in Figure 5.2. For small values of the speed of sound the growth index derived from the perturbation equations clearly differs from that of the case with no dark energy perturbations, which is reproduced by the limiting case in which the speed is unity. The effect of dark energy perturbations leads to an increase of the growth factor of dark matter.

It is not easy to draw any strong conclusion regarding the question of the relevance of our findings for discriminating between dark energy and modified gravity. The issue is already complex without taking into account the effect of dark energy perturbations. As we briefly commented in Chapter 5 , it seems that the more common models of modified gravity like DGP or $f(R)$ theories cannot be told apart

from a sufficiently complex dark energy fluid. However, this conclusion may change if scale effects are taken into account. We have seen that the effect of dark energy perturbations on the growth of structure varies with the comoving scale of the perturbation and the growth index becomes scale dependent. Although this dependence is very small it would be interesting to see if it could be relevant for this discriminating task. In any case, our knowledge of the evolution of perturbations in modified gravity models is still far from being fully settled and it is probably too early to conclude that dark energy and modified gravity cannot be distinguished from such effects.

If we focus on the question of what are the properties of dark energy, the importance of its perturbations is clearer. As we have seen, the value of the dark matter growth index can change by an amount which is of the same order of the estimated accuracy of future probes. The effect is particularly relevant for values of the equation of state which deviate considerably from the cosmological constant case and for small speeds of sound. This means that the detection of dark energy will be easier if it is not a minimally coupled scalar field. It is important to remark that the accuracy forecasts in which this conclusion is based were done assuming no dark energy perturbations and therefore they should be redone to see how different they are when the fluctuations are included. However, we expect that they will not change much and our conclusion should remain valid. Perhaps, one of the more interesting future perspectives of this work is that it may help to measure the sound speed of dark energy, which is currently unconstrained.

Chapter 7

Conclusiones

En esta tesis hemos estudiado algunos aspectos de la aceleración del universo en épocas tempranas y en el momento actual. Hemos visto como la dependencia con la escala del espectro de perturbaciones primordiales puede ser usada para obtener información acerca de la física a muy altas energías. Hemos analizado el efecto que las fluctuaciones en la energía oscura tienen en el crecimiento de las perturbaciones de materia oscura y como esto puede ayudarnos a aprender sobre las propiedades de la primera. Como estos son claramente dos temas distintos hemos decidido explicar por separado las conclusiones principales a las que hemos llegado en su estudio.

7.1 Dependencia del índice espectral con la escala

Hemos considerado modelos inflacionarios que tienen un potencial plano a nivel árbol. Estos modelos están bien motivados desde el punto de vista de la física de partículas. Por ejemplo, las teorías supersimétricas generalmente presentan varias direcciones planas accidentales, que en principio pueden ser descritas por medio del formalismo que hemos usado. En estos modelos existe una correspondencia unívoca entre el valor del campo, la longitud de onda de las perturbaciones primordiales y la escala de renormalización asociada, de manera que el movimiento del campo inflacionario a lo largo del potencial cubre diferentes escalas de energía y distancias cosmológicas. Hemos encontrado que es posible distinguir entre dos regímenes cualitativamente diferentes cuando las correcciones radiativas son tenidas en cuenta. Si los acoplos de la teoría son los suficientemente pequeños las predicciones no dependen de los detalles de la interacción. In este caso, el índice espectral puede ser mayor o menor que la unidad dependiendo del signo de las correcciones radiativas. El running resulta ser pequeño y negativo, un orden de magnitud más pequeño que las indicaciones del satélite WMAP. Por el contrario, si las funciones beta de los acoplos tienen una variación más rápida no es posible extraer muchas conclusiones que sean independientes de un modelo concreto. Una característica general de este segundo caso es que el índice espectral puede cambiar de signo al recorrer diferentes escalas y por lo tanto esto permite conseguir un running más fuerte, lo cual puede reproducir las indicaciones que acabamos de mencionar.

Nos hemos centrado en el problema de obtener los resultados de WMAP concernientes a la parametrización del espectro de potencias con un índice no nulo. El objetivo era encontrar una clase de modelos que además pudiera mantener inflación suficientemente prolongada como para resolver el problema del horizonte y el de la planitud. Como un análisis totalmente independiente de los modelos no resulta posible en el régimen de acoplos grandes, hemos estudiado el efecto de las correcciones radiativas en el caso concreto de la inflación en un modelo híbrido de términos D [254]. Analíticamente, demostramos que existe una tensión entre un running grande del índice espectral y un número de efolds[1] suficientemente alto. Esta parece ser una característica general de los modelos en los que la inflación se produce a causa de las correcciones radiativas a un potencial plano. Hemos considerado las consecuencias de posibles umbrales de masa que el campo inflacionario pudiera atravesar durante su evolución, generalizando el modelo arriba mencionado de inflación con términos D. Descubrimos que un tratamiento adecuado del potencial efectivo y de las condiciones en la frontera en las regiones entre baja y alta energía implica, como sucede en el caso sin umbrales de masa, que no es posible conseguir un running fuerte del índice espectral si al mismo tiempo mantenemos el requisito de conseguir al menos unos 50 efolds de expansión. Sin embargo, hemos mostrado que operadores no renormalizables (NROs) provenientes de física a más altas energías que aquellas a las cuales sucede la inflación tienen un efecto significativo en el problema y permiten una solución al mismo. En este caso, el efecto de la nueva física en un potencial plano hace que el índice espectral se vuelva fuertemente dependiente de la escala a altas energías mientras que las correcciones radiativas contribuyen a mantener la inflación por un tiempo lo bastante largo como para resolver el problema del horizonte y de la planitud. Esto puede lograrse con único término extra en el potencial si su acoplo en unidades de masa es lo suficientemente negativo. En particular, por medio de una estimación sencilla, encontramos que para obtener un running compatible con las indicaciones de WMAP es necesario que el exponente del campo inflacionario en el término extra sea cercano a 20. Hemos explicado porque un orden tan grande en el operador no renormalizable es posible y hemos proporcionado un par de ejemplos de su posible origen en teorías supersimétricas.

Habiendo hecho este análisis teórico de los modelos pasamos a ponerlos a prueba con datos de la estructura del universo a gran escala y del fondo cósmico de microondas. Asumiendo el régimen de acoplos pequeños estudiamos por separado los casos en los que hay o no presente un NRO. Expresamos los resultados en una base de parámetros que proporciona intuición física sobre las características de los modelos y ayuda a contrastarlos con los datos por medio de procesos de Montecarlo. Esta elección es más conveniente para describir el espectro de estas clases de potenciales que la de la parametrización estándar. En particular, en el caso en el que se incluye el NRO, si hubiéramos intentado describir el modelo por medio de la parametrización estándar habríamos necesitado un número de términos muy alto para conseguir una reproducción fidedigna del espectro.

Hemos encontrado que los resultados del ajuste en los parámetros físicos del modelo dependen de las suposiciones que se hacen a priori (llamadas priors) sobre las variables utilizadas para describir el espectro. Además, los valores que dan un mejor

[1] Esta palabra no tiene traducción en castellano. Es una medida de la expansión.

ajuste del número de efolds, que es un parámetro conveniente por su interpretación física y su relación con el índice espectral, también dependen de su prior. Por ejemplo, en el caso en el que solamente tenemos correcciones radiativas, al fijar un prior plano en el número de efolds, los datos dan un ajuste que es relativamente cercano a la cantidad necesaria para resolver los problemas del horizonte y de la planitud, pero no tan bueno como el que se logra con un prior gausiano.

Estos resultados pueden ser vistos y expresados de la siguiente manera: los valores del índice espectral que normalmente se citan están fundamentados en la elección de un prior plano en dicho parámetro y, por lo tanto, en la suposición de que ningún modelo particular es asumido. Esto es algo que siempre debería tenerse en cuenta al interpretar los ajustes clásicos de los datos y al extraer conclusiones sobre modelos de inflación a partir de ellos. No es en absoluto infrecuente dejar de lado los problemas del horizonte y de la planitud al comparar los datos con un modelo determinado y esto puede llevarnos a conclusiones aparentemente paradójicas. Por ejemplo, podría ser que elogiaramos un modelo por tener una región de su espacio de parámetros compatible con los resultados de ajustar los datos con la parametrización estándar, pero ese modelo podría no resolver el problema del horizonte en esa misma región de su espacio de parámetros. Este tipo de contradicciones pueden ser atenuadas por el hecho de que el número total de efolds que podemos observar es solamente una pequeña fracción (no más de un 20%) de la cantidad total que la solución a aquellos problemas requiere. Por lo tanto, podría argumentarse que el modelo es válido en la región observable y recurrir a otros procesos inflacionarios, producidos por otra física, para solucionar los problemas que motivan la idea de inflación cosmológica.

Es un hecho notable que imponiendo un prior de tipo gausiano entorno a 50 efolds, un potencial plano a nivel árbol proporciona un ajuste excelente a los datos, incluso aunque esto corresponde a un valor del índice espectral cercano a 0.98, que es ligeramente diferente de 0.96 (el resultado que se obtiene usando la parametrización estándar). Además, la inclusión de un operador no renormalizable nos lleva a concluir un par de puntos que merece la pena recoger aquí. El ajuste que se obtiene con un NRO de orden lo suficientemente alto es tan bueno como el de la parametrización estándar con running constante. Sin embargo, las formas correspondientes de los dos espectros primordiales son claramente diferentes. La explicación es que lo que realmente se ajusta es el valor de las $\mathcal{C}_l$, que están definidas como integrales del espectro de potencias en las que intervienen ciertas funciones de transferencia. Esto puede ser interpretado como un indicio de que, dada la calidad de los datos actuales, el espectro de perturbaciones primordiales puede no ser tan importante en el ajuste como a veces se asume. Parecería que un espectro primordial con un número suficiente de grados de libertad que no tenga características complicadas podría, en general, dar un buen ajuste a los datos. Esto hace que la comparación de diferentes modelos a un nivel detallado sea una tarea compleja hoy en día. El otro punto interesante es que los resultados del análisis con el NRO indican la necesidad de parametrizar el espectro primordial con formas funcionales específicamente adecuadas si la dependencia con la escala es significante. La comparación con el ajuste proveniente de la parametrización clásica muestra que el número de términos que necesitaríamos en la expansión para dar cuenta de la física que conlleva el NRO es tan grande como el

orden de este. Esto refuerza nuestra conclusión anterior de que es necesario poner un cuidado especial al usar la parametrización estándar para extraer conclusiones acerca de modelos concretos.

La comparación de la efectividad de diferentes parametrizaciones también nos permite extraer algunas conclusiones. Principalmente, que una aproximación estrictamente bayesiana al problema es muy complicada si los modelos no se contienen los unos a los otros. Esto es parcialmente debido a la diferencia cualitativa entre los priors en la parametrización estándar y aquella que describe los modelos planos a nivel árbol con NRO. En el primer caso no hay una gran motivación física para escoger un prior u otro para los parámetros; mientras que en el segundo, el conocimiento teórico sobre los modelos ayuda en la elección. Puede decirse que en una situación en la que las parametrizaciones involucradas tienen motivaciones muy diferentes, la comparación bayesiana de modelos está lastrada desde un principio. Tal vez el método podría mejorarse teniendo en cuenta de manera efectiva el papel que juega la física. De todas formas, hemos mostrado que es posible hacer algunas afirmaciones significativas sobre como unos modelos se comparan con otros. Para más detalles sobre esto sugerimos ver la sección 4.11 . En resumen, los modelos planos a nivel árbol en el régimen de acoplos pequeños, con un operador no renormalizable y con un prior plano sobre el número de efolds, se adecuan a los datos mejor que el resto de modelos analizados. Esta conclusión la obtuvimos usando los datos de WMAP3 y es posible que el resultado pudiera cambiar incluyendo datos más recientes sobre el CMB o la estructura a gran escala. Sin embargo, no esperamos que eso suceda debido a las semejanzas entre WMAP3 y WMAP5. Cualitativamente, los ajustes que llamamos LOG y (NRO+LOG$\mathcal{F}$) están al mismo nivel que los de n constante y running constante, respectivamente. A partir de consideraciones bayesianas, hemos visto que la mejoría del ajuste obtenida con la inclusión de un parámetro extra (como el caso LOG+NRO implica) no es suficiente (de acuerdo con los datos de WMAP3) para requerir dicha modificación desde un punto de vista puramente estadístico. De forma similar, por lo que respecta a la parametrización estándar, nuestros análisis indican que ningún término más allá del running es necesario.

Además, nos gustaría remarcar lo siguiente:

- Ambos escenarios, el caso LOG y el LOG+NRO, predicen fluctuaciones tensoriales pequeñas: $r_0 \lesssim 10^{-3}$ y esto está de acuerdo con los ajustes.

- En el caso LOG hay esencialmente dos parámetros, $P_s(k_0)$ y N_e^0 , y $n(k)$ es aproximadamente constante. Si dejamos que N_e sea un parámetro libre, obtenemos $24 < N_e^0 < 49$ ($16 < N_e^0 < 84$) a 68% (95%) nivel de confianza y el índice espectral correspondiente es cercano a $n_0 = 0.96$. Este resultado es consistente con el requisito teórico $N_e^0 \simeq 50 - 60$, necesario para resolver el problema del horizonte. En el caso LOG$\mathcal{G}$, en el que forzamos el número de efolds a estar cerca de 50, obtenemos $n_0 \simeq 0.98$. Este ajuste tiene en la práctica un único parámetro libre y a pesar de eso ofrece un resultado muy satisfactorio.

- El caso LOG+NRO tiene dos parámetros más que el caso LOG. Puede producir un running sustancial del índice espectral, siendo consistente con los datos, y

un número de efolds razonable, especialmente si N no es demasiado pequeño. Como hemos explicado anteriormente, el efecto del NRO es relevante para valores pequeños de k , lo cual corresponde a las primeras etapas del periodo inflacionario, y después tiende a converger (especialmente si N es lo bastante grande) al caso que llamamos LOG.

Como conclusión final de esta parte, los modelos LOG y LOG+NRO (que están basados en potenciales planos a nivel árbol, incluyendo los efectos de nueva física en el segundo caso) no solamente están bien motivados desde un punto de vista físico sino que proporcionan ajustes notables a los datos del CMB y de la gran escala del universo con gran economía de parámetros. Además son consistentes de manera natural con un numero de efolds razonable. Por lo tanto estos modelos pueden ser considerados como una clase particular de modelos inflacionarios, al mismo nivel que aquellos basados en monomios del campo.

7.2 Perturbaciones en la energía oscura

La mayor parte de las conclusiones relativas a esta parte están contenidas en la sección 5.5 pero merece la pena resumirlas aquí. Hemos estudiado el efecto de fluctuaciones en la energía oscura en el crecimiento de las perturbaciones de materia oscura. Lo hemos hecho analizando las modificaciones que sufre el índice de crecimiento con respecto al caso de energía oscura sin perturbaciones. El crecimiento de las perturbaciones de materia depende del corrimiento al rojo, de la velocidad del sonido y de la ecuación de estado de la energía oscura, de la escala de las perturbaciones (debido a que trabajamos en un espacio de Fourier) y de la abundancia de materia oscura. Hemos obtenido una forma de parametrizar estas dependencias que es precisa en un grado muy elevado porque la desviación con respecto al resultado numérico exacto es menor del 0.2% y en general es mucho menor. Nuestros resultados dependen de la suposición de que la energía oscura no tiene tensión de cizalla y de la constancia de la ecuación de estado y la velocidad del sonido de dicho fluido.

El primer punto importante que queremos reseñar es que las perturbaciones en la energía oscura son necesarias por razones de consistencia, y por lo tanto forzar su valor a zero es una aproximación sesgada al problema de la formación de estructuras. Para ciertas aplicaciones el efecto de estas perturbaciones se puede despreciar sin problemas porque es pequeño para valores razonables de los parámetros físicos. Sin embargo, las perturbaciones de la energía oscura pueden tener un efecto que podría medirse en el índice de crecimiento de las perturbaciones de materia oscura y por lo tanto pueden ser relevantes para distinguir entre diferentes descripciones de la expansión acelerada. Por la misma razón, pueden ser útiles para ganar mayor conocimiento sobre las propiedades de la energía oscura, lo cual es la principal motivación de el trabajo que hemos realizado. El motivo por el cual estas perturbaciones no se pueden descartar de antemano es las ecuaciones de Einstein. Así como los valores promedio de las densidades de energía de los dos fluidos, materia y energía oscuras, se acoplan a través del factor de escala y de su primera derivada (véanse las ecuaciones (3.15) y (3.16)), las perturbaciones se acoplan por medio de los potenciales que introdujimos en la sección 3.3.1 . Esta caracterísitica está escondida en las

ecuaciones diferenciales de segundo orden (5.9) and (5.12) que gobiernan la evolución de las perturbaciones, porque las hemos escrito ex profeso de tal forma que las perturbaciones de la métrica no aparecen en ellas (lo cual es muy conveniente para el análisis numérico). Esto hemos podido hacerlo gracias a utilizar el gauge síncrono. Las ecuaciones (5.9) and (5.12) nos indican que incluso si ponemos inicialmente a cero el valor de las perturbaciones en la energía oscura, se generarán de forma dinámica más tarde. Por lo tanto, la motivación para forzar las perturbaciones en la energía oscura a cero usando la ecuación (5.16) parece bastante poco justificada. El parámetro que controla la relevancia de las perturbaciones en la energía oscura es su velocidad del sonido. Esto se muestra en la figura 5.2 . Para valores pequeños de la velocidad del sonido, el índice de crecimiento derivado de las ecuaciones de las fluctuaciones difiere claramente del caso límite en el que no hay perturbaciones en ese fluido, que puede reproducirse haciendo que la velocidad del sonido sea igual a la unidad. El efecto de las perturbaciones en la energía oscura es un incremento del factor de crecimiento de las perturbaciones de materia oscura.

No resulta sencillo extraer conclusiones definitivas sobre la relevancia de nuestro trabajo para discriminar entre energía oscura y teorías de gravedad modificadas. El asunto es ya bastante complicado de por sí, sin tener en consideración el efecto de las perturbaciones en la energía oscura. Como comentamos de manera breve en el capítulo 5, parece que los modelos más comunes de gravedad modicada como DGP o las teorías $f(R)$ no se pueden distinguir de una componente de energía oscura lo bastante compleja. Sin embargo, esta conclusión podría cambiar si los efectos de escala son tenido en cuenta. Hemos visto que el efecto de las perturbaciones de energía oscura en el crecimiento de estructuras depende de la escala de las perturbaciones y el índice de crecimiento se vuelve una función de la escala. Aunque esta dependencia es pequeña, sería interesante ver si podría ser relevante para discriminar entre los dos tipos de descripción. En cualquier caso, nuestro conocimiento de la evolución de las perturbaciones en modelos de gravedad modificada está todavía lejos de poder considerarse bien establecido y es probablemente muy pronto aún para concluir que la energía oscura y las teorías de gravedad modificada no pueden ser distinguidas entre sí a partir de estos efectos.

Si nos centramos en la cuestión de cuáles son las propiedades de la energía oscura, la importancia de las perturbaciones está clara. Como hemos visto, el valor del índice de crecimiento de las perturbaciones de materia oscura puede cambiar en una cantidad que es del mismo orden que la precisión estimada para futuros experimentos. El efecto es particularmente relevante para valores de la ecuación de estado que se desvían considerablemente del caso de la constante cosmológica y para valores pequeños de la velocidad del sonido. Esto implica que la detección de perturbaciones en la energía oscura será más sencilla si este fluido no es un campo escalar mínimamente acoplado. Es importante recalcar que las predicciones sobre la precisión de los experimentos en los que esta conclusión se basa fueron hechas asumiendo que no hay perturbaciones en la energía oscura y por lo tanto deberían rehacerse para ver cuán diferentes son al tener en cuenta dichas fluctuaciones. En todo caso, no esperamos que cambien mucho y nuestras conclusiones deberían seguir siendo válidas. Tal vez una de las perspectivas más interesantes de este trabajo es que podría ayudar a medir la velocidad del sonido de las perturbaciones de energía

oscura, que actualmente es desconocida.

List of Abbreviations

ΛCDM Model with cosmological constant and cold dark matter

ΛCDMr ΛCDM cosmological model with tensors

$\mathbb{P}_{\rm LOG+NRO}$ See Equation (4.118)

$\mathbb{P}_{\rm LOG}$ See Equation (4.107)

$\mathcal{F}$ Flat prior on the number of efolds

$\mathcal{G}$ Gaussian prior on the number of efolds

2dFGRS Two Degree Field Galaxy Redshift Survey

ACBAR Arcminute Cosmology Bolometer Array Receiver

BAO Baryon Acoustic Oscillations

BOOMERANG Balloon Observations of Millimetric Extragalactic Radiation and Geophysics

c.l. Confidence level

CBI Cosmic Background Interferometer

CMB Cosmic Microwave Background

COBE Cosmic Background Explorer

DGP Dvali–Gabadadze–Porrati model of modified gravity

FLRW Friedmann–Lemaître–Robertson–Walker

HSR Hubble slow roll parameters

ISW Integrated Sachs–Wolfe effect

LAMBDA Legacy Archive for Microwave Background Data Analysis

LOG Logarithmic (small–coupling) regime

LOG+NRO Logarithmic (small–coupling) regime with a NRO

LSS Large Scale Structure

MCMC Montecarlo Markov Chain

MSSM Minimal Supersymmetric Standard Model

nD n–dimensional

NRO Non–renormalizable operator

OCDM Open cold dark matter cosmological model

PCA Principal component analysis

pdf Probability distribution function

PSR Potential slow roll parameters

RGE Renormalization group equation

SCDM Standard cold dark matter cosmological model

SM Standard Model of particle physics

SUSY Supersymmetry

VSA Very Small Array

WL Weak lensing

WMAP Wilkinson Microwave Anisotropy Probe

WMAPe An extended data set. See Table 4.1

WMAPn WMAP year n data release

List of Figures

List of Tables

Bibliography

[1] A. H. Guth, "The Inflationary Universe: A Possible Solution to the Horizon and Flatness Problems," *Phys. Rev.*, vol. D23, pp. 347–356, 1981.

[2] P. Astier *et al.*, "The Supernova Legacy Survey: Measurement of Ω_M, Ω_Λ and w from the First Year Data Set," *Astron. Astrophys.*, vol. 447, pp. 31–48, 2006, astro-ph/0510447.

[3] M. Kowalski *et al.*, "Improved Cosmological Constraints from New, Old and Combined Supernova Datasets," 2008, 0804.4142.

[4] J. E. Lidsey *et al.*, "Reconstructing the inflaton potential: An overview," *Rev. Mod. Phys.*, vol. 69, pp. 373–410, 1997, astro-ph/9508078.

[5] W. H. Kinney, E. W. Kolb, A. Melchiorri, and A. Riotto, "Latest inflation model constraints from cosmic microwave background measurements," 2008, 0805.2966.

[6] J. Lesgourgues and W. Valkenburg, "New constraints on the observable inflaton potential from WMAP and SDSS," *Phys. Rev.*, vol. D75, p. 123519, 2007, astro-ph/0703625.

[7] J. Lesgourgues, A. A. Starobinsky, and W. Valkenburg, "What do WMAP and SDSS really tell about inflation?," *JCAP*, vol. 0801, p. 010, 2008, 0710.1630.

[8] D. J. H. Chung, G. Shiu, and M. Trodden, "Running of the scalar spectral index from inflationary models," *Phys. Rev.*, vol. D68, p. 063501, 2003, astro-ph/0305193.

[9] G. Ballesteros, J. A. Casas, and J. R. Espinosa, "Running spectral index as a probe of physics at high scales," *JCAP*, vol. 0603, p. 001, 2006, hep-ph/0601134.

[10] G. Ballesteros, J. A. Casas, J. R. Espinosa, R. Ruiz de Austri, and R. Trotta, "Flat Tree-level Inflationary Potentials in Light of CMB and LSS Data," *JCAP*, vol. 0803, p. 018, 2008, 0711.3436.

[11] M. Kunz and D. Sapone, "Dark energy versus modified gravity," *Phys. Rev. Lett.*, vol. 98, p. 121301, 2007, astro-ph/0612452.

[12] E. V. Linder, "Cosmic growth history and expansion history," *Phys. Rev.*, vol. D72, p. 043529, 2005, astro-ph/0507263.

[13] E. Bertschinger and P. Zukin, "Distinguishing Modified Gravity from Dark Energy," 2008, 0801.2431.

[14] G. Ballesteros and A. Riotto, "Parameterizing the Effect of Dark Energy Perturbations on the Growth of Structures," 2008, 0807.3343.

[15] S. Weinberg, "Cosmology," *Oxford University Press*, 2008.

[16] S. Weinberg, "Gravitation and cosmology," *John Wiley & Sons*, 1972.

[17] S. Dodelson, "Modern Cosmology," Academic Press (2003) 464 p.

[18] A. R. Liddle and D. H. Lyth, "Cosmological inflation and large-scale structure," Cambridge, UK: Univ. Pr. (2000) 400 p.

[19] R. M. Wald, "General relativity," Chicago, Usa: Univ. Pr. (1984) 491p.

[20] S. Carroll, "Spacetime and Geometry: An Introduction to General Relativity," Addison Wesley (2004) 513 p.

[21] H. P. Robertson. *Astrophys. J.*, vol. 82, p. 284, 1935.

[22] H. P. Robertson. *Astrophys. J.*, vol. 83, pp. 187, 257, 1936.

[23] A. Friedmann. *Z. Phys.*, vol. 10, p. 377, 1922.

[24] A. Friedmann. *Z. Phys.*, vol. 21, p. 326, 1924.

[25] A. G. Walker. *Proc. Lond. Math. Soc.(2)*, vol. 42, p. 90, 1936.

[26] N. A. Bahcall, J. P. Ostriker, S. Perlmutter, and P. J. Steinhardt, "The Cosmic Triangle: Revealing the State of the Universe," *Science*, vol. 284, pp. 1481–1488, 1999, astro-ph/9906463.

[27] C. L. Bennett *et al.*, "4-Year COBE DMR Cosmic Microwave Background Observations: Maps and Basic Results," *Astrophys. J.*, vol. 464, pp. L1–L4, 1996, astro-ph/9601067.

[28] J. Gundersen *et al.*, "Degree Scale Anisotropy: SP94 Results," 1994, astro-ph/9412020.

[29] C. B. Netterfield, M. J. Devlin, N. Jarosik, L. Page, and E. J. Wollack, "A Measurement of the Angular Power Spectrum of the Anisotropy in the Cosmic Microwave Background," *Astrophys. J.*, vol. 474, p. 47, 1997, astro-ph/9601197.

[30] E. S. Cheng *et al.*, "A Measurement of the medium scale anisotropy in the cosmic microwave background radiation," *Astrophys. J.*, vol. 422, p. L37, 1994, astro-ph/9305022.

[31] K. Ganga, B. Ratra, M. A. Lim, N. Sugiyama, and S. T. Tanaka, "MAX 4 and MAX 5 CMB anisotropy measurement constraints on open and flat-Lambda CDM cosmogonies," *Astrophys. J. Suppl.*, vol. 114, pp. 165–175, 1998, astro-ph/9708202.

[32] E. Komatsu *et al.*, "Five-Year Wilkinson Microwave Anisotropy Probe (WMAP) Observations:Cosmological Interpretation," 2008, 0803.0547.

[33] D. Rubin *et al.*, "Looking Beyond Lambda with the Union Supernova Compilation," 2008, 0807.1108.

[34] S. Perlmutter *et al.*, "Discovery of a Supernova Explosion at Half the Age of the Universe and its Cosmological Implications," *Nature*, vol. 391, pp. 51–54, 1998, astro-ph/9712212.

[35] P. M. Garnavich *et al.*, "Supernova Limits on the Cosmic Equation of State," *Astrophys. J.*, vol. 509, pp. 74–79, 1998, astro-ph/9806396.

[36] B. P. Schmidt *et al.*, "The High-Z Supernova Search: Measuring Cosmic Deceleration and Global Cur vature of the Universe Using Type Ia Supernovae," *Astrophys. J.*, vol. 507, pp. 46–63, 1998, astro-ph/9805200.

[37] A. G. Riess *et al.*, "Observational Evidence from Supernovae for an Accelerating Universe and a Cosmological Constant," *Astron. J.*, vol. 116, pp. 1009–1038, 1998, astro-ph/9805201.

[38] S. Perlmutter *et al.*, "Measurements of Omega and Lambda from 42 High-Redshift Supernovae," *Astrophys. J.*, vol. 517, pp. 565–586, 1999, astro-ph/9812133.

[39] A. Einstein, "Kosmologische Betrachtungen zur allgemeinen Relativitätstheorie," *Koniglich Preussische Akademie der Wissenschaften*, 1917.

[40] S. Weinberg, "The cosmological constant problem," *Rev. Mod. Phys.*, vol. 61, pp. 1–23, 1989.

[41] H. B. G. Casimir, "On the Attraction Between Two Perfectly Conducting Plates," *Indag. Math.*, vol. 10, pp. 261–263, 1948.

[42] G. Bressi, G. Carugno, R. Onofrio, and G. Ruoso, "Measurement of the Casimir force between parallel metallic surfaces," *Phys. Rev. Lett.*, vol. 88, p. 041804, 2002, quant-ph/0203002.

[43] S. M. Carroll, "The cosmological constant," *Living Rev. Rel.*, vol. 4, p. 1, 2001, astro-ph/0004075.

[44] I. L. Shapiro and J. Sola, "Can the cosmological 'constant' run? - It may run," 2008, 0808.0315.

[45] B. Zumino, "Supersymmetry and the Vacuum," *Nucl. Phys.*, vol. B89, p. 535, 1975.

[46] P. K. Townsend, "Cosmological Constant in Supergravity," *Phys. Rev.*, vol. D15, pp. 2802–2804, 1977.

[47] V. A. Rubakov and M. E. Shaposhnikov, "Extra Space-Time Dimensions: Towards a Solution to the Cosmological Constant Problem," *Phys. Lett.*, vol. B125, p. 139, 1983.

[48] J.-W. Chen, M. A. Luty, and E. Ponton, "A critical cosmological constant from millimeter extra dimensions," *JHEP*, vol. 09, p. 012, 2000, hep-th/0003067.

[49] C. P. Burgess, "Extra Dimensions and the Cosmological Constant Problem," 2007, 0708.0911.

[50] E. Witten, "The cosmological constant from the viewpoint of string theory," 2000, hep-ph/0002297.

[51] J. Polchinski, "The cosmological constant and the string landscape," 2006, hep-th/0603249.

[52] S. Weinberg, "Anthropic Bound on the Cosmological Constant," *Phys. Rev. Lett.*, vol. 59, p. 2607, 1987.

[53] J. Garriga and A. Vilenkin, "On likely values of the cosmological constant," *Phys. Rev.*, vol. D61, p. 083502, 2000, astro-ph/9908115.

[54] N. Arkani-Hamed, S. Dimopoulos, and S. Kachru, "Predictive landscapes and new physics at a TeV," 2005, hep-th/0501082.

[55] A. De Simone, A. H. Guth, M. P. Salem, and A. Vilenkin, "Predicting the cosmological constant with the scale-factor cutoff measure," 2008, 0805.2173.

[56] R. Fardon, A. E. Nelson, and N. Weiner, "Dark energy from mass varying neutrinos," *JCAP*, vol. 0410, p. 005, 2004, astro-ph/0309800.

[57] J. McDonald, "Dynamical cosmological constant from a very recent phase transition," *Phys. Lett.*, vol. B498, pp. 263–271, 2001, hep-ph/0007117.

[58] F. Mansouri, "Non-vanishing cosmological constant Lambda, phase transitions, and Lambda-dependence of high energy processes," *Phys. Lett.*, vol. B538, pp. 239–245, 2002, hep-th/0203150.

[59] E. W. Kolb, S. Matarrese, and A. Riotto, "On cosmic acceleration without dark energy," *New J. Phys.*, vol. 8, p. 322, 2006, astro-ph/0506534.

[60] T. Padmanabhan, "Cosmological constant: The weight of the vacuum," *Phys. Rept.*, vol. 380, pp. 235–320, 2003, hep-th/0212290.

[61] S. M. Carroll, W. H. Press, and E. L. Turner, "The Cosmological constant," *Ann. Rev. Astron. Astrophys.*, vol. 30, pp. 499–542, 1992.

[62] M. S. Turner, "Dark matter and dark energy in the universe," *Phys. Scripta*, vol. T85, pp. 210–220, 2000, astro-ph/9901109.

[63] V. Sahni and A. A. Starobinsky, "The Case for a Positive Cosmological Lambda-term," *Int. J. Mod. Phys.*, vol. D9, pp. 373–444, 2000, astro-ph/9904398.

[64] P. J. E. Peebles and B. Ratra, "The cosmological constant and dark energy," *Rev. Mod. Phys.*, vol. 75, pp. 559–606, 2003, astro-ph/0207347.

[65] E. J. Copeland, M. Sami, and S. Tsujikawa, "Dynamics of dark energy," *Int. J. Mod. Phys.*, vol. D15, pp. 1753–1936, 2006, hep-th/0603057.

[66] N. Arkani-Hamed, L. J. Hall, C. F. Kolda, and H. Murayama, "A New Perspective on Cosmic Coincidence Problems," *Phys. Rev. Lett.*, vol. 85, pp. 4434–4437, 2000, astro-ph/0005111.

[67] B. Ratra and P. J. E. Peebles, "Cosmological Consequences of a Rolling Homogeneous Scalar Field," *Phys. Rev.*, vol. D37, p. 3406, 1988.

[68] I. Zlatev, L.-M. Wang, and P. J. Steinhardt, "Quintessence, Cosmic Coincidence, and the Cosmological Constant," *Phys. Rev. Lett.*, vol. 82, pp. 896–899, 1999, astro-ph/9807002.

[69] P. G. Ferreira and M. Joyce, "Cosmology with a Primordial Scaling Field," *Phys. Rev.*, vol. D58, p. 023503, 1998, astro-ph/9711102.

[70] E. J. Copeland, A. R. Liddle, and D. Wands, "Exponential potentials and cosmological scaling solutions," *Phys. Rev.*, vol. D57, pp. 4686–4690, 1998, gr-qc/9711068.

[71] A. R. Liddle and R. J. Scherrer, "A classification of scalar field potentials with cosmological scaling solutions," *Phys. Rev.*, vol. D59, p. 023509, 1999, astro-ph/9809272.

[72] P. J. Steinhardt, L.-M. Wang, and I. Zlatev, "Cosmological tracking solutions," *Phys. Rev.*, vol. D59, p. 123504, 1999, astro-ph/9812313.

[73] S. M. Carroll, "Quintessence and the rest of the world," *Phys. Rev. Lett.*, vol. 81, pp. 3067–3070, 1998, astro-ph/9806099.

[74] T. Chiba, "Quintessence, the gravitational constant, and gravity," *Phys. Rev.*, vol. D60, p. 083508, 1999, gr-qc/9903094.

[75] P. Binetruy, "Models of dynamical supersymmetry breaking and quintessence," *Phys. Rev.*, vol. D60, p. 063502, 1999, hep-ph/9810553.

[76] P. Brax and J. Martin, "Quintessence and supergravity," *Phys. Lett.*, vol. B468, pp. 40–45, 1999, astro-ph/9905040.

[77] J. E. Kim, "Axion and almost massless quark as ingredients of quintessence," *JHEP*, vol. 05, p. 022, 1999, hep-ph/9811509.

[78] P. J. E. Peebles and A. Vilenkin, "Quintessential inflation," *Phys. Rev.*, vol. D59, p. 063505, 1999, astro-ph/9810509.

[79] M. Peloso and F. Rosati, "On the construction of quintessential inflation models," *JHEP*, vol. 12, p. 026, 1999, hep-ph/9908271.

[80] T. Chiba, T. Okabe, and M. Yamaguchi, "Kinetically driven quintessence," *Phys. Rev.*, vol. D62, p. 023511, 2000, astro-ph/9912463.

[81] C. Armendariz-Picon, T. Damour, and V. F. Mukhanov, "k-inflation," *Phys. Lett.*, vol. B458, pp. 209–218, 1999, hep-th/9904075.

[82] A. Sen, "Rolling tachyon," *JHEP*, vol. 04, p. 048, 2002, hep-th/0203211.

[83] G. W. Gibbons, "Cosmological evolution of the rolling tachyon," *Phys. Lett.*, vol. B537, pp. 1–4, 2002, hep-th/0204008.

[84] R. R. Caldwell, "A Phantom Menace?," *Phys. Lett.*, vol. B545, pp. 23–29, 2002, astro-ph/9908168.

[85] A. Y. Kamenshchik, U. Moschella, and V. Pasquier, "An alternative to quintessence," *Phys. Lett.*, vol. B511, pp. 265–268, 2001, gr-qc/0103004.

[86] S. Capozziello, S. Carloni, and A. Troisi, "Quintessence without scalar fields," *Recent Res. Dev. Astron. Astrophys.*, vol. 1, p. 625, 2003, astro-ph/0303041.

[87] D. Clowe *et al.*, "A direct empirical proof of the existence of dark matter," *Astrophys. J.*, vol. 648, pp. L109–L113, 2006, astro-ph/0608407.

[88] M. Bradac *et al.*, "Revealing the properties of dark matter in the merging cluster MACSJ0025.4-1222," 2008, 0806.2320.

[89] J. R. Brownstein and J. W. Moffat, "The Bullet Cluster 1E0657-558 evidence shows Modified Gravity in the absence of Dark Matter," *Mon. Not. Roy. Astron. Soc.*, vol. 382, pp. 29–47, 2007, astro-ph/0702146.

[90] G. W. Angus and S. S. McGaugh, "The collision velocity of the bullet cluster in conventional and modified dynamics," 2007, 0704.0381.

[91] S. M. Carroll, V. Duvvuri, M. Trodden, and M. S. Turner, "Is cosmic speed-up due to new gravitational physics?," *Phys. Rev.*, vol. D70, p. 043528, 2004, astro-ph/0306438.

[92] A. D. Dolgov and M. Kawasaki, "Can modified gravity explain accelerated cosmic expansion?," *Phys. Lett.*, vol. B573, pp. 1–4, 2003, astro-ph/0307285.

[93] M. E. Soussa and R. P. Woodard, "The Force of Gravity from a Lagrangian containing Inverse Powers of the Ricci Scalar," *Gen. Rel. Grav.*, vol. 36, pp. 855–862, 2004, astro-ph/0308114.

[94] S. M. Carroll *et al.*, "The cosmology of generalized modified gravity models," *Phys. Rev.*, vol. D71, p. 063513, 2005, astro-ph/0410031.

[95] S. Nojiri and S. D. Odintsov, "Introduction to modified gravity and gravitational alternative for dark energy," *ECONF*, vol. C0602061, p. 06, 2006, hep-th/0601213.

[96] G. R. Dvali, G. Gabadadze, and M. Porrati, "4D gravity on a brane in 5D Minkowski space," *Phys. Lett.*, vol. B485, pp. 208–214, 2000, hep-th/0005016.

[97] G. R. Dvali and G. Gabadadze, "Gravity on a brane in infinite-volume extra space," *Phys. Rev.*, vol. D63, p. 065007, 2001, hep-th/0008054.

[98] C. Deffayet, "Cosmology on a brane in Minkowski bulk," *Phys. Lett.*, vol. B502, pp. 199–208, 2001, hep-th/0010186.

[99] M. Fairbairn and A. Goobar, "Supernova limits on brane world cosmology," *Phys. Lett.*, vol. B642, pp. 432–435, 2006, astro-ph/0511029.

[100] Z.-K. Guo, Z.-H. Zhu, J. S. Alcaniz, and Y.-Z. Zhang, "Constraints on the DGP Model from Recent Supernova Observations and Baryon Acoustic Oscillations," *Astrophys. J.*, vol. 646, p. 1, 2006, astro-ph/0603632.

[101] A. G. Riess *et al.*, "Type Ia Supernova Discoveries at z>1 From the Hubble Space Telescope: Evidence for Past Deceleration and Constraints on Dark Energy Evolution," *Astrophys. J.*, vol. 607, pp. 665–687, 2004, astro-ph/0402512.

[102] D. J. Eisenstein *et al.*, "Detection of the Baryon Acoustic Peak in the Large-Scale Correlation Function of SDSS Luminous Red Galaxies," *Astrophys. J.*, vol. 633, pp. 560–574, 2005, astro-ph/0501171.

[103] K. Koyama and R. Maartens, "Structure formation in the DGP cosmological model," *JCAP*, vol. 0601, p. 016, 2006, astro-ph/0511634.

[104] A. Cardoso, K. Koyama, S. S. Seahra, and F. P. Silva, "Cosmological perturbations in the DGP braneworld: numeric solution," *Phys. Rev.*, vol. D77, p. 083512, 2008, 0711.2563.

[105] I. Sawicki and S. M. Carroll, "Cosmological Structure Evolution and CMB Anisotropies in DGP Braneworlds," 2005, astro-ph/0510364.

[106] I. Sawicki, Y.-S. Song, and W. Hu, "Near-horizon solution for DGP perturbations," *Phys. Rev.*, vol. D75, p. 064002, 2007, astro-ph/0606285.

[107] U. Alam and V. Sahni, "Confronting braneworld cosmology with supernova data and baryon oscillations," *Phys. Rev.*, vol. D73, p. 084024, 2006, astro-ph/0511473.

[108] Y.-S. Song, I. Sawicki, and W. Hu, "Large-scale tests of the DGP model," *Phys. Rev.*, vol. D75, p. 064003, 2007, astro-ph/0606286.

[109] G. Hinshaw *et al.*, "Five-Year Wilkinson Microwave Anisotropy Probe (WMAP) Observations:Data Processing, Sky Maps, & Basic Results," 2008, 0803.0732.

[110] D. Gorbunov, K. Koyama, and S. Sibiryakov, "More on ghosts in DGP model," *Phys. Rev.*, vol. D73, p. 044016, 2006, hep-th/0512097.

[111] A. De Felice, M. Hindmarsh, and M. Trodden, "Ghosts, instabilities, and superluminal propagation in modified gravity models," *JCAP*, vol. 0608, p. 005, 2006, astro-ph/0604154.

[112] J. Yadav, S. Bharadwaj, B. Pandey, and T. R. Seshadri, "Testing homogeneity on large scales in the Sloan Digital Sky Survey Data Release One," *Mon. Not. Roy. Astron. Soc.*, vol. 364, pp. 601–606, 2005, astro-ph/0504315.

[113] W. J. Frith, N. Metcalfe, and T. Shanks, "New H-band Galaxy Number Counts: A Large Local Hole in the Galaxy Distribution?," *Mon. Not. Roy. Astron. Soc.*, vol. 371, pp. 1601–1609, 2006, astro-ph/0509875.

[114] B. R. Granett, M. C. Neyrinck, and I. Szapudi, "Dark Energy Detected with Supervoids and Superclusters," 2008, 0805.2974.

[115] K. Tomita, "Distances and lensing in cosmological void models," *Astrophys. J.*, vol. 529, p. 38, 2000, astro-ph/9906027.

[116] M.-N. Celerier, "Do we really see a cosmological constant in the supernovae data ?," *Astron. Astrophys.*, vol. 353, pp. 63–71, 2000, astro-ph/9907206.

[117] T. Biswas, R. Mansouri, and A. Notari, "Nonlinear Structure Formation and Apparent Acceleration: an Investigation," *JCAP*, vol. 0712, p. 017, 2007, astro-ph/0606703.

[118] S. Alexander, T. Biswas, A. Notari, and D. Vaid, "Local Void vs Dark Energy: Confrontation with WMAP and Type Ia Supernovae," 2007, 0712.0370.

[119] M.-N. Celerier, "The Accelerated Expansion of the Universe Challenged by an Effect of the Inhomogeneities. A Review," 2007, astro-ph/0702416.

[120] J. Garcia-Bellido and T. Haugboelle, "Confronting Lemaitre-Tolman-Bondi models with Observational Cosmology," *JCAP*, vol. 0804, p. 003, 2008, 0802.1523.

[121] J. Garcia-Bellido and T. Haugboelle, "Looking the void in the eyes - the kSZ effect in LTB models," *JCAP*, vol. 0809, p. 016, 2008, 0807.1326.

[122] N. Brouzakis, N. Tetradis, and E. Tzavara, "Light Propagation and Large-Scale Inhomogeneities," *JCAP*, vol. 0804, p. 008, 2008, astro-ph/0703586.

[123] V. Marra, E. W. Kolb, S. Matarrese, and A. Riotto, "On cosmological observables in a swiss-cheese universe," *Phys. Rev.*, vol. D76, p. 123004, 2007, 0708.3622.

[124] V. Marra, E. W. Kolb, and S. Matarrese, "Light-cone averages in a swiss-cheese universe," *Phys. Rev.*, vol. D77, p. 023003, 2008, 0710.5505.

[125] M. P. Dabrowski and M. A. Hendry, "Non-Uniform Pressure Universes: The Hubble Diagram of Type Ia Supernovae and the Age of the Universe," 1997, astro-ph/9704123.

[126] T. Buchert, "On globally static and stationary cosmologies with or without a cosmological constant and the dark energy problem," *Class. Quant. Grav.*, vol. 23, pp. 817–844, 2006, gr-qc/0509124.

[127] S. Rasanen, "Accelerated expansion from structure formation," *JCAP*, vol. 0611, p. 003, 2006, astro-ph/0607626.

[128] A. Ishibashi and R. M. Wald, "Can the acceleration of our universe be explained by the effects of inhomogeneities?," *Class. Quant. Grav.*, vol. 23, pp. 235–250, 2006, gr-qc/0509108.

[129] C.-P. Ma and E. Bertschinger, "Cosmological perturbation theory in the synchronous and conformal Newtonian gauges," *Astrophys. J.*, vol. 455, pp. 7–25, 1995, astro-ph/9506072.

[130] J. M. Bardeen, "Gauge Invariant Cosmological Perturbations," *Phys. Rev.*, vol. D22, pp. 1882–1905, 1980.

[131] H. Kodama and M. Sasaki, "Cosmological Perturbation Theory," *Prog. Theor. Phys. Suppl.*, vol. 78, pp. 1–166, 1984.

[132] R. Bean and O. Doré, "Probing dark energy perturbations: the dark energy equation of state and speed of sound as measured by WMAP," *Phys. Rev.*, vol. D69, p. 083503, 2004, astro-ph/0307100.

[133] S. DeDeo, R. R. Caldwell, and P. J. Steinhardt, "Effects of the sound speed of quintessence on the microwave background and large scale structure," *Phys. Rev.*, vol. D67, p. 103509, 2003, astro-ph/0301284.

[134] J. Weller and A. M. Lewis, "Large Scale Cosmic Microwave Background Anisotropies and Dark Energy," *Mon. Not. Roy. Astron. Soc.*, vol. 346, pp. 987–993, 2003, astro-ph/0307104.

[135] W. Hu and R. Scranton, "Measuring Dark Energy Clustering with CMB-Galaxy Correlations," *Phys. Rev.*, vol. D70, p. 123002, 2004, astro-ph/0408456.

[136] P.-S. Corasaniti, T. Giannantonio, and A. Melchiorri, "Constraining dark energy with cross-correlated CMB and Large Scale Structure data," *Phys. Rev.*, vol. D71, p. 123521, 2005, astro-ph/0504115.

[137] S. Hannestad, "Constraints on the sound speed of dark energy," *Phys. Rev.*, vol. D71, p. 103519, 2005, astro-ph/0504017.

[138] J.-Q. Xia, Y.-F. Cai, T.-T. Qiu, G.-B. Zhao, and X. Zhang, "Constraints on the sound speed of dynamical dark energy," 2007, astro-ph/0703202.

[139] D. F. Mota, J. R. Kristiansen, T. Koivisto, and N. E. Groeneboom, "Constraining Dark Energy Anisotropic Stress," 2007, 0708.0830.

[140] A. Torres-Rodriguez and C. M. Cress, "Constraining the Nature of Dark Energy using the SKA," *Mon. Not. Roy. Astron. Soc.*, vol. 376, pp. 1831–1837, 2007, astro-ph/0702113.

[141] A. Torres-Rodriguez, C. M. Cress, and K. Moodley, "Covariance of dark energy parameters and sound speed constraints from large HI surveys," 2008, 0804.2344.

[142] A. F. Heavens, T. D. Kitching, and L. Verde, "On model selection forecasting, dark energy and modified gravity," 2007, astro-ph/0703191.

[143] A. H. Guth, "The inflationary universe: The quest for a new theory of cosmic origins," Reading, USA: Addison-Wesley (1997) 358 p.

[144] A. R. Liddle and S. M. Leach, "How long before the end of inflation were observable perturbations produced?," *Phys. Rev.*, vol. D68, p. 103503, 2003, astro-ph/0305263.

[145] D. H. Lyth and A. Riotto, "Particle physics models of inflation and the cosmological density perturbation," *Phys. Rept.*, vol. 314, pp. 1–146, 1999, hep-ph/9807278.

[146] C. Amsler *et al.*, "Review of particle physics," *Phys. Lett.*, vol. B667, p. 1, 2008.

[147] S. Dodelson, W. H. Kinney, and E. W. Kolb, "Cosmic microwave background measurements can discriminate among inflation models," *Phys. Rev.*, vol. D56, pp. 3207–3215, 1997, astro-ph/9702166.

[148] W. H. Kinney, E. W. Kolb, A. Melchiorri, and A. Riotto, "Inflation model constraints from the Wilkinson microwave anisotropy probe three-year data," *Phys. Rev.*, vol. D74, p. 023502, 2006, astro-ph/0605338.

[149] A. D. Linde, "Chaotic Inflation," *Phys. Lett.*, vol. B129, pp. 177–181, 1983.

[150] K. Kadota and M. Yamaguchi, "D-term chaotic inflation in supergravity," *Phys. Rev.*, vol. D76, p. 103522, 2007, 0706.2676.

[151] S. C. Davis and M. Postma, "SUGRA chaotic inflation and moduli stabilisation," *JCAP*, vol. 0803, p. 015, 2008, 0801.4696.

[152] A. B. Goncharov and A. D. Linde, "Chaotic inflation in supergravity," *Phys. Lett.*, vol. B139, p. 27, 1984.

[153] M. Kawasaki, M. Yamaguchi, and T. Yanagida, "Natural chaotic inflation in supergravity," *Phys. Rev. Lett.*, vol. 85, pp. 3572–3575, 2000, hep-ph/0004243.

[154] M. Yamaguchi and J. Yokoyama, "New inflation in supergravity with a chaotic initial condition," *Phys. Rev.*, vol. D63, p. 043506, 2001, hep-ph/0007021.

[155] F. Lucchin and S. Matarrese, "Power law inflation," *Phys. Rev.*, vol. D32, p. 1316, 1985.

[156] A. R. Liddle, "Power law inflation with exponential potentials," *Phys. Lett.*, vol. B220, p. 502, 1989.

[157] M. Dine and A. Riotto, "An inflaton candidate in gauge mediated supersymmetry breaking," *Phys. Rev. Lett.*, vol. 79, pp. 2632–2635, 1997, hep-ph/9705386.

[158] F. C. Adams, J. R. Bond, K. Freese, J. A. Frieman, and A. V. Olinto, "Natural inflation: Particle physics models, power law spectra for large scale structure, and constraints from cobe," *Phys. Rev.*, vol. D47, pp. 426–455, 1993, hep-ph/9207245.

[159] K. Freese, J. A. Frieman, and A. V. Olinto, "Natural inflation with pseudo-nambu-goldstone bosons," *Phys. Rev. Lett.*, vol. 65, pp. 3233–3236, 1990.

[160] R. D. Peccei and H. R. Quinn, "CP Conservation in the Presence of Instantons," *Phys. Rev. Lett.*, vol. 38, pp. 1440–1443, 1977.

[161] A. D. Linde, "Axions in inflationary cosmology," *Phys. Lett.*, vol. B259, pp. 38–47, 1991.

[162] E. J. Copeland, A. R. Liddle, D. H. Lyth, E. D. Stewart, and D. Wands, "False vacuum inflation with Einstein gravity," *Phys. Rev.*, vol. D49, pp. 6410–6433, 1994, astro-ph/9401011.

[163] E. D. Stewart, "Flattening the inflaton's potential with quantum corrections," *Phys. Lett.*, vol. B391, pp. 34–38, 1997, hep-ph/9606241.

[164] D. H. Lyth and E. D. Stewart, "More varieties of hybrid inflation," *Phys. Rev.*, vol. D54, pp. 7186–7190, 1996, hep-ph/9606412.

[165] J. A. Adams, G. G. Ross, and S. Sarkar, "Multiple inflation," *Nucl. Phys.*, vol. B503, pp. 405–425, 1997, hep-ph/9704286.

[166] A. D. Linde, "Hybrid inflation," *Phys. Rev.*, vol. D49, pp. 748–754, 1994, astro-ph/9307002.

[167] A. A. Starobinsky, "Multicomponent de Sitter (Inflationary) Stages and the Generation of Perturbations," *JETP Lett.*, vol. 42, pp. 152–155, 1985.

[168] V. F. Mukhanov and P. J. Steinhardt, "Density perturbations in multifield inflationary models," *Phys. Lett.*, vol. B422, pp. 52–60, 1998, astro-ph/9710038.

[169] A. R. Liddle, A. Mazumdar, and F. E. Schunck, "Assisted inflation," *Phys. Rev.*, vol. D58, p. 061301, 1998, astro-ph/9804177.

[170] R. Brandenberger, P.-M. Ho, and H.-c. Kao, "Large N cosmology," *JCAP*, vol. 0411, p. 011, 2004, hep-th/0312288.

[171] S. Dimopoulos, S. Kachru, J. McGreevy, and J. G. Wacker, "N-flation," *JCAP*, vol. 0808, p. 003, 2008, hep-th/0507205.

[172] R. Easther and J. T. Giblin, "The hubble slow roll expansion for multi field inflation," *Phys. Rev.*, vol. D72, p. 103505, 2005, astro-ph/0505033.

[173] P. Adshead, R. Easther, and E. A. Lim, "Cosmology With Many Light Scalar Fields: Stochastic Inflation and Loop Corrections," 2008, 0809.4008.

[174] M. Bucher, A. S. Goldhaber, and N. Turok, "An open universe from inflation," *Phys. Rev.*, vol. D52, pp. 3314–3337, 1995, hep-ph/9411206.

[175] S. W. Hawking and N. Turok, "Open inflation without false vacua," *Phys. Lett.*, vol. B425, pp. 25–32, 1998, hep-th/9802030.

[176] A. Linde, "Fast-roll inflation," *JHEP*, vol. 11, p. 052, 2001, hep-th/0110195.

[177] L. Kofman and S. Mukohyama, "Rapid roll Inflation with Conformal Coupling," *Phys. Rev.*, vol. D77, p. 043519, 2008, 0709.1952.

[178] D. A. Easson, R. Gregory, D. F. Mota, G. Tasinato, and I. Zavala, "Spinflation," *JCAP*, vol. 0802, p. 010, 2008, 0709.2666.

[179] L. H. Ford, "Inflation driven by a vector field," *Phys. Rev.*, vol. D40, p. 967, 1989.

[180] A. Golovnev, V. Mukhanov, and V. Vanchurin, "Vector Inflation," *JCAP*, vol. 0806, p. 009, 2008, 0802.2068.

[181] T. Nihei, "Inflation in the five-dimensional universe with an orbifold extra dimension," *Phys. Lett.*, vol. B465, pp. 81–85, 1999, hep-ph/9905487.

[182] A. Mazumdar, "Extra dimensions and inflation," *Phys. Lett.*, vol. B469, pp. 55–60, 1999, hep-ph/9902381.

[183] N. Arkani-Hamed, H.-C. Cheng, P. Creminelli, and L. Randall, "Extranatural inflation," *Phys. Rev. Lett.*, vol. 90, p. 221302, 2003, hep-th/0301218.

[184] G. R. Dvali and S. H. H. Tye, "Brane inflation," *Phys. Lett.*, vol. B450, pp. 72–82, 1999, hep-ph/9812483.

[185] S. Nojiri and S. D. Odintsov, "Brane world inflation induced by quantum effects," *Phys. Lett.*, vol. B484, pp. 119–123, 2000, hep-th/0004097.

[186] C. Germani, N. E. Grandi, and A. Kehagias, "A stringy alternative to inflation: The cosmological slingshot scenario," *Class. Quant. Grav.*, vol. 25, p. 135004, 2008, hep-th/0611246.

[187] J. Khoury, B. A. Ovrut, P. J. Steinhardt, and N. Turok, "The ekpyrotic universe: Colliding branes and the origin of the hot big bang," *Phys. Rev.*, vol. D64, p. 123522, 2001, hep-th/0103239.

[188] M. Novello and S. E. P. Bergliaffa, "Bouncing Cosmologies," *Phys. Rept.*, vol. 463, pp. 127–213, 2008, 0802.1634.

[189] A. R. Liddle, P. Parsons, and J. D. Barrow, "Formalizing the slow roll approximation in inflation," *Phys. Rev.*, vol. D50, pp. 7222–7232, 1994, astro-ph/9408015.

[190] C. Gordon and R. Trotta, "Bayesian Calibrated Significance Levels Applied to the Spectral Tilt and Hemispherical Asymmetry," 2007, 0706.3014.

[191] R. Trotta, "Applications of Bayesian model selection to cosmological parameters," *Mon. Not. Roy. Astron. Soc.*, vol. 378, pp. 72–82, 2007, astro-ph/0504022.

[192] E. W. Kolb, "Dynamics of the inflationary era," 1999, hep-ph/9910311.

[193] A. Riotto, "Inflation and the theory of cosmological perturbations," 2002, hep-ph/0210162.

[194] M. Sasaki and E. D. Stewart, "A General analytic formula for the spectral index of the density perturbations produced during inflation," *Prog. Theor. Phys.*, vol. 95, pp. 71–78, 1996, astro-ph/9507001.

[195] W. Hu, N. Sugiyama, and J. Silk, "The Physics of microwave background anisotropies," *Nature*, vol. 386, pp. 37–43, 1997, astro-ph/9604166.

[196] M. Giovannini, "A primer on the physics of the cosmic microwave background," Singapore, Singapore: World Scientific (2008) 488 p.

[197] R. Durrer, "The Cosmic Microwave Background," Cambridge University Press (2008) 424 p.

[198] M. Abramowitz and I. Stegun, "Handbook of mathematical functions with formulas, graphs, and mathematical tables," *Dover Publications*, 1968.

[199] J. Martin and R. H. Brandenberger, "The trans-Planckian problem of inflationary cosmology," *Phys. Rev.*, vol. D63, p. 123501, 2001, hep-th/0005209.

[200] U. H. Danielsson, "A note on inflation and transplanckian physics," *Phys. Rev.*, vol. D66, p. 023511, 2002, hep-th/0203198.

[201] R. Easther, B. R. Greene, W. H. Kinney, and G. Shiu, "A generic estimate of trans-Planckian modifications to the primordial power spectrum in inflation," *Phys. Rev.*, vol. D66, p. 023518, 2002, hep-th/0204129.

[202] C. P. Burgess, J. M. Cline, and R. Holman, "Effective field theories and inflation," *JCAP*, vol. 0310, p. 004, 2003, hep-th/0306079.

[203] C. Cheung, P. Creminelli, A. L. Fitzpatrick, J. Kaplan, and L. Senatore, "The Effective Field Theory of Inflation," *JHEP*, vol. 03, p. 014, 2008, 0709.0293.

[204] C. P. Burgess, "Introduction to effective field theory," *Ann. Rev. Nucl. Part. Sci.*, vol. 57, pp. 329–362, 2007, hep-th/0701053.

[205] J. C. Collins, "Renormalization. An introduction to renormalization, the renormalization group, and the operator product expansion," Cambridge, Uk: Univ. Pr. (1984) 380p.

[206] J. C. Collins, "The problem of scales: Renormalization and all that," 1995, hep-ph/9510276.

[207] M. E. Peskin and D. V. Schroeder, "An Introduction to quantum field theory," Reading, USA: Addison-Wesley (1995) 842 p.

[208] M. Srednicki, "Quantum field theory," Cambridge, UK: Univ. Pr. (2007) 641 p.

[209] M. B. Einhorn and D. R. T. Jones, "A new renormalization group approach to multiscale problems," *Nucl. Phys.*, vol. B230, p. 261, 1984.

[210] C. Ford and C. Wiesendanger, "Multi-scale renormalization," *Phys. Lett.*, vol. B398, pp. 342–346, 1997, hep-th/9612193.

[211] M. Bando, T. Kugo, N. Maekawa, and H. Nakano, "Improving the effective potential: Multimass scale case," *Prog. Theor. Phys.*, vol. 90, pp. 405–418, 1993, hep-ph/9210229.

[212] J. A. Casas, V. Di Clemente, and M. Quiros, "The effective potential in the presence of several mass scales," *Nucl. Phys.*, vol. B553, pp. 511–530, 1999, hep-ph/9809275.

[213] T. Appelquist and J. Carazzone, "Infrared Singularities and Massive Fields," *Phys. Rev.*, vol. D11, p. 2856, 1975.

[214] B. M. Kastening, "Renormalization group improvement of the effective potential in massive phi**4 theory," *Phys. Lett.*, vol. B283, pp. 287–292, 1992.

[215] C. Ford, D. R. T. Jones, P. W. Stephenson, and M. B. Einhorn, "The Effective potential and the renormalization group," *Nucl. Phys.*, vol. B395, pp. 17–34, 1993, hep-lat/9210033.

[216] M. Bando, T. Kugo, N. Maekawa, and H. Nakano, "Improving the effective potential," *Phys. Lett.*, vol. B301, pp. 83–89, 1993, hep-ph/9210228.

[217] D. N. Spergel *et al.*, "First year wilkinson microwave anisotropy probe (wmap) observations: Determination of cosmological parameters," *Astrophys. J. Suppl.*, vol. 148, p. 175, 2003, astro-ph/0302209.

[218] H. V. Peiris *et al.*, "First year wilkinson microwave anisotropy probe (wmap) observations: Implications for inflation," *Astrophys. J. Suppl.*, vol. 148, p. 213, 2003, astro-ph/0302225.

[219] D. N. Spergel *et al.*, "Wilkinson microwave anisotropy probe (wmap) three year results: Implications for cosmology," 2006, astro-ph/0603449.

[220] B. S. Mason *et al.*, "The anisotropy of the microwave background to l = 3500: Deep field observations with the cosmic background imager," *Astrophys. J.*, vol. 591, pp. 540–555, 2003, astro-ph/0205384.

[221] J. L. Sievers *et al.*, "Cosmological parameters from cosmic background imager observations and comparisons with boomerang, dasi, and maxima," *Astrophys. J.*, vol. 591, pp. 599–622, 2003, astro-ph/0205387.

[222] C.-l. Kuo *et al.*, "High resolution observations of the cmb power spectrum with acbar," *Astrophys. J.*, vol. 600, pp. 32–51, 2004, astro-ph/0212289.

[223] M. Colless *et al.*, "The 2df galaxy redshift survey: Spectra and redshifts," *Mon. Not. Roy. Astron. Soc.*, vol. 328, p. 1039, 2001, astro-ph/0106498.

[224] W. J. Percival *et al.*, "The 2df galaxy redshift survey: The power spectrum and the matter content of the universe," *Mon. Not. Roy. Astron. Soc.*, vol. 327, p. 1297, 2001, astro-ph/0105252.

[225] L. Verde *et al.*, "First year wilkinson microwave anisotropy probe (wmap) observations: Parameter estimation methodology," *Astrophys. J. Suppl.*, vol. 148, p. 195, 2003, astro-ph/0302218.

[226] N. Kogo, M. Matsumiya, M. Sasaki, and J. Yokoyama, "Reconstructing the primordial spectrum from wmap data by the cosmic inversion method," *Astrophys. J.*, vol. 607, pp. 32–39, 2004, astro-ph/0309662.

[227] M. Tegmark *et al.*, "Cosmological parameters from sdss and wmap," *Phys. Rev.*, vol. D69, p. 103501, 2004, astro-ph/0310723.

[228] M. Viel, J. Weller, and M. Haehnelt, "Constraints on the primordial power spectrum from high resolution lyman-alpha forest spectra and wmap," *Mon. Not. Roy. Astron. Soc.*, vol. 355, p. L23, 2004, astro-ph/0407294.

[229] U. Seljak, P. McDonald, and A. Makarov, "Cosmological constraints from the cmb and ly-alpha forest revisited," *Mon. Not. Roy. Astron. Soc.*, vol. 342, p. L79, 2003, astro-ph/0302571.

[230] J. M. Cline and L. Hoi, "Inflationary potential reconstruction for a wmap running power spectrum," *JCAP*, vol. 0606, p. 007, 2006, astro-ph/0603403.

[231] "http://lambda.gsfc.nasa.gov/,"

[232] H. Hoekstra *et al.*, "First cosmic shear results from the canada-france-hawaii telescope wide synoptic legacy survey," 2005, astro-ph/0511089.

[233] J. K. Adelman-McCarthy *et al.*, "The fourth data release of the sloan digital sky survey," *Astrophys. J. Suppl.*, vol. 162, pp. 38–48, 2006, astro-ph/0507711.

[234] M. Tegmark *et al.*, "The 3d power spectrum of galaxies from the sdss," *Astrophys. J.*, vol. 606, pp. 702–740, 2004, astro-ph/0310725.

[235] J. E. Ruhl *et al.*, "Improved measurement of the angular power spectrum of temperature anisotropy in the cmb from two new analyses of boomerang observations," *Astrophys. J.*, vol. 599, pp. 786–805, 2003, astro-ph/0212229.

[236] T. E. Montroy *et al.*, "A measurement of the cmb spectrum from the 2003 flight of boomerang," 2005, astro-ph/0507514.

[237] C. Dickinson *et al.*, "High sensitivity measurements of the cmb power spectrum with the extended very small array," *Mon. Not. Roy. Astron. Soc.*, vol. 353, p. 732, 2004, astro-ph/0402498.

[238] S. Cole *et al.*, "The 2df galaxy redshift survey: Power-spectrum analysis of the final dataset and cosmological implications," *Mon. Not. Roy. Astron. Soc.*, vol. 362, pp. 505–534, 2005, astro-ph/0501174.

[239] M. Viel, M. G. Haehnelt, and A. Lewis, "The lyman-alpha forest and wmap year three," *Mon. Not. Roy. Astron. Soc. Lett.*, vol. 370, pp. L51–L55, 2006, astro-ph/0604310.

[240] U. Seljak, A. Slosar, and P. McDonald, "Cosmological parameters from combining the lyman-alpha forest with cmb, galaxy clustering and sn constraints," 2006, astro-ph/0604335.

[241] J. R. Kristiansen, H. K. Eriksen, and O. Elgaroy, "Revised wmap constraints on neutrino masses and other extensions of the minimal lambdacdm model," 2006, astro-ph/0608017.

[242] M. Bridges, A. N. Lasenby, and M. P. Hobson, "Wmap 3-year primordial power spectrum," 2006, astro-ph/0607404.

[243] A. Challinor, "Constraining fundamental physics with the cosmic microwave background," 2006, astro-ph/0606548.

[244] J. Dunkley *et al.*, "Five-Year Wilkinson Microwave Anisotropy Probe (WMAP) Observations: Likelihoods and Parameters from the WMAP data," 2008, 0803.0586.

[245] W. M. Wood-Vasey *et al.*, "Observational Constraints on the Nature of the Dark Energy: First Cosmological Results from the ESSENCE Supernova Survey," *Astrophys. J.*, vol. 666, pp. 694–715, 2007, astro-ph/0701041.

[246] C. L. Reichardt *et al.*, "High resolution CMB power spectrum from the complete ACBAR data set," 2008, 0801.1491.

[247] W. J. Percival *et al.*, "Measuring the Baryon Acoustic Oscillation scale using the SDSS and 2dFGRS," *Mon. Not. Roy. Astron. Soc.*, vol. 381, pp. 1053–1066, 2007, 0705.3323.

[248] C.-L. Kuo *et al.*, "Improved Measurements of the CMB Power Spectrum with ACBAR," 2006, astro-ph/0611198.

[249] L. Verde and H. V. Peiris, "On Minimally-Parametric Primordial Power Spectrum Reconstruction and the Evidence for a Red Tilt," 2008, 0802.1219.

[250] "Planck: The scientific programme," 2006, astro-ph/0604069.

[251] www.rssd.esa.int/Planck/

[252] C. Pahud, A. R. Liddle, P. Mukherjee, and D. Parkinson, "When can the Planck satellite measure spectral index running?," *Mon. Not. Roy. Astron. Soc.*, vol. 381, pp. 489–493, 2007, astro-ph/0701481.

[253] M. Cortes, A. R. Liddle, and P. Mukherjee, "On what scale should inflationary observables be constrained?," *Phys. Rev.*, vol. D75, p. 083520, 2007, astro-ph/0702170.

[254] P. Binetruy and G. R. Dvali, "D-term inflation," *Phys. Lett.*, vol. B388, pp. 241–246, 1996, hep-ph/9606342.

[255] R. Allahverdi, K. Enqvist, J. Garcia-Bellido, and A. Mazumdar, "Gauge invariant MSSM inflaton," *Phys. Rev. Lett.*, vol. 97, p. 191304, 2006, hep-ph/0605035.

[256] R. Allahverdi, K. Enqvist, J. Garcia-Bellido, A. Jokinen, and A. Mazumdar, "MSSM flat direction inflation: slow roll, stability, fine tunning and reheating," *JCAP*, vol. 0706, p. 019, 2007, hep-ph/0610134.

[257] D. H. Lyth, "MSSM inflation," *JCAP*, vol. 0704, p. 006, 2007, hep-ph/0605283.

[258] K. Enqvist, L. Mether, and S. Nurmi, "Supergravity origin of the MSSM inflation," *JCAP*, vol. 0711, p. 014, 2007, 0706.2355.

[259] A. Buchel *et al.*, "Radiative corrections to the inflaton potential as an explanation of suppressed large scale power in density perturbations and the cosmic microwave background," *JCAP*, vol. 0503, p. 003, 2005, hep-ph/0410117.

[260] S. P. Martin and M. T. Vaughn, "Two loop renormalization group equations for soft supersymmetry breaking couplings," *Phys. Rev.*, vol. D50, p. 2282, 1994, hep-ph/9311340.

[261] T. Gherghetta, C. F. Kolda, and S. P. Martin, "Flat directions in the scalar potential of the supersymmetric standard model," *Nucl. Phys.*, vol. B468, pp. 37–58, 1996, hep-ph/9510370.

[262] M. Cvetic, "Nonrenormalizable sector of the effective lagrangian from superstring theories," Presented at Strings '88 Workshop, College Park, Md., Mar 24-28, 1988.

[263] A. Font, L. E. Ibanez, H. P. Nilles, and F. Quevedo, "Degenerate Orbifolds," *Nucl. Phys.*, vol. B307, p. 109, 1988.

[264] A. Lewis and S. Bridle, "Cosmological parameters from CMB and other data: a Monte- Carlo approach," *Phys. Rev.*, vol. D66, p. 103511, 2002, astro-ph/0205436.

[265] A. Raftery and S. Lewis, "Implementing MCMC," In *Markov Chain Monte Carlo in Practice*, vol. London: Chapman and Hall, pp. 163–188, 1996.

[266] W. H. Kinney, "How to fool cosmic microwave background parameter estimation," *Phys. Rev.*, vol. D63, p. 043001, 2001, astro-ph/0005410.

[267] G. Hinshaw *et al.*, "Three-year Wilkinson Microwave Anisotropy Probe (WMAP) observations: Temperature analysis," *Astrophys. J. Suppl.*, vol. 170, p. 288, 2007, astro-ph/0603451.

[268] A. C. S. Readhead *et al.*, "Extended mosaic observations with the cosmic background imager," *Astrophys. J.*, vol. 609, pp. 498–512, 2004, astro-ph/0402359.

[269] M. Tegmark *et al.*, "Cosmological Constraints from the SDSS Luminous Red Galaxies," *Phys. Rev.*, vol. D74, p. 123507, 2006, astro-ph/0608632.

[270] W. L. Freedman *et al.*, "Final Results from the Hubble Space Telescope Key Project to Measure the Hubble Constant," *Astrophys. J.*, vol. 553, pp. 47–72, 2001, astro-ph/0012376.

[271] S. M. Leach, A. R. Liddle, J. Martin, and D. J. Schwarz, "Cosmological parameter estimation and the inflationary cosmology," *Phys. Rev.*, vol. D66, p. 023515, 2002, astro-ph/0202094.

[272] M. Dine, L. Randall, and S. D. Thomas, "Baryogenesis from flat directions of the supersymmetric standard model," *Nucl. Phys.*, vol. B458, pp. 291–326, 1996, hep-ph/9507453.

[273] R. Protassov, D. A. van Dyk, A. Connors, V. L. Kashyap, and A. Siemiginowska, "Statistics: Handle with Care, Detecting Multiple Model Components with the Likelihood Ratio Test," 2002, astro-ph/0201547.

[274] R. Trotta, "Forecasting the Bayes factor of a future observation," *Mon. Not. Roy. Astron. Soc.*, vol. 378, pp. 819–824, 2007, astro-ph/0703063.

[275] M. Kunz, R. Trotta, and D. Parkinson, "Measuring the effective complexity of cosmological models," *Phys. Rev.*, vol. D74, p. 023503, 2006, astro-ph/0602378.

[276] L. Knox, Y.-S. Song, and J. A. Tyson, "Two windows on acceleration and gravitation: Dark energy or new gravity?," 2005, astro-ph/0503644.

[277] K. Koyama, "Structure formation in modified gravity models alternative to dark energy," *JCAP*, vol. 0603, p. 017, 2006, astro-ph/0601220.

[278] J.-P. Uzan, "The acceleration of the universe and the physics behind it," *Gen. Rel. Grav.*, vol. 39, pp. 307–342, 2007, astro-ph/0605313.

[279] S. M. Carroll, I. Sawicki, A. Silvestri, and M. Trodden, "Modified-Source Gravity and Cosmological Structure Formation," *New J. Phys.*, vol. 8, p. 323, 2006, astro-ph/0607458.

[280] E. Bertschinger, "On the Growth of Perturbations as a Test of Dark Energy," *Astrophys. J.*, vol. 648, pp. 797–806, 2006, astro-ph/0604485.

[281] E. V. Linder and R. N. Cahn, "Parameterized Beyond-Einstein Growth," *Astropart. Phys.*, vol. 28, pp. 481–488, 2007, astro-ph/0701317.

[282] S. Tsujikawa, "Matter density perturbations and effective gravitational constant in modified gravity models of dark energy," *Phys. Rev.*, vol. D76, p. 023514, 2007, 0705.1032.

[283] V. Acquaviva and L. Verde, "Observational signatures of Jordan-Brans-Dicke theories of gravity," *JCAP*, vol. 0712, p. 001, 2007, 0709.0082.

[284] B. Jain and P. Zhang, "Observational Tests of Modified Gravity," 2007, 0709.2375.

[285] H. Wei and S. N. Zhang, "How to Distinguish Dark Energy and Modified Gravity?," 2008, 0803.3292.

[286] H. Wei, "Growth Index of DGP Model and Current Growth Rate Data," *Phys. Lett.*, vol. B664, pp. 1–6, 2008, 0802.4122.

[287] H. Zhang, H. Yu, H. Noh, and Z.-H. Zhu, "Probing the nature of cosmic acceleration," 2008, 0806.4082.

[288] D. Huterer and E. V. Linder, "Separating dark physics from physical darkness: Minimalist modified gravity vs. dark energy," *Phys. Rev.*, vol. D75, p. 023519, 2007, astro-ph/0608681.

[289] L. Amendola, M. Kunz, and D. Sapone, "Measuring the dark side (with weak lensing)," *JCAP*, vol. 0804, p. 013, 2008, 0704.2421.

[290] D. Sapone and L. Amendola, "Constraining the growth factor with baryon oscillations," 2007, 0709.2792.

[291] S. Nesseris and L. Perivolaropoulos, "Testing LCDM with the Growth Function $\delta(a)$: Current Constraints," *Phys. Rev.*, vol. D77, p. 023504, 2008, 0710.1092.

[292] O. Dore *et al.*, "Testing Gravity with the CFHTLS-Wide Cosmic Shear Survey and SDSS LRGs," 2007, 0712.1599.

[293] A. Mantz, S. W. Allen, H. Ebeling, and D. Rapetti, "New constraints on dark energy from the observed growth of the most X-ray luminous galaxy clusters," 2007, 0709.4294.

[294] C. Di Porto and L. Amendola, "Observational constraints on the linear fluctuation growth rate," *Phys. Rev.*, vol. D77, p. 083508, 2008, 0707.2686.

[295] K. Yamamoto, D. Parkinson, T. Hamana, R. C. Nichol, and Y. Suto, "Optimizing future imaging survey of galaxies to confront dark energy and modified gravity models," *Phys. Rev.*, vol. D76, p. 023504, 2007, 0704.2949.

[296] V. Acquaviva, A. Hajian, D. N. Spergel, and S. Das, "Next Generation Redshift Surveys and the Origin of Cosmic Acceleration," 2008, 0803.2236.

[297] A. Refregier and t. D. collaboration, "The Dark UNiverse Explorer (DUNE): Proposal to ESA's Cosmic Vision," 2008, 0802.2522.

[298] J. K. Erickson, R. R. Caldwell, P. J. Steinhardt, C. Armendariz-Picon, and V. F. Mukhanov, "Measuring the speed of sound of quintessence," *Phys. Rev. Lett.*, vol. 88, p. 121301, 2002, astro-ph/0112438.

[299] B. A. Bassett, M. Kunz, D. Parkinson, and C. Ungarelli, "Condensate cosmology - Dark energy from dark matter," *Phys. Rev.*, vol. D68, p. 043504, 2003, astro-ph/0211303.

[300] H. Sandvik, M. Tegmark, M. Zaldarriaga, and I. Waga, "The end of unified dark matter?," *Phys. Rev.*, vol. D69, p. 123524, 2004, astro-ph/0212114.

[301] L. M. G. Beca, P. P. Avelino, J. P. M. de Carvalho, and C. J. A. P. Martins, "The Role of Baryons in Unified Dark Matter Models," *Phys. Rev.*, vol. D67, p. 101301, 2003, astro-ph/0303564.

[302] L. Amendola, F. Finelli, C. Burigana, and D. Carturan, "WMAP and the Generalized Chaplygin Gas," *JCAP*, vol. 0307, p. 005, 2003, astro-ph/0304325.

[303] M. Kunz and D. Sapone, "Crossing the phantom divide," *Phys. Rev.*, vol. D74, p. 123503, 2006, astro-ph/0609040.

[304] L.-M. Wang and P. J. Steinhardt, "Cluster Abundance Constraints on Quintessence Models," *Astrophys. J.*, vol. 508, pp. 483–490, 1998, astro-ph/9804015.

[305] D. Polarski and R. Gannouji, "On the growth of linear perturbations," *Phys. Lett.*, vol. B660, pp. 439–443, 2008, 0710.1510.